THE UNIVERSITY
of EDINBURGH

MMP-12 Activity During Vascular Remodelling

Holly Rosannah Stott

THE UNIVERSITY *of* EDINBURGH

Doctor of Philosophy

The University of Edinburgh

2016

Declaration

The thesis herein is solely my own work. Apart from where stated the experiments were performed entirely by me. I confirm that this work has not been previously submitted for any other degree.

……..

Acknowledgements

I am grateful to my all my supervisors, Dr. Paddy Hadoke, Prof. Mark Bradley and Dr. Kev Dhaliwal for their guidance during my Ph.D. I would also like to thank Dr. Annamaria Lilienkampf, Dr. Nicolaos Avlonitis, Dr. Mark Macaskill, Dr. Ruth Morgan, Eileen Miller, Dr. Chesney Michels, Gary Borthwick and all the support staff who have helped or given me advice over the past 4 years.

I would like to thank The British Heart Foundation for supporting me thoughout my Ph.D.. It has been a wonderful experience and I will always be grateful for the opportunity.

Paddy was a brilliant mentor; always enthusiastic, knowledgeable, motivating, patient and reassuring. He always found the time to discuss upcoming experiments and new results. I am a much better scientist now because of him.

To all the friends I made over the past 4 years, thank you for sharing this experience with me. I would like to say a special thanks to Catherine Rose, Jess Clavadetscher, Andrew Nolan, Martha Mackay, Aurélie Brunet, Neil Norouzi, Tracy Mak, Gianna Panagakou, Lyam Hollis, Callam Davidson, Rob Ogley, Amber Abernethie, Cairnan Duffy and Junxi Wu. You kept me sane and helped me laugh when things didn't go to plan, which was often. Thanks must also to friends from home who helped me survive the writing process.

I am forever thankful to my family, particularly my parents who helped me develop into the person I am today. Every day they still broaden my horizons through conversation and travel. They celebrate my highs and help me through the lows; forever encouraging, supportive and loving. Thank you for everything.

Finally, I must thank Dr. Alex Saunders. I know I couldn't have done this without him. Hopefully life will never again be so stressful. I'm so proud of both of us. Endless love x

Abstract

Matrix metalloproteinases (MMPs) are required for tissue remodelling processes, including angiogenesis. MMP activity is generally proangiogenic but MMP-12 is suggested to be antiangiogenic and its precise role is still unclear. The work in this thesis describes the synthesis of an MMP-12 inhibitor and activity probe to address the hypothesis that MMP-12 inhibits angiogenesis.

An inhibitor, synthesised in-house, selectively inhibited MMP-12 in *in vitro* recombinant enzyme assays. An activity probe, also synthesised in-house, was selective for MMP-12 in *in vitro* recombinant enzyme assays.

The function of MMP-12 during angiogenesis was assessed using murine models of angiogenesis; the *in vivo* sponge implantation, and the *ex vivo* aortic ring assays. Angiogenesis and MMP activity were imaged *in vivo* in sponges in C57Bl6/J mice over 7 − 21 days (D) using commercial probes (MMPSense™ and AngioSense™). MMP-12 protein concentration and activity were higher in sponges during early angiogenesis (D 3 − 7) when gene expression of vascular endothelial growth factor (a proangiogenic marker) was also high. Gene expression for MMP-12 and platelet-derived growth factor receptor (a marker of vascular maturation) were both higher on D 21 as angiogenesis started to stabilise. The MMP-12 activity probe was unsuccessful in selectively detecting MMP-12 activity in sponge lysate mixtures from D 7 − 21.

Administration of an MMP-12 inhibitor did not increase angiogenesis in the sponges *in vivo*. Additionally, sponges implanted in MMP-$12^{-/-}$ mice did not exhibit significant changes in angiogenesis or MMP activity when imaged *in vivo* using commercial probes (MMPSense™ and AngioSense™) on D 7. Supporting this, histological analysis of the sponges (removed on D 21) showed that deletion of MMP-12 also did not increase angiogenesis within the sponges.

Furthermore, in the ex vivo aortic ring assay, the inhibition or deletion or MMP-12 did not increase the number or length of microvessel outgrowths.

To summarise, MMP activity and angiogenesis can be imaged in vivo with commercial probes. The inhibition or deletion of MMP-12 did not inhibit angiogenesis in the in vivo sponge implantation, or the ex vivo aortic ring assays. These results suggest that MMP-12 does not inhibit angiogenesis in these models.

Lay Abstract

The cardiovascular system consists of the heart, blood and vessels. It is required for delivering nutrients and removing harmful by-products from around the body. New vessels are formed as part of normal day-to-day body maintenance or in response to an increased oxygen demand of a tissue. Angiogenesis is the formation of new blood vessels from existing blood vessels. Angiogenesis requires the temporary dismantling of the existing vessel structure to allow the cells to move and multiply to form a new vessel structure.

Matrix metalloproteinases (MMPs) are a large family of enzymes (26+) which are required for the breakdown of the network of structural fibres found between cells. The disassembly of this fibrous network creates new space for cells to move and multiply. It is generally accepted that MMPs encourage new vessel formation. MMP-12 is an exception: whilst its precise role is unclear, there is some evidence that MMP-12 creates molecules that inhibit angiogenesis.

This thesis explores the influence of MMP-12 on angiogenesis. This was achieved by making molecules that would inhibit or detect MMP-12, and applying them to two models of angiogenesis in which MMP-12 was thought to be involved. In the first model new vessel growth (over a 21day period) is stimulated by insertion of small sponges under the skin of adult mice. Using this model, new methods of visualising angiogenesis and MMPs within live animals were tested. For the first time commercially-available agents were used to image angiogenesis and MMP activity in mice (over a period of 2 weeks) within sponges implanted under the skin. The second model of angiogenesis involved stimulating new vessel growth in the lab using vessels taken from mice. It was proposed that blocking MMP-12 activity would increase the number of new vessels formed in both models but it was shown that blocking MMP-12 (either using drugs or genetic manipulation) did not alter angiogenesis.

This study showed that angiogenesis and MMPs can be imaged in sponges during vascular remodelling in live mice. However, MMP-12 is not required for angiogenesis in the models used in this study.

List of Presentations

Oral Presentations:

H. Stott, K. Dhaliwal; M. Bradley; P. Hadoke (2015). The Role of Matrix Metalloproteinases-12 in Vascular Remodelling. *The Scottish Cardiovascular Forum 2015, Abstract R5.*

H. Stott, K. Dhaliwal; M. Bradley; P. Hadoke (2015). Optical Imaging of Angiogenesis and MMP Activity in a Murine Model of Vascular Remodelling. *World Molecular Imaging Congress 2015, Abstract SS 106.*

Poster Presentations:

H. Stott, K. Dhaliwal; M. Bradley; P. Hadoke (2014). Imaging Matrix Metalloproteinases During Vascular Remodelling *In Vivo. The Scottish Cardiovascular Forum 2014.*

H. Stott, K. Dhaliwal; M. Bradley; P. Hadoke (2014). Characterisation of MMP-12 expression and activity in the sponge model of angiogenesis. *Centre for Cardiovascular Science Symposium Day 2014*

H. Stott, K. Dhaliwal; M. Bradley; P. Hadoke (2015). Optical imaging of angiogenesis and MMP activity in a murine model of angiogenesis. *Centre for Cardiovascular Science Symposium Day 2015*

Table of Contents

List of Figures

List of Schemes

List of Tables

List of Abbreviations

aa	amino acid
AAA	abdominal aortic aneurysm
ACN	acetonitrile
ANVOA	analysis of variance
ApoE	apolipoprotein E
Boc	tert-butyloxycarbonyl
CD31	cluster of differentiation 31
cDNA	complementary deoxyribonucleic acid
COSY	correlation spectroscopy
Cp	crossing point
CT	X-ray computed tomography
CV	cardiovascular
CVD	cardiovascular disease
D	day
DAB	3,3'-diaminobenzidine
DAPI	4',6-diamidino-2-phenylindole
DCM	dichloromethane
Dde	1-(4,4-Dimethyl-2,6-dioxocyclohex-1-ylidene)-3-ethyl
DIC	diisopropylcarbodiimide
DIPEA	*N*,*N*-diisopropylethylamine
DMAP	4-dimethylaminopyridine
DMEM	Dulbecco's modified Eagle medium
DMF	dimethylformamide
DMSO	dimethyl sulfoxide
EC	endothelial cell
ECM	extracellular matrix

ELSD	evaporative light scattering detector
FA	formic acid
FAI	femoral artery injury
FAM	5(6)-carboxyfluorescein
Fmoc	fluorenylmethyloxycarbonyl
FMT	fluorescent molecular tomography
FRET	Förster resonance energy transfer
GAPDH	glyceraldehyde 3-phosphate dehydrogenase
GF	growth factors
h	hour
HPLC	high pressure liquid chromatography
hrp	horseradish peroxidase
HSQC	heteronuclear single quantum coherence spectroscopy
IFNα	interferon alpha
IR	infrared
KO	knockout
m	murine
MALDI - TOF	matrix-assisted laser desorption/ionization - time of flight
MI	myocardial infarction
min	minute
MMP	matrix metalloproteinase
MMPI	matrix metalloproteinase inhibitor
MR	methyl red
MRI	magnetic resonance imaging
MS	mass spectroscopy
MTT	3-(4,5-dimethylthiazol-2-yl)-2,5-diphenyltetrazolium bromide
NIR	near infrared
NMP	N-methyl-2-pyrrolidone

NMR	nuclear magnetic resonance
P	post-natal
PBS	phosphate buffered saline
PDGFR	platelet-derived growth factor receptor
PEG	polyethylene glycol
PET	positron emission tomography
PS	polystyrene
r	recombinant
rh	human recombinant
RhodB	5(6)-carboxyrhodamine B
RNA	ribonucleic acid
ROI	region of interest
RT-qPCR	real time- quantitative polymerase chain reaction
sec	seconds
SMC	smooth muscle cell
SPPS	solid phase peptide synthesis
TBP	TATA-binding protein
TFA	trifluoroacetic acid
TIMP	tissue inhibitors of metalloproteinases
TIS	triisopropylamine
TL	tissue lysates
TLC	thin layer chromatography
TMB	3,3′,5,5′-tetramethylbenzidine
TNFα	tumor necrosis factor alpha
uPA	urokinase-type plasminogen activator
uPAR	urokinase-type plasminogen activator receptor
VEGF	vascular endothelial growth factor
WT	wild type

Chapter 1

Introduction

1 Chapter 1: Introduction

1.1 Overview

Blood vessels have evolved to supply oxygen and nutrients to tissues and dispose of carbon dioxide and other waste products. A healthy network of blood vessels supports tissue maintenance, growth and repair but structural and functional abnormalities in the network can contribute to disease. Poor blood supply can cause ischemia in tissues, leading to myocardial infarction or stroke; whilst abnormal vessel remodelling and excessive blood supply is implicated in poor cancer prognosis and inflammatory diseases. The ability to image this network and blood flow could contribute towards the assessment of disease states.

The activity of matrix metalloproteinases (MMPs) is associated with increased vessel growth and the progression of several cardiovascular diseases. Interestingly, MMP-12 is suggested to inhibit vessel growth but its precise role is still unclear (Li *et al*., 2012). The ability to selectively image and/or manipulate MMP-12 activity *in vivo* could contribute to a better understanding of its role during vessel formation and diseases where MMP-12 is suggested to have an active role.

This introduction will first discuss the MMP family, with emphasis on MMP-12, and its role in angiogenesis and disease. Next, tools for molecular imaging of MMPs and angiogenesis will be considered, followed by a discussion on MMP-12 inhibitors, with a focus on the choice of inhibitor for use in this study.

1.2 Matrix metalloproteinases

MMPs constitute a large family of zinc dependent endopeptidases which are required for the breakdown of the extra cellular matrix (ECM) and regulation of cell behaviour. MMPs contribute to tissue remodelling by cleaving the ECM, basement membrane and cell-cell junctions (Page-McCaw *et al.,* 2007). This connective tissue is found between cells and comprises structural material such as collagens, elastin, proteoglycans, and laminins (Visse & Nagase, 2003). MMPs create space to enable cell migration and tissue remodelling (Figure 1.1). Furthermore, MMPs can manipulate cell behaviour by processing (activating or disabling) signalling molecules or creating substrate cleavage fragments which have independent biological activity (Figure 1.2); the role of MMPs and cell behaviour has been reviewed comprehensively by Sternlicht & Werb (2001) and Newby (2006).

MMP activity is under tight endogenous regulation and is essential for many physiological processes, including: embryo development (Shi *et al.,* 2008), bone formation (Paiva & Granjeiro, 2014), ovulation (Goldman & Shalev, 2004), and wound healing (Gill & Parks, 2008). However, unregulated and excessive MMP activity is associated with the progression of disease pathology. Rheumatoid arthritis (Burrage *et al*., 2006), tumour angiogenesis (Kerkelä *et al.,* 2002) and atherosclerosis (Liang *et al.,* 2006) are all conditions in which MMP activity contributes to disease pathology. Consequently, the pharmaceutical industry now targets, or has targeted, MMPs to treat diseases including COPD (Dahl *et al*., 2012), arthritis (Dubois *et al*., 1998) and cancer (Lee *et al.,* 2004; Whelan 2004; Cathcart *et al.,* 2015).

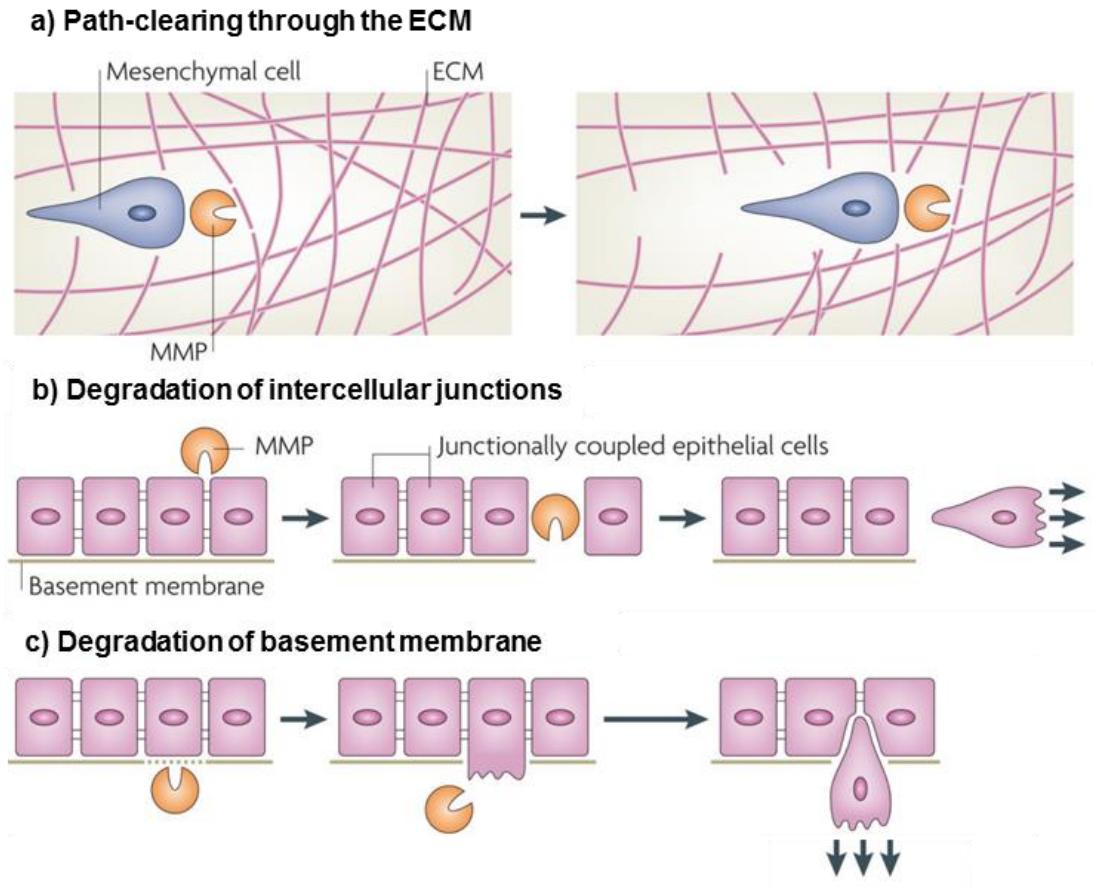

Figure 1.1 Matrix metalloproteinases (MMP) can cleave components of the extracellular matrix (ECM), basement membrane and intercellular junctions, resulting in space for cell movement. a) MMPs cleave components of the ECM which creates space for cell migration through tissue. b) MMPs can also directly regulate epithelial tissue architecture through cleavage of intercellular junctions or (c) the basement membrane which facilitates cell migration. Figure reproduced with permission from Page-McCaw and colleagues (2007) and modified.

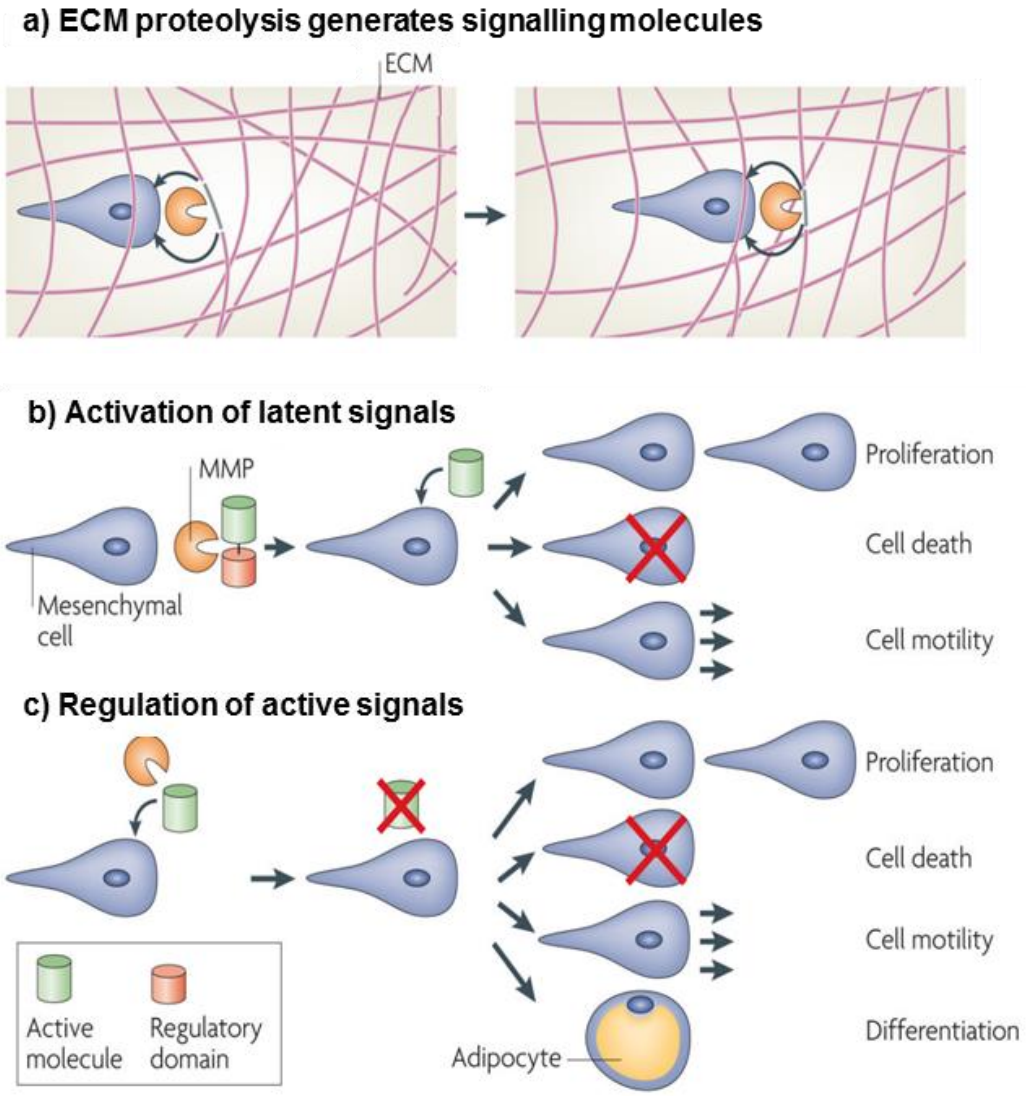

Figure 1.2 Matrix metalloproteinases (MMPs) proteolysis of extracellular matrix (ECM) components or signal molecules can generate specific cleavage products that then signal in an autocrine or paracrine manner. a) MMP proteolysis of the ECM matrix can generate biologically active cleavage products (for example, MMP -9, -3, -12 and -13 can generate an antiangiogenic peptide, endostatin, from collagen XIII (Ferreras *et al.*, 2000; Halfter *et al.*, 1998)). b) MMPs can activate or modify the action of latent signalling molecules (for example vascular endothelial growth factor (Lee *et al.*, 2005). c) MMPs can also deactivate or modify the action of active signalling molecules, the resulting molecules can affect cell proliferation, death, differentiation or motility. Reproduced with permission from Page-McCaw and colleagues (2007) and modified.

1.2.1 MMP Evolution and structure

Members of the MMP family, which comprises at least 26 members, share a similar gene arrangement, suggesting that they arose through duplication of a single ancestor gene (Shapiro *et al.*, 1998). The MMP family can be split approximately into two distinct groups; those that are secreted and those that are membrane associated (membrane-type; Table 1.1). Membrane-type MMPs include MMP-14, -15, -16, -17, -23, -24 and -25; these are anchored to the cell membrane. The secreted MMPs fall into several categories, including the: gelatinases (MMP-2, -9); collagenases (MMP-1, -8, -13), and stromelysins (MMP-3, -10, -11). Other secreted MMPs which are not in these categories are MMP-7 and 12. MMP-7 lacks an anchor domain like membrane type MMPs but instead is membrane associated through binding to cholesterol sulfate in cell membranes (Yamamoto *et al*., 2006). MMP-12 also lacks an anchor domain but the catalytic domain is suggested to have favourable electrostatic attraction to cell membranes (Koppisetti *et al*., 2014). MMPs have a wide variety of ECM substrates (Table 1.1).

Table 1.1 MMP family classifications and substrates. MMPs have multiple substrates and can be sub-classified into collagenases, gelatinases, stromelysins, matrilysins and membrane-type. MMP-4, -5, -6 and -22 are missing from the table since they were shown to be identical to other members. MMP-18 (collangense-4) has only been identified in Xenopus. Table is adapted from MMP review paper (Visse & Nagase, 2003).

Table 1.1 MMP family classifications and substrates

Class	MMP No.	*Enzyme*	ECM Substrates
Collegenases	MMP-1	*Collagenases Collagenase-1*	Collagens (type I, II, III, VII, VIII, X, and XI), gelatin, fibronectin, laminin.
	MMP-8	*Neutrophil collagenase*	Collagens (type I, II, and III), gelatin, aggrecan.
	MMP-13	*Collagenase-3*	Collagens (type I, II, III, IV3, VI, IX, X, and XIV), gelatin, fibronectin.
Gelatinases	MMP-2	*Gelatinase-A*	Gelatin, collagens (type I, II5, III, IV, V, VII, X, and XI), elastin, fibronectin.
	MMP-9	*Gelatinases-B*	Collagens (type IV, V, XI, and XIV), gelatin, elastin, vitronectin, laminin.
Stromelysins	MMP-3	*Stromelysin-1*	Collagens (type III, IV, V, VII, IX, X, and XI), gelatin, elastin, fibronectin.
	MMP-10	*Stromelysin-2*	Collagens (type III, IV, and V), gelatin, elastin, fibronectin.
	MMP-11	*Stromelysin-3*	gelatin, fibronectin, collagen type IV, laminin.
	MMP-27	*52 % homology to stromelysin-2*	gelatin.
Matrilysins	MMP-7	*Matrilysin (PUMP)*	Collagens (type I, and IV), gelatin, elastin, fibronectin, laminin, entactin.
	MMP-26	*Matrilysin-2*	Collagen type IV, gelatin, fibronectin, vitronectin.
Membrane type	MMP-14	*MT-MMP*	Collagens (type I, II, and III), gelatin, fibronectin, laminin, entactin, aggrecan.
	MMP-15	*MT2-MMP*	fibronectin, tenascin, entactin, laminin.
	MMP-16	*MT3-MMP*	Collagen type III, gelatin, fibronectin, vitronectin, laminin.
	MMP-17	*MT4-MMP*	Gelatin.
	MMP-24	*MT5-MMP*	Fibronectin, Gelatin, chondroitin sulphate proteoglycan.
	MMP-25	*MT6-MMP*	Collagen type IV, gelatin, fibronectin.
Others	MMP-12	*Macrophage elastase*	Collagens (type I, V, and IV), gelatin, elastin, fibronectin, vitronectin, laminin.
	MMP-19	*RASI 1*	Collagen type IV, gelatin, laminin, entactin, fibronectin.
	MMP-20	*Enamelysin*	Amelogenin, aggrecan.
	MMP-28	*Epilysin*	

MMPs are multi-domain proteases but all have a signal peptide domain, pro-domain and catalytic domain (Figure 1.3). Most MMPs also have a hemopexin domain for recognition of substrates and tissue inhibitors of metalloproteinases (TIMPs) (Nagase *et al.,* 2006). Membrane bound MMPs have additional anchor domains which binds the MMP to the membrane. They generally also have a furin cleavage site in the pro-peptide for activation. MMP-2 and -9 uniquely also have a fibronectin recognition construct.

The 3D structures of some MMP catalytic domains have been resolved using X-ray crystallography and NMR techniques (Lang *et al.,* 2001; Iyer *et al.,* 2006; Rush & Powers 2004). The catalytic domains are almost superimposable within the MMP family; they consist of a 5-stranded β-pleated sheet, three α-helices and a selectivity loop. The site contains two zinc ions, one catalytic (bound by three histamines) and one which provides a structural support (Lang *et al.,* 2001). MMPs also have 3 calcium counter ions to stabilise the structure but are also suggested to play role in regulating MMP activity (Gossas & Danielson 2006).

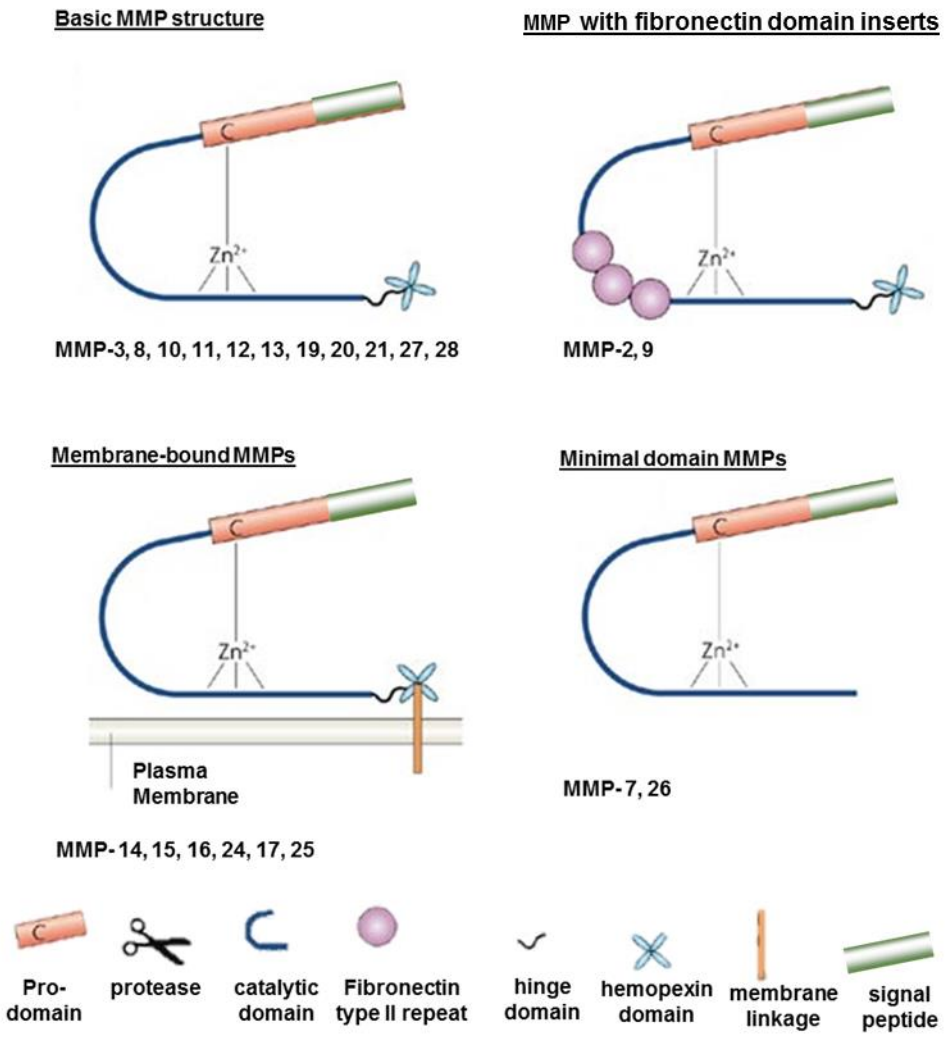

Figure 1.3 The structure of sub-groups in the MMP family. MMPs are multi-domain proteases that are initially inactive due to the pro-domain which binds to the catalytic zinc blocking its activity. Each MMP also has a signal peptide which directs it towards the secretory pathway. The hemopexin-like domain contributes to substrate and/or ligand specificity, subcellular localisation and activation/inhibition; MMP-2 and -9 also have a gelatin-binding domain (fibronectin type II repeat). MMPs located on the cell membrane normally have a transmembrane domain with a cytoplasmic tail. However, MMP-17 and -25 are glycosylphosphatidylinositol anchored. Linkers are short peptide sequences connecting the domains. Reproduced with permission from Page-McCaw and colleagues (2007) and modified.

1.2.2 Regulation of MMP activity

Generally, regulation of MMP activity can occur at several stages within the life of an MMP protein: transcription, post-translational modifications, secretion, activation of latent MMP, endogenous inhibition and, finally, degradation. MMP transcription can be promoted by transcription factors (including activator protein-1 (AP-1) and nuclear factor kappaB (NF-$_k$B)), inflammatory cytokines (such as TNFα), growth factors, hormones and by cell–cell and cell–matrix interactions (Vincenti & Brinckerhoff 2002; Yabluchanskiy *et al.,* 2013; Nagase & Woessner 1999; Sternlicht & Werb 2001).

MMPs are released as zymogens (proMMPs) and so require activation to become functional (Figure 1.4). A thiol group (cysteine) from the pro-domain inactivates the enzyme by binding to the catalytic zinc within the active site, this is known as the "cysteine switch". Membrane bound MMPs are activated in the Golgi apparatus before delivery to the cell membrane. Secreted proMMPs are generally activated by serine proteases (such as plasmin) or by other active MMPs already in the extracellular space. When the pro-domain is cleaved it breaks the interaction of cysteine–zinc, opening the active site to substrates for hydrolysis (Figure 1.5).

Active MMPs can be endogenously inhibited by α_2-macroglobulin and TIMPs (Baker *et al.,* 2002). Four TIMPs (TIMP-1, 2, 3, 4) have been described; each are 184–194 amino acids long and folded into 2 domains to form a ''wedge-like'' molecule (Gomis-Rüth *et al.,* 1997). TIMPs inhibit MMPs in a 1:1 stoichiometry; the N-terminal domain of a TIMP blocks the active site of a MMP (Murphy *et al.,* 1991). α_2-Macroglobulin, a 725 KDa plasma glycoprotein, can engulf extracellular MMPs (and other proteinases), irreversibly blocking their activity, the complex is then rapidly cleared from the circulation (Sternlicht & Werb 2001).

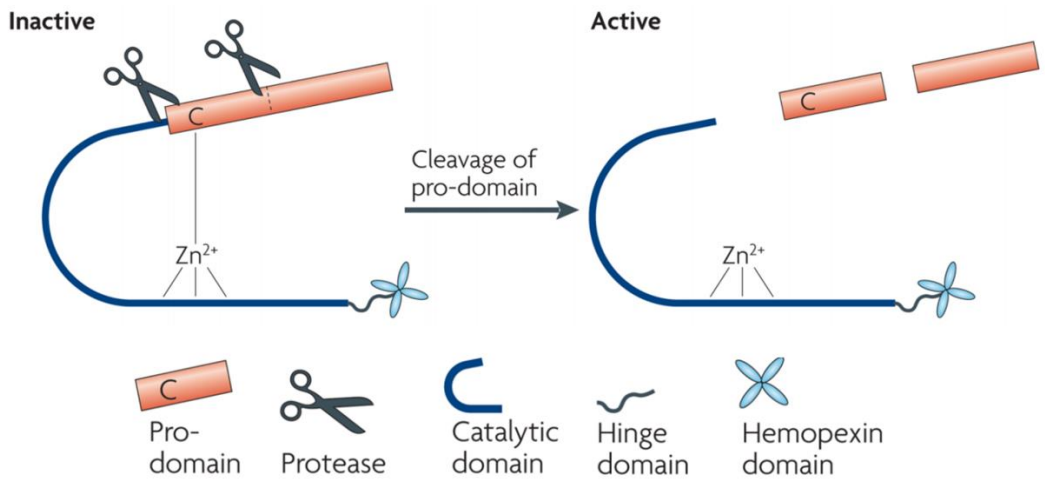

Figure 1.4 The cysteine switch activation of MMPs. MMPs are secreted in the inactive form. This is due to the integration of the catalytic zinc molecule with a thiol group from a cysteine residue in the pro-domain. Proteases can cleave the pro-domain, breaking this interaction and activating the MMP. Reproduced with permission from Page-McCaw and colleagues (2007) and modified.

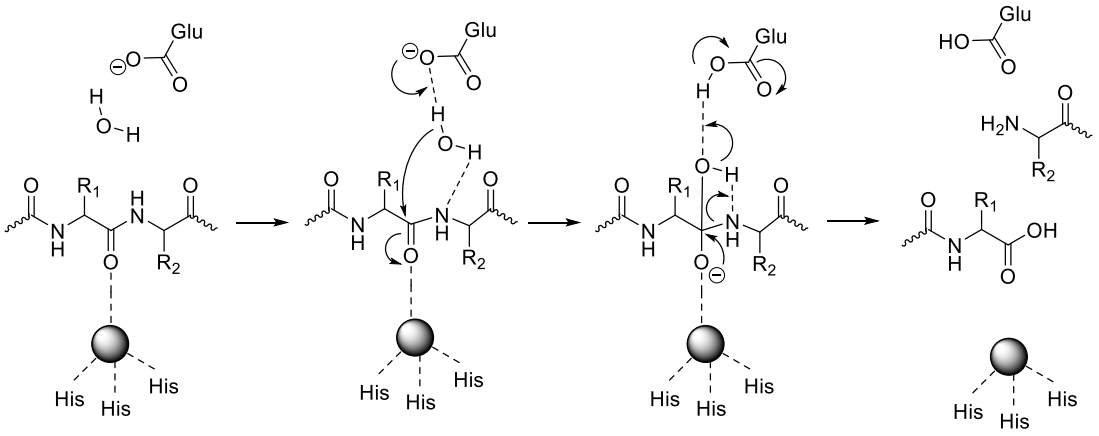

Figure 1.5 Mechanism of proteolysis of a peptide by an MMP. During proteolysis, the carbonyl of the peptide bond to be cleaved coordinates with the catalytic zinc (sphere); the peptide bond is hydrolysed by nucleophilic attack of water (polarised by the carboxylate group of the glutamate (Glu) residue in the active site) on the carbonyl carbon of the peptide bond. After rearrangement, the resulting hydrolysis products are a carboxylic acid and amine.

1.3 MMP-12

MMP-12 (macrophage elastase, MME) was first found in lung alveolae of cigarette smokers (Shapiro *et al.*, 1993). MMP-12 activity has since been recognised in other diseased tissues (Liu *et al.*, 2004; Scholtes *et al.*, 2012; Houghton *et al.*, 2006) but its expression is rarely found in normal tissue (Belaaouaj *et al.*, 1995). It is predominantly secreted by pro-inflammatory macrophages and is required for their migration across the basement membrane (Shipley *et al.*, 1996). MMP-12 can degrade ECM components (elastin, IV collagen, laminin and fibronectin, (Gronski *et al.*, 1997)) and other proteins including plasminogen (Xu *et al.*, 2008).

1.3.1 Structure

The domain structure of MMP-12 is similar to most other MMPs (Figure 1.3) and consists of a five-stranded β-sheet and three α-helices constructed into 4 domains: catalytic, propetide and a helmopexin and signal peptide (cleaved off early in the life of MMP-12) (Figure 1.6). The zymogen (54 KDa) is activated by proteinases; initially the pro-domain is lost to produce an active 45 KDa metalloproteinase, then the C-terminal hemopexin domain can also be lost to produce the 22 KDa mature MMP-12 (Nar *et al.*, 2001). The full human and mouse MMP-12 enzymes have amino acid sequences that are 64% identical (Shapiro *et al.*, 1993). Endogenously the active MMP-12 can be inhibited by TIMP-1 (Nagase *et al.*, 2006).

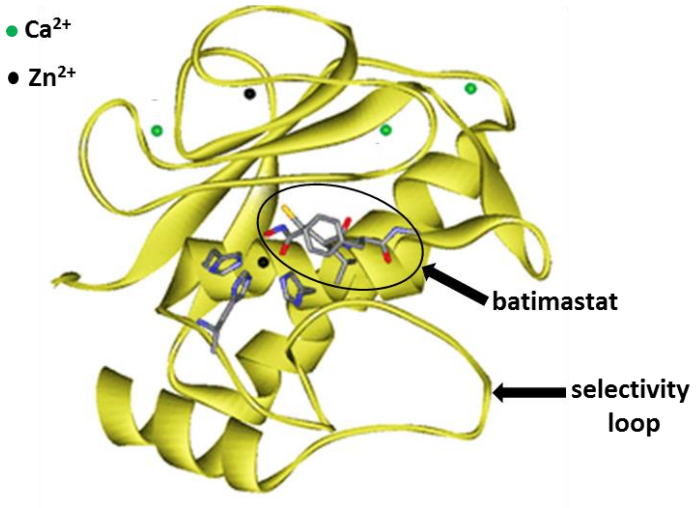

Figure 1.6 A 3D image of the active site of MMP-12 bound to a MMP inhibitor (batimastat). Here the binding sites of the 2 zinc ions (black dots) and 3 calcium ions (green dots) are shown on the tertiary structure of MMP-12 (yellow ribbon). The inhibitor batimastat (circled) is a broad spectrum MMP inhibitor; it binds to the catalytic zinc ion (which itself is coordinated to 3 histidine residues). The selectivity loop is highly influential for the selectivity of substrates and inhibitors for all MMPs. Image is modified from Gossas & Danielson (2006).

1.3.2 MMP-12 contributes to protection against infection

Interestingly, MMP-12 has antiviral and antibacterial properties, which are not necessarily a direct result of its proteinase action. MMP-12 is secreted by macrophages in response to bacterial lung infection (Houghton *et al*., 2006); however, MMP-12$^{-/-}$ mice with this infection exhibit impaired bacterial clearance and increased mortality (Houghton *et al.*, 2009). Interestingly, proteolysis is not responsible for this antimicrobial activity. Rather a unique four amino acid sequence on an exposed beta loop of the C-terminal is responsible, although the exact mechanism remains unknown. MMP-12 is also antiviral, Marchant and colleagues (2014) found that MMP-12 promotes the secretion of interferon alfa (IFN-α) from the host cell which enhances its antiviral protection. Briefly, *in vitro* studies showed that macrophage-secreted MMP-12 can be transported into the nucleus of virus-infected cells where it binds to

the promotor of the $I_KB\alpha$ gene and enhances its transcription. $I_KB\alpha$ protein then promotes the export of IFN-α from cells (extracellular IFN-α stimulates an antiviral immune response (Taniguchi & Takaoka, 2002)). In MMP-$12^{-/-}$ mice, infected cells do not express $I_KB\alpha$ and do not export INF-α. MMP-12, therefore, promotes the secretion of antiviral IFN-α which enhances the host cell protection. However, MMP-12 was also found to inactivate extracellular INF-α which prevented an unchecked immune response and contributed towards resolving inflammation. This evidence was supported by an MMP-12 inhibitor study (Marchant *et al*., 2014); selective inhibition of only extracellular MMP-12 resulted in an increase of IFN-α secretion and a reduction of viral replication. Although these properties of MMP-12 are beneficial for health, MMP-12 activity is also associated with disease.

1.3.3 MMP-12 and disease

Unregulated MMP-12 activity generally inflicts the greatest damage in tissues with a high elastin content. Elastin is a highly crosslinked hydrophobic ECM protein found in tissues which require elasticity, such as: skin, ligaments, arterial vessel walls and lungs. In inflammatory lung disease, breakdown of elastin can lead to permanently compromised lung function and ongoing degenerative disease (Shifren & Mecham 2006). Chronic obstructive pulmonary disease (COPD) is an umbrella term for a collection of inflammatory lung diseases including chronic bronchitis, emphysema and chronic obstructive airways disease. Patients with COPD often have high levels of MMP-12 and MMP-9 in their lungs (Demedts *et al.,* 2006; Molet *et al.,* 2005). In preclinical models MMP-12 activity was found to be necessary for the development of COPD (Hautamaki *et al.,* 1997; Valença *et al.,* 2004). Inhibitors targeting MMP-12 are suggested to be a good potential treatment option for COPD (Lagente *et al.,* 2009; Dahl *et al.,* 2012).

The skin has multiple layers of ectodermal tissue which are joined together with connective tissues. The disappearance of normal elastic fibres is a typical feature of skin damage; MMP-12 expression is increased in granulomatous skin diseases (Vaalamo *et al.,* 1999) and in areas of sun-damaged skin (Saarialho-Kere *et al.,* 1999). Therefore, MMP-12 activity is suggested to play a detrimental role in these conditions.

The vascularisation and subsequent dissemination of tumours are key stages in the development of cancer. MMPs generally play important roles in facilitating these processes (Kessenbrock *et al.,* 2010), but the role of MMP-12 is unclear. MMP-12 is expressed in human skin and liver cancers; indeed increased MMP-12 expression is correlated with tumour invasiveness or a negative long term prognosis (Kerkelä *et al.,* 2000; Kerkelä *et al.,* 2002; Yang *et al.,* 2007; Ng *et al.,* 2011). Conversely, other *in vivo* preclinical cancer studies have found the presence of MMP-12 to be protective. In a model of lung cancer (Lewis lung metastases) MMP-12$^{-/-}$ mice had increased tumour growth and metastasis (Houghton *et al.,* 2006). In models of breast cancer and colon cancer MMP-12 reduced tumour growth (Margheri *et al.,* 2009; Shi *et al.,* 2006; Xu *et al.,* 2008; Gorrin-Rivas *et al.,* 2001). This discrepancy between the roles of MMP-12 in cancer pathology and prognosis in pre-clinical models may be due to the cancer type and/or the cellular source of MMP-12. Kerkelä and colleagues (2002) found that MMP-12 expression in human squamous cell carcinoma promoted tumour invasiveness whereas expression of MMP-12 in macrophages was protective against cancer.

In the clinic, MMP-12 activity is protective against gastric cancer; patients with increased MMP-12 expression within their tumours, had reduced metastasis size and had a higher "two-year survival rate" (Zhang *et al.,* 2007). Furthermore in human samples of colorectal cancer, increased mRNA expression of MMP-1, -2, -3, -7, -9, -13 correlated negatively with disease stage and prognosis; whereas over expression of MMP-12 was associated with an increased

patient survival (Zucker & Vacirca 2004; Yang *et al.,* 2001). Interestingly, most studies which report a protective effect of increased MMP-12 expression in cancer, also tended to report reduced vascular growth within the tumours (Margheri *et al.*, 2009; Yang *et al.,* 2001; Gorrin-Rivas *et al.,* 2001; Shi *et al.,* 2006).

MMPs, including MMP-12, are required for remodelling of the cardiovascular system. MMP-12 has been suggested to be antiangiogenic (Li *et al.*, 2012), it has also been identified as playing an active role in the progression of vascular disease involving remodelling, such as atherosclerosis (Johnson *et al.,* 2011; Yamada *et al.,* 2008) and aortic aneurysms (Curci *et al.*,1998).

1.4 MMP activity during vascular remodelling and disease.

1.4.1 The cardiovascular system and disease

The cardiovascular (CV) system consists of the heart, blood vessels and blood, and is the first operational organ system in vertebrate embryos. Blood is pumped through vessels by the heart, from large arteries down to the fine capillary beds where chemical exchange takes place before blood is returned to the heart by the veins. The primary role of the CV system is to meet the metabolic demands of tissues by transporting nutrients, gases and waste products; it also transports immune cells, endocrines and some cytokines around the body.

Cardiovascular disease (CVD) includes coronary artery disease (angina and myocardial infarction), stroke, cardiomyopathy, aortic aneurysms, peripheral artery disease, hypertensive heart disease and venous thrombosis. CVD is the primary cause of death globally. Approximately 17.5 million people died from CVDs in 2012 accounting for 31% of all global deaths (World Health Organisation, cardiovascular disease fact sheet N°317). The underlying biological mechanisms of disease development vary depending on the disease in question.

1.4.2 Atherosclerosis

Atherosclerosis is a chronic inflammatory disease; it can remain asymptomatic for decades but can also quickly deteriorate with deadly consequences. Atherosclerotic plaques are a build-up of fatty material and inflammatory cells within the walls of arteries. These cause the affected vessel to become narrowed which can result in ischemia of downstream tissues (Figure 1.7). Most plaques are generally considered stable but those with a thin fibrous cap, high macrophage content and increased vascularity are vulnerable to rupture (Ross, 1999). Plaque erosion and rupture can lead to thrombus formation and often occlusion of the vessel. Tissue ischemia follows and, if left untreated, can have catastrophic consequences. Depending on

location, this can induce a myocardial infarction (heart attack) or stroke (in the brain); both can cause sudden death. Highly aerobic tissues (such as the heart) can suffer irreversible damage in just a few minutes post occlusion. If the patient survives such an event, there is gradual scarring of the damaged tissue post injury which normally leaves it unable to perform its function efficiently. Therapies to regenerate damaged tissue would be highly beneficial; this process may be aided by promoting healthy angiogenesis into the scared tissue.

MMP activity worsens atherosclerosis pathology

The degradation of extracellular matrix (ECM) proteins in the vessel walls is critical for the development, increased vulnerability and eventual rupture of atherosclerotic plaques (Newby 2005). MMPs can facilitate macrophage invasion (Shipley *et al*., 1996) and promote angiogenesis (Pepper 2001; Li *et al.,* 2012) in plaques; both of which contribute towards increased plaque vulnerability. In preclinical models, MMP-9 activity increased lesion size (Johnson *et al.,* 2005). Furthermore, MMPs can weaken the fibrous cap: MMP-1, -3, -9, -13, -12 and -14 have all been found in plaque regions with a thinning fibrous cap (Galis *et al*., 1994; Formato *et al*., 2004; Deguchi *et al*., 2005; Newby, 2006). Generally, MMP activity, especially MMP-12, is considered to promote atherosclerotic plaque development.

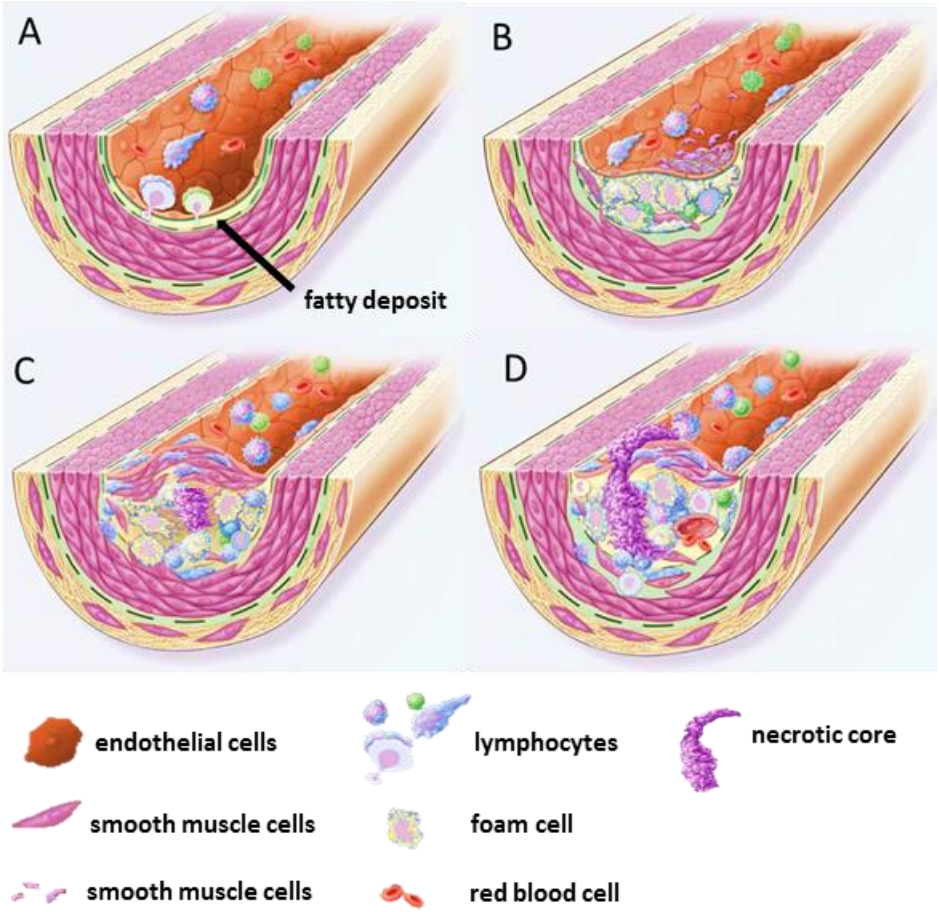

Figure 1.7 Mechanism of atherosclerosis. a) Atherosclerosis is initiated by endothelial cell dysfunction, characterised by increased permeability to lipoproteins (yellow) and increased adhesion and migration of inflammatory cells (lymphocytes) into the arterial wall. b) A fatty steak forms: inflammatory cells phagocytose the free lipids, forming foam cells. Smooth muscle cells migrate from the vessel wall into the plaque which begins to stabilise the lesion. c) An advanced lesion: a necrotic core forms as a result of lipid accumulation and cell apoptosis/ necrosis; a fibrous cap made of smooth muscle cells (SMC) and connective tissue stabilises it. d) Plaques are generally stable in this state; however, those with thin caps and/or under high shear stress and/or highly vascularised are prone to rupture. A ruptured plaque results in the necrotic core contents entering the lumen and thrombosis formation which often results in occlusion of the artery. Figure reproduced with permission from Ross (1999) and modified, copyright Massachusetts Medical Society.

MMP-12 activity accelerates atherosclerosis

MMP-12 has been shown to be pro-atherosclerotic in two murine models. Mice do not naturally develop extensive lesions on a high fat diet so genetically modified animals are used. Murine models of atherosclerosis are based on deletion of either the low density lipoprotein (LDL) receptor ($LDLr^{-/-}$) or apolipoprotein E ($ApoE^{-/-}$). ApoE is a circulatory fat transporter protein whereas the LDLr recognises the ApoE protein and removes it and free LDL from the circulation. Mice lacking either of these proteins develop hyperlipidaemia and spontaneously develop atherosclerotic plaques throughout the arterial tree when fed a high fat diet (Ishibashi *et al.*, 1993; Nakashima *et al.*, 1994).

$LDLr^{-/-}$ mice fed a high fat diet for 16 weeks have a 22 fold higher expression of MMP-12 mRNA in their aortic lesions (compared to aorta from $LDLr^{-/-}$ mice on a normal diet which did not develop lesions), double that of other MMPs investigated (Prescott *et al.*, 1999). The administration of a broad spectrum MMP inhibitor did not inhibit lesion development in this model but did decrease elastin destruction in the vessel wall. Double knockout $ApoE^{-/-}$: $MMP\text{-}12^{-/-}$ mice have smaller brachiocephalic artery lesions (with increased smooth muscle cell content and reduced macrophage content) compared to single $ApoE^{-/-}$ knockouts (Johnson *et al.*, 2005). In a subsequent study, $ApoE^{-/-}$ mice treated with a selective MMP-12 inhibitor had lesions with a significantly reduced (50 %) cross sectional area (Johnson *et al.*, 2011). Both murine models support the hypothesis that MMP-12 promotes atherosclerosis.

Non-genetically altered rabbits fed a high cholesterol diet (1%, 16 weeks) developed aortic plaques which contained foam cells and MMP-12 (mRNA and protein); this was compared to aortae from rabbits on normal chow which have no MMP-12 expression and do not develop lesions (Matsumoto *et al.*, 1998). Another study utilised transgenic (Tg) rabbits modified to overexpress human (h) MMP-12 in the macrophages (hMMP-12 Tg). These hMMP-12 Tg rabbits were fed a cholesterol rich diet (1%) for 6 −9 weeks; they exhibited lesions 3 times (6

weeks) to 2.3 times (9 weeks) larger than those in their WT counterparts (Yamada *et al.,* 2008). The lesions from the hMMP-12 Tg rabbits exhibited increased elastolysis and macrophage content (which had a negative impact on the appearance of plaque stability) and a small increase in smooth muscle cell content (which is considered to improve plaque stability). In a longer study, rabbits were fed a high cholesterol diet (0.8%) for 28 weeks; hMMP-12 Tg rabbits had a greater total number of lesions (up to 50% more) and twice as many advanced lesions compared with their non-transgenic counterparts (Liang *et al.,* 2006). The lesions also contained an increased number of macrophages and more disruption of the elastic lamina. This data further supports the role of MMP-12 in the progression of atherosclerosis in animal models.

The pro-atherosclerotic role of MMP-12 has also been indicated in human disease. Unstable human carotid plaques (obtained from endarterectomy) have higher levels of MMP-12 expression compared to stable plaques and healthy vessel controls (Müller *et al.,* 2014). Moreover, MMP-12 mRNA expression is higher in ruptured plaques than in those without cap disruption; again highlighting the role of MMP-12 in elastin degradation and disease pathogenesis (Morgan *et al.,* 2004). Studies on human carotid endarterectomy samples found that those with a high ratio of MMP-12/CD68 (a marker for monocytes/macrophages, both detected by immunohistochemistry) had a high lipid and macrophage content and a reduced number of vascular smooth muscle cells, all characteristics of vulnerable plaques (Scholtes *et al.,* 2012). Furthermore, those patient samples possessing the highest MMP-12/ CD68 ratio (highest quartile) had a $3-4$ fold higher risk of subsequent stroke compared to the lowest quartile. However, endarterectomies are an invasive surgical procedure and are of little use for diagnosis and prognosis. Jguirim-Souissi and colleagues (2007) found that the circulating level of MMP-12 in the patients plasma could predict the presence of a carotid stenosis but not the severity. Interestingly, those patients on statin therapy had a marked reduction of MMP-12

protein concentrations compared to those without treatment, suggesting that statin therapy, as well as reducing CVD risk, also reduces MMP-12 protein expression in carotid stenosis.

The evidence presented here supports that MMP-12 has an important role in the initiation, progression and prognosis of atherosclerosis in preclinical and clinical studies. Lesions with MMP-12 expression have high inflammatory cell infiltration and thinner caps, while advanced lesions exhibit accelerated ECM breakdown in the protective cap, leading to increased vulnerability to rupture. This supports the need for a simple way to measure MMP-12 in plaques as a marker of plaque vulnerability.

1.4.3 Neointimal hyperplasia

Neointimal hyperplasia refers to proliferation and migration of vascular SMC, primarily in the tunica intima, resulting in the thickening of arterial walls, a decrease in the luminal diameter and arterial stiffening. Restenosis after angioplasty can occur as a result of neointimal hyperplasia (Johnson *et al.*, 1990). Mice subject to the fine-wire femoral artery injury model (FAI; in which a wire is briefly inserted into the femoral artery which denudes and stretches the arterial wall, and is followed by neointimal hyperplasia) have increased vessel permeability, leukocyte adhesion, and smooth muscle proliferation, all contributing towards neointimal hyperplasia (Sata *et al.*, 2000; Roque *et al.*, 2000). MMP-2 and -9 are expressed in the artery after FAI and contribute towards remodelling (Zou *et al*. 2009). MMP-12 mRNA expression and activity were increased in vessels post FAI which contributed towards an observed elastin breakdown; mice with a selective deletion of MMP-12$^{-/-}$ only in the SMC had a reduced proliferative response to FAI with reduced neointimal thickening (Liu *et al.*, 2015). This evidence supports the role of MMP-12 in neointimal hyperplasia in murine models.

1.4.4 Aneurysms

Aneurysms are a life-threatening condition and are associated with aging, atherosclerosis and family history (Kent *et al.*, 2010). An aneurysm is an abnormal bulge in an artery formed when the vessel wall is weakened by progressive connective tissue destruction and distorted by blood pressure (Figure 1.8). True aneurysms may be classified by morphology and location; they can be saccular or fusiform (Figure 1.8). Saccular aneurysms are spherical shaped and tend to only affect one side of the vessel wall, while fusiform are "spindle shaped" and often involve a large portion of the aorta. Aneurysms can occur throughout the arterial vascular system and cause abnormal blood flow within the artery. Abdominal aortic aneurysm (AAA) generally remain clinically silent until rupture; the risk of rupture increases with increased expansion rate (diameter dilates > 0.5 cm in 6 months is at high risk of rupture) and size (an aneurysm with a diameter of 8 cm has a 30 to 50% risk of rupture) (Aggarwal *et al*., 2011). A ruptured AAA can result in sudden internal bleeding, hypovolemic shock, leading to death in > 55% of cases (Harris *et al*., 1991). Asymptomatic aneurysms are normally detected during screening or a routine physical examination or incidentally during imaging for other purposes. Patients with AAA are regularly monitored and those with an aneurysm greater than 5.5 cm are recommended to undergo surgery to stabilise the vessel. MMPs play a destructive role weakening the vessel wall which promotes aneurysm formation and later rupture (Keeling *et al.*, 2005).

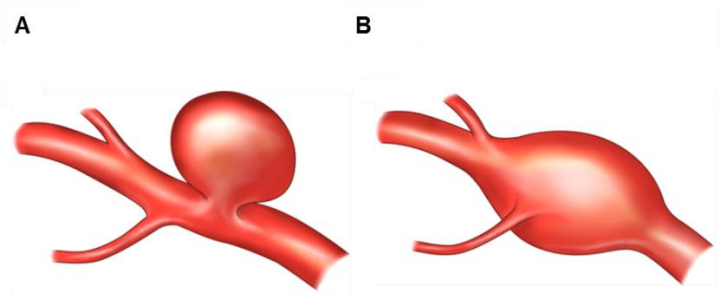

Figure 1.8 Example structures of aneurysms. a) Saccular aneurysm; these are typically found in smaller vessels and are more common in the brain (cerebral aneurysm). b) fusiform aneurysm; these are typically found in larger vessels, such as the aorta. They are at higher risk of rupture which can lead to hypovolemic shock and sudden death. Aneurysms rupture as a result of structural weakening and can cause massive internal bleeding and death. Figure reproduced with permission from (Withers *et al.*, 2013) and modified.

MMP activity increases the size of aortic aneurysms

MMP-9 levels in patient plasma can be used as a marker of AAA size (Lindholt *et al.*, 2000). Pre-clinical models are needed to explore the mechanisms contributing towards AAA formation and the development of treatment. AAA can be induced by the application of a calcium chloride solution to the abdominal aorta; this disrupts the elastic network within the media and induces an inflammatory response (Chiou *et al.*, 2001). Application of calcium chloride solution to the aorta of MMP-$2^{-/-}$ mice results in a 52% increase in aortic diameter compared with controls, whereas MMP-$9^{-/-}$ mice show a 75% increase (Longo *et al.*, 2002).

Elastin is a major component of the aorta and is a principal substrate for MMP-12. MMP-$12^{-/-}$ mice treated with an aortic application of calcium chloride solution exhibited a reduced size of AAA, combined with lower macrophage cell numbers within the aortic wall compared to their WT counterparts (Longo *et al.*, 2005). Studies on donated human AAA samples found that diseased tissues contained more macrophages and showed higher MMP-12 activity compared with normal aorta (Curci *et al.*, 1998; Annabi *et al.*, 2002). Curci and colleagues

(1998) also found that the expression of MMP-12 was uniquely co-localised to residual elastin fibre fragments within the aneurysm tissue in a distinct pattern, unlike MMP- 2, -7 and -9 which did not co-localise. Therefore, MMP-12 likely plays an important role in the pathogenesis of AAA.

1.4.5 Angiogenesis

Mechanisms of vascular growth

New vessels grow as a result of either angiogenesis or vasculogenesis which are both multi-step processes. Vasculogenesis requires *de novo* production of endothelial cells (EC) from angioblasts which assemble to form primitive vessels. Vasculogenesis has been observed in adults during tumour vascularisation and endometriosis but is primarily observed during embryonic development (Ribatti *et al.*, 2001; Laschke *et al.*, 2011). The cardiovascular system is the first functioning organ system in the developing embryo (Chung *et al.*, 2010). In embryos, an organised network of vessels grows as a result of vasculogenesis. These eventually develop into arteries, capillaries and veins. Vessels mature and expand by the recruitment of vascular smooth muscle cells and pericytes which encompass the EC tubes to provide support and control perfusion (arteriogenesis) (Jain, 2003).

In contrast, angiogenesis is the formation of new vessels from existing blood vessels (Figure1.9). Stimulation of angiogenesis can be by mechanical (activity induced) or chemical signals, with the former being poorly characterised and somewhat controversial (reviewed in depth by Egginton (2009)). Angiogenesis is controlled by a balance between a host's pro- and anti-angiogenic factors. Angiogenesis most commonly occurs in response to the oxygen demands of the tissue and is triggered by the release of potent pro-angiogenic stimuli. Hypoxic cells release hypoxia-inducible factors (HIF) to stimulate angiogenesis (Krock *et al*., 2011).

HIF-1α is an important transcriptional regulator of a broad array of genes including the potent angiogenic stimulator vascular endothelial growth factor (VEGF) (Forsythe *et al*., 1996). VEGFs play a key role in activating EC (Ferrara *et al.*, 2003); VEGF-A regulates EC chemotaxis and proliferation during angiogenesis. Sprouting angiogenesis is characterised by sprouts composed of ECs, which usually grow towards an angiogenic stimulus such as VEGF-A. Briefly, sprouting angiogenesis can be divided into 4 key stages (Figure 1.9) which are well reviewed in the literature (Adams & Alitalo, 2007).

Firstly, proangiogenic signals and growth factors (GFs) stimulate pericytes and SMC to detach from the vessel wall and proteases (including MMPs) break down the basement membrane and surrounding ECM. In the absence of potent endogenous inhibitors, such as angiostatin and endostatin (which inhibit EC migration and proliferation (Moser *et al.*, 1999; Ferreras *et al.*, 2000)), ECs (tip cells) protrude filopodia, become motile and begin to move into the surrounding tissue. Next, the endothelial cell-cell adherins of the surrounding ECs break down; these ECs (stalk cells) then detach from the ECM and follow the tip cell. The stalk cells proliferate and migrate from the mother vessel, elongating the sprout along a chemotactic gradient. ECs form stable cell-cell connections and generate a lumen. Blood flow is established when neighbouring sprouts fuse to form a vascular loop. The third stage of angiogenesis is the maturation of the new vessels. This is stimulated by GFs such as platelet-derived growth factor (PDGF) which promotes the proliferation, migration and adhesion of smooth muscle cells (Hellström *et al.*, 1999). The adhesion of pericytes and the deposition of a basement membrane is also key for the stability of the new vessel. The final stage is the pruning and remodelling of the new network to best fit the needs of the surrounding environment. Once the pro-angiogenic signals and the remodelling cease, the vascular cells return to their quiescent state.

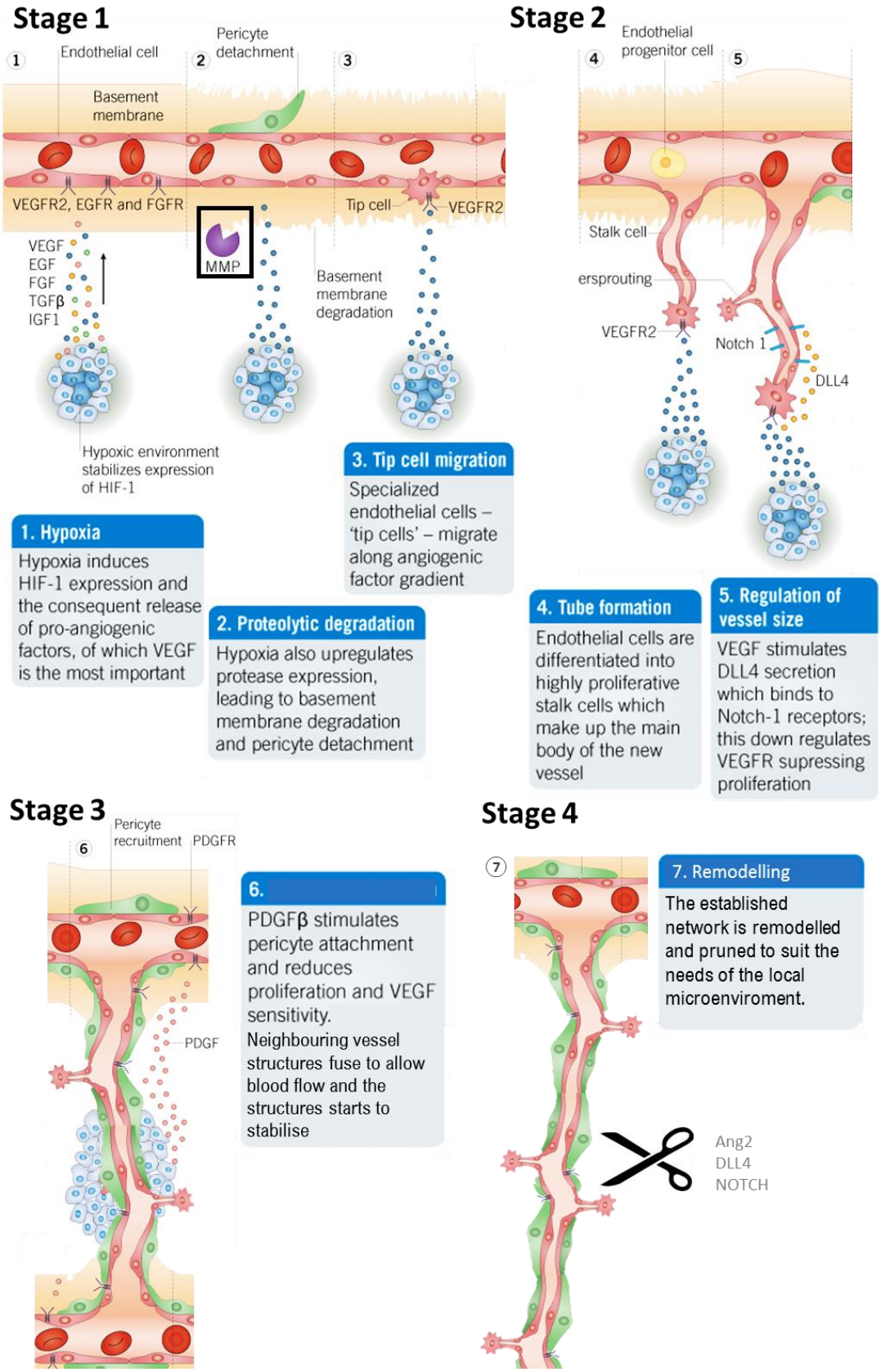
Stage 1
Endothelial cell
Pericyte detachment
Basement membrane
VEGFR2, EGFR and FGFR
Tip cell
VEGFR2
VEGF
EGF
FGF
TGFβ
IGF1
MMP
Basement membrane degradation
Hypoxic environment stabilizes expression of HIF-1
1. Hypoxia
Hypoxia induces HIF-1 expression and the consequent release of pro-angiogenic factors, of which VEGF is the most important
2. Proteolytic degradation
Hypoxia also upregulates protease expression, leading to basement membrane degradation and pericyte detachment
3. Tip cell migration
Specialized endothelial cells – 'tip cells' – migrate along angiogenic factor gradient
Stage 2
Endothelial progenitor cell
Stalk cell
ersprouting
VEGFR2
Notch 1
DLL4
4. Tube formation
Endothelial cells are differentiated into highly proliferative stalk cells which make up the main body of the new vessel
5. Regulation of vessel size
VEGF stimulates DLL4 secretion which binds to Notch-1 receptors; this down regulates VEGFR supressing proliferation
Stage 3
Pericyte recruitment
PDGFR
PDGF
6.
PDGFβ stimulates pericyte attachment and reduces proliferation and VEGF sensitivity.
Neighbouring vessel structures fuse to allow blood flow and the structures starts to stabilise
Stage 4
7. Remodelling
The established network is remodelled and pruned to suit the needs of the local microenviroment.
Ang2
DLL4
NOTCH

Figure 1.9

Figure 1.9 The four stages of sprouting angiogenesis. Stage 1) Hypoxic tissues release vascular growth factors (GF, such as vascular endothelial growth factor (VEGF)) and fibroblast growth factor (FGF)) which simulate vascular remodelling. Stage 2) Matrix metalloproteinases (MMPs) break down the basement membrane and weaken inter-endothelial contacts to facilitate their migration. Some endothelial cells (ECs) are polarised (tip cells) and migrate in the direction of the GF to form the body of a new vessel. The trailing EC (stalk cells) divide to form a solid core around which there is deposition of new matrix. EC in the core of the stalk form vacuoles which fuse to form the eventual lumen. This process continues until it is stopped by angiogenesis inhibitors (e.g. Notch-1). Stage 3) New vessels can fuse with neighbouring vessels and mature through the attachment of pericytes and smooth muscle cells, leading to vessel maturation. Stage 4) The new vascular network is remodelled to best suit the needs of the microenvironment. Figure taken from TOCRIS, 2015 and modified.

MMPs, other than MMP-12, promote angiogenesis

MMP activity generally promotes angiogenesis by degrading basement membrane and other ECM components, allowing vascular cells to detach and migrate, and also by releasing ECM-bound pro-angiogenic factors (reviewed by Rundhaug *et al*., 2005*)*. Interestingly, various cancer studies have shown that tumour samples with increased MMP-12 expression also had reduced vascular content (Margheri *et al.,* 2009; Yang *et al.,* 2001; Gorrin-Rivas *et al.,* 2001; Shi *et al.,* 2006). MMP-12 activity is not only suggested to be anti-angiogenic in cancer but also in a murine model of (hypoxia-induced) retinal damage. MMP-12$^{-/-}$ mice had a reduced inflammatory response and increased revascularisation 5 days post injury (Figure 1.10; Li *et al.,* 2012). Subsequent studies treated WT mice with a selective MMP-12 inhibitor: these mice also exhibited increased angiogenesis in response to hypoxia-induced retinal damage (Li *et al.,* 2012).

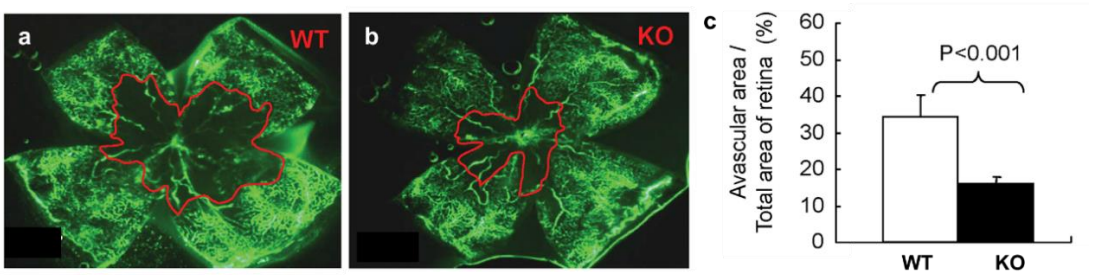

Figure 1.10 MMP-12 deficiency increases angiogenesis *in vivo* during oxygen-induced retinopathy. New born post-natal mice were kept in a hyper-oxygen environment (75%) for 5 days (postnatal day (P) 7 to P 12), then returned to a normoxic environment for a further 5 days (P 17 to P 21). The mice were then culled, retinas dissected and their vessels imaged by retinal fluorescein angiography (green). Images show retinas from (a) MMP-$12^{+/+}$ (wild type, WT) and (b) MMP-$12^{-/-}$ (knockout, KO) mice. The red line indicates the area considered to be avascular. (c) Quantification of the avascular area showed that MMP-12 KO mice exhibit faster revascularisation post ischeamia, resulting in a reduced avascular area. Figure reproduced with permission from Li *et al.,* (2012) and modified.

MMP-12 has also been identified as an inhibitor of angiogenesis in peripheral vascular disease. Systemic sclerosis (SSc) is a disease of defective angiogenesis (mostly of small vessels) which can result in significant damage to the peripheral vasculature, tissue ischemia and damage to vital organs. D'Alesso and colleagues (2004) isolated microvascular EC (MVECS) from the skin from SSc patients. When cultured, these expressed more MMP-12 than MVECs from unaffected controls. Matrigel assays are used to assess EC behaviour and growth in vitro; on Matrigel covered surfaces, EC form a network (suggestive of the microvascular capillary systems) that is otherwise difficult to observe under normal EC culture conditions (Arnaoutova *et al*., 2009). Cultured, human MVECs, when treated with conditioned medium from patient-derived cultured SSc-fibroblasts, developed impaired proliferation, invasion and capillary morphogenesis in Matrigel assays (Serrati *et al*., 2006). However, if conditioned medium from SSc-fibroblasts was pre-treated with MMP-12 antibodies, it restored normal MVEC behaviour

in the Matrigel assay (Serrati *et al.,* 2006). These observations suggest that MMP-12 activity disrupts EC network formation. MMP-12 is suggested to be antiangiogenic; two potential mechanisms underlying this action have been proposed but their relative importance has not been established.

Mechanisms of MMP-12-mediated inhibition of angiogenesis

It has been suggested that MMP-12 inhibits angiogenesis in two ways: firstly, by the inhibition of pro-angiogenic protease activation and, secondly, by the production of inhibitors of angiogenesis.

The pro-Urokinase plasminogen activator (uPA) and urokinase plasminogen activator receptor (uPAR) system has a complex role in regulating cell function, inflammation, cancer and cell signalling processes (Crippa 2007; Blasi & Carmeliet 2002; Smith & Marshall 2010). The EC uPAR is bound to the cell surface (Figure 1.11) and binds to extracellular pro-uPA, converting it to active uPA. The uPA can then catalyse the production of plasmin from plasminogen in the extracellular space. Plasmin is a broad-spectrum protease which can activate proteases, including pro-MMPs, and hydrolyse ECM proteins, notably fibrin (Pepper 2001). This generates a "leaky" matrix and, combined with the presence of angiogenic stimulants, this stimulates the migration of ECs required for angiogenesis (Blasi & Carmeliet, 2002). Mice lacking uPA have impaired revascularisation in infarcted murine hearts, this was suggested to be as a result of impaired EC migration (Heymans *et al.,* 1999).

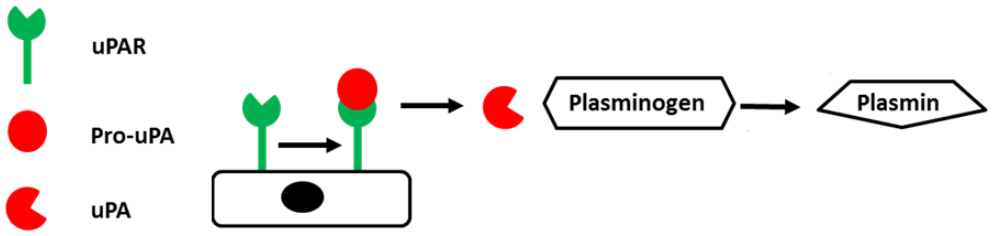

Figure 1.11 The activation of plasmin by pro-Urokinase plasminogen activator (uPA) and urokinase plasminogen activator receptor (uPAR) on the surface of endothelial cells (ECs). The uPAR is present on the EC surface where it is able to bind extracellular pro-uPA, activating it to uPA. Active uPA can convert the zymogen plasminogen into active plasmin. Plasmin is a broad spectrum protease which can activate MMPs and hydrolyse many extracellular proteins. Its activity is considered proangiogenic.

MMP-12 can cleave endothelial uPAR *in vitro*, generating a truncated form; this may render it unable to sustain its role in promoting angiogenesis via the activation of plasmin *in vivo* (Serrati *et al.*, 2006; D'Alessio *et al.*, 2004; Koolwijk *et al.*, 2001). In this way MMP-12 is suggested to indirectly inhibit the activation of plasmin and, therefore, inhibit plasmin-dependent angiogenesis.

An alternative mechanism by which MMP-12 may inhibit angiogenesis is by the production of the anti-angiogenic substrate cleavage products angiostatin and endostatin. Angiostatin is an inhibitor of angiogenesis. The mechanism involved remains unclear but it can bind to many proteins, including angiomotin and EC surface adenosine triphosphate (ATP) synthase (Troyanovsky *et al.*, 2001; Moser *et al.*, 1999). This can inhibit EC migration and proliferation, and can induce EC apoptosis (O'Reilly *et al.*, 1994; Moser *et al.*, 1999). Preclinical *in vivo* studies of Lewis lung carcinoma found that both active MMP-12 (suggested to be from infiltrating macrophages) and angiostatin protein were present within the tumours (Dong *et*

al., 1997). MMP-12 is the most efficient member of the MMP family at cleaving plasminogen to form angiostatin, which inhibits EC proliferation *in vitro* and *in vivo* (Cornelius *et al.,* 1998; Serrati *et al.,* 2006). Additionally, macrophages from MMP-12$^{-/-}$ mice cannot produce angiostatin from plasminogen (Cornelius *et al.,* 1998).

MMP -9, -3, -12 and -13 can also produce endostatin, a 20 kDa C-terminal fragment of collagen XVIII (found in the vascular basement membrane) which also acts as a potent inhibitor of angiogensis (Ferreras *et al*., 2000; Halfter *et al.,* 1998). As with angiostatin, its mechanism of action is not clear but it can bind to pro-angiogenic growth factors, such as VEGF (Kim *et al.,* 2002), or induce EC apoptosis (Dhanabal *et al.,* 1999). Endostatin significantly inhibits microvessel formation in the *ex vivo* aortic ring assay (Kruger *et al.,* 2000; Li & Olsen 2004) and in tumours *in vivo* (O'Reilly *et al.,* 1997).

To summarise, MMP-12 is suggested to inhibit angiogenesis in two ways (Figure 1.12): firstly by the production of pro-angiogenic plasmin by inhibiting the uPA/ uPAR system. Secondly by the production of the angiogenic inhibitors endostatin (from collagen) and angiostatin (from plasminogen).

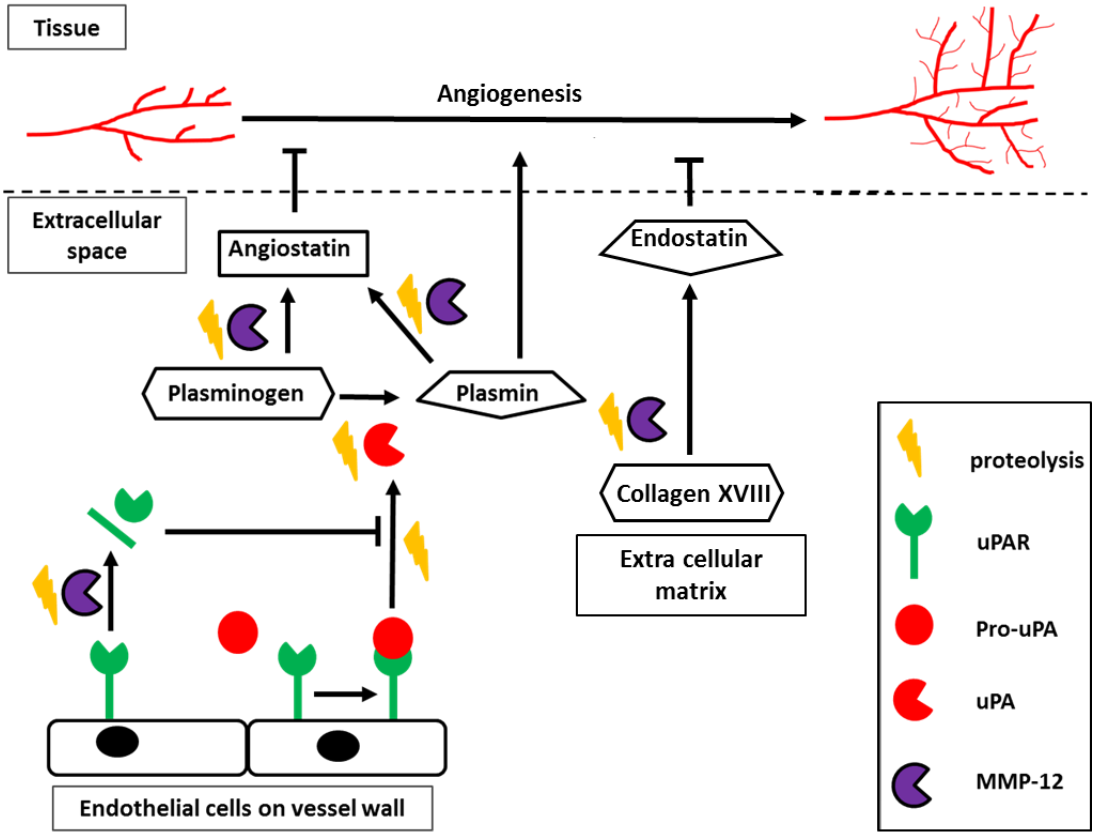

Figure 1.12. Suggested mechanisms for MMP-12-induced inhibition of angiogenesis. Two suggested mechanisms for the inhibition of MMP-12. Firstly, by the production of angiogenic inhibitors: direct cleavage of plasminogen/ plasmin by MMP-12 creates angiostatin fragments (potent inhibitors of angiogenesis) or MMP-12 can generate endostatin, a 20 kDa C-terminal fragment of collagen XVIII (also a potent inhibitor of angiogenesis). Secondly, by cleaving uPAR from the ECs, which subsequently inhibits the activation of pro-uPA to uPA. This limits the production of plasmin; plasmin is considered to be pro-angiogenic as it activates proMMPs and promotes the breakdown of the ECM and angiogenesis.

1.4.6 Summary: MMP-12 and tissue remodelling

CVD is the primary killer in the developed world and MMP-12 is implicated in the progressive pathogenesis of atherosclerosis, aneurysms, restenosis and arterial stiffening. MMP-12 is also suggested to be anti-angiogenic but its precise role is still unclear. Drugs to manipulate vessel

growth or regression are highly sought after by the pharmaceutical industry. For example, angiogenesis is undesirable in advanced atherosclerotic plaques (as it is a risk factor for rupture) or in cancerous tissue (as it promotes growth and metastasis). The promotion of angiogenesis is, however, desirable in ischemic tissue and in biomedical implants which require tissue adhesion and integration. Therefore, there are continuing efforts to develop biomedical strategies to manipulate the process. The ability to image and inhibit MMP-12 activity *in vivo* could allow for the development of new drugs and better understanding of the role of MMP-12 in tissue remodelling and disease.

1.5 Molecular imaging

Traditional clinical imaging modalities generally provide structural information of the scanned tissues, but there is increasing excitement and movement into the field of molecular imaging. Molecular imaging often utilises a labelled functional group to target a disease biomarker or pathway. Labels could be contrast agents such as gadolinium (magnetic resonance imaging (MRI)), radionuclides (positron emission tomography (PET)), single photon emission computed tomography (SPECT)), or microbubbles (ultrasound) (Figure 1.13) (Molecular imaging has been reviewed by James & Gambhir, 2012). Alternatively, selective fluorophores can be made optically "silent" until presented with certain environmental conditions (e.g. low pH or hypoxia). Preclinical tracers have already been designed to image enzyme activity (Lim *et al.,* 2014), low pH in tissues (Urano *et al.,* 2009) and bacterial infections (Akram *et al.,* 2015). In doing so, these probes can provide a real-time dynamic assessment of the molecular processes and micro-environment of diseased or infected tissues. This technology has the potential to provide vital lifesaving information to doctors who are currently unable to quickly assess these attributes. In the clinic, molecular imaging could also provide, in real-time, information about the effectiveness of treatments and, thus, contribute to the development and use of personalised medicine for patients (Garland *et al*., 2016; Willmann *et al*., 2008).

Clinical molecular imaging has mainly focused on the use of radionuclides such as ^{18}F (PET) or ^{111}In and ^{99m}Tc (both SPECT) (reviewed by James & Gambhir, 2012). However, these species are short lived, expensive, time intensive to prepare and expose patients to radiation. Optical molecular imaging, however, has the potential to be a safer and simpler method for molecular imaging.

1.5.1 Optical molecular imaging

Optical detection methods are commonly used in *in vitro* assays (such as enzyme-linked immunosorbent assays (ELISA), reverse transcription polymerase chain reaction (RT-qPCR) or fluorescent immunohistochemistry). Until recently use of optical detection methods *in vivo* has been limited due to lack of user-friendly tools and equipment. Now, commercial optical molecular imaging probes and benchtop *in vivo* detection equipment (which is less bulky than MRI or PET) have become available for preclinical studies (Groves *et al*., 2010). Commercial optical probes have been designed to target a selection of molecular processes. New probes are also being synthesised and tested by small companies and research groups, which has led to an increase *in vivo* optical molecular imaging publications (Aslam *et al*., 2015; Akram *et al.*, 2015; Groves *et al*., 2010; Lim *et al*., 2014; Waschkau *et al*., 2013).

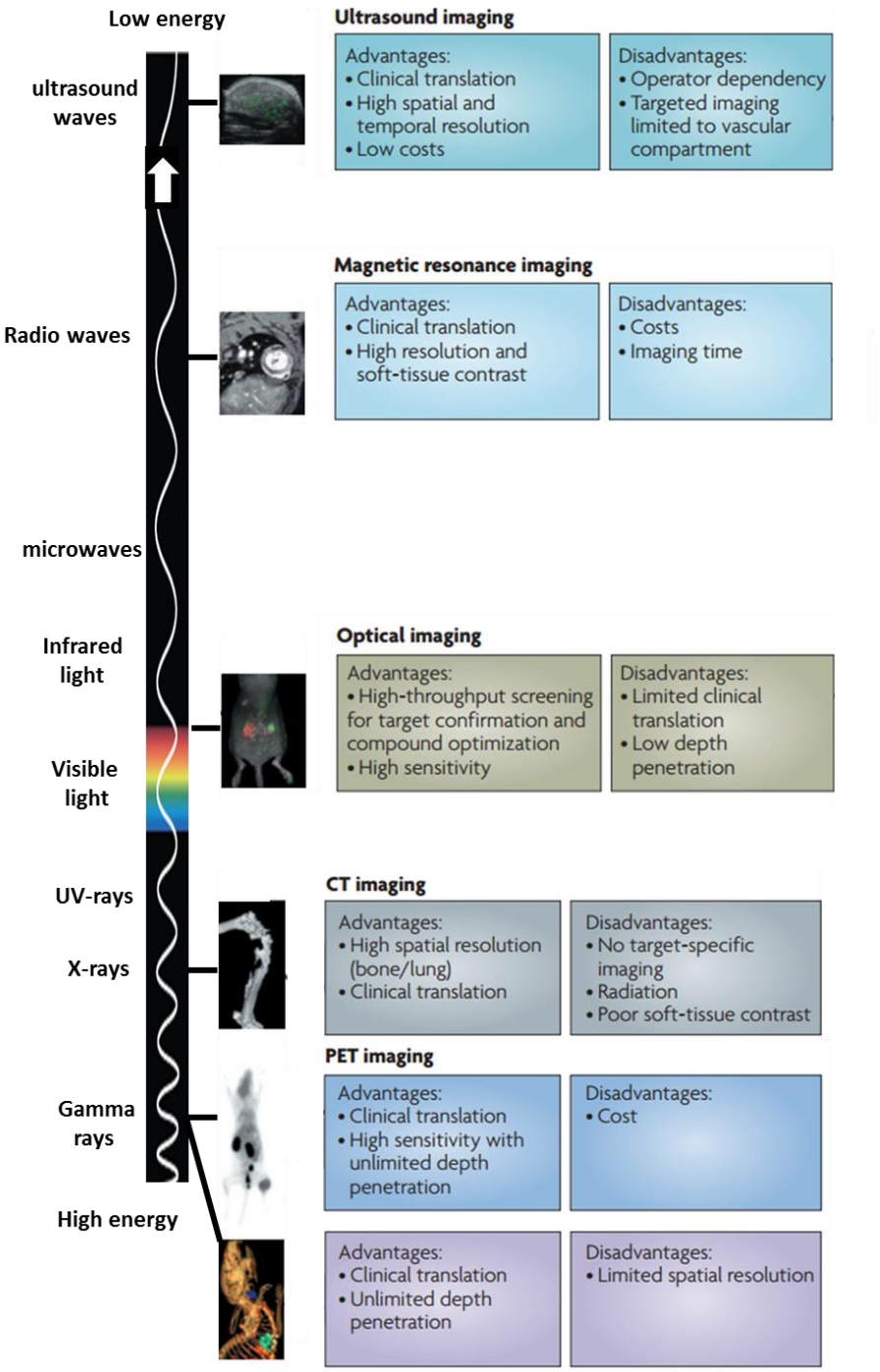

Figure 1.13 Summary of some modalities used for molecular imaging. Listed is the energy sources and the advantages/disadvantages of: ultrasound imaging, magnetic resonance imaging (MRI) optical imaging, computed tomography (CT) imaging, positron emission tomography (PET) and single positron emission computer tomography (SPECT). Figure reproduced with permission from Willmann and colleagues (2008) and modified.

Regrettably there has been limited utilisation of optical molecular imaging techniques. This is because, unlike other molecular imaging methods, there are still considerable limitations that preclude clinical translation. Disadvantages of *in vivo* optical molecular imaging include: 1) short tissue penetration depth and high scattering of light (even with near infrared (NIR) dyes, it is only a few cm); 2) low signal-to-noise ratio and a lack of specificity and sensitivity of some optical molecular imaging probes; 3) limited equipment and probes commercially available for human imaging (reviewed by Keereweer *et al*., 2013). Despite this, optical molecular imaging has great potential for endoscopy and bornchoscopy (Akram *et al*., 2015), camera guided surgery (Figure 1.14, Mito *et al*., 2012) and intravascular imaging (Osborn & Jaffer 2013).

Furthermore, unlike other molecular imaging modalities, optical molecular imaging is also not limited to imaging a single contrast agent per scan; multiple optically-tagged probes can be administered and imaged in one session. This is possible provided the excitation and emission profiles of the attached fluorophores do not interfere, and the imaging system is capable of discriminating one from the other (Troyan *et al*., 2009). Using this system, more information about a disease state could be gained in a single imaging session, improving disease understanding and diagnostic medicine.

In vivo optical molecular imaging generally requires the injection of a fluorescent contrast agent into the vasculature which accumulates in a specific region. Accumulation can occur as a result of using a fluorescently-labelled inhibitor or an antibody which targets and collects in the location of the protein of interest (the excess is metabolised/excreted) (Waschkau *et al*., 2013). Secondly probes can be designed to be silent until "switched on" by a target protease or environmental trigger. This results in an increase in fluorescence in a tissue region(s) (Lim *et al*., 2014).

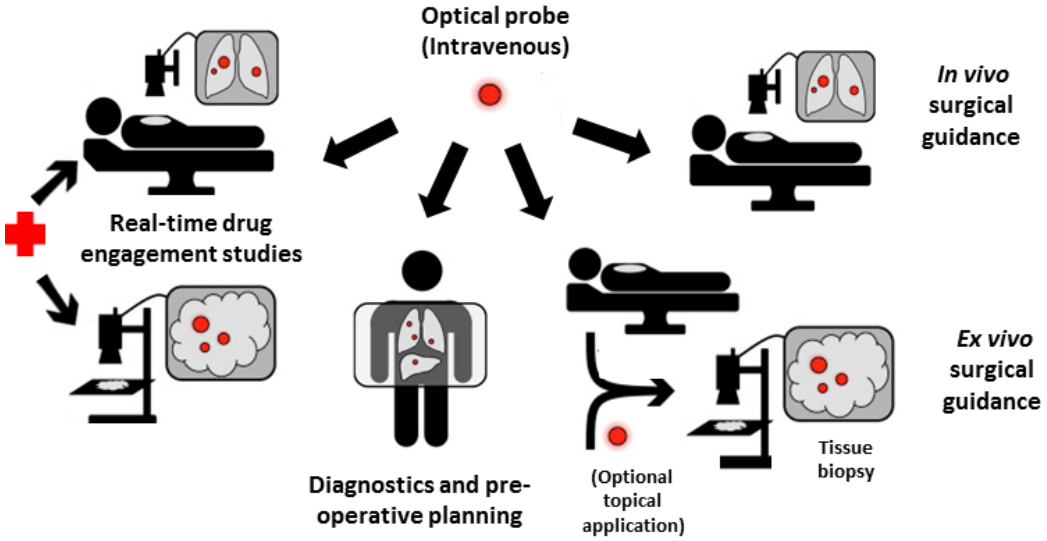

Figure 1.14 Molecular imaging using optical probes. Possible future applications of optical molecular imaging tools, including: diagnostics, real-time drug engagement studies and surgical guidance (*in vivo* and *ex vivo*). *In vivo* fluorescent imaging with indocyanine green, methylene blue and 5-aminolevulinic acid has already been successful in small clinical trials for the detection of cancerous tissue during surgery (Mito *et al.*, 2012). Figure reproduced with permission from Garland *et al*., 2016 and modified.

1.5.2 Förster resonance energy transfer (FRET) probes

Substrate-based Förster resonance energy transfer (FRET) probes, also known as activity FRET probes, are fluorescent molecules that are quenched until activated by one or more targeted proteases (Figure 1.15). Briefly, substrate-based FRET probes are constructed from two or more fluorophores (or a fluorophore and a dark quencher) tethered with a short peptide sequence. The distance between fluorophores is typically in the range of 1 −10 nm (peptide and linkers) (Jares-Erijman & Jovin, 2003) for efficient FRET but rapidly drops if this distance between the fluorophores increases (Equation 1.1). When fluorophores with overlapping excitation and emission spectra are held close in space, the donor excitation energy is transferred to the acceptor (Figure 1.15a) resulting in quenched fluorescence or a shift in the observed fluorescence wavelength (λ).

$$E = \frac{1}{1 + \left(\frac{r}{R_0}\right)^6}$$

Equation 1.1 FRET rapidly drops if the distance between the fluorophores increases. The Förster resonance energy transfer efficiency (E) is the fraction of energy transfer event occurring per donor excitation event (the quantum yield of the energy of transfer transition). E depends on the donor-to-acceptor separation distance (r). R_0 is the Förster distance, which is the distance at which the energy transfer efficiency is 50%, (Jares-Erijman & Jovin, 2003).

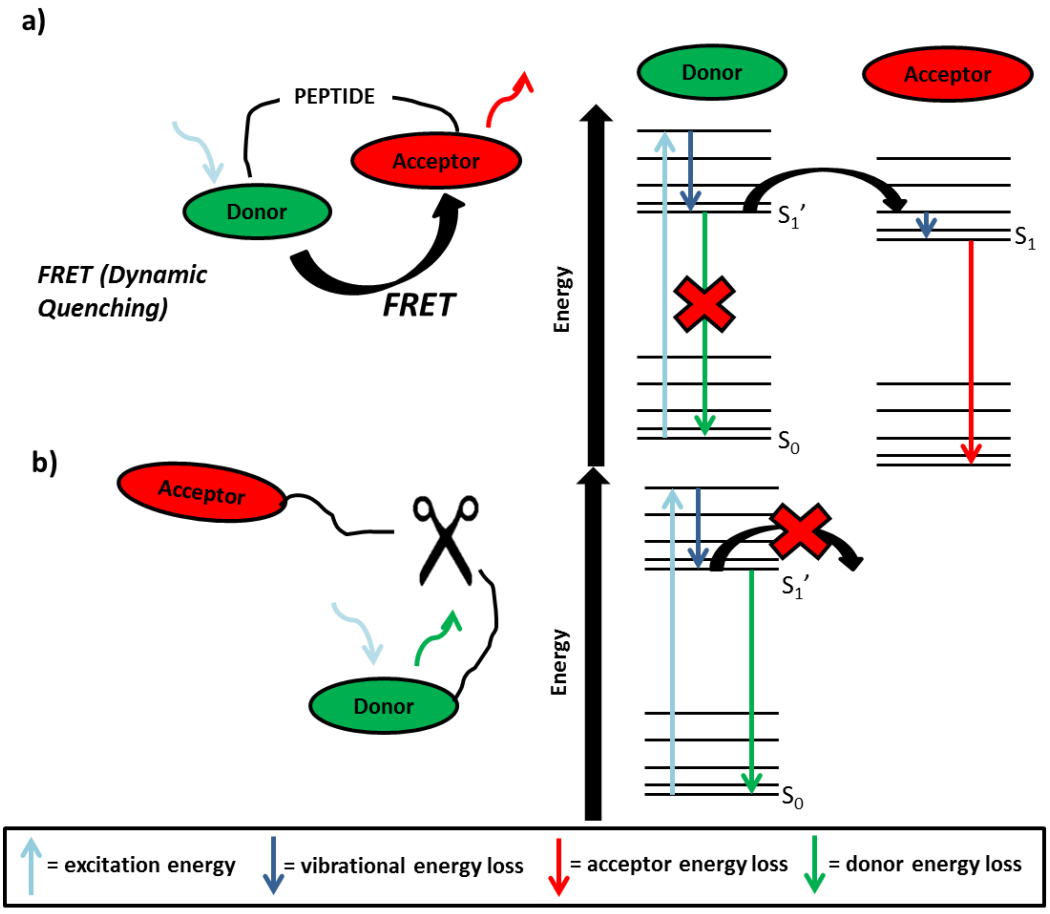

Figure 1.15 Activity probes using Förster resonance energy transfer (FRET) systems. FRET requires a donor–acceptor spectral overlap, short distance and the relative orientation of the donor and acceptor transition dipole moments. a) In an intact probe the FRET pair is in close proximity (distance (r), up to 10 nm) and the donor excitation energy is transferred to the acceptor should the dipoles align (falling off at a rate of $1/R^6$). The acceptor then loses the transferred energy by fluorescence at a lower

wave number (λ) and/or by vibrations. b) Cleavage of the peptide sequence causes the FRET fluorophore system to break down as the distance between the fluorophores is too great (R > 100 Å). This results in an increase in the donor fluorophore emissions combined with a decrease in the observed emissions from the acceptor. Therefore, monitoring fluorophore emissions can provide information about the proximity of the fluorophores and, consequently, the state of the probe construct.

The FRET system breaks down when the peptide sequence is cleaved and the fluorophores disperse, with the distance between them becoming too great to allow FRET (Figure 1.15b). Break down of FRET results in an increase in emissions from the donor fluorophore whereas the emission from the acceptor fluorophore decreases. Therefore, by monitoring these emissions from the fluorophores, information about their proximity can be gained. Thus they can be used as a tool to monitor biological activity and interactions. Another great advantage of FRET probes is that they generally have low toxicity; most peptides and selective fluorophores are not toxic (Choyke *et al*., 2009; Nolting *et al*., 2011). Furthermore, molecular imaging generally requires low quantities of probes. However, there are still regulatory and approval challenges associated with the design of clinical trials for these agents (Garland *et al*. 2016).

1.5.3 Commercial probes for optical molecular imaging.

The advancement of optical molecular imaging has been, in part, due to the advances in preclinical technology. There are now many commercially-available probes which can be used *in vitro* and *ex vivo* in combination with confocal and multiphoton microscopy, or *in vivo* using fluorescence molecular tomography (FMT) which allows for 3D localization and quantification of fluorescent light in tissue (Zhang *et al*., 2014; Ntziachristos *et al*., 2003; Zhang *et al*., 2011; Lee *et al*., 2012). The work described in this thesis was conducted using

FMT imaging with the FMT 2500, Perkin-Elmer™; further details on the FMT machine are available in Appendix 1. There is a wide range of optical imaging agents for different targets (Perkin-Elmer™) which take advantage of NIR dyes (700-900 nm) (Groves *et al*., 2010; Peterson 2011). This region is where the absorption coefficient of tissue is at its lowest, allowing for better tissue penetration (Frangioni *et al*., 2003).

In this project AngioSense 680 and MMPSense 750 FAST were used to measure vascular leakiness and MMP activity *in vivo*, respectively. The AngioSense 680 is a blood pool imaging agent (and not a FRET probe). It is high-molecular-weight (250 kDa) pegylated macromolecule made of copolymers which are non-immunogenic (Peterson 2011); each macromolecule is conjugated to a fluorophore (Montet *et al.*, 2007). After intra-venous injection, the initial high circulating level of the probe drives its extravasation from circulation. Depending on the time of imaging, two different measurements can be made about the vasculature. AngioSense probes can be used to measure vascular density 3-4 h post injection (as the macromolecule is still mostly in the vasculature) (Montet *et al*., 2007; Montet *et al*., 2005; Zhang *et al*., 2014). Although AngioSense can be used to measure vascular density in a whole subject it has proved challenging due to a low signal to noise ratio; therefore this measurement is better suited to intravital window microscopy. Alternatively AngioSense can be used to measure vascular leakiness after 24 h (vascular leakiness increases in tissues undergoing angiogenesis), at this point the probe is accumulated in tissues with leaky vasculature and the circulating probe is mostly cleared from circulation (Zhang *et al.*, 2011; Zhang *et al.*, 2014).

MMPSense 750 FAST (MMPSense) is a 43 kDa FRET probe constructed of a peptide (PLGVR) labelled with NIR fluorophores and conjugated to a pharmacokinetic modifier (Figure 1.16 A) (Groves *et al.*, 2010). MMP -2, 7, 9, 12 and 13 enzymatically cleave the peptide and the signal to noise/ratio is generally most desirable for imaging 24 h post

intravascular injection (Groves *et al.*, 2010). MMPSense has been used to image MMP activity in a number of inflammatory disease models, including: atherosclerosis (Hermus *et al*., 2010), deep vein thrombosis (Ripplinger *et al.*, 2012), aneurysms (Kaijzel *et al*., 2010) and arthritis (Ibarra *et al*., 2011). MMPSense was also successfully used to detect MMP activity in *ex vivo* human carotid artery samples (Wallis de Vries *et al.*, 2009).

MMPSense 750 is not specific to a particular member of the MMP family member and, therefore, the data collected using this tool consequently lack important information on the specific roles of individual MMPs in the disease model. The ability to image these relationships selectively would be a fantastic tool to interrogate the dynamic nature of these proteases *in vivo*.

Members of the Bradley and Dhaliwal group have synthesised and tested FRET probes for: the selective detection of neutrophil elastase in *in vitro* cell based assays (Avlonitis *et al.*, 2013); for the selective *in vitro* imaging of Caspase 3 activity (Mackay *et al.*, 2016); tracking of intracellular labelled murine macrophages during pulmonary inflammation (Dhaliwal *et al.*, 2011), and imaging live bacterial infections in *ex vivo* human lungs (Akram *et al.*, 2015). More recently, research has focused on the development of new imaging systems (data not shown or published) and of new selective FRET probes for new substrates including MMP-9 (data not shown or published).

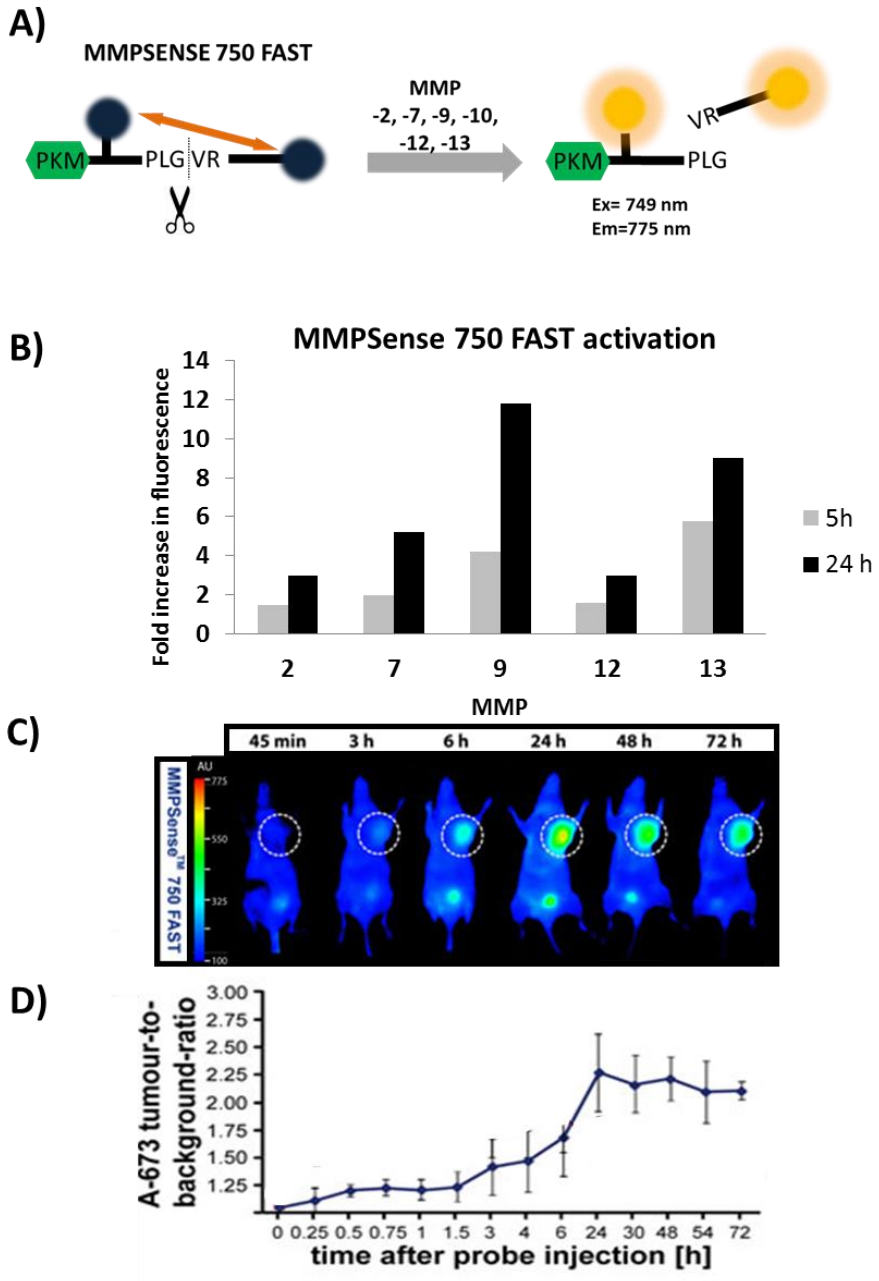

Figure 1.16 MMPSense 750 FAST: structure, activation and *in vivo* imaging. a) The structure of MMPSense 750FAST before and after activation by MMPs. The probe is a peptide (PLGVR) labelled with 2 NIR fluorophores and conjugated to a pharmacokinetic modifier (PKM) designed to effect rapid accumulation and activation in target tissues. The fluorophores are self-quenched by their close proximity imposed by the peptide link. When the peptide is cleaved by the MMPs the fluorophores are no longer self-quenched. b) MMPSense 750 FAST (0.5 µM final concentration in the assay) was cleaved in the presence of 0.05-0.1 µM activated MMPs. Reactions for MMPs were carried out in

optimal buffers, pH and temperature (Groves *et al.*, 2010). c) Representative images of reflectance imaging of MMPSense *in vivo* in a mouse tumour xenograph (dashed circle) over 72 h. (d) The measured tumour-to-background-ratio over 72 h after injection of MMPSense. Figure reproduced with permission from Waschkau *et al.*, 2013 and modified, or redrawn from Groves *et al.*, 2010**.**

1.5.4 MMP-12-targeting substrate FRET probes.

Due to the strong links between MMP-12 activity and vascular remodelling, it was decided that an optical molecular imaging FRET probe for MMP-12 detection would be a very useful tool. MMP-12 selective FRET probes have already been synthesised. The peptide substrate sequence PLGLEEA is selective for MMP-12, but showed minor cross reactivity with MMP-13 and -9 (Figure 1.17; Devel *et al.*, 2006). This is likely to be the result of the high structural homology between the MMP family members. A similar FRET probe (PLGLEEA peptide sequence with a lipid tail and 2 fluorophores) was found to selectively label macrophages stimulated to express MMP-12 (Figure 1.18; Cobos-Correa *et al.*, 2009). Lim and colleagues (2014) have more recently found that a NIR fluorophore-labelled FRET probe (with the PLGLEEA sequence) could be used to detect active MMP-12 *in vivo* in a murine model of arthritis (Figure 1.19). As of yet, there are no examples of a similar probe with the PLGLEEA sequence being used to detect MMP-12 activity in models of cardiovascular disease.

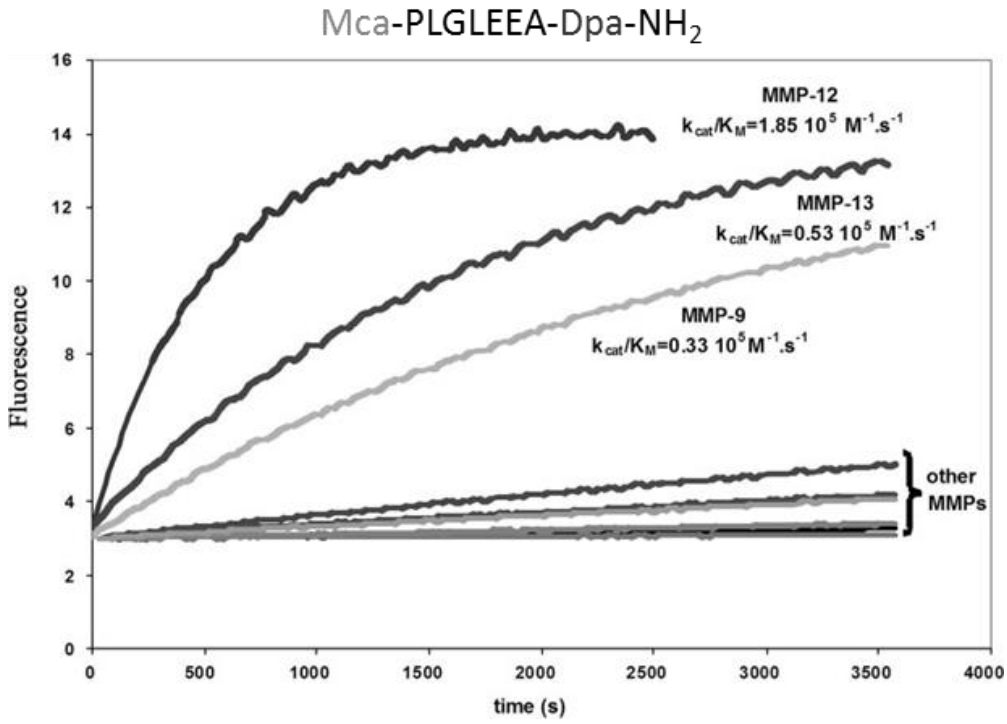

Figure 1.17 The peptide sequence PLGLEEA is selective for MMP-12. First order full-time reaction curves observed for the breakdown of the 7-methoxycoumarin-4-acetic acid (Mca) and 9,10-diphenylanthracene (Dpa) Förster resonance energy transfer **(**FRET) pair; Mca-PLGLEEA-Dpa-NH_2 (0.5 nM) by MMPs (11 nM), 50 mM Tris, pH 6.8, 10 mM $CaCl_2$, 25 °C. Nonlinear regression fitting of these curves with the integrated Michaelis-Menten Equation 1 was used to determine the kcat/Km values for MMP-12, -9, and -13. This probe is selective for MMP-12 but can also be cleaved by MMP-9 and MMP-13 with slower Michaelis-Menten kinetics. Figure reproduced with permission from Devel and colleagues (2006) and modified.

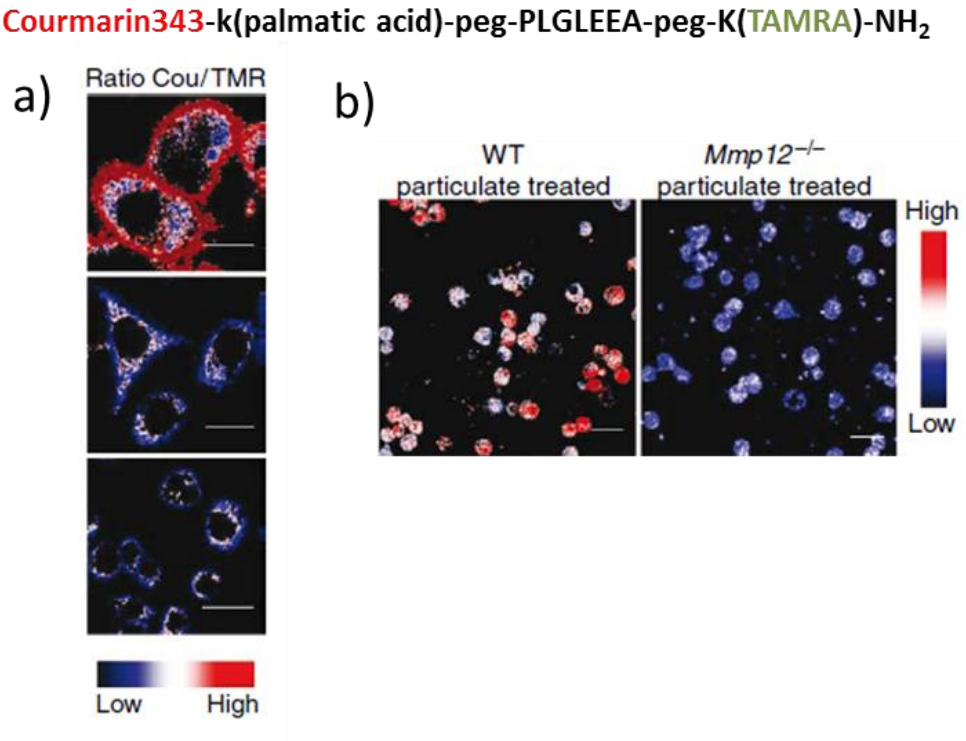

Figure 1.18 An MMP-12-selective peptide sequence utilised by Cobos-Correa to create an MMP-12 probe (Courmarin 343 and TAMRA adapted to integrate a lipid tail to allow binding to a lipid membrane. a) MMP-12 selective FRET probe was activated by inflammatory macrophages. The probe (1 µM) was incubated with LPS-stimulated macrophages (top, LPS simulates an inflammatory response and MMPs are released) and non-stimulated cells (centre) or those stimulated but also treated with an MMP inhibitor (bottom) (scale bar, 25µm). b) This probe showed an MMP-12 specific response. C57BL6/J (WT, left) and MMP-12$^{-/-}$ (right) mice which were challenged with particulate fraction PM10 by intra-tracheal instillation (stimulated an inflammatory response)); bronchoalveolar lavage fluid was then incubated with the FRET probe (3 µM). Figure reproduced with permission from Cobos-Correa *et al.*, 2009 and modified.

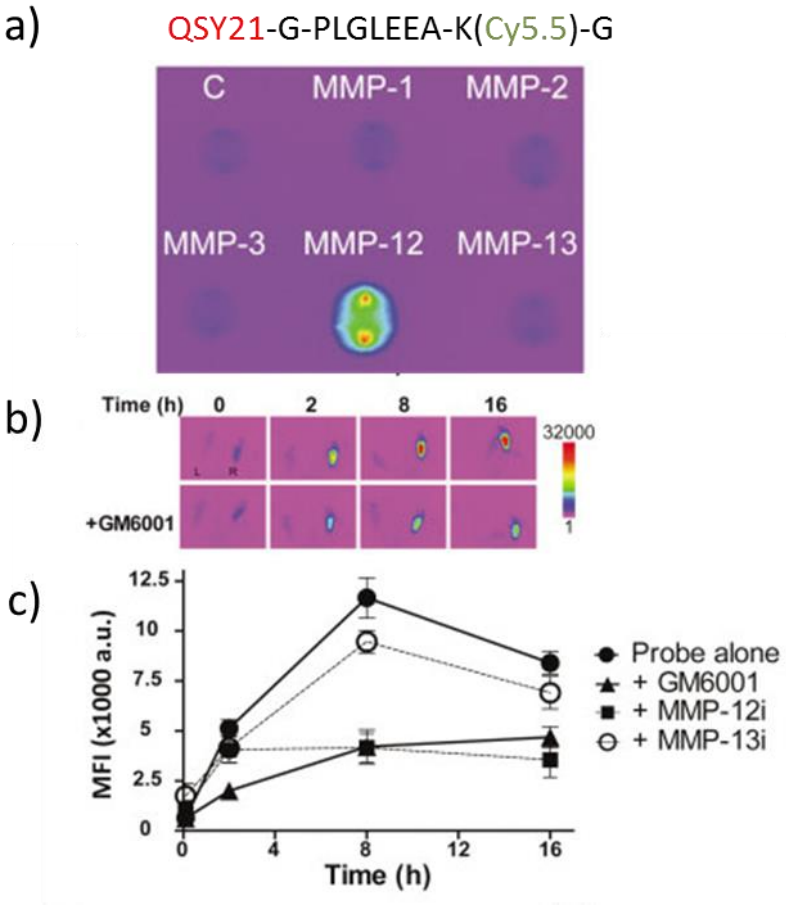

Figure 1.19. FRET probe MMP12ap (QSY21-GPLGLEEAK[Cy5.5]G) is shown to be selective for MMP-12 *in vitro* and *in vivo*. a) Fluorescence images of 1 µM MMP12ap solutions spotted on glass slides after incubation with 50 nM of an MMP (MMP-1 (cat), MMP-2, MMP-3 (cat), MMP-12 (cat) or MMP-13) for 30 min at 37°C. b) Representative fluorescence images of zymosan-induced inflammation and oedema over 16 h in a single animal showing specific activation of the MMP-12 activity probe (MMP12ap) after intra-plantar injection with or without MMP inhibition (GM6001). c) Quantification of probe activation after intra-plantar injection of the probe alone or in combination with a broad-spectrum MMP inhibitor (GM6001) or selective MMP-12 inhibitor (MMP-12i) or a selective MMP-13 inhibitor (MMP-13i) (n = 3/group). These data strongly suggest that this probe is selectively activated by MMP-12 *in vivo*. Figure reproduced with permission from Lim *et al.*, 2014 and modified.

1.6 MMP-12 inhibitors

1.6.1 MMP inhibitors in clinical trials

Unregulated MMP activity is closely associated with progressive disease pathology (Hu *et al.*, 2007; Johnson *et al.*, 2005; Burrage *et al.*, 2006). Consequently these zinc-dependent extracellular enzymes appeared to be promising targets in a range of diseases, including CVD (Hu *et al.*, 2007) and cancer (Cathcart *et al.*, 2015). The first clinically-tested, broad spectrum MMP inhibitors (batimastat (**1**) and the orally available marimastat (**2**); Figure 1.20) were developed to target cancers (Hidalgo & Eckhardt, 2001).

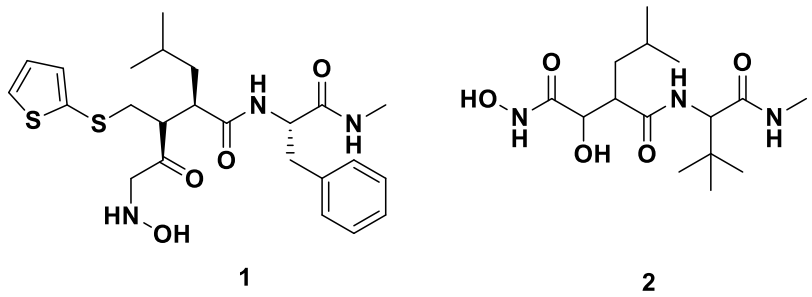

Figure 1.20 Structures of batimastat (1) and the orally available marimastat (2).

Studies in murine models of gastric (Kimata *et al.*, 2002; Wada *et al.*, 2003), lung (Wojtowicz-Praga *et al.*, 1998) and prostate (Somlyo *et al.*, 2003) cancer showed improvements after treatment with marimastat, which generally resulted in reduced tumour size and vascularity. Unfortunately, these results were not easily reproduced in human clinical studies. Some trials observed no change compared to placebo (for example, in breast cancer; Sparano *et al.*, 2004), but patients with gastric cancer did demonstrate a small improvement in overall survival (Bramhall *et al.*, 2002). These MMP inhibitor drugs were also found to have muscoskeletal toxicity so they never became the breakthrough cancer treatments once hoped (Wojtowicz-Praga *et al.*, 1998; Bramhall *et al.*, 2002; Jacobsen *et al.*, 2010). It has been suggested that

future generations of MMP inhibitors could have reduced toxicity if they are designed to target a single MMP (prominent in the pathology of the disease being targeted), or that the zinc binding could be weakened to limit the off target effects (Saghatelian *et al.*, 2004).

1.6.2 MMP imaging using selective inhibitors

Therapeutic targeting of MMPs with broad spectrum inhibitors has proved challenging due to toxicity. However, some MMP inhibitors could still be used as molecular imaging probes by labelling with a reporter. This may have reduced toxic effects as only a single, low dose would be required for imaging.

MMP-12 has been successfully covalently labelled *in vitro* with fluorescent or radiolabelled labelled MMP inhibitors (Figure 1.21), but these probes utilised reactive species such as a photo labile group (**3**) (Nury *et al.*, 2013) or an electrophile (**4**) (Morell *et al.*, 2013) which are prone to cross reactivity. The latter also required MMP-12 to be engineered to incorporate a cysteine near the active site. These are time consuming processes and quicker techniques would be beneficial. Furthermore, these attributes are not practical for *in vivo* studies. Covalent bonding of MMP-12 *in vivo* is unlikely to be possible. An alternative strategy is to use high potency MMP-12 inhibitors to target the enzyme and localise the reported group to the site of action.

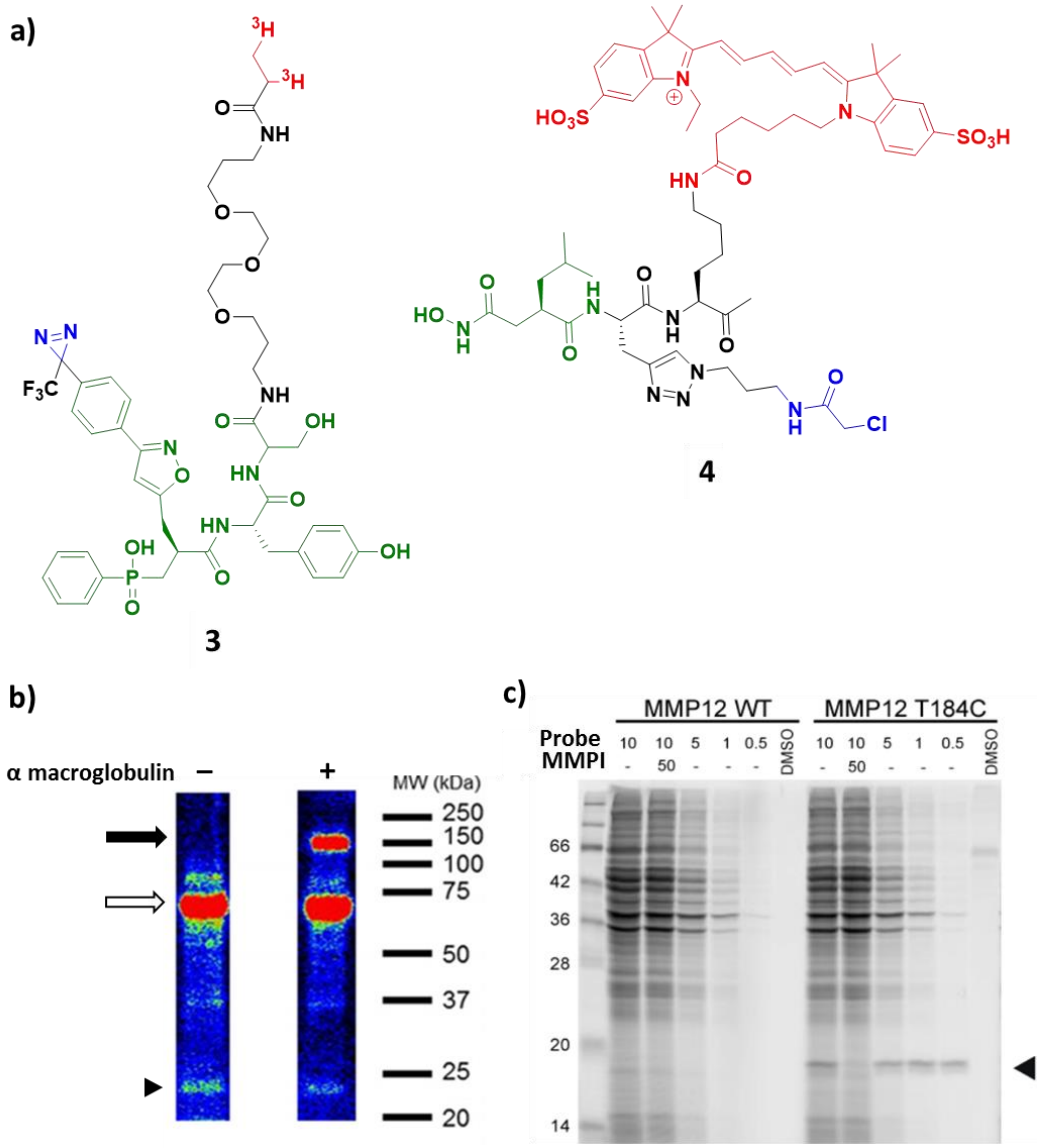

Figure 1.21 Molecular tools for covalently and selectively labelling MMP-12 *in vitro*. a) Structures of MMP-12 targeting probes: Probe **3** utilises a phosphinic peptide (green) designed to selectively target the MMP-12 active site (Devel *et al.*, 2006), this was conjugated to a photo-labile group (blue) and radionuclide (tritium) reporters (red) (Nury *et al.*, 2013). Probe **4** utilises an MMP targeting, zinc-binding (hydroxamic acid) group (green) conjugated to an α-chloroacetamide electrophile (blue) and a fluorophore (Cy5.5, red) (Morell *et al.*, 2013). b) Imaging protein bound probe **3** in BALf separated by electrophoresis and imaged using radio imaging. Irradiated probe **3** (100 nM) labelled free MMP-12 (arrow head) and MMP-12 bound α-macroglobulin (black filled arrow) in BALf collected from mice exposed to nanoparticles; probe **3** also bound to mouse serum albumin (empty arrow). The addition of

α macroglobulin (protease inhibitor) prior to irradiation blocked MMP-12 binding to probe **3**. c) Probe **4** was designed to, and did, selectively react with a mutant recombinant form of MMP-12 with a cysteine residue within the active site (T184C MMP-12, arrowhead, compared to wild type (WT) MMP-12) in spiked rat liver lysates (50 μg) with negligible background labelling (when used at low probe concentrations). This labelling could be blocked using a broad spectrum inhibitor (GM6001, 10 μM, 30 min, 37℃). Samples were analysed by electrophoresis gel and then imaged Cy5 fluorescence. Figure reproduced with permission from Nury *et al.*, 2013 and Morell *et al.*, 2013 and modified.

Non-covalently bound MMP imaging probes have been developed for i*n vivo* use (Figure 1.22). Wagner and colleagues (2009) synthesised an ^{18}F labelled MMP inhibitor (**5**) designed for PET imaging. Probe **5** displayed no accumulation in the heart and aorta of C57BL/6J mice and was predominatly found in the liver and bladder; it has yet to be used in a disease model. Schäfers and colleagues (2004) developed a very similar ^{123}I labelled MMP inhibitor (**6**) which was successfully used to image carotid atherosclerotic lesions in $ApoE^{-/-}$ mice *in vivo* using planer scintigraphy. Waschkau and colleagues (2013) optically labelled a related MMP inhibitor (Cy5.5-AF489, **7**). *In vivo* optical molecular imaging of probe **7** showed that it accumulated in tumour xenographs (Ewing's sarcoma) in minutes (with a higher signal to noise ratio) after tail vain injection (Figure 1.23). This was much faster than the commercial MMPSense™ 750 but after 6 h post injection, the MMPSense probe had a higher signal to noise ratio in the xenograph compared to the probe **7**.

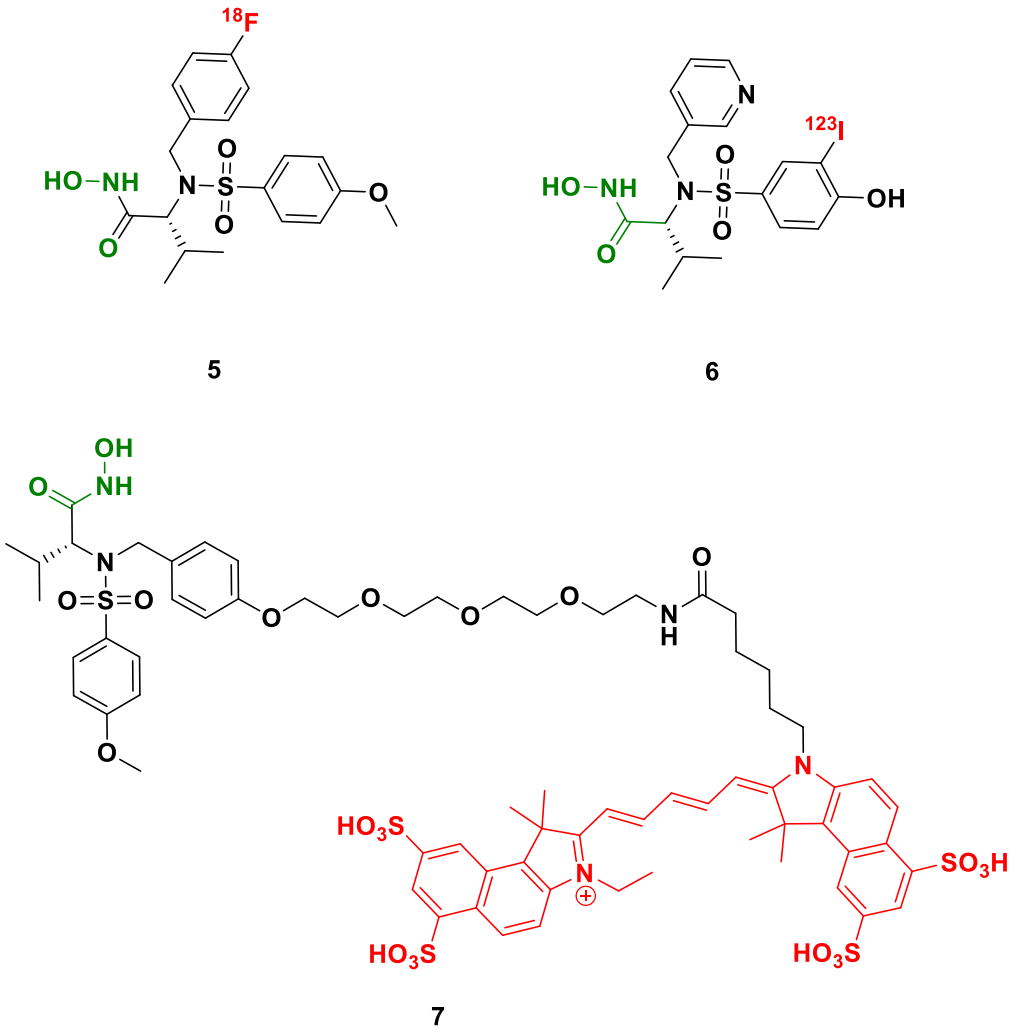

Figure 1.22 Structures of imaging probes, based on MMP inhibitors, that are suitable for *in vivo* imaging. Probes have a zinc binding hydroxamic acid group (green) and a reporter (red). Probes **5** and **6** are labelled with radionuclide and are suitable for radio imaging methods whereas **7** is conjugated to a fluorophore (Cy5.5) and is suitable for optical molecular imaging.

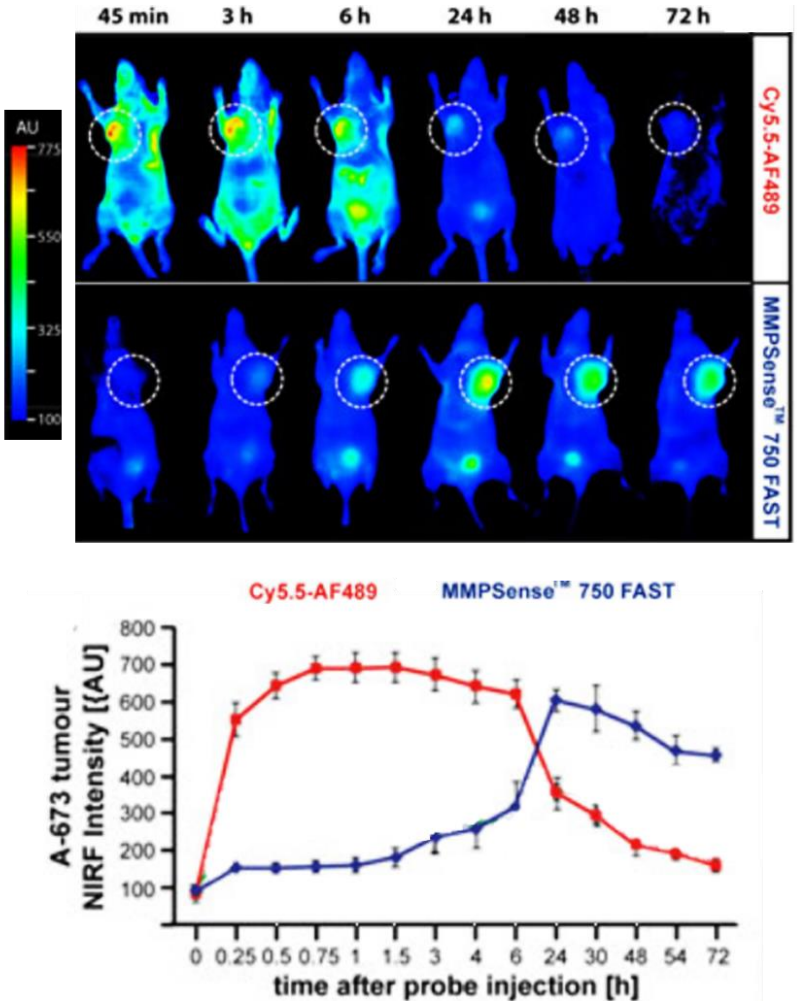

Figure 1.23 Optical imaging of MMP activity with an MMP inhibitor and FRET probe. Top) Fluorescent *in vivo* images were captured of mice with tumour xerographs over a 72 h period post administration of probe **7** or commercial MMPSense™ 750 (MMP activity FRET probe). Images clearly demonstrate the accumulation of the probes within the tumours; this could be blocked by co-administering a broad spectrum MMP inhibitor (data not shown). Bottom) The signal intensity of the two probes was quantified within the xenograph over the 4 day period. Probe **7** (which targeted MMP-2, -8, -9, -13) accumulated within the tumour xerographs within minutes but started to be cleared after 6 h; whereas MMPSense took longer to accumulate and was best imaged 24 h post administration. Figure reproduced with permission from Waschkau *et al.*, 2013 and modified.

Overall this demonstrates the capacity of labelled MMP inhibitors as optical molecular imaging contrast agents. They can quickly accumulate in target tissues *in vivo* in the target tissue allowing for quick imaging (compared to FRET probes). Furthermore, structural changes to the inhibitor moiety could tune the probe to target specific MMPs. To date labelled MMP-12 selective inhibitors have not been used to image MMP activity in CVD tissues.

1.6.3 MMP-12-targeting inhibitors

MMPs have very similar structures (for example, all have a zinc atom chelated to three histamines in the active site, Figure 1.3). Therefore to obtain selectivity attempts have mostly concentrated in the S1′ pocket where some differences between the MMPs are present (Morales *et al*., 2004). The S1′ pocket is surrounded by a "selectivity loop" which varies in length, flexibility and chemical properties between MMPs. MMP-12 also has a large, predominantly hydrophobic, S1′ pocket which is part of a channel running through the protein (Morales *et al*., 2004).

Selective inhibitors for MMP-12 have been predominantly developed for the treatment of chronic obstructive pulmonary disease (COPD) (Lagente *et al*., 2009). Compound AZD1236 (**8**) is an MMP-9 and -12 selective inhibitor; it was in Phase II clinical trials for the treatment of COPD but failed to meet its biomarker endpoints to progress (Magnussen *et al.,* 2011; Dahl *et al.,* 2012). Compound RXP470.1 (**9**) is a phosphinic peptide inhibitor of MMP-12, which has been successful in preclinical trials for reducing atherosclerotic plaque development (Devel *et al.,* 2006; Czarny *et al.,* 2013; Johnson *et al.,* 2011). Compound MMP408 (**10**) is a potent MMP-12 inhibitor which significantly reduced (>70%, $p<0.001$) the number of macrophages collected in the BALf from a model of murine lung inflammation (Li *et al*., 2009).

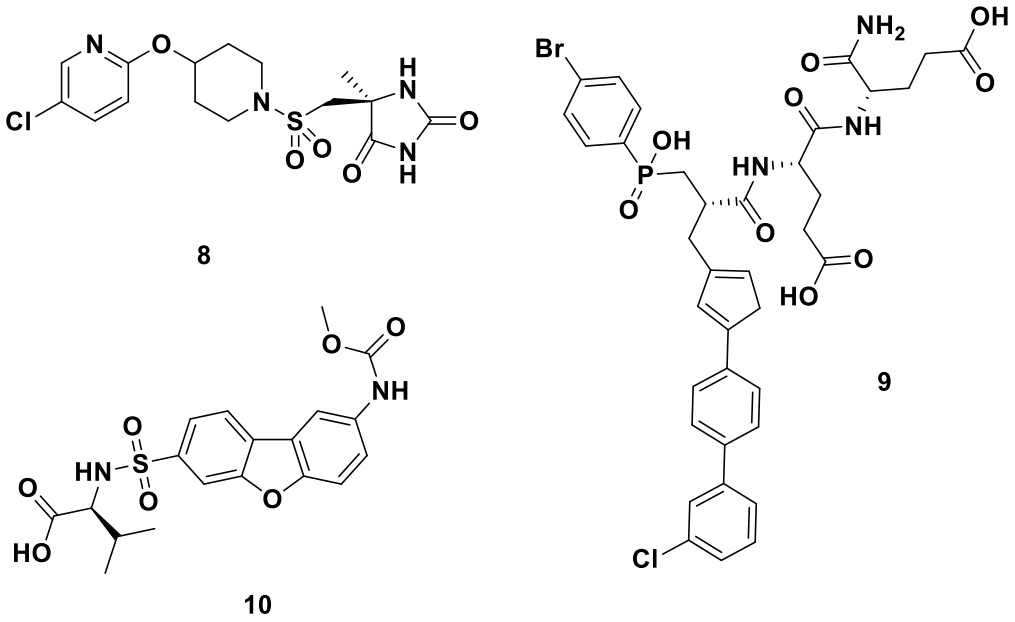

Figure 1.24 MMP-12 selective inhibitors. The suggested structure of AZD1236 (**8**) which is still under patent by AstraZeneca (Barnwell *et al.,* 2007). The exact mechanism of action has not been published. Compound RXP470.1 (**9**) binds to zinc within the active site of MMP-12 via the phosphoryl group. The peptide backbone interacts with the MMP-12 selectivity loop and the long muti-ring (P1′) group sits deep in the activity site (S^1) pocket (Czarny *et al.,* 2013). Compound MMP408, (**10**) is a highly potent MMP-12 inhibitor (IC_{50} = 2 nM). The affinity of **10** for MMP-12 is primarily due to the presence of the carboxylic acid which binds to Zn^{2+} within the active site of MMP-12, rendering it inactive.

1.6.4 MMP-12 inhibitor selection

It was hoped that in future studies a selective MMP-12 inhibitor could be labelled for optical molecular imaging of CV remodelling. Compound MMP408 was selected as a starting compound for this study on the basis of its high potency and selectivity towards MMP-12. The binding of MMP408 to MMP-12 is primarily due to the presence of the carboxylic acid which binds to the active site Zn^{2+} of MMP-12 (Figure 1.25) rendering it inactive.

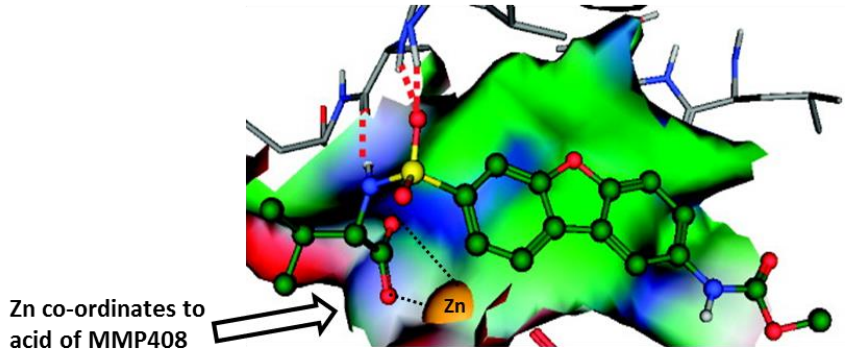

Figure 1.25 MMP408 and analogue inhibitors. The co-crystal structure of MMP408 docking in the active site (S1′ pocket) of MMP-12. The carboxylic acid of MMP408 forms ionic bonds to the zinc atom, blocking its proteolytic activity. Selectivity of MMP408 for MMP-12 over other MMPs was due to various factors. The dibenzofuran ring provides rigidity and stability to the compound. It also formed pi-stacking bonds with histamine and tyrosine residues (HIS218 and TYR240) in the MMP-12 S1′ pocket (Shamsara *et al*., 2014). The addition of substituents to the ring was also limited to the C2, C3, C7 and C8 positions of dibenzofuran ring as others were blocked by the limited size of the S1′ channel (Shamsara *et al*., 2014). The sulphonamide moiety also had favourable hydrogen bond interactions (red dotted lines) with the protein backbone in the S1′ pocket. Figure reproduced with permission from Li *et al.,* 2009 and modified.

Following consideration of analogues of MMP408, compound LiMMPI-12 (**11**, Table 1.3) was selected for this study as it was very potent for MMP-12 and had a relatively simple synthesis (Li *et al*., 2009). Encouragingly, it showed potential to also carry large functional groups and still have acceptable potency towards MMP-12 (Table 1.; Li *et al*., 2008). This could allow for future MMP inhibitor labelling and imaging studies should LiMMPI-12 elicit the desired effects in preliminary *in vivo* inhibitor studies.

Table 1.2 Structural differences of between MMP408 (10) and analogue LiMMPI-12 (11). Table was adapted from Li *et al.*, 2009.

Structure	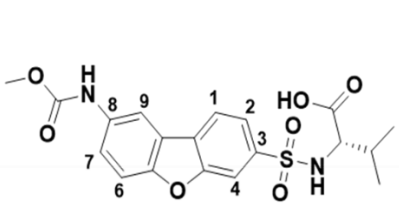 10	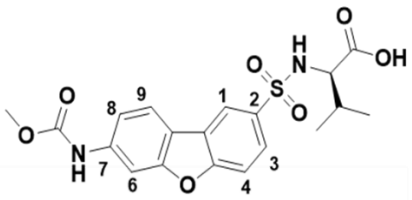 11
Name	MMP408	Li MMPI-12
Sulfonoamide	3	2
Carbamate	8	7
Amino acid chirality	S	R
IC_{50} (nM)	2	7.2

Table 1.3 MMP-12 selective inhibitors. The structure activity relationships of LiMMPI-12 and its analogues (Li *et al*., 2008).

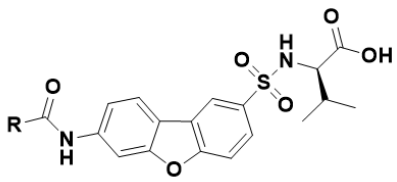

R		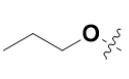	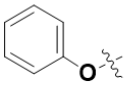	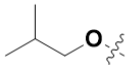	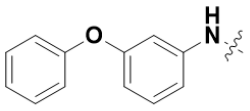
IC_{50} (nM)	7.2	13.2	29. 2	180	430

1.7 Hypothesis and aims

1.7.1 Hypothesis

The work described in this thesis uses commercial and in-house synthesised MMP inhibitors and FRET probes to address the hypothesis that MMP-12 activity is anti-angiogenic.

1.7.2 Aims

1. To synthesise and characterise an MMP-12 selective inhibitor and to use it in *in vitro, ex vivo* and *in vivo* models of angiogenesis.

2. To synthesise and characterise a small library of MMP-12 selective FRET probes and to test them *in vitro* using recombinant enzymes and tissue extracts.

3. To characterise a preclinical model of angiogenesis with MMP-12 activity.

4. To image MMP activity and angiogenesis *in vivo* using a model of angiogenesis using commercial probes.

Chapter 2

Material and Methods

2 Chapter 2: Materials and Methods

2.1 Materials and reagents

All reagents and solvents were from Sigma Aldrich or Fisher Scientific unless otherwise stated and were used without further purification.

2.1.1 Buffers

MMP buffer: 50 mM Tris, 10 mM $CaCl_2$, 0.15 M NaCl, 0.05% polyethylene glycol dodecyl ether (Brij® 35), pH 7.5, 0.2 µm filtered.

Sample buffer*:* 3X solution; 6 mL 20% sodium dodecyl sulfate (SDS), 6 mL 0.5M Tris pH 6.8, 6 mL glycerol, 1.2 mL 0.5% bromophenol blue (BoB) (in EtOH), 240 µL 0.5M ethylenediaminetetraacetic acid (EDTA) made up to 20 mL using H_2O.

Phosphate buffered saline (PBS): 0.01 M phosphate buffer, 2.7 mM potassium chloride and 0.137 M sodium chloride, pH 7.4, at 25 °C.

Citrate buffer: 10 mM citric acid, 0.05% Tween 20, pH 6.

PBlec: 0.1 mL $MnCl_2$ (1M) in PBS (1 L) with 1% (*v/v*) Tween 20.

2.1.2 Reagents and solutions

MTT solubilising solution: 10% Triton-X 100 in acidic isopropanol (0.1 M HCl)

Sinapic acid matrix solution: 15 mg/mL of sinapic acid dissolved in a 30% solution of acetonitrile (ACN) in H_2O (70%) with trifluoroacetic acid (TFA) (0.1%).

Picro-sirius red staining solution: Pico-sirius red solution was prepared: 1% direct red, 1% fast green FCF in water; immediately before use, this was diluted 1:9 in picric acid saturated aqueous solution, filtered and protected from light.

Dde deprotection stock solution: $NH_2OH \cdot HCl$ (1.25 g, 1.8 mmol) and imidazole (0.918 g, 0.35 mmol) in 5 mL of N-Methyl-2-pyrrolidone (NMP) (stable for 2 weeks at −20 °C).

Kaiser test reagents*: Reagent A* Solution 1: Reagent grade phenol (40 g, 0.43 mol) was dissolved in absolute ethanol (10 mL). Aberlite mixed bead resin MB3 (4 g) was added, stirred for 45 min and then filtered. Solution 2: KCN (65 mg, 1 mmol) was dissolved in water (100 mL). The KCN solution (2 mL) was diluted to 100 mL with pyridine (freshly distilled). Aberlite mixed bead resin MB3 (4 g) was added, stirred for 45 min, filtered and mixed with solution 1 to give *Regent A. Regent B:* ninhydrin (2.5 g, 14 mmol) was dissolved in absolute ethanol (50 mL).

Chloronil test reagents: *Reagent A*: 2% acetaldehyde in dimethylformamide (DMF); *Reagent B*: 2% chloranil in DMF.

2.2 Animals

All animal experiments were carried out according to the Home Office Animals (scientific procedures) Act of 1986 (PPL: 60/4523 19b1/19b2 and PILs (Stott) 13818 / I16D1B9E2, Hadoke 60/7976/ I93FA603D) and approved by the University of Edinburgh ethics committees. C57BL6/J mice were purchased from Harlan or Charles River, MMP-12$^{-/-}$ mice (B6.129X-Mmp12tm1Sds/J) were purchased from The Jackson Laboratories (USA) via Charles River (UK). Animals were housed in groups, where appropriate, and maintained under controlled conditions of light (lights on 08:00 – 20:00) and temperature (21 – 22 ˚C). All surgical procedures were performed by myself, or under the direct supervision of Dr Hadoke until competent. Gary Borthwick undertook the intravenous injections for imaging agent administration.

2.3 Data analysis and statistics.

Data groups were checked for outliers using a Grubb's test. Prism (GraphPad version 5) software was used to plot the data and check for normality within groups (Kolmogorov–Smirnov test). Differences between groups were then tested for significance using an appropriate assay:

- Student's t-test (2 data groups, two-sided, normally distributed)
- A one–way ANOVA (3 or more normally distributed groups with a single variable)
- A two–way ANOVA (2 or more normally distributed groups with > one variable)
- Kruskal–Wallis-test (3 or more not normally distributed data sets)

These tests were followed by an appropriate Post-Hoc test: a Bonferroni multiple comparisons test; Dunnett's multiple comparison test *vs* the control or samples collected on day (D) 3; Dunn's multiple comparison test *vs* the control or samples collected on D 3. A comparison was considered statistically significant when $P < 0.05$. When a trend was reported, $P < 0.01$ but > 0.05. In general results are presented as mean ± standard error of the mean (SEM). See figure legends for details of analysis for the data presented.

2.4 General equipment, software and analytical procedures.

2.4.1 Equipment and software

Microsoft Office: Microsoft Corporation, version 2013; with NormFinder Excel Add-In, version 0.953 (MOMA - Department of Molecular Medicine, Aarhus University Hospital, Denmark, http://moma.dk/normfinder-software)

ImageJ: Wayne Rasband, National institute for health, USA, version 1.48.

Plate reader: Synergy HT machine with GEN 5 software version1.1 (Bio-Tek).

Fluorescence molecular tomography (FMT) machine: FMT 2500 with TrueQuant software version 3.1 (VisEn medical, Perkin Elmer).

Slide Scanner: Zeiss AxioScan.z1 with Zen lite Software (blue version 6.1.7 and black 8.1.0 editions) 2012 (Carl Zeiss Microscopy GmbH).

NanoDrop: NanoDrop 1000 Spectrophotometer with Nanodrop 100 software version 3.8.1 (ThermoScientific).

Lightcycler: Lightcycler 480 with Lightcycler 480 software version 1.5.1.62 (Roche Diagnostics).

Thermocycler: TC-512 gradient thermal cycler (Techne, Bibby Scientific Ltd).

Nuclear magnetic resonance (NMR) spectrometers: 1D and 2D ^{1}H and ^{13}C NMR spectra were recorded using an automated Bruker advance NMR spectrometer operating at 500 MHz and 125 MHz, respectively. Results were analysed using MetReNova software (version 6.2, 2009 Mestrelab Research S. L.).

Mass spectrometers (MS): *Low resolution analysis(LRMS):* recorded using an Agilent 1100 series LC/MSD quadropole mass spectrometer under both positive and negative electrospray ionisation (ESI) conditions. Spectra were analysed using LC/MS Chem Station Rev B.04.03.SPI. *High resolution analysis (HRMS)*: ESI recorded using Thermo Finnigan Sector (LCQ) mass spectrometer or ThermoElectron MAT 900; EI recorded using ThermoElectron MAT 900 by the School of Chemistry Mass Spectroscopy department. *Matrix assisted laser desorption ionisation – time of flight (MALDI TOF*) *MS*: Samples were analysed on an Ultraflex Extreme MALDI TOF MS (Bruker) and analysed using Data Analysis Viewer software (version 4.1, Bruker).

Infra-red (IR) spectrometer: IR spectra were run using a Bruker Tenzor 27 and analysed using OPUS software (SS-Build 5.5.66 [317], 1997-2005).

High performance liquid chromatography (HPLC) systems: *Analytical:* Reverse phase HPLC was performed on an Agilent 1100 HPLC system equipped with an ultraviolet detector connected to a Polymer lab 100 ES evaporative light scattering detector (ELSD). Columns: reverse phase Supelco Discovery C18, 5 µm, 50 × 4.6 mm column (FRET probes) or Kinetix XB-C18 (100A) 5 µm, 50 × 4.6 mm column (HS1-22 synthesis). Solvents: HPLC grade, Acetonitrile (ACN, 0.1 % formic acid (FA)) and water (0.1% FA). Analysis software: ChemStation for LC systems, Agilent technologies 2001-2007 Rev: B.13.01.

Semi-preparative HPLC: the compound was dissolved in HPLC grade ACN/ H_2O solution and placed in an HPLC vial. Reverse phase HPLC was performed on an Agilent 1260 HPLC system equipped with a UV absorption detector and connected to a fraction collector. Column: C18 reverse phase column, Agilent Eclipse XB-C18 9.4 × 250 mm, 5 µm. Solvents: HPLC grade, ACN (0.1% FA) and water (0.1% FA). Analysis: ChemStation for LC systems, Agilent technologies, Open Labs CD, 2001-20011 Rev: C.01.03[37].

Preparative HPLC Reverse HPLC was performed on an Agilent 1100/1200 HPLC system equipped with an ultraviolet absorption detector and connected to a fraction collector. Column: C18 reverse phase column, Kinetix XB-C18 21.2 × 150 mm C18 column. Solvents: HPLC grade, ACN (0.1% formic acid) and water (0.1% formic acid). Analysis: ChemStation edition for LC systems, Agilent technologies 2001-2007 Rev: B.03.01.SR1 [317].

2.4.2 General compound analytical procedures

NMR spectroscopy: Compound (5 mg) was dissolved in 1 mL of deuterated solvent.

Mass spectrometry (MS): *Low/ High MS: c*ompound (0.25 mg) was dissolved in 1 mL of HPLC grade methanol or ACN. *MALDI-TOF MS*: A solution of the compound (1 µL, serially diluted to 0.01M,) was mixed with a sinapinic acid solution (1 µL) on the MALDI plate and allowed to dry at room temperature for 10 min prior to analysis.

HPLC: *Analytical HPLC:* Compound (0.5 mg) was dissolved in 1 mL of HPLC grade methanol or ACN. Method: GE15ACN was used unless otherwise stated (GE15ACN: ACN in water with (0.1% FA) on a gradient 5 to 95% (8 min); Isocratic (4 min); gradient 95% to 5% (5 sec) then isocratic (3 min) at a flow rate of 1 mL/ min). *Semi-preparative HPLC*: the compound was dissolved in HPLC grade ACN/ H_2O solution for purification on the HPLC semi-preparative system. Method: see compound experimental (Section 2.5.5 and 2.6). Collected fractions were analysed by analytical HPLC. Those with pure product were combined and the solvent removed under reduced pressure. *Preparative* HPLC: the compound was dissolved in HPLC grade MeOH or ACN and placed in an HPLC vial for purification on the HPLC preparative system. Method: the solvent gradient used for purification depended on the compound, see the compound experimental. Collected fractions were analysed by analytical HPLC, those with pure product were combined and the solvent removed under reduced pressure.

2.5 General procedures for solid phase synthesis of FRET probes

2.5.1 Materials

Reagents for the free amine assays were prepared as described in Section 2.1. Fmoc-Lys (Dde)-OH was synthesised in-house using a published method and prepared by Andrew Nolan (Chhabra *et al.,* 1998). All other reagents were commercially available and used without further purification.

2.5.2 Free amine assays

Kaiser test

Mini reactions, on solid phase, were conducted to test for the presence of free primary amines as follows: *Reagent A* (3 drops) and *reagent B* (1 drop) were added to a small sample of resin (< 0.5 mg) in a small test tube. The mixture was heated to 100 °C for 2 min and the sample inspected. The intensity of the blue colour of the solution gives a qualitative indication of the presence of the free primary amine groups; a negative test is yellow.

Chloranil Test

Mini reactions, on solid phase, were conducted to test for the presence of free secondary amines as follows: *Reagents A* and *B* (3 drops of each) were added to a sample of resin (< 0.5 mg) in a small test tube. After brief mixing, the mixture was left at room temperature for 10 min and the beads inspected. The intensity of the colour change from yellow to blue gives a qualitative indication to the presence of the free secondary amine groups; a negative test remains yellow.

2.5.3 General methods

Peptide synthesis

Reactions were conducted in a polypropylene syringe fitted with a polyethylene porous frit. Heating was assisted by microwave radiation in a SP Wave (Biotage). Lysine(Dde) deprotection and coupling of dyes (and quencher) was achieved without microwave heating.

Resin

Peptides were prepared using standard Fmoc synthesis on H-Gly-Trityl-ChemMatrix resin (Sigma Aldrich, loading = 1.1 mmol/g) (Amblard *et al*., 2006). Note: 3 equivalents (eq) of reagents were used for coupling reactions (3.3 mmol of reagent/g of resin used).

Resin wash: On a vacuum manifold, the resin was isolated by filtration and washed with DMF (3 × 2*v/v*), dichloromethane (DCM, 3 × 2*v/v*) and MeOH (3 × 2*v/v*).

Swelling: The beads were swollen in (DCM, 10 min), the resin should not fill > 1/3 of the vessel.

Resin-peptide storage: After completed coupling and a standard *resin wash***,** an additional wash with ether (2 *v/v*) shrank the resin. This was then stored at -20 °C

2.5.4 Deprotection reactions

Fmoc deprotection

In the SP Wave the pre-swollen resin was treated with 20% piperidine in DMF (*v/v*) and vortexed (3 min) then washed with DMF (*v/v*). The resin was then treated again with 20% piperidine in DMF (*v/v*) and vortexed (10 min). After a *resin wash,* the presence of free amines was detected using an appropriate free amine test solid phase test.

Lysine Dde deprotection

Immediately before use the stock Dde deprotection solution was dissolved in DCM (1:5 DCM stock), added to the pre-swollen resin (2 *v/v*) and gently shaken (3 × 1 h) (Díaz-Mochón *et al*., 2004).

Deprotection of side chains and cleavage from the resin

Beads were stirred with a cleavage cocktail (TFA: DCM: TIS, 95: 2.5: 2.5) for 45 min (*v/v*), and the filtrate collected in a 25 mL falcon tube; the solvent was then evaporated under N_2 gas. Cold ether (10 mL) was then added to the remaining mixture to precipitate out the peptide; this solution was centrifuged 4500 rpm (2 min) to form a pellet. The supernatant was discarded and the solid washed a further 2 times with ether; the remaining solid was then purified by HPLC.

Amino acid (aa) and spacer coupling

To a solution of 8-(Fmoc-amino)-3,6-dioxaoctanoic acid (peg_2) or Fmoc-aa-OH (3 eq) in DMF, oxyma (3 eq) was added and stirred for 5 min. *N*,*N'*-Diisopropylcarbodiimide (DIC, 3 eq) was added to the mixture and stirred for a further 10 min. This solution was then added to the pre-swollen resin beads and the mixture heated and vortexed (75 °C, 5 min) in the SP wave microwave. After a *resin wash*, the completion of the couplings was confirmed by an appropriate free amine test on solid phase.

Fluorophore Coupling

Three equivalents of 5(6)-carboxyfluorescein (FAM) or 5(6)-carboxyrhodamine B (RhodB) or methyl red (MR) were dissolved in DMF (2*v/v*); coumarin 343 was dissolved in 1:1:3 dimethyl sulfoxide (DMSO): *N*-Methyl-2-pyrrolidone (NMP): DMF. To a fluorophore solution, oxyma (3 eq) was added and stirred for 5 min at room temperature. DIC (3 eq) was then added and the mixture and the solution stirred for 10 min. This solution was then added to the pre-swollen resin beads and the mixture stirred for 50 min at RT. Excess fluorophore was then washed off the resin as follows: 5(6)-carboxyfluorescein: 20% piperidine in DMF (× 10) followed by an appropriate number of *resin washes* until the filtrate was colourless. Coumarin 343 and MR: *resin wash* (× 4) or until the filtrate was colourless. 5(6)-carboxyrhodamine B: *resin wash* (× 4) followed by hexane wash (× 10), this was repeated until the filtrate was clear. Coupling was then confirmed using a *Kaiser test.*

2.5.5 FRET probe purification and characterisation

FRET probes were synthesised using standard solid phase Fmoc chemistry, purified by HPLC (ACN in water with (0.1% FA with a flow rate of 2 mL/ min. Compounds were characterised by MS and analytical HPLC (spectra/ traces in Appendix 2 and 3, respectively).

HS1-58 (12): (Coumarin343)-peg$_2$-PLGLEEA- peg$_2$-K(RhodB)G-OH

Semi-preparative HPLC. Gradient: 5 to 80% (20 min); Isocratic (1 min); gradient 80% to 5% (1 min). Collection at 254 nm. MALDI-TOF MS: calculated for $C_{97}H_{133}N_{15}O_{27}^{+}$ $[M]^{+}$ 1940.2, found 1940.14. Analytical HPLC (GE15ACN): 7.65 min. Yield: 1.06 mg, 560 nmol, 10%.

HS1-59 (13): (FAM)- peg$_2$-PLGLEEA- peg$_2$-K(RohdB)G-OH

Semi-preparative HPLC. Gradient: 5 to 95% (30 min); Isocratic (5 min); gradient 95% to 5% (5 sec) then isocratic (1 min). Collection at 495 nm, this allowed the isolation of the rhodamine 2 isomers. MALDI-TOF MS: calculated for $C_{102}H_{129}N_{14}O_{30}^+$ $[M]^+$ 2031.22 found 2031.68. Analytical HPLC (GE15ACN): 5.62 min. Yield of a single isomer: 0.38 mg, 188 nmol, 4%.

HS1-65 (14): (MR)-peg$_2$-PLGLEEA- peg$_2$-K(FAM)-G-OH

Semi-preparative HPLC. Gradient: 5 to 95% (25 min); Isocratic (5 min); gradient 95% to 5% (5 sec) then isocratic (1 min). Collection at 495 nm. MALDI -TOF MS: calculated for $C_{88}H_{113}N_{15}O_{27}Na$ $[M+Na]^+$ 1835.95 found 1835.6. Analytical HPLC (GE15CN): 7.45 min. Yield: 0.85mg, 468 nmol, 8%.

2.5.6 Absorption spectroscopy yield determination

Linear equations were derived from a plot of dye absorbance (Y) vs concentration ((X) μM) of probe. RhodB was used to quantify HS1-58 and HS1-59 due to the minimal absorbance of Coumarin 343 and 5(6)-carboxyfluorescein (FAM) at 546 nm, See Appendix 4.

Table 2.1 Experimentally-derived linear equations for FRET probe yield quantification.

Dye	Abs (nm)	Equation	R^2	Used to Quantify yields of:
RhodB	546	Y = 0.0054X+0.0821	1.00	HS1-58, HS1-59
FAM	495	Y = 0.0086X+0.0919	1.00	HS1-65

2.6 Synthesis of HS1-22

3-Nitrodibenzo[b,d]furan (15)

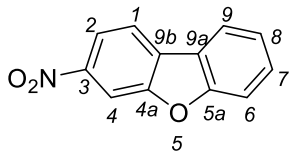

Experimental method was adapted from published by Keumi and colleagues (1991).

Dibenzofuran (5.00 g, 30.0 mmol) dissolved in TFA (200 mL) was cooled to -20 ˚C. Fuming nitric acid (>90% HNO_3, 1.7 g (1.3 mL), 27.0 mmol) in TFA (4 mL) was added dropwise into the dibenzofuran solution. After 1 h the reaction mixture was warmed to 0˚C and stirred for a further 3 h. Upon completion, the solution was warmed to room temperature and ice water (40 mL) added, and the resulting precipitate was collected by vacuum filtration. The solid was dissolved in DCM (30 mL), dried ($MgSO_4$), and the solvent removed under reduced pressure to give **15** as a yellow solid (5.2 g, 91% yield).

^{1}H NMR (500 MHz, d_6-DMSO) δ: 8.62 (d, *J* = 1.9 Hz, 1H, **4**), 8.42 (d, *J* = 8.5 Hz, 1H, **1**), 8.34 (dd, *J* = 8.4, 1.2, 0.7 Hz, 1H, **9**), 8.32 (dd, *J* = 8.5, 1.9 Hz, 1H, **2**), 7.83 (dt, *J* = 8.4, 0.7, 0.7 Hz, 1H, **6**), 7.69 (ddd, *J* = 8.4, 7.3, 1.2 Hz, 1H, **7**), 7.53 (ddd, *J* = 8.4, 7.3, 0.7 Hz, 1H, **8**). ^{13}C NMR (125 MHz, DMSO) δ: 157.8 (C, **4a**), 154.5 (C, **5a**), 146.6 (C, **3**), 130.2 (CH, **7**), 129.9 (C, **9b**), 124.3 (CH, **8**), 122.8 (CH, **2**), 122.1 (C, **9a**), 121.9 (CH, **1)**, 118.8 (CH, **9**), 112.3 (CH, **6**) 108.0 (CH, **4**). IR (neat), cm^{-1}: 3101 (aromatic C–H stretch), 1629 (aromatic C=C stretches), 1522 (N–O asymmetric stretch), 1359 (N–O symmetric stretch), 1198 (C–O aryl stretch). HRMS: (EI+) calculated for $C_{12}H_7NO_3$ 213.0420 $[M]^+$ found 213.0425 (δ 2.0 ppm). HPLC retention time: 9.91 min (GE15ACN).

7-Nitrodibenzo[b,d]furan-2-sulfonic acid (16)

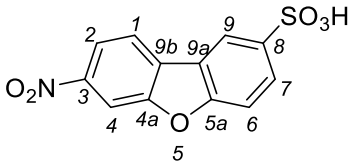

To a solution of **15** (0.50 g, 2.4 mmol) in DCM (15 mL), cooled to 0 ˚C, chlorosulfonic acid (0.20 mL, 300 mmol) was added dropwise. After 30 min, the reaction mixture was warmed to room temperature and stirred for 4 h. Upon completion the reaction mixture was cooled to 0 ˚C and the precipitate collected by filtration. This was dissolved in DCM:MeOH (1:5), dried ($MgSO_4$), and the solvent removed under reduced pressure to give a quantitative yield of **16**.

^{1}H NMR (500 MHz, d_6-DMSO, ppm) δ: 8.61 (d, *J* = 2.0 Hz, 1H, **9**), 8.57 (d, *J* = 1.8 Hz, 1H, **4**), 8.52 (d, *J* = 8.5 Hz, 1H, **6**), 8.29 (dd, *J* = 8.5, 2.0 Hz, 1H, **7**), 7.93 (dd, *J* = 8.6, 1.8 Hz, 1H, **2**), 7.77 (d, *J* = 8.6 Hz, 1H, **1**). ^{13}C NMR (125 MHz, DMSO, ppm) δ: 157.5 (C, **8**), 155.0 (C, **3**), 146.6 (C **4a**), 144.8 (C, **5a**), 129.9 (C, **9b**), 128.0 (CH, **7**), 122.2 (CH, **1**), 121.4 (C, **9a**), 120.0 (CH, **9)**, 118.8 (CH, **2**), 111.4 (CH, **6)**, 108.0 (CH, **4)**.

IR (neat), cm^{-1}: 3093 (aromatic C−H stretch), 2901 (SO−H broad stretch), 1631 (aromatic C=C stretches), 1546 (N−O asymmetric stretch), 1419 (S=O stretch), 1344 (N−O symmetric stretch), 1141 (C−O stretch). HRMS: (EI+) calculated for $C_{12}H_8NO_6S$ $[M+H]^+$ 294.0067 found 294.0067 (δ 0.0 ppm). HPLC retention time: 5.91 min (GE15ACN).

Tert-butyl D-valinate (17)

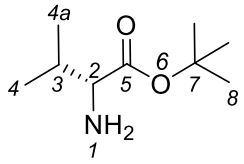

The synthesis was adapted from that published by (Chen and colleagues (2005), compound analysis data agree with literature values.

To a solution of D-valine (1.0 g, 8.5 mmol) in *tert*-butyl acetate (20 mL) at 0 ˚C, perchloric acid (1.2 mL, 13 mmol) was added dropwise. The reaction mixture was warmed to room temperature and stirred for 18 h. Upon completion the solution was washed with water (10 mL) and 1M HCl (10 mL). The aqueous fractions were combined and adjusted to pH 9 using K_2CO_3 (0.1 M). The basic solution was extracted with DCM (5 × 10 mL). The organic fractions were combined, dried over $MgSO_4$ and the solvent removed under reduced pressure to yield a clear oil of D-valine *tert*-butyl ester **17** (0.50 g, 40%).

^{1}H NMR (500 MHz, CDCl3) δ: 3.22 (d, *J* = 4.8 Hz, 1H, **2**), 2.04 (qqd, *J* = 6.9, 6.9, 4.8 Hz, 1H, **3**), 1.53 (s, 9H, **8**), 1.02 (d, *J* = 6.9 Hz, 3H, **4**), 0.98 (d, *J* = 6.9 Hz, 3H, **4a**).^{13}C NMR (125 MHz, CDCl3) δ: 175.1 (C, **5**) 82.4 (C, **7**), 61.2 (CH, **2**), 33.4 (CH, **3**), 28.3 (3(CH_3), **8**), 19.2 (CH_3, **4**), 17.9 (CH_3, **4a**). HRMS: (ESI+) calculated for $C_9H_{2o}NO_2$ $[M+H]^+$ 174.1489 found 174.1489 (δ 0.45 ppm).

D-valine, *N*-[[7-(hydroxyoxoammonio)-2-dibenzofuranyl]sulfonyl]-, 1,1-dimethylethyl ester (18)

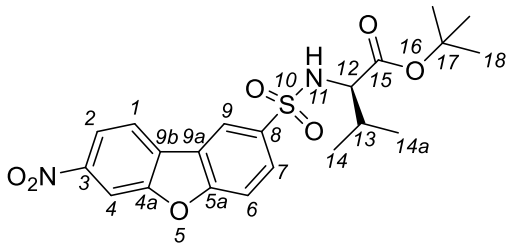

To a suspension of **16** 1.6 g, 5.0 mmol) in $SOCl_2$ (20 mL), DMF (10 drops) was added. The reaction mixture was refluxed at 80 ˚C for 1 h under N_2 atmosphere, then cooled to RT and stirred for a further 16 h. Excess $SOCl_2$ was removed from the filtrate under reduced pressure to give a green solid. To a solution of the green solid (1.7 g, 5.0 mmol) in dry DCM (20 mL), **17** (0.95 g, 5.0 mmol) was added and the reaction mixture stirred and cooled to 0 ˚C. This was followed by the slow addition of DIPEA (3.8 mL, 22 mmol), the reaction mixture was then warmed to RT stirred for 4 h. Upon completion the solvent removed under reduced pressure and the crude compound was purified by silica gel chromatography (20 – 30% EtOAc/ Hex) to yield a yellow solid **18** (1.9 g, 71%).

^{1}H NMR (500 MHz, $CDCl_3$, ppm) δ: 8.57 (d, *J* = 1.9 Hz, 1H, **9**), 8.50 (d, *J* = 1.5 Hz, 1H, **4**), 8.36 (dd, *J* = 8.5, 2.0 Hz, 1H, **2**), 8.13 (d, *J* = 8.5 Hz, 1H, **1**), 8.08 (dd, *J* = 8.7, 1.9 Hz, 1H, **7**), 7.75 (d, *J* = 8.7 Hz, 1H, **6**), 5.27 (d, *J* = 9.9 Hz, 1H, **11**), 3.72 (dd, *J* = 9.9, 4.5 Hz, 1H, **12**), 2.12 – 2.04 (m, 1H, **13**), 1.10 (s, 9H, **18**), 1.02 (d, *J* = 6.8 Hz, 3H **14**), 0.86 (d, *J* = 6.8 Hz, 3H **14a**). ^{13}C NMR (125 MHz, $CDCl_3$, ppm) δ: 170.4 (C, **15**), 160.1 (C, **8**), 156.0 (C, **3**), 147.8 (C, **4a**), 136.1 (C, **5a**), 129.1 (CH, **9b**), 128.7 (CH, **7**), 123.2 (C, **9a**), 122.3 (CH, **9**), 121.5 (CH, **1**), 119.5 (CH, **2**), 113.1 (CH, **6**), 108.6 (CH, **4)**, 82.6 (C, **17**), 61.6 (CH, **12**), 31.8 (CH, **13**), 27.7 (3(CH_3), **18**), 19.3 (**14**), 17.2 (**14a**). IR (neat), cm^{-1}: 3269 (N−H secondary amine) 3099 (C−H aromatic stretch), 1721 (C=O ester), 1571 and 1340 (N−O asymmetric and symmetric stretch), 1159 (S=O stretch). HRMS:(ESI+) calculated for $C_{21}H_{21}N_2O_7NaS$ $[M+Na]^+$ 471.1196 found 471.1182 (δ 3.1 ppm). HPLC retention time: 11.49 min (GE15ACN).

D-valine, *N*-[(7-amino-2-dibenzofuranyl)sulfonyl]-, 1,1-dimethylethyl ester (19)

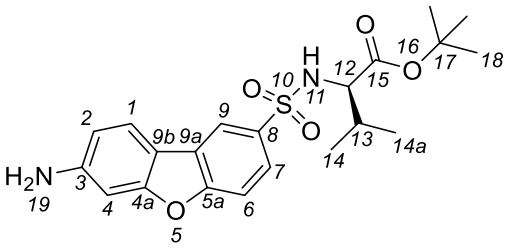

To a solution of nitro-aryl compound **18** (0.29 g, 0.12 mmol) in DCM (3 mL), zinc dust (0.2 g) was added with acetic acid (1.0 mL). The reaction was stirred for 1 h (30 °C); upon completion the reaction mixture was filtered through celtite and the solvent (and acetic acid) removed under reduced pressure. The crude material was purified by silica gel chromatography (50 % EtOAc/Hex) to afford a yellow solid **19** (0.23 g, 86%).

^{1}H NMR (500 MHz, $CDCl_3$) δ: 8.25 (d, *J* = 1.9 Hz, 1H, **9**), 7.79 (dd, *J* = 8.6, 1.9 Hz, 1H, **7**), 7.69 (d, *J* = 8.3 Hz, 1H, **1**), 7.50 (d, *J* = 8.6 Hz, 1H, **6**), 6.83 (d, *J* = 1.9 Hz, 1H, **4**), 6.71 (dd, *J* = 8.3, 1.9 Hz, 1H, **2**), 5.19 (d, *J* = 9.7 Hz, 1H, **11**), 4.04 (s, 2H, **19**), 3.68 (dd, *J* = 9.7, 4.5 Hz, 1H, **12**), 2.10 – 1.98 (m, 1H, **13**), 1.08 (s, 9H, **18**), 1.00 (d, *J* = 6.8 Hz, 3H, **14**), 0.85 (d, *J* = 6.8 Hz, 3H**, 14a**). ^{13}C NMR (125 MHz, $CDCl_3$) δ: 170.5 (C, **15**), 159.0 (C, **8**), 158.1 (C, **3**), 148.1 (C, **4a**), 134.2 (C, **5a**), 125.7 (C, **9a**), 124.6 (CH, **7**), 121.9 (CH, **1**), 119.3 (CH, **9**), 114.3 (C, **9b**), 112.2 (CH, **2**), 111.6 (CH, **6**), 97.4 (CH, **4**), 82.4 (C, **17**), 61.5 (CH, **12**), 31.9 (CH, **13**), 27.7 (3(CH_3), **18**), 19.2 (CH_3, **14**) 17.3 (CH_3, **14a**). IR (neat), cm^{-1}: 3467 and 3378 (N−H primary amine stretch); 3269 (N−H secondary amine stretch), 2966 and 2932 (C−H aromatic stretch), 1722 (C=O ester stretch) 1634 and 1603 (aromatic C=C stretches), 1132 (S=O stretch). HRMS: (ESI+) calculated for $C_{21}H_{27}N_2O_5S$ $[M+H]^+$ 419.1635 found 419.1628 (δ 1.71 ppm). HPLC retention time: 9.80 min (GE15ACN).

Tert-butyl *N*-({7-[(ethoxycarbonyl)amino]dibenzo[b,d]furan-2-yl}sulfonyl) -D-valinate (20)

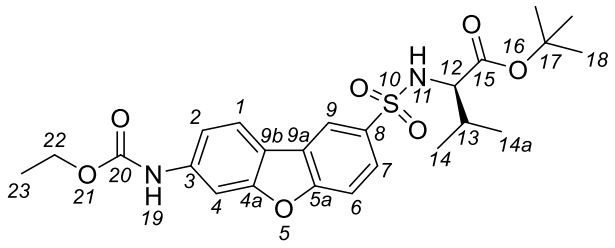

The aryl amine **19** (50 mg, 0.12 mmol) and ethyl chloroformate (13 μL, 0.13 mmol) were dissolved in 1.0 mL DCM followed by the addition DMAP (17 mg, 0.14 mmol). The solution was stirred at RT for 5 h then the reaction mixture as washed with H_2O (mildly acidic), dried ($MgSO_4$) and the solvent removed under reduced pressure to give **20** (36 mg, 61 %).

^{1}H NMR (500 MHz, $CDCl_3$) δ: 8.37 (d, *J* = 1.8 Hz, 1H, **9**), 7.89 (dd, *J* = 8.6, 2.0 Hz, 1H, **2**), 7.87 (d, *J* = 8.3 Hz, 1H, **6**), 7.61 (d, *J* = 8.6 Hz, 1H, **1**), 7.19 (dd, *J* = 8.3, 1.8 Hz, 1H, **7**), 6.82 (d, *J* = 2.0 Hz, 1H, **4**), 5.15 (d, *J* = 9.8 Hz, 1H, **11**), 4.28 (q, *J* = 7.1 Hz, 2H, **22**), 3.69 (dd, *J* = 9.8, 4.6 Hz, 1H, **12**), 2.10 – 2.02 (m, 1H, **13**), 1.35 (t, *J* = 7.1 Hz, 3H, **23**), 1.08 (s, 9H, **18**), 1.01 (d, *J* = 6.8 Hz, 3H, **14**), 0.86 (d, *J* = 6.8 Hz, 3H, **14a**). ^{13}C NMR (125 MHz, $CDCl_3$) δ 170.5 (C, **15**), 158.7 (C, **8**), 158.5 (C, **3**), 158.0 (C, **20**), 149.0 (C, **4a**), 137.3 (CH, **2**) 134.6 (C, **5a**), 125.7 (CH, **7**), 124.9 (C, **9a**), 121.4 (CH, **1**), 120.3 (CH, **9**), 118.3 (C, **9b**), 112.1 (CH, **6**), 108.8 (CH, **4**), 82.5 (C, **17**) 67.9 (CH_2, **22**), 61.5 (CH, **12**), 31.8 (CH, **13**), 27.7 (3(CH_3, **18**), 19.2 (CH_3, **14)**, 17.2 (CH_3, **14a**), 14.1 (CH_3, **23**). IR (neat), cm^{-1}: 3284 (N−H secondary amine stretch); 2968 and 2931(C−H stretch), 1719 (C=O ester stretch), 1602 and 1537 (aromatic C=C stretches), 1210 (C−O stretch), 1135 (S=O stretch) HRMS: (ESI+) calculated for $C_{24}H_{31}N_2O_7S$ 491.1847 $[M+H]^+$ found 491.1832 (δ 3.04 ppm). HPLC retention time: 11.05 min (GE15ACN).

N-({7-[(Ethoxycarbonyl)amino]dibenzo[b,d]furan-2-yl}sulfonyl)-D-valine (21)

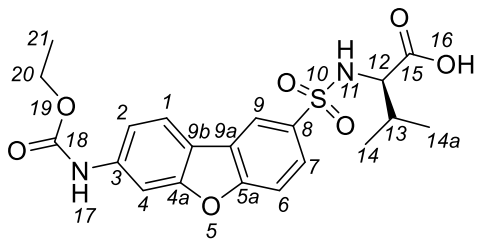

Compound is named HS1-22 in the subsequent chapters.

Compound **20** (44 mg, 0.090 mmol) was dissolved in 1.0 mL of DCM followed by the addition of TFA (1.0 mL), the resulting solution was stirred at room temperature for 1 h. Upon completion toluene (0.5 mL) was added to the mixture and solvent removed under reduced pressure. The crude sample was purified by preparative HPLC: 70 − 83% ACN (8 min) then 70% isocratic (1 min) collection detection at 254 nm. Fractions containing pure compound were combined and solvent removed under speed vacuum to give **21** (26 mg, 50%).

^{1}H NMR (500 MHz, MeOD,) δ: 8.47 (d, *J* = 1.8 Hz, 1H, **9**), 7.99 (d, *J* = 8.4 Hz, 1H, **1**), 7.98 (d, *J* = 1.7 Hz, 1H, **4**)**,** 7.93 (dd, *J* = 8.6, 1.8 Hz, 1H, **7**), 7.68 (d, *J* = 8.6 Hz, 1H, **6**), 7.37 (dd, *J* = 8.4, 1.7 Hz, 1H, **2**), 4.26 (q, *J* = 7.1 Hz, 2H, **20**), 3.66 (d, *J* = 4.6 Hz, 1H, **12**), 2.07 (m, 1H, **13**), 1.36 (t, *J* = 7.1 Hz, 3H, **21**), 1.00 (d, *J* = 6.8 Hz, 3H, **14**), 0.92 (d, *J* = 6.8 Hz, 3H, **14a**). ^{13}C NMR (125 MHz, MeOD,) δ: 173.1 (C, **15**) 159.6 (C, **8**), 159.2 (C, **3**), 155.9 (C, **18**), 141.5 (C, **4a**), 137.0 (C, **5a**), 126.8 (C, **9b**), 126.0 (CH, **7**), 122.4 (C, **9a**), 121.0 (CH, **1**), 119.2 (CH, **9**), 115.9 (CH, **2**), 112.7 (CH, **6**), 102.6 (CH, **4**), 62.1 (CH, **12**) 57.5 (CH_2, **20**), 32.6 (CH, **13**), 18.1 (CH_3, **14**), 17.4 (CH_3, **14a**), 14.9 (CH_3, **21**). IR (neat), cm^{-1}: 3326 (O−H) 3226 (N−H stretch); 3070 and 2964(C−H stretch), 1718 (C=O stretch), 1600 and 1547 (aromatic C=C stretches), 1246 (C−O stretch), 1167 (S=O stretch). HRMS: (ESI+) calculated for $C_{20}H_{22}N_2O_7NaS$ 457.10 found $[M+Na]^+$ 457.10 (δ 1.39 ppm). HPLC retention = 8.89 min (GE15ACN).

2.7 *In vitro* Förster resonance energy transfer (FRET) probe and inhibitor assays with recombinant enzymes

2.7.1 Materials

Compounds were tested against a panel of recombinant (r) catalytic (cat) domain MMPs (MMP_{cat}-1, 2, 3, 7, 8, 9, 10, 11, 12 and 13, Enzo Life Sciences). Full MMP-12 proteins were also purchased (recombinant human (rh) MMP-12 and recombinant murine (rm) MMP-12 (R&D systems) and activated prior to use. Neutrophil elastase (Elastin Products Company, Inc.) was diluted in PBS to the desired concentration. Inhibitors used were: marimastat (Tocris bioscience, R&D Systems, low molecular weight broad spectrum MMP inhibitor (Rasmussen & McCann 1997)), AZD1236 (donated by AstraZeneca, MMP-9 and 12 inhibitor) and HS1-22. **MMP activation**: amino-phenyl mercuric acetate (AMPA) (1 mM) was incubated with recombinant proteins (1 µM) in MMP buffer for 18 h (37 °C). MMP proteins were then diluted in MMP buffer to the desired concentration.

2.7.2 FRET probe plate assays

General protocol: In a 384 well plate 15 µL reactions we set up in triplicate as follows: enzyme (5 µL, 30 nM final concentration unless otherwise stated) and MMP buffer (5 µL) or inhibitor (various concentrations, 5 µL) were incubated (37 °C). Plates were then cooled to 0 °C followed by the addition of a FRET probe (made in house, 5 µL, 10 µM final concentration) and then immediately transferred to the plate reader. MMP buffer was used to replace components of the reaction mix to act as the corresponding controls. The plate reader was programmed to detect fluorescence from the probes. Data were exported in Microsoft Excel and analysed in PRISM; see figure legends in the results chapters for further details on study design and the statistical tests used (Section 2.3).

Enzyme activation of FRET probes

FRET probes were tested against MMP_{cat}-12 without inhibitors. Spectral fluorescence emissions of reactions were monitored after the addition of the probe in a plate reader (37 °C, at wavelengths in Table 2.2) until fluorescence intensity reached a plateau. The fold change in fluorescence was calculated.

Table 2.2 Wavelengths used for spectral scanning of FRET probes.

	Excited dye	Excitation (nm)	Emission detected (nm)
HS1-58	Coumarin 343	440	460–700
HS1-59	FAM	460	495–700
HS1-65	FAM	460	490–700

FRET Probe selectivity assay

The selectivity of FRET compounds was tested against a library of enzymes (MMP_{cat} -1, -2, -3, -7, -8, -9, -10, -11, -12, -13 and activated rh-MMP-12, rm-MMP-12, rh-neutrophil elastase). Enzymes were incubated with marimastat (200 nM final concentration) for 2 h at 37 ˚C. The plate was cooled, probe added and transferred to the plate reader set at 37 ˚C to detect fluorescence of the respective FRET probe dyes (Table 2.3). The reaction was allowed to procced for 2 h, the fold change in fluorescence was calculated.

Table 2.3 Excitation and emission wavelengths of FRET probes.

	Excited dye	Excitation (nm)	Emissions monitored for:
HS1-58	Coumarin 343	440	coumarin (490 nm)
HS1-59	FAM	485	FAM (528 nm),
HS1-65	FAM	485	FAM (528 nm)

IC_{50} assays for MMP inhibitors

Inhibitors (AZD1236, marimastat or HS1-22, 5 µL, 0.5-500 nM final concentration) and MMP_{cat}-12 were incubated in MMP buffer (37 °C, 1 h). The plate was then cooled to 0 °C before the addition of an MMP activity sensor probe (FAM-PEG2-G-P-K-G-L-K-G-K(MR)-NH2). Reactions were monitored in a plate reader (37 °C, ex = 495, em = 525, 1 h). Data were processed in PRISM; a scatter plot for each inhibitor was created (as log concentration *vs* log fluorescence) and analysed using a best-fit non-linear regression plot.

Inhibitor selectivity assays

Enzymes (MMP_{cat} -1, -2, -3, -7, -8, -9, -10, -11, -12 and -13; rh-MMP-12, rm-MMP-12 and rh-neutrophil elastase) were incubated with marimastat or HS1-22 (200 nM final concentration) for 2 h at 37 ˚C. The plate was cooled before the addition of HS1-65; this was then immediately transferred to the plate reader set at 37 ˚C to detect the fluorescence (Table 2.3). Data were analysed in PRISM by calculating the fold change in fluorescence.

2.7.3 MTT toxicity assay

The toxicity of compounds was assessed using the colorimetric MTT assay. HEK 293T cells were plated in a 96 well plate (approx. 1 × 106/ well) and incubated for 24 h (100 µL, 37 °C, 5% CO2) in Dulbecco's modified Eagle medium (DMEM) with added L-Glutamine (4 mM) and antibiotics (100 units/ mL of penicillin and 100 units/mL streptomycin) and heat inactivated fetal bovine serum (FBS,10%). HS1-22 was dissolved in sterile DMSO to give a 200 mM stock solution; this was diluted in media (1mM - 1 µM final concentrations). When the cells were > 80 % confluent, they were incubated with the drug for 20 h before removing the media and briefly washing the cells with PBS (100 µL). MTT ((3-(4, 5-dimethylthiazol-2-yl)-2,5-diphenyltetrazolium bromide) was dissolved in phenol-free DMEM to give a final

concentration of (0.5 mg/mL) and incubated will cells for 4 h (100 µL, 37 °C, 5% CO_2). The solubilising solution was added to the wells (100 µL) and the solutions gently mixed by pipetting up and down; the plate was then agitated until all of the formazan crystals had dissolved. The absorbance of formazan was measured at 570 nm using a plate reader. The "% viability" of cells was evaluated using background corrected absorption values; these were averaged for each treatment and compared. The data was analysed as described in Section 2.3.

2.8 Angiogenesis *ex vivo:* mouse aortic ring assay

The aortic ring assay is a popular quantitative *ex vivo* model of angiogenesis in which developing microvessels undergo many key features of angiogenesis, it has recently been reviewed by Baker *et al.*, 2012.

2.8.1 Materials

Medium, DMEM and Opti-MEM, was purchased from LONZA and the collagen type 1 (rat tail, Millipore) was used to make the gel. Drugs and growth factors were: marimastat (Tocris bioscience, R&D Systems) and VEGF (Sigma Aldrich) and HS1-22.

2.8.2 Collection of aortae

Mice (8 − 10 weeks) were sacrificed by a schedule one method (asphyxiation in CO_2) and the aorta carefully dissected out and washed in serum free medium (DMEM). At room temperature, using fine tools and a microscope, the peri-adventitial tissue was carefully removed and the aorta divided into 1 − 2 mm rings which were stored in fresh medium on ice until embedding.

2.8.3 Embedding and culture conditions

Under sterile conditions, gels were prepared using collagen and serum free medium (DMEM) to make a 1 mg/mL collagen solution; this was then re-basified with NaOH solution (1 M) and stored on ice until use. In 96 well plates, 1 aortic ring was embedded on its side in each well in 50 µL of collagen solution. This was then left at room temperature for 15 min before being transferred to an incubator (37 ˚C, 1 h) to solidify. Treatments were made in Opti-MEM (1% P/S) supplemented with 2% Foetal calf serum (FCS) for the first 3 days then VEGF (5 ng/mL)

for the rest of the experiment; to this MMP inhibitors were added (HS1-22 or marimastat, 25 μM)). Treatment was randomised to ensure the observer was blinded to the treatment during analysis. Treatments were added to embedded aortic sections (150 μL/ well) in triplicate and cultured (37 ˚C, 0.05% CO_2) for up to 7 days.

2.8.4 Quantification of angiogenesis

Images of aortic vessels were captured at × 20 magnification on D 3, 5 and 7 post embedding. The images from mice with different genotypes were randomised and angiogenesis was quantified by:

- Counting the number of sprouts and branches from the ring; the average value of the replicates was taken for each mouse.
- Quantifying the maximum vessel length. The length of the three longest vessels for each aortic ring was quantified using ImageJ. The freehand line drawing tool was used to measure the length of microvessels (in pixels); the average value of the replicates was taken for each mouse.

This data was analysed as described in Section 2.3.

2.9 Angiogenesis *in vivo:* subcutaneous sponge implantation assay

Subcutaneous sponge implantation allows the study of the components of the fibrovascular tissue that infiltrates the sponge compartment. The model was adapted from Andrade and colleagues (1987) and Small and colleagues (2005).

2.9.1 Materials

Sponges were cut from a larger sheet of polyurethane sponge (grade XE1700V, Caligen foam Ltd., UK) into 1 cm^3 cubes and sterilised by autoclaving. All surgical instruments and Michel Wound clips (7.5 × 1.75mm) (Fine Scientific Tools, UK) were sterilized by autoclaving prior to surgery; between animals, instruments were placed in a bead sterilizer for 10 seconds (sec), then allowed to cool. For drug studies, marimastat (Tocris Bioscience, R&D Systems) or HS1-22 were administered using a micro-osmotic pump (model 1004, Alzet) via a polyethylene catheter (0.76 mm diameter, Alzet).

Surgical procedure

Male C57Bl/6J or MMP-$12^{-/-}$ mice aged 8 − 10 weeks were weighed and anaesthetised by isoflurane inhalation with suitable analgesic cover (0.05 mg/Kg, Buprenorphine (Vetergesic)) by sub-cutaneous injection. The area around the scruff was shaved and disinfected with sterilizing iodine solution. A 1 cm incision was made into the skin between the shoulder blades and a subcutaneous tunnel made using blunt forceps to lift the skin from the back of the body. Two sponges were inserted into flank; one on the left and one on the right of the lower back (Figure 2.1). The incision was then closed with 2 − 3 Michel wound clips. The animal was allowed to recover and closely monitored for signs of infection for the following week. The metal clips were removed 10 days post-surgery once the wound had healed sufficiently.

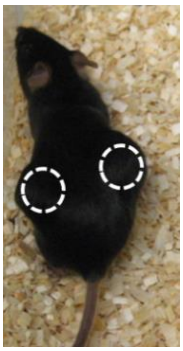

Figure 2.1 C57Bl/6J mouse post sponge implantation surgery, the dashed circles indicate the position of the sponges.

2.9.2 *In vivo* Matrix metalloproteinase inhibitor drug study

Mini pump preparation

Drugs were administered to mice at 150.6 nmol/mouse/day (marimastat: 2 mg/kg/day, HS1-22: 2.6 mg/kg/day) for 21 days (25 g mouse) in DMSO: propylene glycol: H_2O (1:1:1). Pumps were prepared under sterile conditions (see Appendix 1 for method). The pumps were primed by incubation in a saline solution (0.9% NaCl, 37 °C, 48 h) prior to surgery.

Surgical procedure

Immediately prior to surgery, the catheter was cut to approximately 1.5 inches, inserted into the centre of a sponge and glued in place with 1 drop of tissue adhesive (Vetbond, 3M). The surgical procedure was similar to that previously described for sponge implantation (Section 2.9.2). Briefly, male mice were anaesthetised and given analgesic cover before a dorsal subcutaneous tunnel was made. The sponge and the mini-pump were inserted, the catheter was then tucked in under the scruff and the incision closed with Michel wound clips. The mouse was allowed to recover and closely monitored for signs of infection or toxicity for the remaining experiment. The clips were removed 10 days post-surgery once the wound had healed sufficiently.

2.10 Fluorescence molecular tomography imaging

2.10.1 Materials

Imaging probes, MMPSense 750 FAST and Angiosense 680, and tissue mimic solution were purchased from PerkinElmer. The alfalfa free diet, Teklad 2914 maintenance diet, was from Harlan Teklad Laboratory. Hair was removed using depilitory cream (Veet, Reckitt Benckiser Group).

2.10.2 General FMT procedure

Further explanation of fluorescence molecular tomography (FMT) method and protocols are in Appendix 1. Briefly, mice were fed an alfalfa free diet for 10 days prior to imaging (Inoue *et al.*, 2008). Imaging agents were reconstituted, under sterile conditions, with PBS (1.2 mL/ vial); agents were combined (2.4 mL). With assistance from Gary Borthwick, 24 h prior to imaging the mice were warmed (30 °C, 15 min) and briefly anaesthetised and agent administered by intravenous tail vein injection (200 µL, containing 2 nmol of each agent or PBS as a control).

Imaging *in vivo*

Mice were anaesthetised (isoflurane for the duration of the experiment) and hair was removed from the chest and abdomen (clippers followed by depilitory cream). The mouse was positioned in the imaging cassette so that the tissue of interest was in the centre. The cassette was closed and placed in the FMT 2500 machine. The TrueQuant software was used to acquire the data (see Appendix 1). The mouse was then removed from the chamber and either allowed to recover or culled by a schedule 1 method, as required.

Imaging *ex vivo*

Once mice had been killed, sponges were removed and placed in a dish and covered with tissue mimic solution (PerkinElmer). The dish was placed in the imaging cassette and inserted into the FMT machine and the data acquired. After scanning, each sponge was gently cleaned in PBS, cut in half and either fixed in paraformaldehyde solution (24 h and then stored in 70% ethanol) or snap frozen on dry ice and subsequently stored at -80 ˚C.

Data acquisition

Using TrueQuant software, a database was created with subject (mouse) numbers and selected agents. A reflectance image was acquired onto which the scan field was drawn around the ROI to have < 50 laser source positions (Figure 2.2). The mouse was then scanned and data reconstructed into a 3D image.

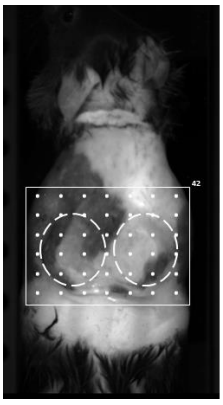

Figure 2.2 FMT2500 Reflectance image and ROI determination. The scan field (solid line) was drawn around the sponges (dashed circles, added here for clarity) with the maximum number of laser points (dots) limited to 50 (total on top right of scan field).

2.10.3 FMT data analysis

The fluorescent signal from within the sponges was reconstructed into a 3D image by the TrueQuant software.

In vivo imaging data analysis

Thresholds were set to eliminate the endogenous background signal found in the controls (those injected with PBS rather than agent): AngioSense 680 = 51 nM and MMPSense 750 = 39 nM. A ROI around each sponge was drawn using the cylindrical drawing tool, the X, Y and Z axis lengths were relatively well conserved for all *in vivo* analyses. The software converted the fluorescent signals, using a calibrated algorithm, into pmol of each reagent within the ROI. For each agent the average number of pmols detected from the two sponges was used to give a value for each mouse. These data were analysed as described (Section 2.3).

Ex vivo imaging data analysis

Thresholds were set to zero for both agents (no signal in controls) and an ROI was made with the cuboid drawing tool which captured all the signal detected. The software converted the fluorescent signals, using a calibrated algorithm, into moles (pmol) of each reagent within the ROI. For each agent the average pmols from the two sponges was used to give a value for each mouse. These data were analysed as described (Section 2.3).

2.11 *Ex vivo* FRET probe assays with tissue lysates

2.11.1 Quantification of total protein in tissue lysates

Tissue homogenisation

One half of the sponge was thoroughly homogenised in 1 mL of cold cell lysis buffer (Cell Signalling) or PBS using the ultra turrax homogeniser (IKA T10 Basic). Samples were then centrifuged at 13,000 rpm for 2 min and the supernatant transferred to a new Eppendorf tube. The sample was then centrifuged (13,000 rpm, 10 min) and the lysate supernatant transferred to a new Eppendorf and stored at -80 ˚C.

Total protein quantification

The total protein in the lysate samples was quantified colourimetrically using a Bradford's assay against bovine serum albumin (Fisher, ThermoScientific). Briefly, protein standards were made by serial dilutions (250, 125, 50, 25, 5 µg/mL) of the supplied BSA standard using the working reagent (50:1, Reagent A:B). In triplicate, each standard or unknown sample (25 µL) was mixed with the working reagent (200 µL) and the plate mixed thoroughly before incubation at 37 °C for 30 min. The plate was then cooled to RT and the absorbance measured at 562 nm on a plate reader (blank-corrected at 652 nm). A linear standard curve was constructed by plotting the average blank-corrected 562 nm measurement for each BSA standard vs. its concentration in µg/mL; the fit was deemed satisfactory if $R^2 < 0.98$. This was used to determine the protein concentration of each unknown sample. Tissue homogenate samples were standardised to 800 µg of protein using PBS.

2.11.2 Quantification of MMP-12 and TIMP-1 protein

The enzyme-linked immunosorbent assay (ELISA) assay method is explained in more detail in Appendix 1.

MMP-12 ELISA

MMP-12 protein concentrations (zymogen and active forms) in the sponge tissue lysates were quantified using an MMP-12 ELISA (CUSABIO) and the reagents and standards were prepared according to manufacturer's instructions. Standards were analysed in duplicate; tissue lysates (800 µg/mL) were diluted (1/400) and analysed in triplicate. Briefly, standards and samples were added to the appropriate wells and incubated (100 µL, 2 h, 37 °C). The liquid was removed and the biotin antibody was added (100 µL, 1 h, 37 °C). Wells were washed with wash buffer (3 × 200 µL, 2 min, 37 °C) and the plated inverted and blotted on clean paper towels. The horseradish peroxidase (HRP)-avidin antibody was added and incubated (100 µL, 1 h, 37 °C) and then the wells washed (5 × 200 µL, 2 h, 37 °C). The 3,3′,5,5′-tetramethylbenzidine (TMB) substrate was added to each well for (15-30 min, protected from light, 90 µL, 37 °C) before addition of the stop solution (50 µL, 2 h, 37 °C). The absorbance was measured at 450 nm and 540 nm using a microplate reader. Absorbance readings from 450 nm were subtracted from those at 540 nm for each well. A standard curve was constructed (x-axis: log concentration, y-axis: absorbance) and deemed acceptable if R^2 > 0.96. The MMP-12 concentrations in the replicate were calculated and the average calculated for each sample, the data were then analysed as described (Section 2.3).

TIMP-1 ELISA procedure

Tissue inhibitors of metalloproteinases (TIMP)-1 protein concentrations (zymogen and active forms) in the sponges were quantified using a TIMP-1 ELISA (Quantikine, R&D Systems). Standards were analysed in duplicate; tissue lysate samples (800 µg/mL) were diluted (1/50) and analysed in triplicate. Briefly the reagents and standards were prepared according to manufacturer's instructions. Assay diluent was added to each well (50 µL); standards and samples were added to the appropriate wells and incubated (50 µL, 2 h, 25 °C). The liquid was

removed, the wells washed with wash buffer (5 × 400 µL, 2 min, 37 °C), and the plate inverted and blotted on clean paper towels. Mouse TIMP-1 conjugate was added to each well and incubated (100 µL, 2 h, 37 °C). The liquid was removed, the wells were washed with wash buffer (5 × 400 µL, 2 min, 37 °C), and the plate inverted and blotted on clean paper towels. The TMB substrate was added to each well (30 min, protected from light, 100 µL, 37 °C) before addition of the stop solution (100 µL, 2 h, 37 °C). The absorbance was measured at 450 nm and 540 nm using a microplate reader. Absorbance readings from 450 nm were subtracted from those at 540 nm for each well. A standard curve was constructed (x-axis: log concentration, y-axis: absorbance) and deemed acceptable if $R^2 > 0.99$. The TIMP-1 concentrations in the samples were calculated and the mean of the reading taken. Data was then analysed as described (Section 2.3).

2.11.3 Zymography

Materials

All gels (12% Tris-Glycine gel with 0.05% casein), the colloidal blue stain, a *sharp* pre-stained protein standard, the XCell SureLock Mini-Cell and all buffers were purchased from the Novex range (Life Technologies) and used according to manufacturer's instructions.

Sample preparation and electrophoresis

12 well precast 12% Zymogram gels were prepared and loaded into the electrophoresis tank, which was then filled with Tris-Glycine SDS Running Buffer and cooled (4˚C). Tissue lysate samples were standardised to 1 µg/µL protein with 33.3% sample buffer in PBS. The samples (15 µL) and protein standard (10 µL) were loaded and electrophoresis started (4 ˚C, 120 min, 150 V).

Renaturing and development of gels

Gels were carefully removed from their casts (a note of the ladder position taken on clear plastic) and submerged in Zymogram Renaturing Buffer (1.5 h, 4 ˚C) with gentle agitation. The gel was then moved into Zymogram Developing Buffer (30 min, 4˚C, with gentle agitation), the buffer was refreshed and the gel allowed to develop (18 h, 37 ˚C).

Staining and imaging

The digestion of the gel was imaged using a colloidal blue staining kit, and the gel was submerged in the stain (4 h), followed by destaining in H_2O (17 h). Gels were digitally imaged using a scanner to create a TIFF file.

Densitometry image analysis

The TIFF files images were analysed by densitometry using Image J as described (Hu & Beeton 2010). Briefly, TIFF files were opened in Image J and visualised in black and white. The rectangular tool was used to select the first band (drawing a rectangle twice the height of the width) and selected as the first lane; this process was repeated for the other lanes. The software was then used to generate a profile plot of the regions of interests selected. The area of each plot was evaluated by drawing a straight line to form an enclosed area under the curve; this area is proportional to the extent of gel digestion. The quantitative value for the enclosed area was generated (using the wand tool) and was plotted. Gel digestion was directly related to MMP activity.

MMP-12 activity inhibition assays

For MMP inhibition studies, a gel was loaded with duplicated samples, loaded in a mirror image, and run as described above. The gel was removed from the cast, cut in half (resulting

in each half having the same sample arrangement) and incubated in denaturing buffer (1.5 h, 4 ˚C with gentle agitation). One half of the gel was then placed in developing buffer containing marimastat (50 µM), the other (control gel) was placed in drug free developing buffer. The subsequent protocol was the completed as described above.

2.11.4 FRET probe assays with tissue lysates

Plate assay with MMP inhibitors

In a 384 well plate, 15 µL reactions were prepared in triplicate: tissue lysates (D 3 − 35, 5 µL, final concentration 1.67 µg/µL) and marimastat (5 µL, final concentration 500nM; MMP buffer was used as a control) were incubated together (37 °C, 1 h). The plate was then cooled to 0 °C before HS1-65 was added (5 µL, final concentration 10 µM). Reactions were monitored in a plate reader (37 °C, ex = 495 nm, em = 525 nm, 2 h). Results were analysed as a fold change in the fluorescent signal (compared to HS1-65 with no treatment). The proteins in the tissue lysates were denatured (95 °C, 5 min and then cooled to 4 °C in a thermocycler) and used as a negative control; MMP_{cat}-12 (5 µL, 30 nM) was used as a positive control.

MS analysis of probe cleavage in tissue lysate

Tissue lysate reaction mixtures from plate assays were purified and concentrated using pipette tips containing C18 resin cartridges for reverse phase purification (Millipore Zip Tip® pipette tips, 10 µL). Briefly, tips were prepared by washing with ACN (1 × 5 µL) then H_2O with 0.1% TFA (2 × 10 µL). Sample was loaded by gently pipetting 10 µL of sample in and out of the cartridge 5 times. The cartridge was then washed with H_2O with 0.1% TFA (2 × 10 µL). Sample was eluted from the cartridge with 80% ACN in H_2O, 0.1% TFA (1 × 5 µL) into a clean vessel; filtrate was analysed by MALDI TOF MS.

Plate assay with protease inhibitors

In a 384 well plate, 15 µL reactions were prepared in triplicate: tissue lysates (D 3 − 35, 5 µL, final concentration 1.67 µg/ µL; MMP-12_{cat} (5 µL, 90 nM) was used as a positive control) were mixed with protease inhibitors, see **Table 2.4** (Sigma Aldrich, 5 µL, MMP buffer was used as a control) and then incubated (37 °C, 2 h). The plate was then cooled to 0 °C before the addition of HS1-65 (5 µL, final concentration 10 µM). Reactions were monitored in a plate reader (37 °C, ex = 495, em = 525, 2 h). Results were analysed as a fold change in the fluorescent signal (compared to HS1-65 with no treatment).

Table 2.4 Protease inhibitors used in the tissue lysate assay with HS1-65

Drug	Final Concentration
Sivelestat	100 µM
Antithombin III	400 nM
Protease cocktail block	1/3 stock solution

2.12 Immunohistochemistry

Tissue section preparation

Fixed tissues were embedded in paraffin and cut into 5 µm thin sections using a microtome. Tissue sections were floated on a water bath to smooth out creases and attached to Apex superior adhesive glass slides (Leica) and allowed to dry in an oven (30 °C, 24 h).

Hydration and dehydration of tissue sections

Before staining, slides were deparaffinised in xylene (2 × 5 min) and rehydrated though a series of ethanol solutions (100% 2 min, 100% 2 min, 95%, 1 min and 80% 1 min) and washed in H_2O. After non-fluorescent staining, slides were dehydrated through a series of alcohols (50% 2 min, 75% 1 min, 95% 1 min and 100% 1 min) and then mounted using DPX solution. After fluorescent staining, sections were washed and then mounted using permaflour mountant (Thermo Scientific).

2.12.1 Quantification of angiogenesis

Staining

Antigen retrieval was achieved by autoclaving rehydrated slides in citrate buffer (pH 6). Slides were then loaded onto Sequenza cassettes and washed with 0.5% BSA in PBS. Tissues were blocked in 10% donkey serum (1 h, RT) before addition of primary CD31 antibody (1 in 200, Rabbit anti mouse, ABCAM AB28364, 18 h, 4 ˚C). The excess primary antibody was washed away with 0.5% BSA in PBS followed by incubation with the secondary Alexa 488 conjugated antibody (donkey anti-rabbit, 1 in 1000, RT, 1 h, Sigma Aldrich) and alpha smooth muscle actin (α-SMA) antibody conjugated to Cy3 (rabbit anti-mouse, 1 in 1000, RT, 1 h). The excess antibodies were then washed off and the sections incubated with DAPI (1 in 1000, RT, 5 min) before a final thorough wash and then mounting.

Imaging and analysis

Slides were imaged at ×20 magnification, using the slide scanner, and the image files randomised. Files were viewed in Zen software and the total area of the section was measured using the line tool.

The images were analysed as follows:

1) The mean signal intensity across the whole area of tissue for the three fluorescent channels was measured using Zen software.

2) The area of signal was measured by creating 4 ROI (5000 × 5000 pixels) in vessel hot spots, for each channel (Figure 2.3a). Image J was then used to measure the % area covered by the signal in each ROI; the mean was taken of the 4 ROI for each signal per section.

3) The number of vessels was counted across the whole section; vessels were identified as green (CD31, Alexa 488) tubular structures with a black lumen possibly containing erythrocytes. Mature vessels were also counted; these were identified as those positive for CD31 and α-SMA (red). This was corrected for the area of the section analysed.

Data were unblinded and analysed as described in Section 2.3.

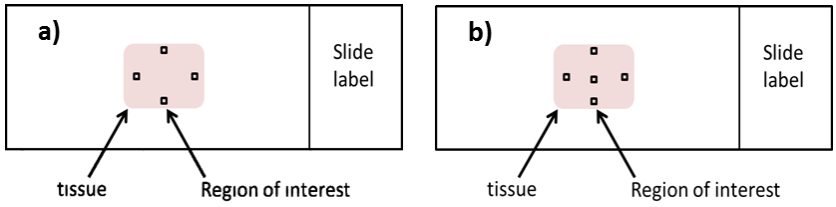

Figure 2.3. The areas where the ROIs were sampled from each section for image analysis. ROI were selected near the edge of the section in an area with no staining artefacts and saved as TIFF files: a) 1 ROI on each of the 4 sides of the section, b) 1 ROI on each of the 4 sides and 1 in the centre of the section**.**

2.12.2 Quantification of macrophage infiltration

Staining was performed by L. Boswell based at the Shared University Research Facilities (SuRF) within The Queen's Medical Research Institute.

F4/80 Immunohistochemistry

Staining was achieved using a staining robot (Leica Bond-III, leica Biosystems) and the Leica refine detection kit. Slides were rehydrated and treated with trypsin (0.5 mg/mL, 10 min at 37 ˚C) before being bathed in hydrogen peroxide (3 – 4%, 5 mins, RT) and then blocked in rat impress blocking serum (30 min, Vector labs). The F4/80 antibody was applied (eBiosciences, 1:300, 30 min) followed by an incubation with the ImmPRESS™ anti-rat Ig reagent (30 min, vector labs) which contains a "micropolymer" of a very active peroxidase coupled to an affinity-purified anti-rat IgG (H+L) secondary antibody. A solution of 3,3'-diaminobenzidine (DAB) was applied to the tissues (10 min), which were then counterstained with haematoxylin. Slides were dehydrated and mounted, as previously described.

Imaging and analysis

Slides were imaged using the slide scanner and image files randomised. Files were viewed in Zen software and images were analysed as follows:

1. The maximum depth of staining into the tissue was measured using the line tool.

2. The percentage area stained stain was measured by creating 4 ROI per section (3000 × 3000 pixel; Figure 2.3a). The percentage area of stain was measured by colour thresholding for the brown DAB stain using ImageJ. The percentage stain over the 4 ROI was averaged for each section.

Data was unblinded and analysed as described (Section 2.3).

2.12.3 Quantification of neutrophil infiltration

Staining with H&E

Rehydrated slides were washed with water and stained using Harris haematoxylin solution for 4 min and washed under running water for 1 min before 15 sec in acidified water and another rinse under running tap water. Slides were placed in Scott's tap water for 20 sec before a further rinse under tap water. Sections were counter stained in Eosin for 2 min, excess stain was washed off using running tap water. Slides were dehydrated and mounted as previously described.

Imaging and analysis

Slides were imaged at × 20 magnification using the slide scanner and image files randomised and viewed in Zen software. For each section, 5 regions of interest were selected (500 × 500 µm; Figure 2.3b). In each ROI the number of neutrophils was counted; the average number of neutrophils in the 5 ROIs was taken for each section, data were unblinded and analysed as described (Section 2.3).

2.12.4 Quantification of matrix deposition

Staining was performed by L. Boswell based at the Shared University Research Facilities (SuRF) within the The Queen's Medical Research Institute. All reagents are commercially available.

Staining with picro-sirius red

Rehydrated slides were washed with water and stained in the picro-sirius red solution for 3 h, briefly washed with water, dehydrated and mounted as previously described.

Imaging and analysis

Slides were imaged at ×20 magnification using the slide scanner and image files randomised and viewed in Zen software. Samples were analysed in 2 ways:

1. The maximum depth of staining into the tissue was measured using the line tool (μm).

2. The % stain was measured by creating 4 ROI per section (5000 × 5000 pixel, near the perimeter, Figure 2.3a). The % area of stain was measured by colour thresholding for the red stain using ImageJ. The % stain over the 4 ROI was averaged for each section.

Data were unblinded and analysed as described (Section 2.3).

2.13 Gene expression analysis

2.13.1 Materials

The RNeasy mini kit, QIAzol Lysis Reagent and the QuantiTect Reverse Transcription kit were all purchased from Qiagen. Tissues were homogenised using an ultra turrax homogeniser (IKA T10 Basic). UPL probes, Probes mastermix and Lightcycler water were from Roche Diagnostics. For quantification by real-time polymerase chain reaction (RT-qPCR) a light cycler 480 (Roche Diagnistics) was used.

2.13.2 Isolation of RNA from sponges

Ribonucleic acid (RNA) extraction from the tissue in the sponges was achieved using the RNeasy mini kit. Briefly, under strict RNAse free conditions, one half of a frozen sponge was homogenised in 700 µL of QIAzol (2 min) until the mixture was smooth. It was then split into 2 sterile 2 mL Eppendorfs (500 µL sample in each) and another 350 µL of QIAzol added to each. The samples were then homogenised (1 min) and left to rest (5 min, RT). Subsequently chloroform (200 µL) was added to each and mixed (not vortex) and left to stand (2 min) at RT. Samples were spun (12,000 × g, 4 ˚C, 15 min) and the aqueous fractions from the same sample were combined (if there was only a little aqueous phase and a large white colloidal phase, QIAzol (200 µL) was added and the sample mixed and spun again), this totalled approximately 1 mL/ sponge sample. Ethanol (70%, 1 *v/v*) was added to the aqueous phase and mixed well by pipetting. The sample (700 µL) was loaded on to an RNeasy Mini spin column, placed in a 2 mL collection tube, and centrifuged (8000 × g, 15 sec), the flow through was then discarded; this was repeated until all the sample was loaded. Buffer RW1 (700 µL) was loaded onto the column and centrifuged (15 sec 8000 × g), the flow through was then discarded. Buffer RPE (500 µL) was loaded onto the column and centrifuged (15 sec, 8000 × g), the flow through was then discarded. Buffer RPE (500 µL) was loaded onto the column and centrifuged (2 min, 8000 × g), then the flow through was discarded. The column was

placed in a new 1.5 mL collection tube and the RNA was eluted out with different volumes of RNAse free water depending on the sample collection time (Table 2.5). RNA concentration and quality by 260/280 nm ratio was determined using Nanodrop. RNA integrity was determined by Gel Red agarose gel electrophoresis for the integrity of the abundant ribosomal RNA fragments. RNA was stored at -80 ˚C.

Table 2.5 Volumes of RNase free water required to elute RNA from different time point samples (days, D) from the spin column.

Sample collected (D)	Volume of RNAse free water to wash column (µL)	
	1st elution	2nd elution
3 and 7	40	Reuse flow though
14, 21, 28 and 35	30	30

2.13.3 Preparation of cDNA

Complementary deoxyribonucleic acid (cDNA) synthesis was performed using a QuantiTect Reverse Transcription Kit and used according to the manufacturer's instructions. Briefly, genomic DNA was removed by incubating the RNA sample (500 ng) with gDNA Wipeout buffer (42 °C, 2 min). Then reverse transcription was performed using a reaction master mix. Per 500 ng of RNA, master mix consisted of: Quantiscript Reverse Transcriptase (1 µL), Quantiscript Reverse Transcription buffer (4 µL) and Quantiscript Reverse Transcription primer mix (1 µL) adjusted to a total volume of 20 µL with RNase free water. Negative controls for cDNA reactions were also performed: 1) without the addition of the reverse transcriptase as a control for DNA contamination; 2) without the addition of RNA as a control for transcription kit/ processing contamination. Samples were incubated (42 °C for 15 min, then 95 °C for 3 min and cooled to 4 °C) using a thermocycler and then stored at -20 ˚C. The cDNA was diluted 1 in 40 with RNase free water before performing RT-qPCR.

2.13.4 Primers and genes

Primers were purchased from Invitrogen Life Technologies. Primers (Table 2.6) were designed to match intron spanning probes within the Roche Universal Probe Library (UPL). PubMed nucleotide gene resources was utilised with the online software, UPL assay design centre by Roche. The program assigns primers to give a melting temperature between 59-60 ˚C, intron spanning, a molecular weight between 6100 and 7100 µg/µmol and assigns a corresponding UPL probe.

(https://lifescience.roche.com/shop/CategoryDisplay?catalogId=10001&tab=Assay+Design+Center&identifier=Universal+Probe+Library&langId=-1).

2.13.5 Real-time quantitative polymerase chain reaction

The RNA transcript levels of genes were assessed by RT-PCR. A standard curve was constructed using pooled cDNA (2 µL of cDNA from every sample excluding the negative controls). This was subsequently diluted 1/8 with PCR water, followed by serial half dilutions to give 1/16, 1/32, 1/64, 1/128, 1/256, 1/512.

Reactions (10 µL) were performed in triplicate on a 384 well plate. Each reaction contained: 6 µL LightCycler® 480 Probes Master; 2.7 µL RNase free water; 0.1 µL of the forward primer; 0.1 µL reverse primer; 0.1 µL of the UPL probe assigned to the designed gene primers and 2 µL of the sample cDNA.

Reactions were incubated in the light cycler using the following programme: 95 ˚C for 5 min followed by 50 cycles of 95 ˚C for 10 sec, 60 ˚C for 30 sec. Reactions were then incubated at 40 ˚C for 30 sec. Once the programme was complete, sample results were analysed in triplicate using the absolute quant/ 2nd derivative max setting on the light cycler. A standard curve was constructed using the pooled cDNA (x axis = concentration, y axis = crossing point (Cp)), an

efficiency between 1.8 and 2.1 was optimal. Triplicates were deemed acceptable if the standard deviation of their Cp was less than or equal to 0.5 cycles. One replicate could be removed per sample to improve standard curve efficiency or to reduce variation within sample replicates.

Table 2.6. Primer sequences for RT-PCR. Invitrogen custom primers for housekeeping genes and genes of interest

Gene symbol (full name)	Accession number	Primers		UPL #
		Forward	Reverse	
MMP-12 (Matrix metalloprotease 12)	NM_008605.3	ttgtggataaacactactggaggt	aaatcagcttggggtaagca	51
MMP-13 (Matrix metalloprotease 13)	NM_008607.2	tggaccttctggtcttctgg	ggcatccccaccatagttt	79
MMP-2 (Matrix metalloprotease 2)	NM_008610.2	taacctggatgccgtcgt	ttcaggtaataagcacccttgaa	77
MMP-9 (Matrix metalloprotease 9)	NM_013599.2	cagaggtaacccacgtcagc	gggatccaccttctgagactt	7
MMP-10 (Matrix metalloprotease 10)	NM_019471.2	gagtctggctcatgcctacc	caggaataagttggtccctga	81
Actβ (Beta Actin)	NM_007393.3	ctaaggccaaccgtgaaaag	accagaggcatacagggaca	64
GAPDH (Glyceraldehyde 3-phosphate dehydrogenase)	NM_008084.2	tgtccgtcgtggatctgac	cctgcttcaccaccttcttg	80
TBP (TATA box binding protien)	NM_01368.3	gatgggaattccaggatgtca	gggagaatcatggaccagaa	97
18S rRNA (18S ribosomal RNA)	AY248756.1	ctcaacacgggaaacctcac	cgctccaccaactaagaacg	77
CD31 (cluster of differentiation 31)	NM_001032378.1	cggtgttcagcgagatcc	actcgacaggatggaaatcac	45
HIF1α (hypoxia inducible factor 1, alpha subunit)	NM_010431.2	gcactagacaaagttcacctgaga	cgctatccacatcaaagcaa	95
PDGFRβ (platelet derived growth factor receptor, beta polypeptide)	NM_008809.2	tgcagagacctcaaaaggtg	cctgatcttcctcccagaaa	63
Thbs1 (thrombospondin-1)	NM_011580.3	cacctctccgggttactgag	gcaacaggaacaggacaccta	22
VECAD (vascular endothelial cadherin (Cdh5))	NM_009868.4	gttcaagtttgccctgaagaa	gtgatgttggcggtgttgt	56
Vegfa (vascular endothelial growth factor A, transcript variant 2)	NM_009505.4	gcagcttgagttaaacgaacg	ggttcccgaaaccctgag	4
VWF (von Willebrand factor)	AY208897.1	ccaaggagggtctgcaact	aaaggaagactctggcaagcta	15
TNFα (Tumour necrosis factor α)	NM_013693.2	ttgagatccatgccgttg	ctgtagcccacgtcgtagc	25

2.13.6 Reference genes and analysis

The sponge does not contain any endogenous biological tissue when implanted and the subsequent cell populations present within the sponge varied depending on the time point investigated. Therefore, it was beneficial to investigate for genes with stable expression despite the changing cell population to use as reference genes to normalise against. The housekeeping genes investigated in this project were βActin (βAct), glyceraldehyde-3-phosphate dehydrogenase (GAPDH), ribosomal 18s (rRNA18s) and TATA-binding protein (TBP). RT-qPCR for these genes was run with the samples from different groups (D 3, 7, 14 and 21). The Microsoft Excel plug-in "NormFinder" was used to assess the variation in expression between groups (Andersen *et al.*, 2004). The average of TBP and GAPDH had least variation between the groups and was used in this study to normalise expression from genes of interest (Table 2.7). Furthermore, the samples from D 3 had minimal gene expression that could not be compared to that of samples collected on D 7, 14 and 21. For each sample the gene of interest transcript expression was normalised against the reference genes (TBP and GAPDH); this value was analysed as described in Section 2.3

Table 2.7 The recorded stability values for samples taken over D 7, 14 and 21.

Gene name	Stability value			
βAct	0.483		**Best gene**	TBP
rRNA18s	0.551		**Stability value**	0.254
TBP	0.254			
GAPDH	0.408		**Best combination of two genes**	TBP + GAPDH
			Stability value for best combination	0.206

Chapter 3

Synthesis and *In vitro* Testing of MMP-12 Targeting Compounds

3 Chapter 3: Synthesis and *In Vitro* Testing of MMP-12 Targeting Compounds

3.1 Introduction

The extracellular matrix (ECM) is the structural connective tissue between cells which helps give tissue its structure, it also enables basic cellular behaviour such as cell division (Hynes, 2009). Structural changes in the ECM are also required for vascular remodelling (Liu *et al*., 2006) with matrix metalloproteinases (MMP) required for the breakdown of the ECM. An increase in MMP-12 mRNA, protein expression and protease activity has been associated with the progression of vascular disease pathology (Longo *et al*., 2005; Liang *et al*., 2006). MMP-12 has also been suggested to be anti-angiogenic (Li *et al*., 2012). Tools to enable the interrogation and real-time assessment of MMP-12 activity could lead to a better understanding of its precise role in angiogenesis and disease pathogenesis. Furthermore, molecular imaging of MMP-12 could facilitate real-time drug engagement studies, assessment of disease progression and *in vivo* and *ex vivo* surgical guidance (Figure 1.14).

In this chapter, two molecules were synthesised to target MMP-12. Firstly, an MMP-12 selective FRET probe (discussed in detail in Section 1.5.4); secondly an MMP-12 inhibitor (MMP-12 selective inhibitors are discussed in Section 1.6.4). These molecules have the potential to be used to monitor MMP-12 activity and to test the effects of MMP-12 activity in tissue samples undergoing angiogenic remodelling.

3.2 Hypothesis and aims

3.2.1 Hypothesis

Molecules can be synthesised in-house to aid investigation into the roles of MMP-12 in biological systems.

3.2.2 Aims

1. To synthesise a small molecule MMP-12 inhibitor based on those described by Li and colleagues (2009). This molecule will be tested *in vitro*, for selectivity against a panel of MMPs and for potency against MMP-12.

2. To synthesise a small family of MMP-12 selective FRET imaging probes based on those made by Cobos-Correa and colleagues (2009). These will be tested *in vitro* for selectivity against a panel of MMPs.

3.3 Methods

3.3.1 MMP-12 inhibitor HS1-22 (21)

Synthesis

The synthesis of the MMP-12 inhibitor was adapted from compounds MMP408 and LiMMPI-12 (Section 1.6.4) described by Li and colleagues (2009). The MMP-12 inhibitor, HS1-22, differed from LiMMPI-12 by changing a methyl to an ethyl group on the carbamate moiety. HS1-22 was built in 6 synthetic steps from commercial reagents. The experimental procedures are detailed in Section 2.6.

In vitro assays to test the selectivity, potency and toxicity of HS1-22

The inhibition selectivity of HS1-22 was tested against a panel of recombinant (r) MMP catalytic domains (MMP_{cat}). The IC_{50} of HS1-22 with MMP_{cat}-12 was tested against marimastat and AZD1236 (MMP- 9 and 12 inhibitor). The toxicity of HS1-22 was tested using an MTT assay. These assays are described in Section 2.7.

3.3.2 MMP-12 activity FRET probes

Synthesis

FRET probes were synthesised using standard solid phase peptide synthesis (SPPS) using the Fmoc strategy as described in Section 2.5.

Quantification of FRET probes

As less than 1 mg of each FRET probe was synthesised, yield determination by weighing the masses was challenging. Therefore, standard curves of the associated dyes were created. The absorbance of the FRET probes was measured, and then using the standard curve, used to calculate the mass of FRET probe synthesised (as described in Section 2.5 and Appendix 4).

Selectivity of FRET probes

The activation of the FRET probes was tested initially against MMP_{cat}-12 and the fluorescence emission monitored over time. The peptide sequence PLGLEEA was tested as a substrate for MMP-12 against a panel of recombinant MMP catalytic domains as described in Section 2.7.

3.3.3 Statistics

Data were analysed, firstly by checking for outliers and then using appropriate statistical tests as described in Section 2.3.

3.4 Results and discussion

3.4.1 Synthesis of HS1-22

The synthesis of HS1-22 (**21**) was completed in 6 steps, starting from commercially available dibenzofuran (**22**) (Scheme 3.1).

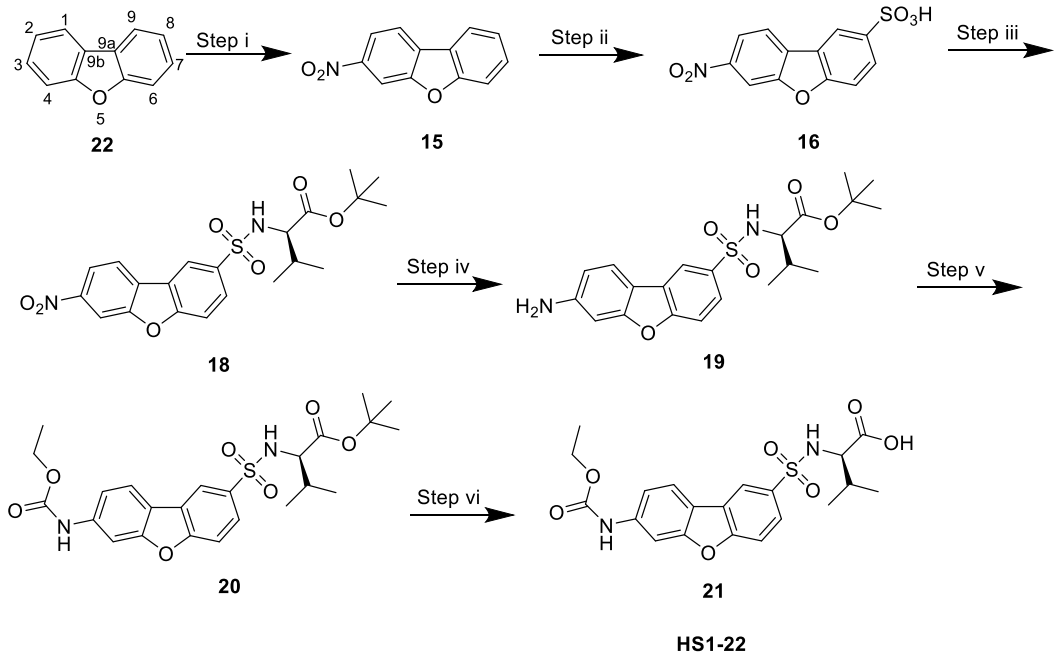

Scheme 3.1 Synthetic route for HS1-22. Step i) Nitration: HNO_3, TFA, -20 °C, 4 h, 91%; Step ii) Sulfonation: SO_3HCl, DCM, 0 °C, 4 h, quantitative; Step iii) a) Chlorination: $SOCl_2$, reflux, 18 h, quantitative, b) Sulfonamide formation: *t*-butyl D-valine, DIPEA, DCM, 0°C, b) 4 h, RT, 55%; Step iv) Nitro reduction: Zn dust, acetic acid, THF, RT 86%. Step v) Carbamate formation: Ethylchloroformate, DIPEA, 5 h, RT, 61%. Step vi) TFA : DCM (1:1), 1 h, RT, 50%.

Step i) Nitration of Dibenzofuran

The synthesis started with the selective nitration of the dibenzofuran **22** at the 3' position, this was achieved with fuming nitric acid (HNO_3, > 90%) in trifluoroacetic acid (TFA) to give 3-nitrodibenzofuran **15** in 91% yield (Scheme 3.2).

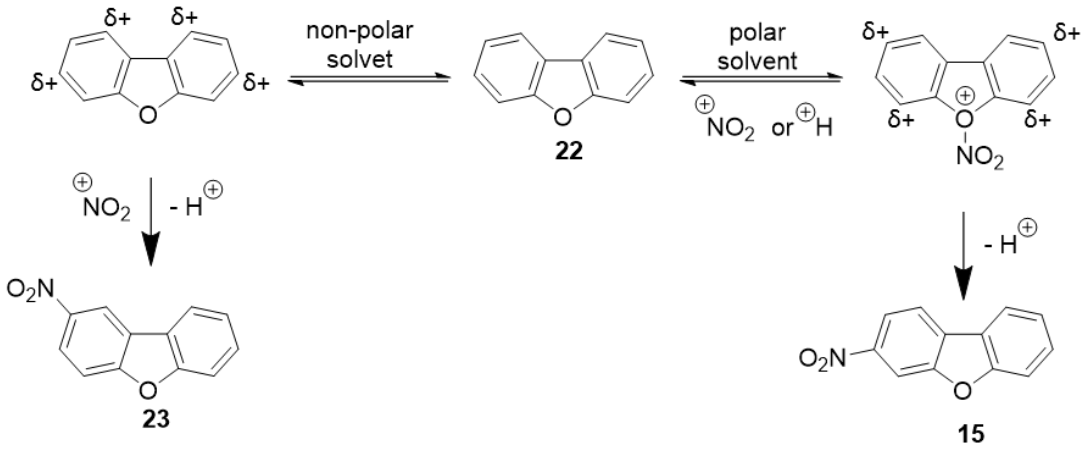

Scheme 3.2 Nitration of the dibenzofuran (22) with the nitronium ion derived from nitric acid. The nitronium ion (Equation 3.1) can coordinate to the oxygen on the furan ring, this is stabilised in more polar solvents (solvent with a high ε). The coordinated ion donates a positive charge into the ring system which directs the nitronium attack to the 3' (**15**) over the 2' (**23**) position.

The dibenzofuran (**22**) ring system reacts through electrophilic aromatic substitution; the first aromatic substitution reaction with nitric acid (to give **15**) was exothermic. The resulting nitrated tricyclic ring system is deactivated towards a second reaction as electron density is withdrawn by the nitro group. Furthermore, reaction conditions were disadvantageous for a second reaction due to excess of **22** and the low reaction temperature. Traditionally electrophilic aromatic substitution reactions with dibenzofuran are favoured at the 2' position (*para* to the oxygen) over the 4' position (*ortho* to the oxygen) owing to the effect of the furan ring (**23**). Conversely, for nitration reactions the 3' position is favoured but interestingly, the substitution position is solvent dependent: TFA favoured the 3' position (≥ 93%) whereas Ac_2O favoured the 2' position (≥ 39%) (Keumi *et al*., 1991). The reaction is dependent on the nature of HNO_3 reacting species in the organic solvents; this is thought to be a nitronium (NO_2^+) species stabilised by the nitrate ion (NO_3^-), (Equation 3.1).

$$2HNO_3 \rightleftharpoons NO_2^+ + NO_3^- + H_2O$$

Equation 3.1 The ionisation of nitric acid in an organic solvent.

Although the exact mechanism is unclear, it is suggested by Keumi and collegues (1991) that preferential formation of the 3' isomer was less dependent on the pH of the solvent than on its dielectric constant (ε); solvents with a higher ε (higher polarity) stabilized the nitronium ion (NO_2^+). The nitronium ion is suggested to coordinate with the oxygen on **22** and then rearrange to the 3' position to give **15**. The conversion of **22** was > 90% by NMR and was purified by silica gel chromatography. The regioselectivity was confirmed using 2D NMR experiments (correlation spectroscopy (COSY, proton-proton), heteronuclear single-quantum correlation spectroscopy (HSQC, proton-carbon) and heteronuclear multiple-bond correlation spectroscopy (HMBC, long range correlations)) (raw data not presented).

Step ii) Sulfonation of 3-Nitrodibenzofuran

Traditionally in sulfonation reactions, sulfur trioxide is used as the electrophile, which is generated from concentrated sulphuric acid (at > 80 °C). However, chlorosulfonic acid is now a more popular choice; chlorine acts as a good leaving group in this reagent, so is reactive in milder conditions. Compound **15** was sulfonated by a dropwise addition of chlorosulfonic acid in $CHCl_3$ to give compound **16** in quantitative yield. This electrophilic aromatic substitution reaction with compound **15** was directed to the 8′ position by the electronic properties of the nitro group (Scheme 3.3); i) the nitro deactivates the ring it is bound to and makes the opposite ring more attractive to substitution, ii) the oxygen in the furan ring is *para* directing. Double sulfonation of **15** was aided by the nature of the reagents and the experimental set-up. Firstly, the rings are deactivated by the nitro group present and are further deactivated by the sulfonic acid group after the first addition. Secondly, experimentally a second reaction was avoided by:

i) conducting the experiment at low temperatures and, ii) using a low ratio of reagents (1:1.3, **15:** chlorosulfonic acid). The regioselectivity and number of substitutions was confirmed using 2D NMR experiments (COSY (proton-proton), HSQC (proton-carbon), HMBC (long range correlations), raw data not presented). This reaction produced a quantitative yield of 3-nitro-8-sulfonyldibenzofuran **16** which was taken onto the next step without further purification.

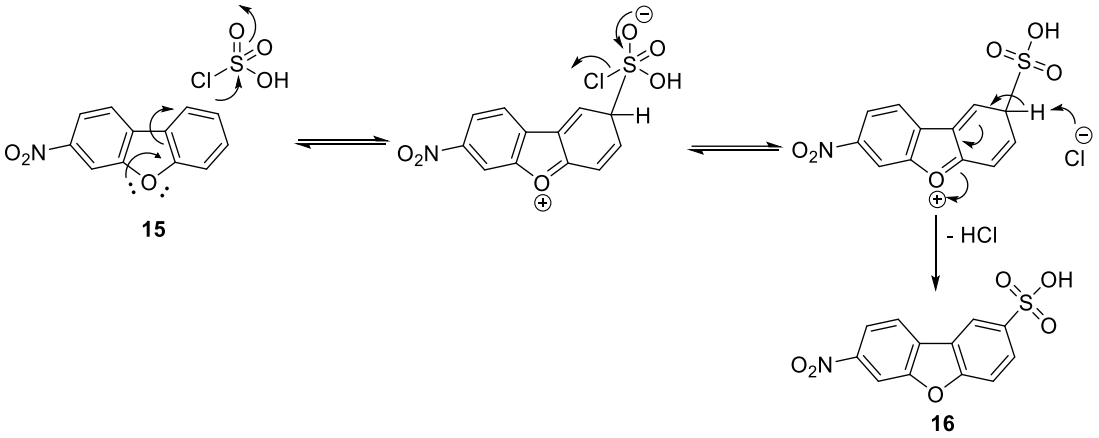

Scheme 3.3 Mechanism of sulfonation of compound 15 with chlorosulfonic acid to give 16. The electrophilic aromatic substitution reaction is directed to the 8' position by the electronic properties of the nitro group and the oxygen; the oxygen is *para* directing but the nitro group deactivates the ring it is bound to and makes the opposite ring more attractive to substitution.

Step iv) *t*-butyl Protection of D-Valine and Sulfonamide Coupling

The next stage of the synthesis was to react the aryl sulfonic acid with an amine on the D-valine to form the sulfonamide. The carboxylic acid on the D-valine **24** needed to be protected (made chemically unreactive) in this and subsequent reactions to allow chemoselectivity. It was, therefore, protected with a *t*-butyl group. Many L amino acid (L-aa) enantiomers are commercially available with the carboxylic acid (which would form part of the peptide backbone) protected with a *t*-butyl ester, but the commercially available D-aa enantiomer

equivalents are rarer. Therefore compound **24** was functionality protected with a *t*-butyl ester in-house; **24** was reacted with *t*-butyl acetate and perchloric acid to give **17**, this was purified by an acid-base extraction and used without further purification (40%, Scheme 3.4) (Chen *et al*., 2005). Notably, the *t*-butyl methyl groups were observed as a singlet (9 H) by ^{1}H NMR spectroscopy, whereas the aa sidechain methyl groups were observed as two sets of doublet peaks (3H) (Figure 3.1).

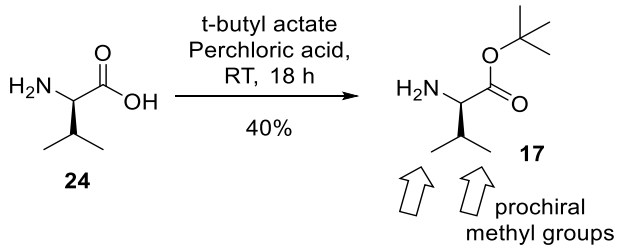

Scheme 3.4 Protection of the acid using a *t*-butyl group. The D-valine carboxylic acid was protected with a *t*-butyl group by a reaction with *t* butyl acetate and perchloric acid at room temperature overnight to give *t*-butyl D valinate.

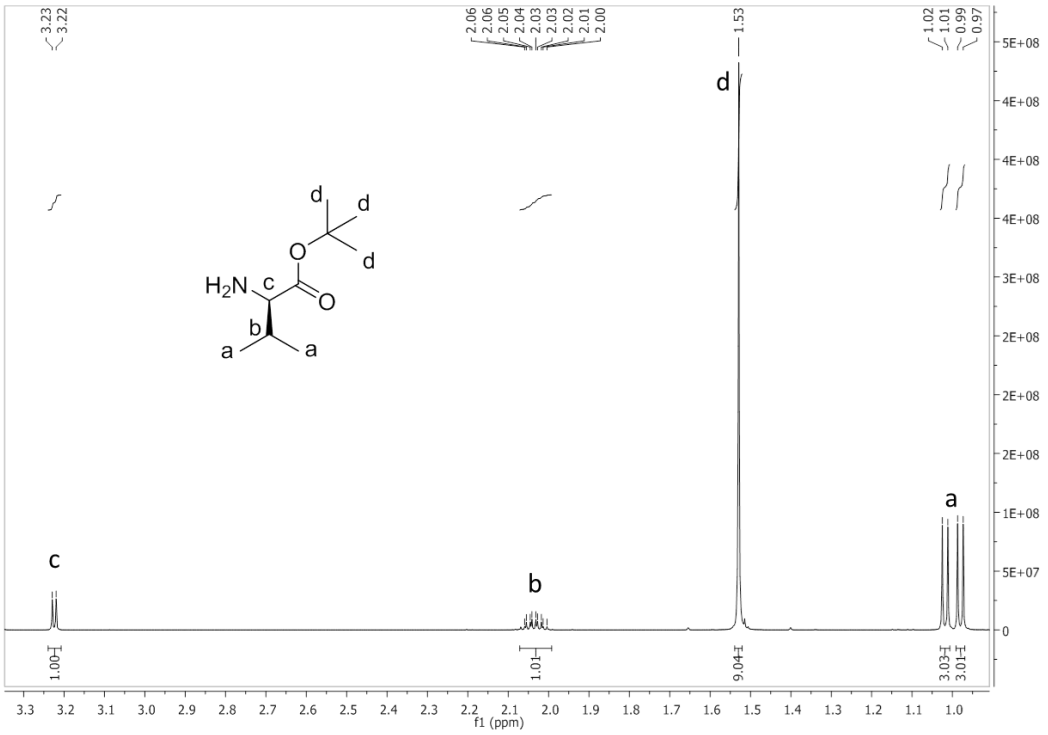

Figure 3.1 ^{1}H NMR spectrum of *t*-butyl D-valine (24). The *t*-butyl methyl groups were observed as a singlet δ 1.5 ppm, whereas the D-valine sidechain methyl groups were observed as two sets of doublet peaks (3H), δ 1.02 -0.97 ppm. The two sets of doublets were observed, not as a result of a racemic mixture, but because of the diastereotopic nature of the methyl groups. The chemical non-equivalence of the methyl groups results in the splitting of apparently identical methyl groups in the (^{1}H and ^{13}C) NMR spectrum.

The sulfonic acid **16** was converted to the sulfonyl chloride **25** using thionyl chloride and a catalytic volume of DMF. Compound **16** was insoluble in thionyl chloride but compound **25** was soluble, making monitoring of the reaction simple. This conversion was not analysed by NMR or MS due to rapid hydrolysis during the analytical process; therefore, solid IR spectroscopy was used to monitor the loss of the S–OH bond around 2901 cm^{-1} (Figure 3.2).

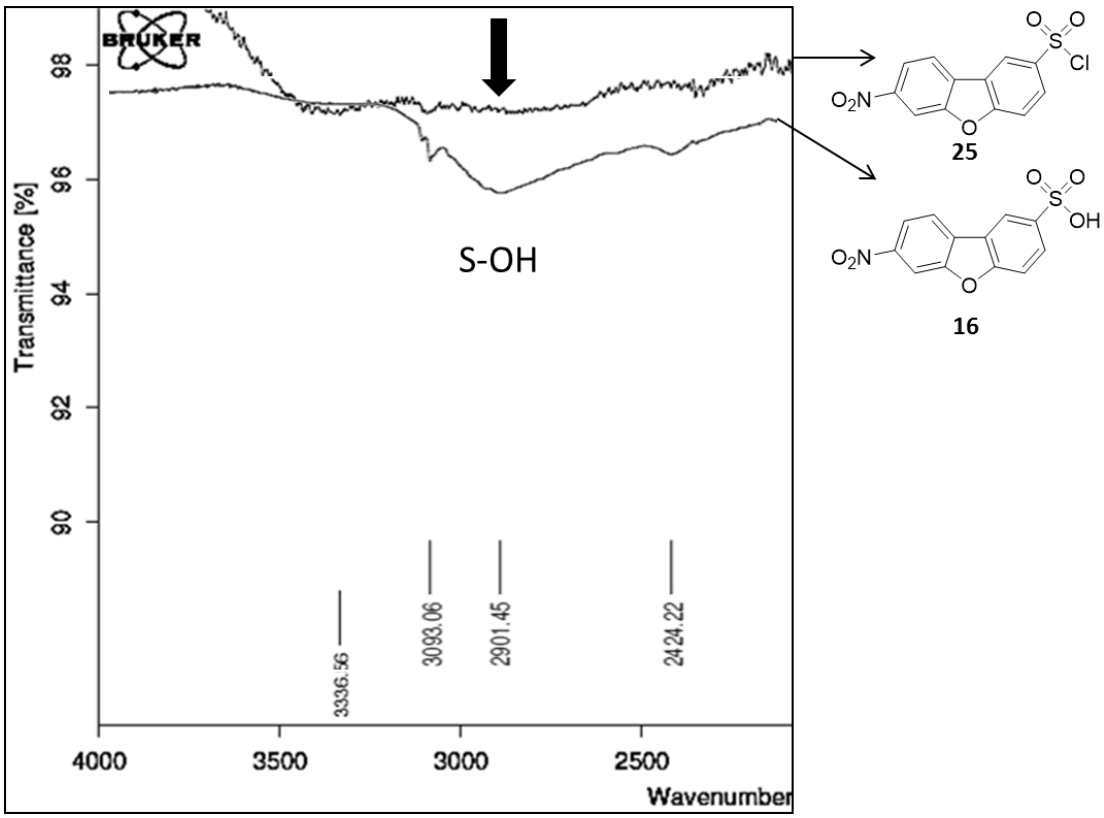

Figure 3.2 Superimposed IR spectra confirm chlorination of sulfonic acid group to give 25. The chlorination of **16** with thioyl chloride could be observed by the loss of the S-OH stretch at 2901 cm^{-1} (thick black arrow) of **25**.

The aryl sulfonyl chloride **25** was reacted with the *t*-butyl D-valine **17** in the presence of a base, DIPEA, to give a 55% yield of **18** (Scheme 3.5). DIPEA was used as a non-nucleophilic base to "mop up" excess protons which drove the reaction forward.

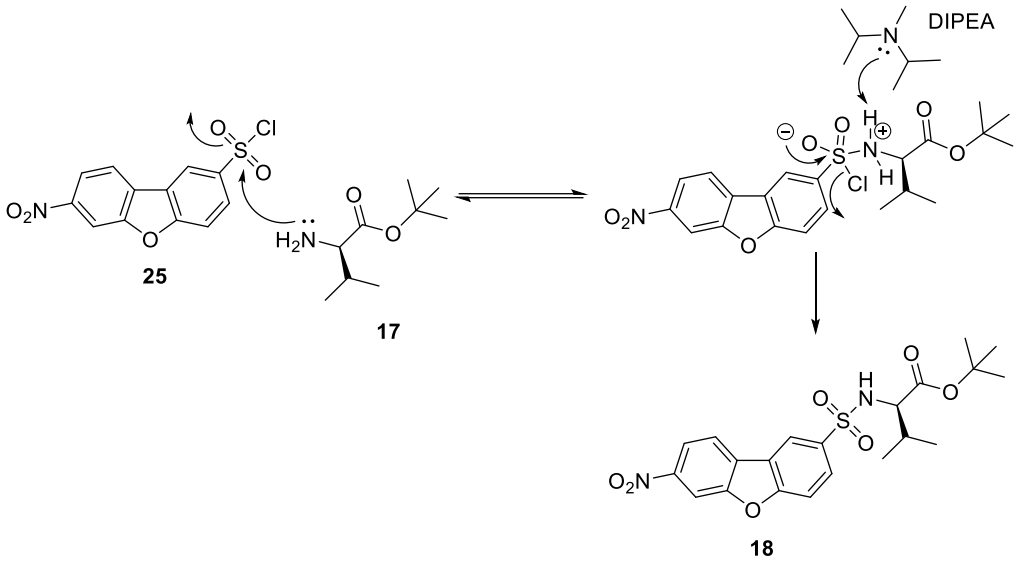

Scheme 3.5 Mechanism of the sulfonoamide formation reaction between compound 25 and 17 in the presence of DIPEA to give 18.

Step v) Nitro group reduction

The reduction of the nitro-group, **18,** to generate the aryl amine **19**, was achieved using two methods. Firstly, by stirring **18** with 10 % Pd/C under H_2 (24 h): but the reaction resulted in numerous by-products (observed by thin layer chromatography (TLC) and NMR spectroscopy). These impurities had similar polarities to **19** and, consequently, chromatographic purification proved difficult. Secondly, an alternative reaction using zinc dust and acetic acid (DCM, 20 °C, 1 h) was employed (Channe Gowda *et al*., 2001). In this reaction the protons are donated by the acetic acid, whereas the electrons are donated by the zinc metal (Scheme 3.6). Importantly the acetic acid (pKa = 4.75) was not strong enough to remove the *t*-butyl group from the carboxylic acid so was conserved. Furthermore, zinc dust and acetic acid were cheaper (compared to H_2 and Pd) and the equipment set up was much simpler, making this a favourable approach. This gave a crude product that was easier to purify by silica gel chromatography to afford **19** (55%).

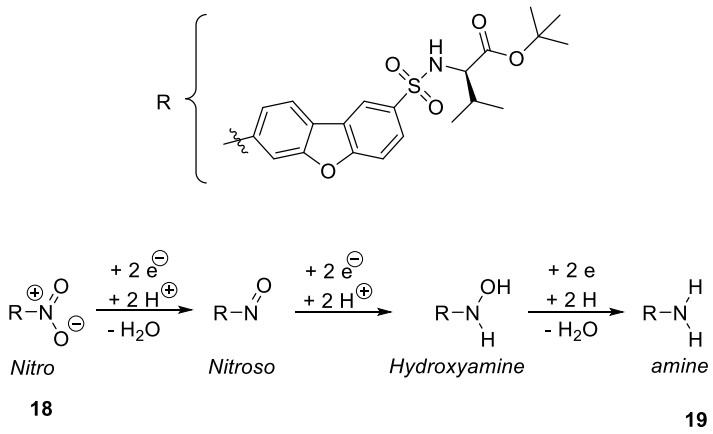

Scheme 3.6 The reduction of the nitro group on 18 to an amine (19). In this reduction reaction, the protons were donated by the acetic acid whereas the electrons were donated by the zinc metal (reagents were in > 4 fold excess to **18**). The nitroso and hydroxyamine intermediates were not isolated.

Step vi and vii) Carbamate formation and *t*-butyl deprotection

The carbamate, **20**, was synthesised by a reaction between **19** and ethylchloroformate in the presence of 4-dimethylaminopyridine (DMAP) to give **20** (61% yield). DMAP is a nucleophilic catalyst, sometimes referred to as an acyl transfer reagent, which activates the acid and is an improved leaving group compared to chlorine (Scheme 3.7).

Subsequently, the final compound HS1-22, **21**, was made by the deprotection of *t*-butyl-acid of compound **20** under strong acidic conditions (TFA, pKa = 0.5). The loss of the *t*-butyl protecting group was confirmed by the loss its distinctive peak in the ^{1}H NMR the spectra (Figure 3.3).

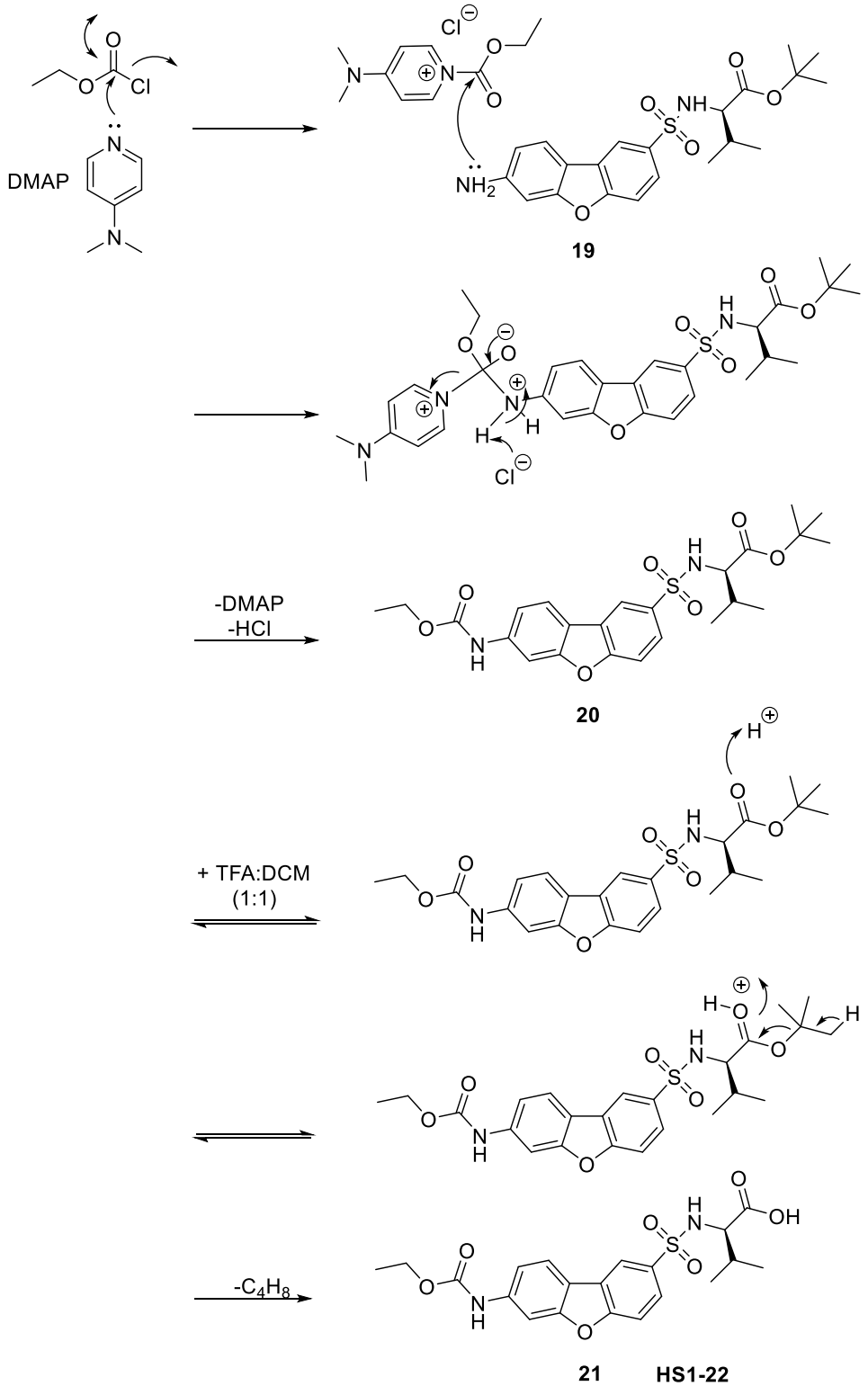

Scheme 3.7 Step vi and Step vii: carbamate formation and acid deprotection. The reaction mechanism between **19** and ethylchloroformate was catalysed by DMAP to give **20**. Step vii: *t*-butyl deprotection **20** with TFA in DCM (1:1) resulted in **21** (HS1-22).

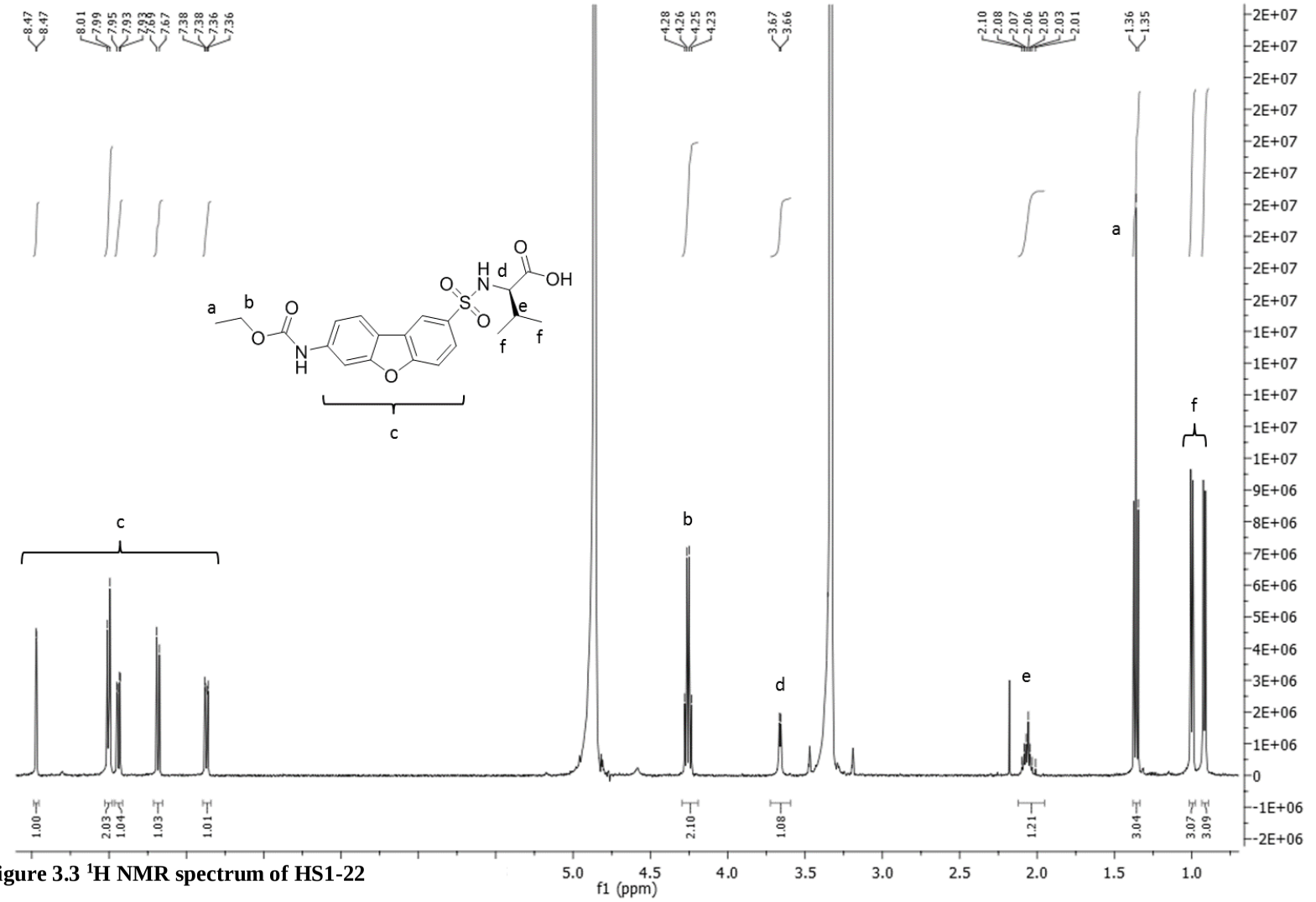

Figure 3.3 ^{1}H NMR spectrum of HS1-22

3.4.2 HS1-22 is a selective and potent inhibitor of MMP-12

MMP Selectivity of HS1-22

In the selectivity assay, commercially available marimastat, a broad spectrum inhibitor, appeared to inhibit all the MMPs (200 nM, broad spectrum inhibitor, black bars) however only MMP-9, 12 and 13 reached significance (**Error! Reference source not found.**). HS1-22 was shown to be selective against MMP_{cat}-12. Due to the high homology between MMPs it is not surprising that there is also minor inhibition of other MMPs in the panel. These data are consistent with analogues of HS1-22 which were designed to be selective inhibitors of MMP-12 (Li *et al*., (2009) and patent WO 2008/057254 A2).

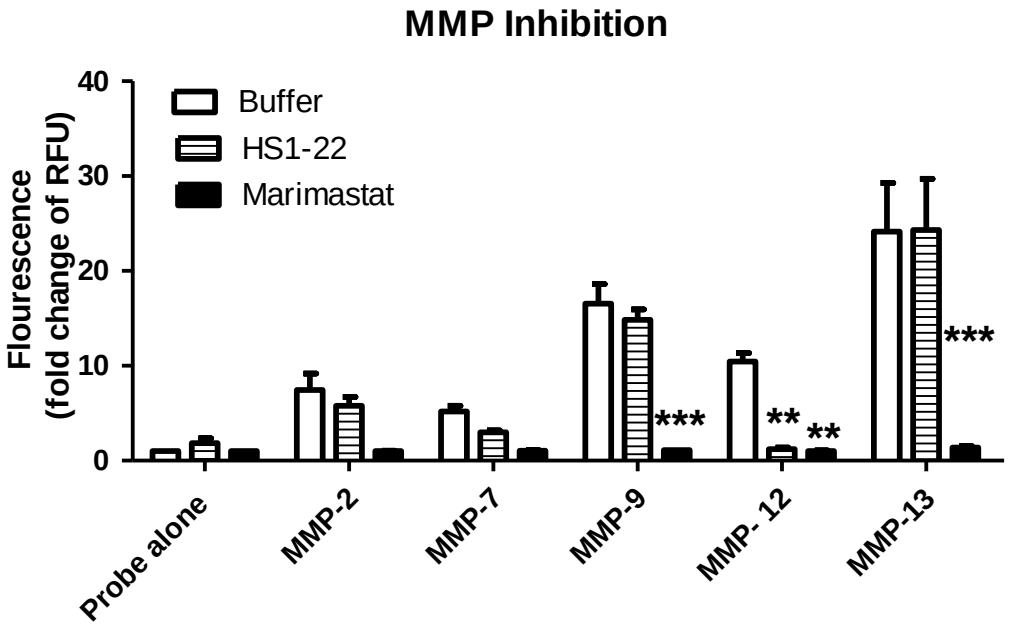

Figure 3.4 HS1-22 is relatively selective for MMP-12. In this selectivity assay, the substrate probe (10 µM) was activated by MMPcat- 2, 7, 9, 12 and 13 (30 nM) (white bars). The addition of marimastat appeared to inhibit all the MMPs (200 nM, broad spectrum inhibitor, black bars) however only MMP-9, -12 and 13 reached significance. The addition of HS1-22 (stripped bars) was selective for MMP-12. Bar represents mean ± SEM (n = 3), and multiple comparisons where made using a two-way ANOVA followed by Bonferroni post hoc tests comparing groups to buffer alone (**P < 0.01, *** P < 0.001).

Potency and toxicity

The IC_{50} of HS1-22 for MMP_{cat}-12 was measured against marimastat (Wojtowicz-Praga *et al*., 1998) and AZD1236 (an MMP-9/12 inhibitor in Phase I clinical studies (Dahl *et al*., 2012; Magnussen *et al*., 2011) Figure 3.5). The data suggest that as the selectivity of the MMPI compound increased, the potency decreased: HS1-22 had an experimental IC_{50} value of 68.2 nM, marimastat of 3.4 nM and AZD1236 of 22.1 nM. The latter two had higher values than expected from the literature (AZD1236: data on file, marimastat (Zucker *et al.,* 2001)). This may be because the assay was not set up identically to those used in previous studies. For example, different substrate probe, machines and equipment were used. Furthermore, this experiment has an n of 1 due to limited resources and difficulty in running the assay. Despite this, this IC_{50} experiment showed that HS1-22 is a relatively selective MMP-12 inhibitor at nM concentrations; this compound was, therefore, taken forward to toxicity assays. MTT assays showed that HS1-22 was not toxic to HEK293 cells *in vitro* at concentrations below 100 µM (Figure 3.6). HEK 293 cells are a common immortal cell line and are very easy to grow so have been widely used in cell biology research for many years. From the data collected it was decided to take this compound forward to further biological assays as a tool to help better understand the roles of MMP-12 in healthy and diseased tissue.

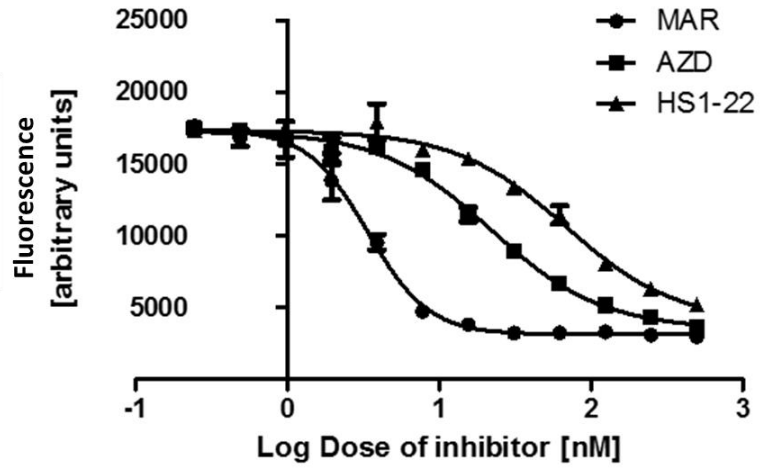

Inhibitor	IC_{50} (nM)	
	Experimental	Literature
Marimastat	3.4	3-16
AZD1236	22.1	6.1
HS1-22	68.2	7.2 - 13.2

Figure 3.5 Inhibitor potency for MMP-12 is dependent on its selectivity over other MMPS. This example IC_{50} graph was generated using MMPcat-12 (30 nM) and a FRET probe (10 µM) and inhibitors at various concentrations (500 - 0.5 nM). Inhibitors tested were: marimastat (circles), a broad spectrum inhibitor; AZD1236 (squares), advertised as an MMP-9 and MMP-12 selective inhibitor; and HS1-22 an MMP-12 inhibitor (triangles). The table illustrates the experimentally (in-house) determined IC_{50} values compared with those quoted in the literature (HS1-22: estimate WO 2008/057254 A2, AZD1236: data on file, marimastat: (Zucker *et al.*, 2001)). Data are plotted as mean ± SEM, experiments were run in duplicate (n = 1), a best fit non-linear regression curve was fitted to the data using PRISM software.

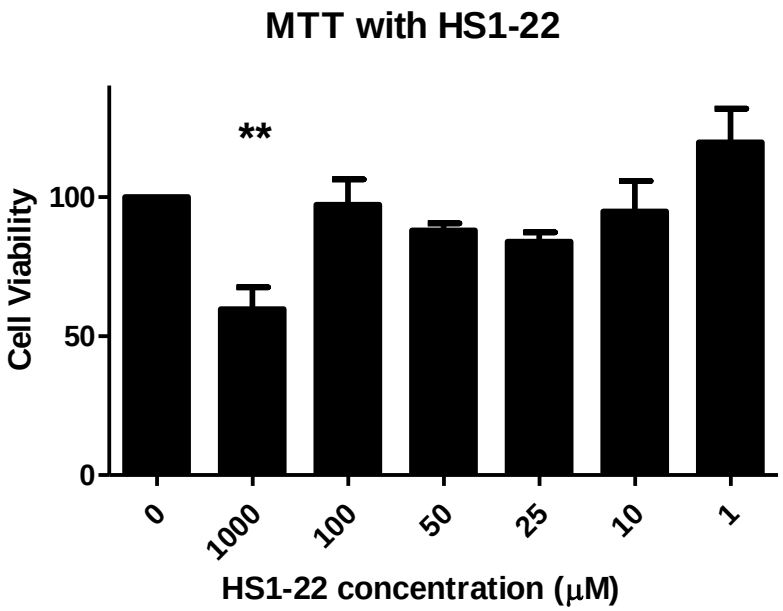

Figure 3.6 HS1-22 is not toxic at concentrations below 100 μM. An MTT assay was used to test toxicity with HEK 293 cells *in vitro*. Bars represent mean ± SEM (n = 3 − 6) and comparisons were made using a one-way ANOVA followed by a Dunnett's multiple comparison post hoc test comparing all inhibitor treatments to the control (0 μM) (** P > 0.01)

3.4.3 Synthesis of activity FRET probe

Fmoc-based solid phase peptide synthesis

The advent of solid phase peptide synthesis (SPPS) was pioneered by Merrifield in the 1960s (Merrifield *et al*., 1966), which won him a Nobel prise in 1984. Unlike natural protein synthesis, SPPS proceeds in a C to N terminal fashion. There are two general strategies that can be used: the *tert*-butyloxycarbonyl (Boc) or fluorenylmethyloxycarbonyl (Fmoc) protecting group methods (Stawikowski & Fields, 2012). In this study the FRET probes were synthesised in-house using the standard solid phase Fmoc method, which generally employs reagents which are safer and more easily handled than those used for Boc SPPS chemistry. This strategy utilised Fmoc protected N-termini of aa monomers (Fmoc–aa-COOH). The solid supported peptide was extended by a single aa by reacting the free carboxylic acid of the monomer with the amine on the peptide terminal to form a new peptide bond (Scheme 3.8). The Fmoc protected amine of the newly added monomer to the peptide inhibits any further reactions but this Fmoc group could be removed under basic conditions to reveal the free amine ("deprotection") so another monomer could then be added; this cycle was continued until the peptide was finished. The peptide could then be cleaved from the resin under acidic conditions. In this chapter, peptides were constructed with an MMP-12 selective peptide sequence, PLGLEEA (Cobos-Correa *et al*., 2009). The FRET system was constructed with fluorophore–fluorophore or fluorophore–quencher systems; these moieties were conjugated to the peptide on solid phase through orthogonal amine deprotection and coupling reactions.

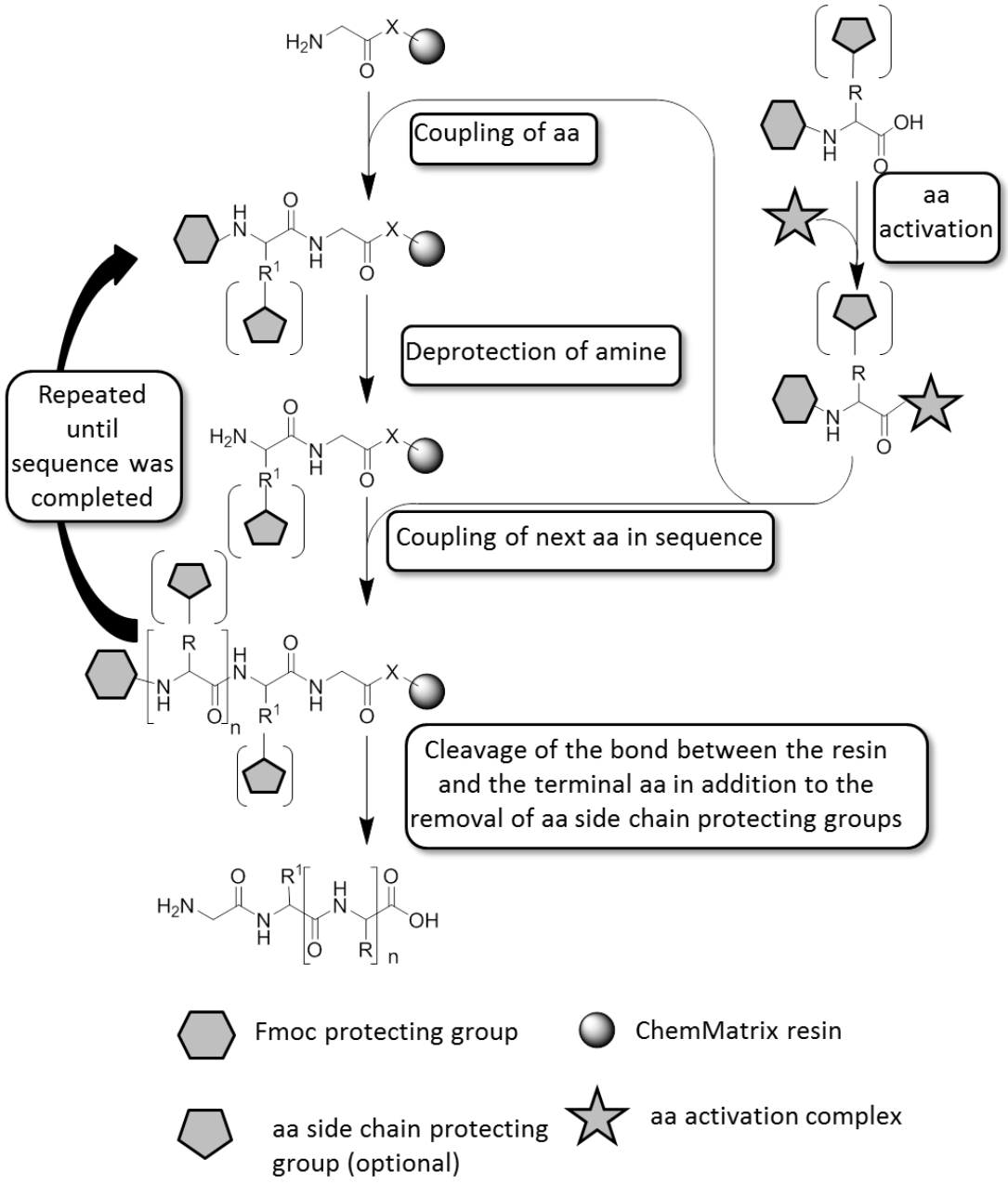

Scheme 3.8 General method for Fluorenylmethyloxycarbonyl (Fmoc) based solid phase peptide synthesis (SPPS). SPPS was started with a commercially available resin (sphere) conjugated to an acid labile trityl linker (X) coupled to glycine. The amino acid (aa) were commercially available with the amine protected with an Fmoc group (hexagon) and any reactive side chains protected with a suitable protecting group (pentagon). The acid on the Fmoc-aa-OH was activated (star) with oxyma and *N*,*N*'-dicyclohexylcarbodiimide (DIC) before the addition to the NH-aa$_n$-X-resin. Fmoc deprotection was achieved by incubation with 20% piperidine in dimethylformamide (DMF). Couplings and deprotection reactions were confirmed using the Kaiser or chloranil test on solid phase. Once synthesis was complete,

removal of all protecting groups on the aa side chains and cleavage of the peptide from the resin was achieved in a single step by incubating the resin beads in a solution of trifluoroacetic acid (TFA), dichloromethane (DCM) and triisopropylsilane (TIS). The solution (containing the peptide) is then isolated from the resin and the solvent evaporated; the peptide was the precipitated out from the remaining mixture with ether and then purified by HPLC.

Resin and linker

Within the Bradley group, aminomethyl functionalised polystyrene (PS) resin is frequently used as the polymer support scaffold for the synthesis of peptides. A linker, normally 2-chlorotrityl (trityl), is coupled to the amine handle on the scaffold. This trityl moiety is an acid labile functional group which facilitates cleavage of the peptide from the PS scaffold at the end of the synthesis; its bulk also prevents the diketopiperazide formation with the first 2 coupled amino acids. In this project commercially available trityl-PS resin (1.6 mmol/g, 100-300 mesh) was activated and then the first amino acid was loaded (Scheme 3.9) followed by standard Fmoc-mediated peptide synthesis. Unfortunately, this method resulted in low loading and the crude peptide had many impurities; disappointingly this ultimately resulted in very low yields post purification (< 1%). An alternative resin, ChemMatrix (made predominantly with polyethylene glycol (PEG)) was utilised instead; it had greater stability (thermal and chemical) and swelling properties (almost double in volume) compared to PS which enabled higher loading. Moreover, the preloaded resin (1.1 mmol/g, 75-150 μm) was commercially available (H_2N-G-trityl-ChemMatrix) saving time and resources.

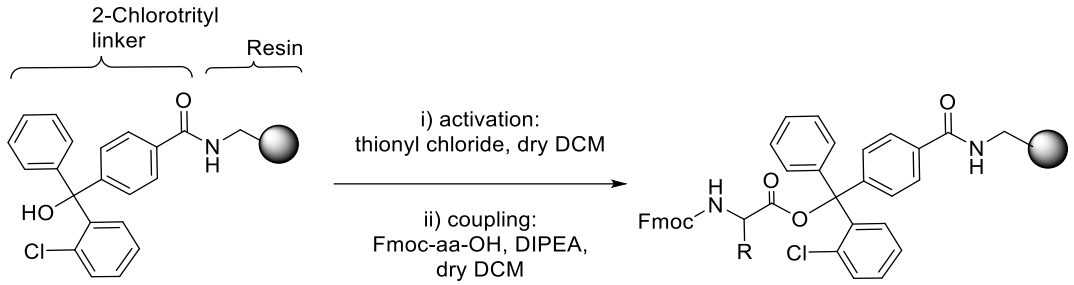

Scheme 3.9 The activation of 2-chlorotrityl-resin. The reaction between thionyl chloride and the linker alcohol gave 2-chlorotrityl chloride; this was then coupled to an Fmoc-aa-OH in the presence DIPEA.

Amino acid coupling reactions

The peptide was built using SPPS procedures in a C to N terminal fashion. The free amine on the first aa (H_2N-G-trityl-ChemMatrix) was reacted with the next amino acid (Fmoc-aa-OH) in the sequence. The free acid on the HO-aa-Fmoc was activated with *N,N'*-diisopropylcarbodiimide (DIC, **26**) using Oxyma Pure (Oxyma, ethyl 2-cyano-2-(hydroxyamino)acetate, **27**) as an additive prior to the addition to the free amine on the peptide chain terminus (Subirós-Funosas *et al*., 2009; Scheme 3.10). Carbodiimides are used in peptide synthesis to activate the carboxylate as an *O*-acylisourea, which is a good leaving group; thus improving the reaction speed. However, this complex is also prone to undesirable reactions such as aa racemisation and the formation of stable *N*-acylisoureas. To solve the problem of racemisation, triazoles (HOBt and HOAt and their derivatives) are introduced which react with the *O*-acylisourea to form an active ester; this is slightly less reactive and consequently at a reduced risk of racemisation reactions. Unfortunately, these triazoles are relatively expensive and potentially explosive. Conveniently a safer alternative, **27**, has been developed (which has similar reactivity profiles to the triazols without their major disadvantages) and has unsurprisingly become a popular choice for SPPS chemistry. The coupling additives and the Fmoc-aa-OH were used at high concentrations so reactions proceeded in pseudo-first order to

the amine which maximised yields. Additionally, the reactive groups on the aa side chains (amines, thiols and acids) were also protected (*t*-butyl, Boc or Dde (1-(4,4-Dimethyl-2,6-dioxocyclohex-1-ylidene)-3-ethyl) to prevent unwanted reactions, these are discussed further below (Deprotection reactions; Figure 3.7).

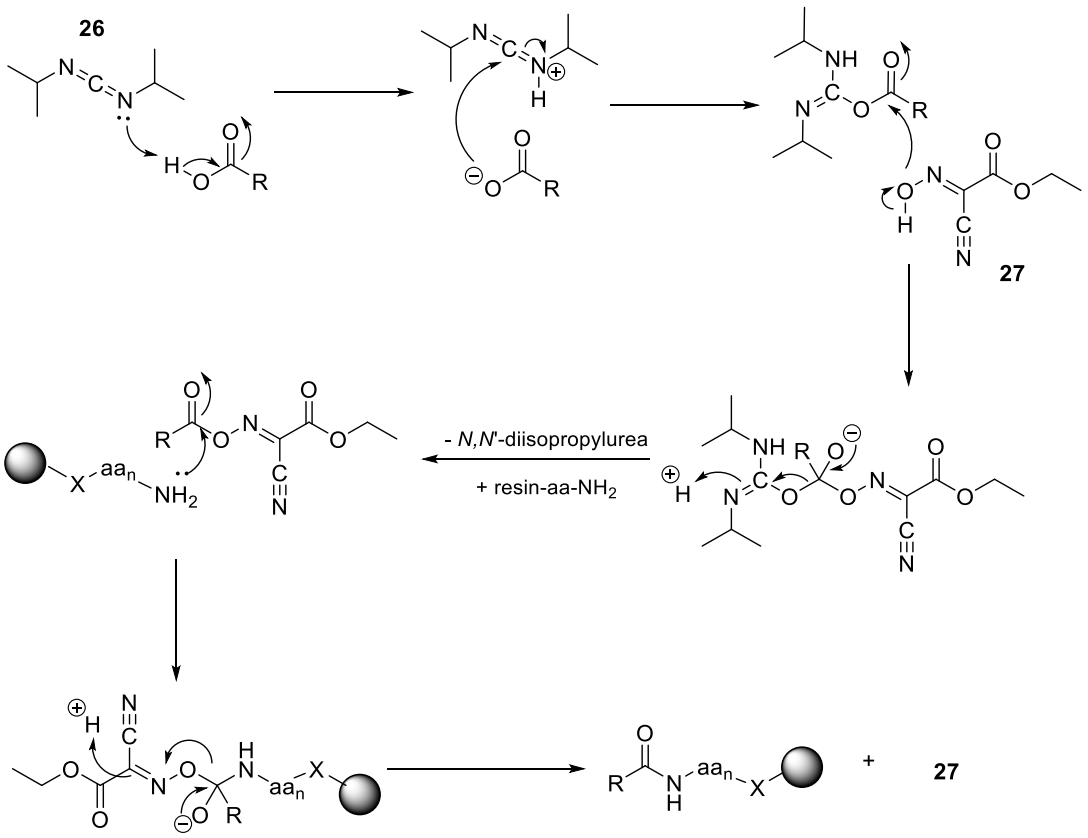

Scheme 3.10 Peptide coupling reaction with Oxyma (27) and DIC (26) additives. First the electrophilicity of the carboxylate is improved by "activating" the negatively charged oxygen by a reaction with **27** to create a highly reactive *O*-acylisourea, this is then reacted with **27** to form an activated ester (*N*-acylisourea). This active ester is then introduced to the peptide terminus free amine which react to form a new peptide bond and regenerates **27**. R = aa-Fmoc, X = trityl linker, sphere = resin.

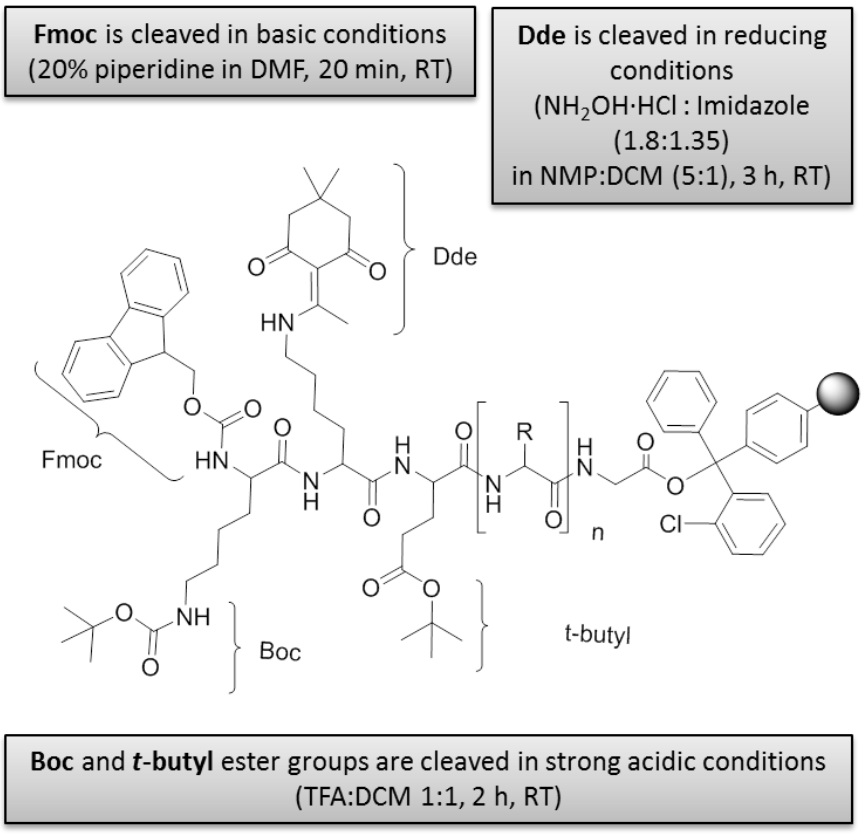

Figure 3.7 Common protecting groups for reactive species used in SPPS. Orthogonal protecting groups are functional groups which can be removed under different chemical conditions. For example, Dde is removed using a reducing solution, Fmoc is removed by in basic conditions and *t*-butyl in the presence of a strong acid. These groups could all be removed selectively from the peptide with minimal impact on the stability of the others.

The rate of peptide synthesis can be increased, not just chemically but by heating the reaction between the amine and the activated acid. Traditionally this reaction is completed with conventional thermal conductive heating but, more recently, microwave irradiation has been employed (Murray *et al*., 2011). In this study, aa coupling reactions at RT took 40 min whereas reactions using microwave energy were complete, in some cases, in just 5 min (75 °C). Additionally, this method of heating has been shown to increase the purity of the synthesised peptides, with reduced aa racemisation (Palasek *et al*., 2007). Chemical microwaves heat

reactions by interacting directly with the solvent (and some reagent) molecules with a high dielectric constant (ε) (de la Hoz *et al*., 2005). Molecules with a high ε have bond dipoles or ions which align with the alternating electromagnetic field (microwave). This energy is then converted to heat energy by dielectric loss (inherent dissipation of electromagnetic energy (heat)). Put simply, these molecules can absorb energy from the microwaves which is then dissipated as heat. This method allows for more rapid and even heating compared to traditional convention methods. Solvent can also undergo superheating (liquid temperatures above the boiling point), which is suggested to also contribute towards increased reaction rates (Klán *et al*., 2001). Microwave irradiation has been suggested to catalyse peptide synthesis not only through heating, but by preventing peptide aggregation on the surface of the resin (Palasek *et al*., 2007). Aggregation is caused by intramolecular hydrogen bonding in the peptide which can obstruct the agents from accessing the peptide end. The alternating microwave electromagnetic radiation is suggested to cause the polar backbone of the polypeptide to continuously align with the radiation, preventing any aggregation. This is difficult to prove experimentally but Basca and colleagues (2008) showed little or no changes between conventional heating and microware irradiation for yields or purity for their peptide synthesis. The improved yields may be primarily down to loss of any aggregation due to disrupted hydrogen bonding at warmer temperatures (75 °C) rather than the direct interaction with the peptide backbone and the microwaves. Therefore, microwave irradiation may simply be a means for convenient, rapid, even heating of the reaction mixture.

Deprotection reactions

Unwanted reactions with chemically reactive moieties can be stopped by masking their behaviour with a "protecting group" (Isidro-Llobet *et al*., 2009). Protecting groups are moieties that are easily attached to reactive species, which renders them inert but can be selectively removed under certain chemical conditions (Figure 3.7). Many aa are commercially

available with the amine on the backbone protected with Fmoc and any reactive side chain moieties (amines, thiols and acids) also protected (predominantly with *t*-butyl or Boc). In this study SPPS with the Fmoc method was utilised to make the FRET probes. The Fmoc deprotection was achieved in basic conditions allowing the prolongation of the backbone; therefore, the aa sidechains are orthogonally protected using acid labile groups (e.g. *t*-butyl or Boc). To incorporate other moieties into the peptide molecule (such as fluorophores or lipids) a lysine protected with the side chain amine protected with Dde (Fmoc-Lys(Dde)-OH) was integrated into the peptide; Dde is commonly used and enables orthogonal amine deprotection with no interference with Fmoc, Boc or *t*-butyl groups (Díaz-Mochón *et al*., 2004). This enables the selective incorporation of functional moieties on to the side chains (Dde deprotection).

PEG and Fluorophore coupling

To minimise the steric hindrance between the MMP active site and the peptide sequence, PEG ((2-[2-(Fmoc-amino)ethoxy]ethoxy}acetic acid) spacers were added to either end of the peptide sequence to distance the bulky fluorophores. The integration of PEG also improved the solubility of these compounds in aqueous solutions. Free amines can be functionalised with a reporter with a carboxylate handle, or by conversion of the amine to another functional species: for example, an azide (diazo transfer) for Cu^{I} click reactions with alkyne species. Normally, fluorophores are conjugated to the molecule once the peptide backbone (with spacers) is complete. In this project, fluorophores were conjugated at the N-terminus and via a lysine residue near the C terminus with simple amide bonds. Interestingly, microwave radiation worked well for aa couplings but caused decomposition during fluorophore coupling; these reactions were therefore completed at room temperature. Fluorophores used were coumarin 343, 5(6)-carboxyfluorescein (FAM), 5(6)-carboxyrhodamine B (RhodB) and the quencher methyl red (MR).

Simultaneous cleavage from the resin and side chain deprotection

Once the sequence was complete the peptide was cleaved from the ChemMatrix resin via the trityl linker. This was achieved using weakly acidic conditions (1% TFA/DCM) if the aa side chains still required their acid labile protecting group, or using a stronger conditions (TFA : DCM (1:1) with 5% triisopropylsilane (TIS)) if not. TIS acts as a scavenger for the carbo-cations and the TFA anion formed in the deprotection reaction. The crude compound was purified using semi-preparative HPLC as detailed in Section 2.5.5.

Probe purification and characterisation

Probes were purified by semi-preparative HPLC and then characterised by analytical HPLC and MALDI mass spectroscopy.

Probes synthesised

To enable MMP-12 selective imaging three FRET probes, HS1-58 (**12**), HS1-59 (**13**) and HS1-65 (**14**), were synthesised with the previously published MMP-12 specific sequence (PLGLEEA) (Table 3.1). The structures differed by the conjugated FRET pairing (the structures and mass (found by MALDI) are shown in Figure 3.8 (HS1-58 HS1-59) and Figure 3.9 (HS-65). The fluorophore FRET combinations were tested with MMP-12 to establish the best indicator of MMP-12 activity.

Table 3.1 FRET probe sequences and yields

[Fluorophore1]-PEG_2-PLGLEEA-PEG_2-K[Fluorophore 2]-G-OH				
Compound	**compound name**	**fluorophore1**	**fluorophore 2 or quencher**	**yield**
12	HS1-58	coumarin 343	RhodB	10%
13	HS1-59 (single isomer)	FAM	RhodB	4%
14	HS1-65	FAM	MR	8%

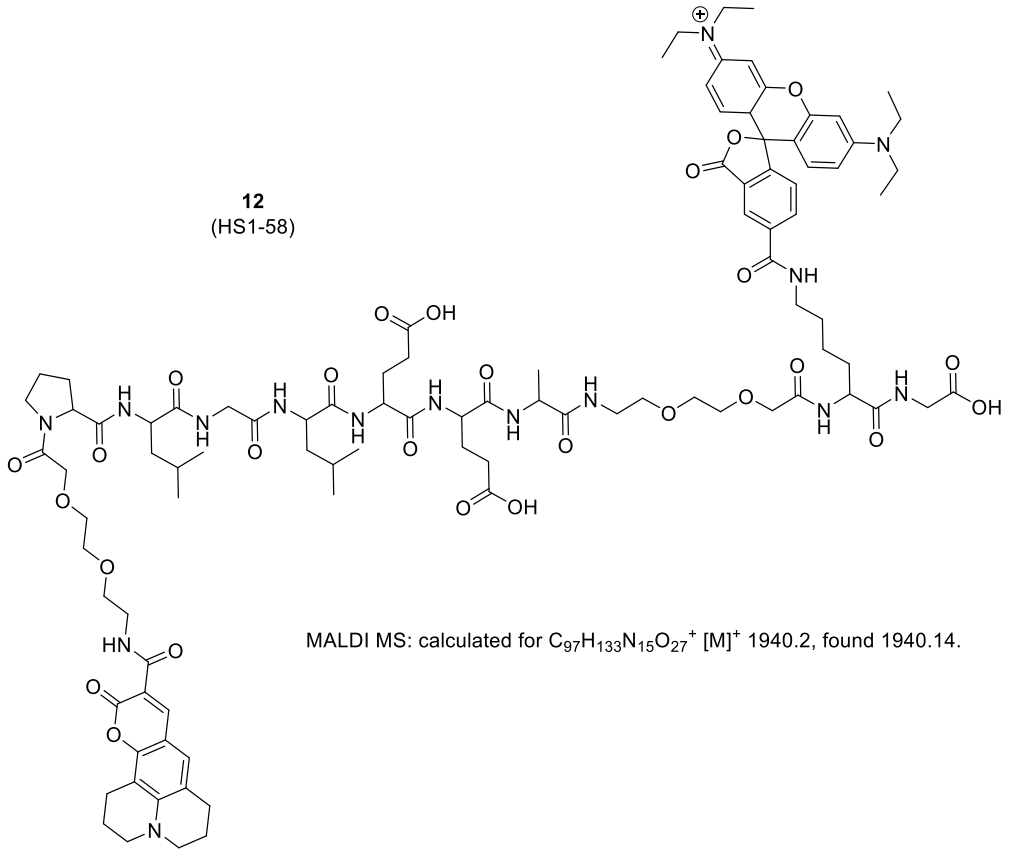

12
(HS1-58)

MALDI MS: calculated for $C_{97}H_{133}N_{15}O_{27}^{+}$ $[M]^{+}$ 1940.2, found 1940.14.

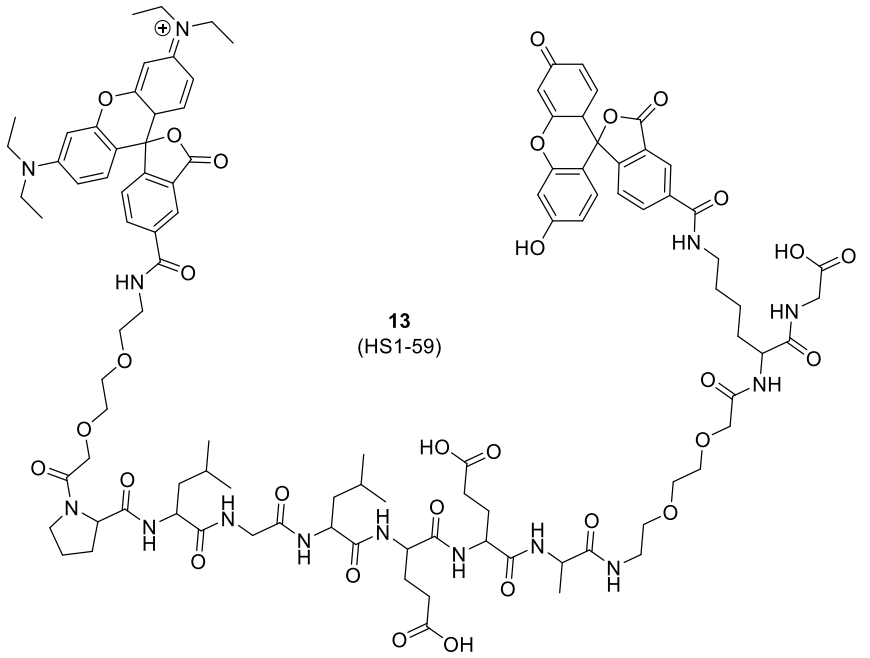

13
(HS1-59)

MALDI Mass Spectrometry: calculated for $C_{1102}H_{129}N_{14}O_{30}^{+}$ $[M]^{+}$ 2031.22 found 2031.68

Figure 3.8 Structures of HS1-58 and HS1-59 are their corresponding mass found by MALDI mass spectroscopy.

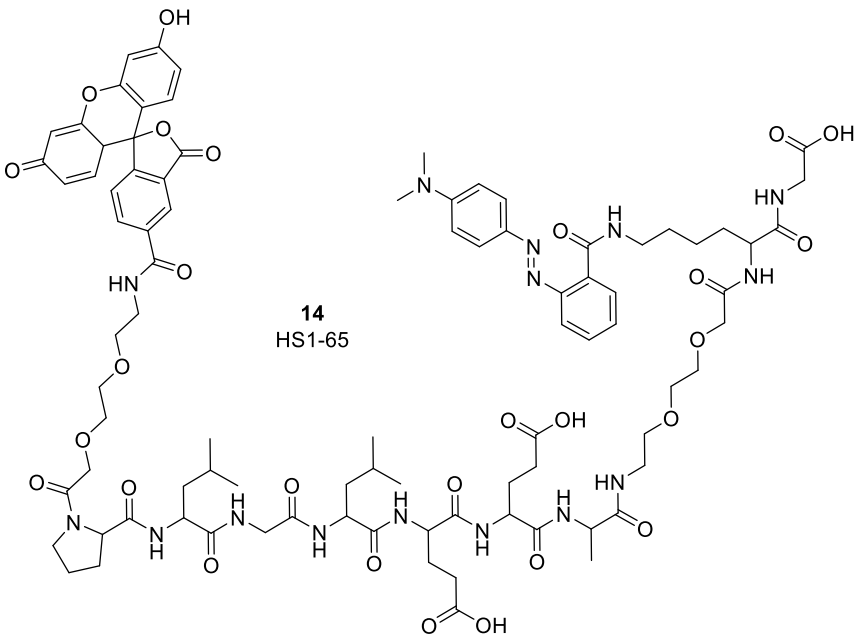

MALDI Mass Spectrometry: calculated for $C_{88}H_{113}N_{15}O_{27}Na$ $[M+Na]^+$ 1835.95 found 1835.6.

Figure 3.9 Structure of HS1-65 and corresponding mass found by MALDI mass spectroscopy.

3.4.4 Probes undergo FRET and are cleaved by MMP-12

The emission of the donor fluorophore of the activity probes was monitored over time in the presence of the catalytic domain of MMP-12 (Figure 3.10). The emissions from the donor fluorophore did increase over time, as expected, for all three probes. Interestingly the emissions from the acceptor fluorophore, in compounds HS1-58 and HS1-59, RhodB (λ ex = 440 or 485 respectively, em = 590 – 600 nm), also increased. This was unexpected as the acceptor emission was expected to decrease; this would suggest that there is a complex interaction between the donor fluorophores (coumarin 343 and FAM) and RodB and is not as simple as energy loss by fluorescence (but does agree with published data from Cobos-Correa *et al*., 2009). A possible reason for FAM and Rhod B to exhibit quenched fluorescence in the intact probe, but not after cleavage, is that the fluorophores do not undergo just FRET, but also interact by static quenching. Static quenching occurs when similar planar aromatic

fluorophores are close in space as they can stack with the aid of hydrophobic effects and hydrogen bonding. The stacked fluorophores can then form a complex which interacts through proton coupled electron transfers. This mechanism allows an excited complex to lose energy (and return to the ground state) by emitting phonons (heat) instead of the usual fluorophore emission of photons (light, e.g. fluorescence). A characteristic of complex formation is a change in absorption spectra of the fluorophores when the complex is formed: there is a small shift to the right for the absorbance of probe HS1-58 and HS1-59 (Appendix 4**)**. Although these complexes had a high fold change in fluorescence post cleavage, there was high background signal from the RhodB. To minimise the background and costs, a frequently utilised fluorophore–quencher system in the Bradley group FAM (fluorophore) and MR, quencher) activity probe was synthesised, HS1-65**.**

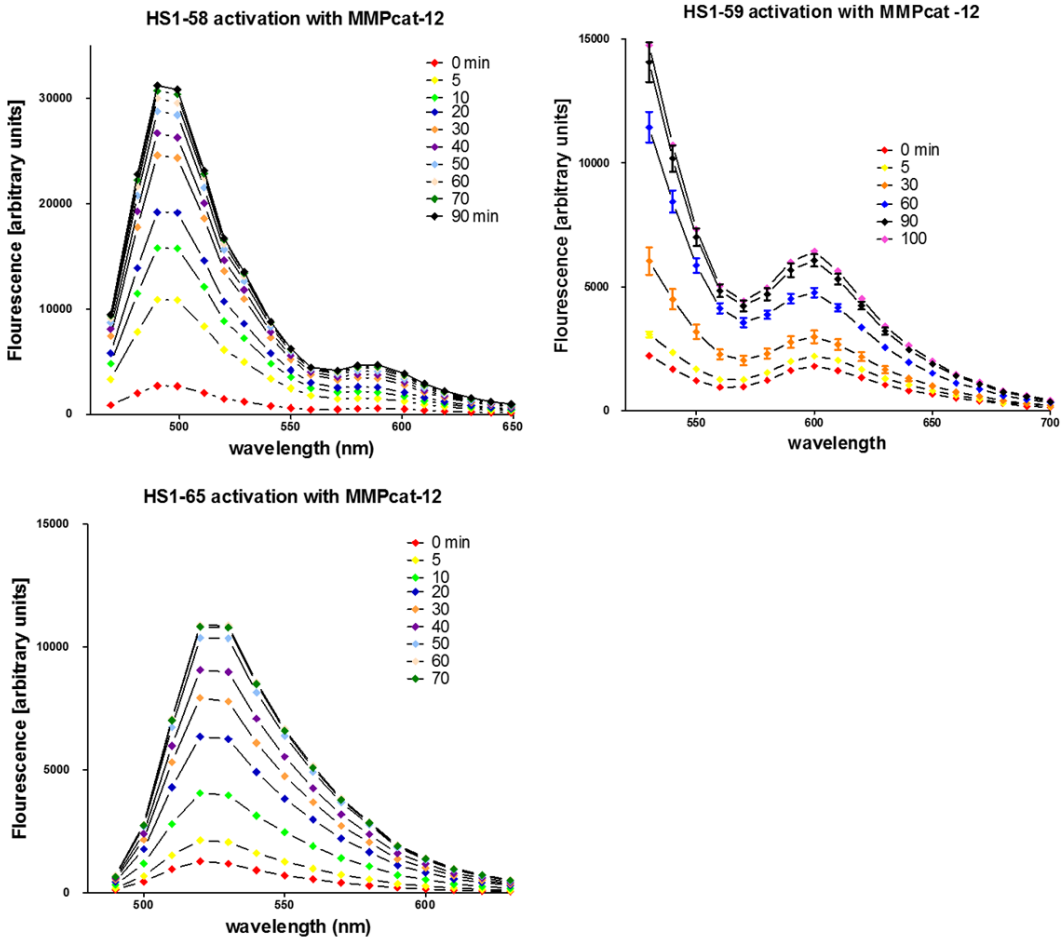

Figure 3.10 Activation of FRET probes *in vitro*. MMP_{cat}-12 (30 nM) cleaved the FRET probes (10 µM) and the emission of the donor and actor fluorophores monitored over time. All reactions were complete by 90 min. HS1-58 λ ex = 440 nm, HS1-59 and HS1-65 λ ex = 485 nm. Data are plotted as mean, reactions were conducted in duplicate and error bars removed for clarity (n = 1).

FRET probes are selective for MMP-13 and MMP-12 *in vitro*.

Compound HS1-65 was tested against a panel of proteolytic enzymes and shown to be activated by human and murine MMP-12 (Figure 3.11). The addition of marimastat (MMP inhibitor) suppressed the fluorescence of HS1-65 in the presence of MMPs; this is consistent with activation due to MMP proteolysis. In addition, neutrophil elastase did not activate HS1-65. However, HS1-65 was also activated by MMP-7 and -13 (Figure 3.12). This was not

completely unexpected due to the high structural and functional homology in the MMP family. Furthermore, other groups have shown that this peptide sequence is not 100% specific for MMP-12 (Cobos-Correa *et al*., 2009; Lim *et al*., 2014). Nonetheless, this assay confirmed that this probe is relatively selective for MMP-12 (murine and human) and, therefore, it was taken forward for further investigation.

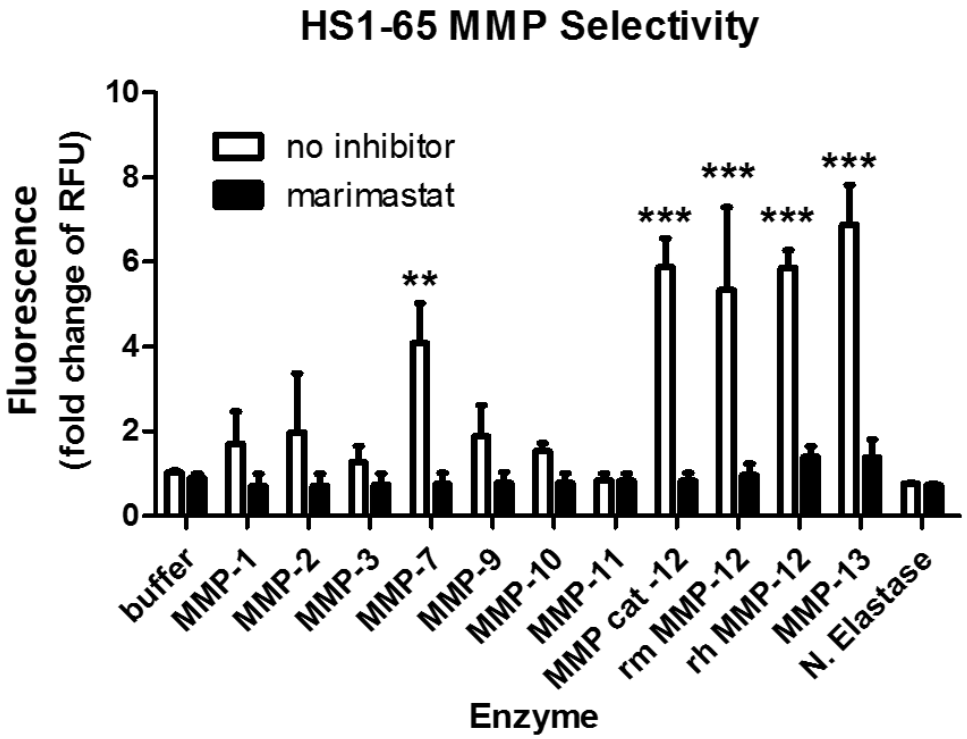

Figure 3.11 HS1-65 is selective for MMP-7, 12 and 13. The emission of fluorescein from HS1-65, in the presence of MMPs, monitored over time (120 min). HS1-65 was activated by MMP-1, -2, -3, -7, -9, -10, -12 (catalytic and full activated murine and human MMP-12) and -13 (no inhibitor, white bars), but the signal from MMP-1, -2, -3, -9 and -10 reactions were small and not significant. marimastat treated reactions (black bars) did not exhibit an increase in fluorescence from HS1-65. Neutrophil elastase was also shown to not activate HS1-65. Bar represents mean ± SEM (n = 3) and multiple comparisons where made using a two-way ANOVA followed by Bonferroni post hoc tests comparing groups to buffer alone (** $P < 0.01$, *** $P < 0.001$).

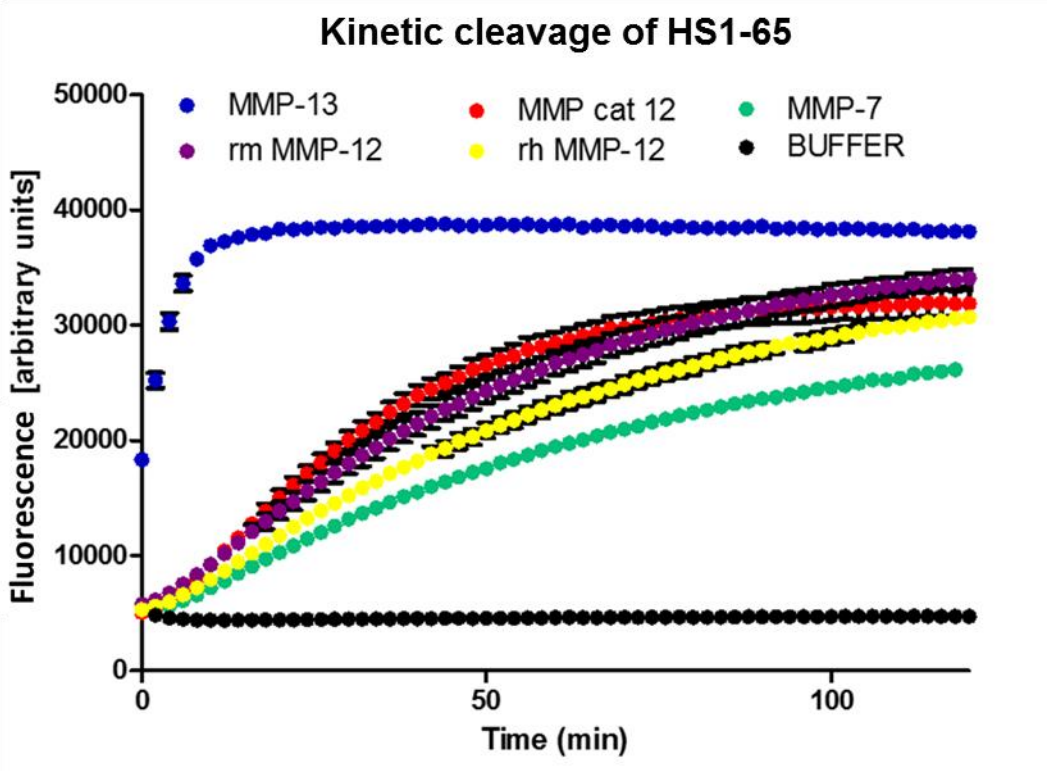

Figure 3.12 Flourescence of HS1-65 in the presence of MMPs over a 2 h period MMP- 7, 12 and 13 (30nM) were incubated with HS1-65 (10 µM) and the emission monitored over 2 h (λ ex = 485 nm, em = 528 nm). MMP -13 (blue) cleaved the probe fastest followed by MMP-12 (catalytic domain (red)> murine (purple)> human (yellow) then MMP-7 (green). Data are plotted as mean ± SEM; reactions were conducted in triplicate; this graph is one of three experiments.

3.5 Summary

In this chapter, a small molecule MMP-12 inhibitor, HS1-22, was synthesised in 6 steps and a small library of FRET probes with an MMP-12 targeting sequence was made using SPPS. *In vitro* assays have shown both of these compounds to have selectivity for MMP-12. HS1-22 is a relatively selective inhibitor for MMP-12 (IC_{50} 68 nM) that is not toxic in concentrations below 100 µM. HS1-65 is an activity probe which is predominantly activated by MMP-12 and 13. Both compounds were taken forward to the next phase of the study; to be used in *ex vivo* and *in vivo* assays to interrogate MMP-12 in biological processes.

Chapter 4

Development of a Bioassay for MMP-12

4 Chapter 4: Development of a Bioassay for MMP-12

4.1 Introduction

The extracellular matrix (ECM) is the connective tissue between cells which helps give tissue its structure, it can also facilitate basic cellular behaviour such as cell division. (Hynes 2009). The ECM scaffold is constructed from collagens, elastin, glycoproteins and fibronectin; structural changes in the ECM, such as during would repair or growth, require a collection of enzymes to break down and rebuild the complex network. (Frantz *et al*., 2010) Matrix metalloproteinases comprise a large family (24+) of zinc dependent proteases, each capable of degrading one or many components of the ECM (Nagase *et al*., 2006). The MMP family is essential for physiological processes, including: embryonic development, bone formation and wound healing (Vu & Werb, 2000). Conversely, unregulated MMP activity is associated with the progression of pathology of diseases such as: inflammatory bowel disease (O'Sullivan *et al*., 2015), rheumatoid arthritis (Burrage *et al*., 2006) , cardiovascular diseases (Liu *et al*., 2006) and tumour development (Overall & Kleifeld 2006). This dual sided nature of tissue remodelling by MMPs requires their catalytic domain to be tightly regulated. Due to their powerful capabilities, these proteases are under tight regulation: from translational and transcriptional control, to activation of the excreted zymogen and, later, inhibition by endogenous tissue inhibitors of metalloproteinases (TIMPs) (Löffek *et al*., 2011).

MMP-12 is considered one of the most important enzymes in the degradation of elastin but also breaks down fibronectin and collagen IV (Shipley *et al*., 1996). Interestingly, MMP-12 activity has protective properties such as: anti-tumour (Houghton *et al*., 2006), anti-inflammatory (Dean *et al*., 2008), antibacterial (Houghton *et al*., 2009), and antiviral (Marchant *et al*., 2014). But its presence is also associated with several cardiovascular diseases including atherosclerosis (Johnson *et al*., 2011; Yamada *et al*., 2008) and aneurysms (Curci *et*

al,1998; Longo *et al*., 2005). MMP-12 is also suggested to inhibit angiogenesis (Li *et al*., 2012).

Tools that enable inhibition and visualisation of MMP-12 activity could contribute towards a better understanding of its role during vascular remodelling and other diseases (Lim *et al*., 2014; Hensley *et al*., 2012). This project aims to develop MMP-12-targeting inhibitors and imaging probes to do this. Assessment of these compounds required the development of a robust *in vivo* model of vascular remodelling with characterised MMP-12 activity profiles. Animal models are useful for improving and developing tools to enhance our understanding of the regulation of vascular remodelling (Nakashima *et al.*, 1994; Small *et al*., 2005).

Pilot studies were undertaken to establish a murine model of vascular remodelling with MMP activity detectable by fluorescent molecular tomography (FMT) using commercial imaging agents activated by active MMPs. Greater detail on the commercial probes and FMT is provided in Appendix 1 and Section 1.4. Three models of vascular remodelling were investigated:

- Atherosclerosis: ApoE$^{-/-}$ mice fed on a western diet (up to 30 weeks) (Nakashima *et al*., 1994).
- Neointimal hyperplasia: hyperplasia in the femoral artery following wire injury (Sata *et al*., 2000).
- Angiogenesis: stimulated by subcutaneous implantation of a sponge (Small *et al*., 2005).

The strongest and most consistent MMPSense signal was detected in the angiogenic remodelling model (sponge implantation, data not shown). This is a murine model of angiogenesis achieved by the subcutaneous dorsal implantation of two 1 cm^3 polyurethane

sponges, usually for 20 days. Spontaneous angiogenesis in the sponge implants is facilitated by the porous framework accompanied by the cytokines and chemokines secreted in the local environment during the inflammatory response (Leibovich *et al*., 1987; Barcelos *et al*., 2005). In this model, there is a steady increase in deposition of fibrovascular tissue and growing vessels are present at different stages of maturation (Xavier *et al*., 2010). Angiogenesis is a complicated process; during the sprouting phase the surrounding connective network is broken down by proteases, such as MMPs, and endothelial cells lead the formation of new vessels (Heissig *et al.*, 2003). These vessels then mature by the recruitment of other cells such as smooth muscle and pericytes (Jain 2003). MMP-12 has been suggested to be anti-angiogenic in other angiogenic models but has not been investigated in this model. For this reason, we proposed to examine if and when MMP-12 was present in this model, and its relationship towards the angiogenic and inflammatory process.

4.1.1 Hypothesis

Angiogenesis in subcutaneous implanted sponges is accompanied by MMP-12 activity.

4.1.2 Aims

1. To characterise angiogenesis in sponges implanted beneath the skin for 3 − 35 days.

2. To characterise MMP expression and activity in these sponges.

3. To use commercial probes and FMT to image angiogenesis and MMP activity in sponges *in vivo*.

4.2 Methods

4.2.1 Study design

Two studies were set up to investigate angiogenesis, inflammation and MMP profiles in this model (Figure 4.1). The first study aimed to investigate the early stages of angiogenesis in this model; days (D) 3, 7, 14 and 21. The second looked at the later stages of this model: D 21, 28, and 35. FMT imaging for angiogenesis and MMP activity was achieved using commercial probes, AngioSense 680 (AngioSense) and MMPSense 750 F.A.S.T. (MMPSense), respectively. FMT imaging of sponges was conducted both *in vivo* and *ex vivo* on D 7, 14 and 21.

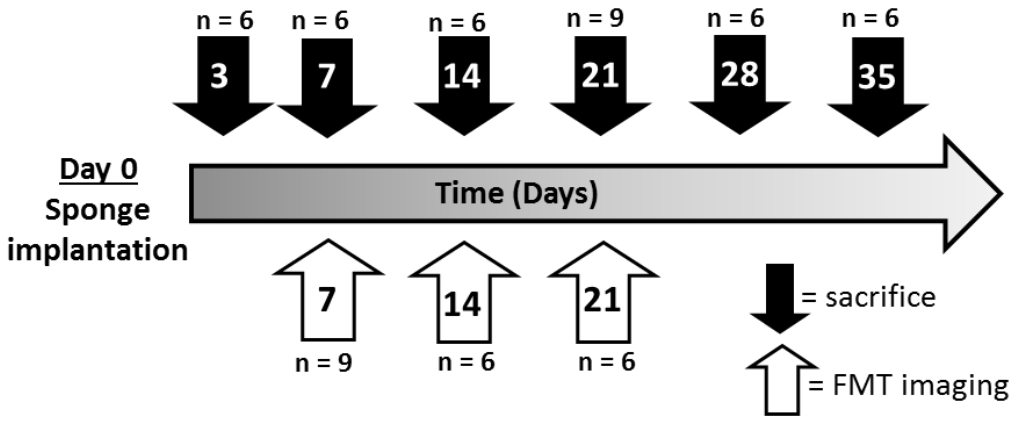

Figure 4.1 Study design for time course study. The number inside the arrow indicates the time-point (days) and the number above/ below relates to the number (n) of mice used at the stage of the experiment. Black arrows indicate when mice were killed and the sponge tissue collected for molecular analysis and histology. White arrow indicates when FMT imaging of sponges (*in vivo* and *ex vivo*) was conducted.

4.2.2 Animals

Male C57BL6/J (age 8 − 10 weeks) were obtained from Harlan (UK). All mice were housed for at least 1 week, with constant access to food and water and a 12 h light/dark cycle, before use in experiments.

4.2.3 *In vivo* imaging of MMP activity and angiogenesis in the murine sponge model of angiogenesis by FMT.

Surgery

Each mouse was placed under general anaesthesia and two sponges were implanted subcutaneously, the mouse was then allowed to recover. This procedure is described in greater detail in section 2.9.

FMT imaging and analysis

Briefly, mice were placed on an alfalfa free diet to reduce autofluorescence and injected with MMPSense and AngioSense 24 h prior to FMT imaging. Sponges were imaged *in vivo* and *ex vivo* by FMT, the data was analysed using the Truequant® software to determine the concentration of probe within the sponges. The mean value of probe concentration over the 2 sponges was taken for each mouse, this was then tested for statistical significance. See Section 2.10 and Appendix 1 for the imaging procedures and data analysis; Section 1.4 and Appendix 1 contain more information on FMT and the commercial agents used.

Tissue collection

The sponges were collected after *ex vivo* imaging, gently washed in PBS to remove tissue mimic solution, cut in half and either snap frozen on dry ice before storage at -80 °C or fixed in 4% PFA (18 h) before storage in 70% ethanol.

4.2.4 Characterisation of angiogenesis, inflammation and MMP profiles over time in the murine sponge model

Surgery

Each mouse was placed under general anaesthesia and two sponges were implanted subcutaneously, the mouse was then allowed to recover. This procedure is described in greater detail in section 2.9.

Tissue collection and histology

The sponges were collected and cut in half then either snap frozen on dry ice before storage at -80 °C or fixed in 4% PFA (12 h) before storage in 70% ethanol. Fixed tissues were prepared for histology by embedding in paraffin wax and 5 µm sections cut from the centre of each sponge for staining and immunohistochemistry. One section for each mouse was used for:

1. Staining with haematoxylin and eosin (H&E) to image different cell types and tissue structures.
2. Immunostaining for F4.80 to identify macrophages.
3. Immunostaining for CD31 and α-SMA to visualise vessel structures.

Staining and immunohistochemistry procedures are described in section 2.12. Whole sections were imaged using a slide scanner and the images appropriately analysed (described in section 2.12).

Molecular analysis of gene expression

RNA was isolated from frozen sponges from the two experiments. From this, cDNA was synthesised and RT-qPCR was performed. Gene expression was measured for the following:

MMP-2, 7, 9, 10, 12, 13, CD31, PDGFR, VEGF, and TNFα (gene transcripts were normalised against the mean of TBP and GAPDH). The protocols are described in Section 2.13. Due to difficulties in acquiring genes able to normalise between the earlier and later time points, the data from D 7 − 21 are presented in this chapter. Data from D 21 − 35 are presented in Appendix 5. Data from D 3 were excluded as they could not be normalised with the housekeeping genes.

Quantification of total MMP-12 and TIMP-1 protein

Quantification of MMP-12 (zymogen and active forms) and TIMP-1 protein concentrations in the sponges over D 3 − 35 was achieved using ELISAs (protocols in Section 2.11).

Zymography

MMP-12 activity was assessed by zymography using tissue homogenates made from sponges collected on D 3 – 35 (protocols in Section 2.11).

4.2.5 Statistics

Data were checked for outliers and presented as mean ± SEM. Comparisons were made using Students T-test or ANOVA as appropriate. More detail on statistics used in Section 2.3.

.

4.3 Results

4.3.1 Sponge implantation stimulated an angiogenic response

Angiogenesis in the sponges was observable *ex vivo*

In this model, upon dissection of the sponges there was an observable increase in the encapsulation and vascularisation over D 3 − 35 (Figure 4.2a). Tissue lysates collected from the sponges had increased in redness, this suggested that haemoglobin content, and therefore vascularisation, within the implanted sponges increased over time (Figure 4.2b).

Implantation of sponges results in cell infiltration and tissue deposition

Microscopy analysis of sections of sponge from D 3 − 35 stained with H&E showed an increase in cell infiltration and development of large tubular structures (Figure 4.3). On D 3 there is no tissue structure but purple nuclei could be discerned and isolated cells could be identified throughout the sponges. There was gradual increase in deposition of tissue and matrix within the sponge over the duration of the study which was associated with vessel development, large vessels could be clearly identified by D 35.

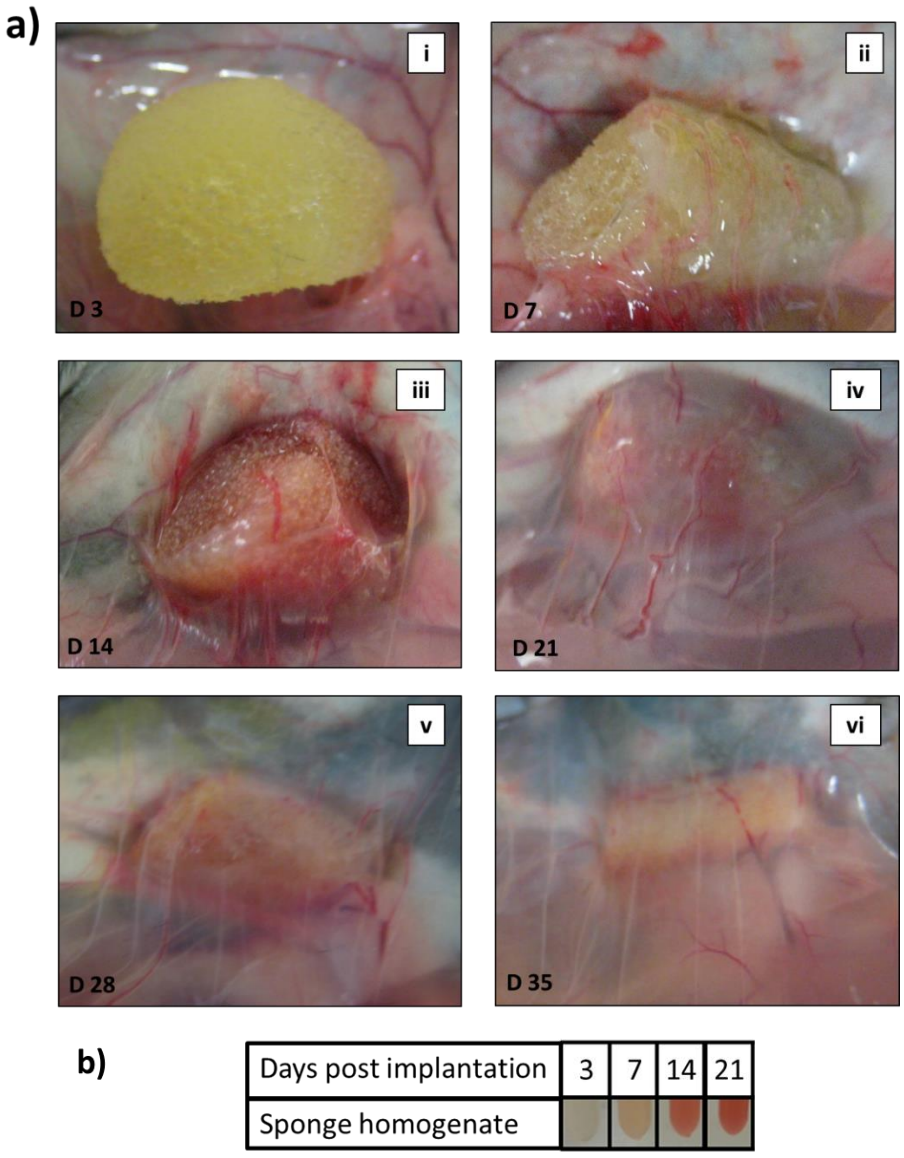

Figure 4.2. *Ex vivo* observations of angiogenesis in the subcutaneous implanted sponges. a) Representative images of sponges during dissections on D 3 − 35. There was no vascular ingrowth on D 3 (i) but the sponges were full of fluid. By D 7 (ii) vessels were observed growing into the sponges. The number and size of vessels entering the sponges steadily appeared to increase over D 14 (iii) and D 21 (iv), connective tissue gradually encapsulated the sponges which was generally complete by D 21. Sponges appeared to be further incorporated (v) and gradually compressed over the remaining time course to D 35 (vi). b) Representative images of sponge homogenates from samples collected on D 3 − 21. There is a progressively darker red colour suggesting increasing haemoglobin content in the sponges over this period.

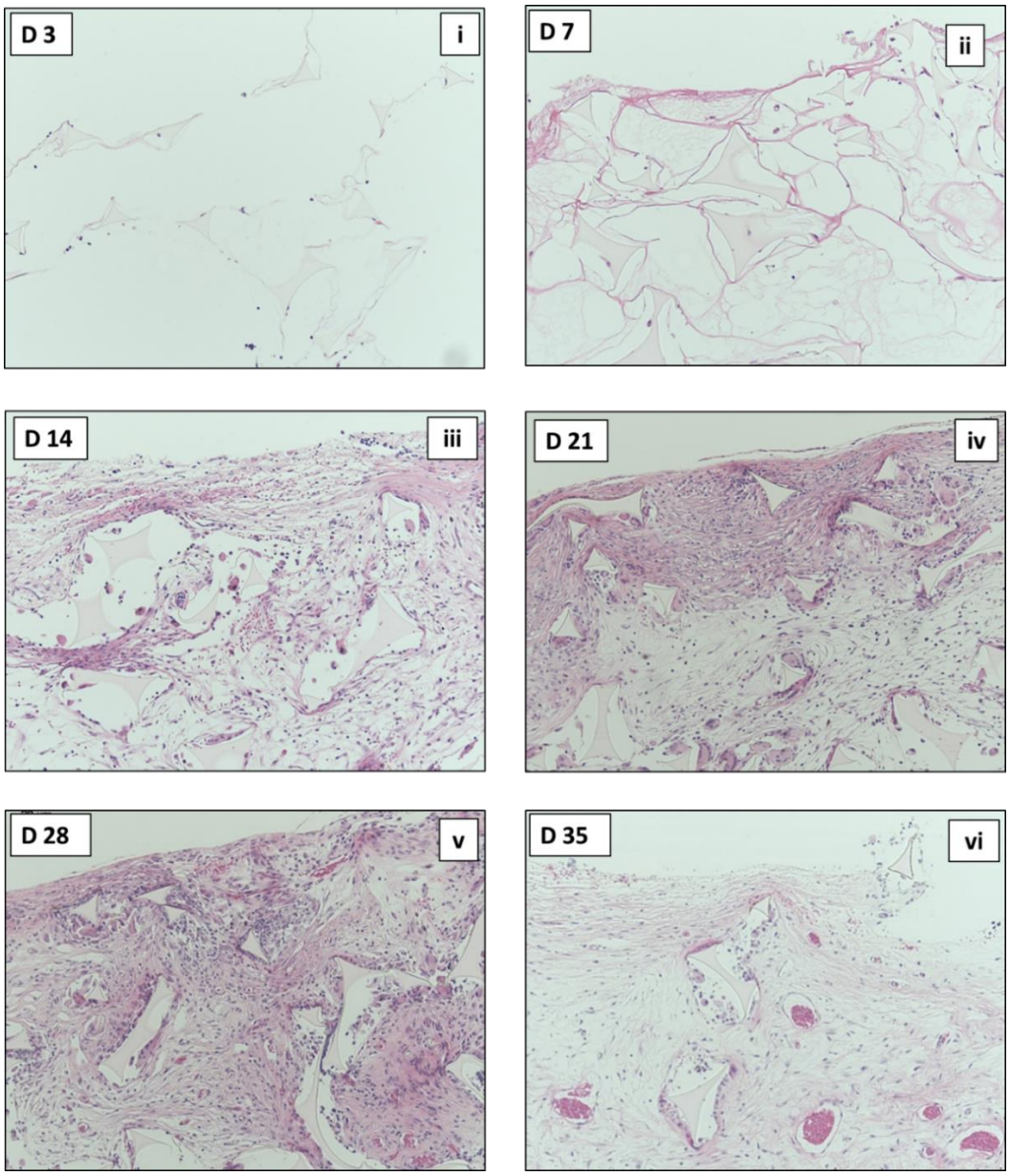

Figure 4.3. Representative haematoxylin and eosin-stained sections, images taken from the edge towards the centre of the sponges collected on D 3 − 35. Sponge plastic can be clearly identified as triangular or rectangular structures with concave edges. On D 3 (i) there was no tissue structure but isolated cells could be identified, individual cells were observable within the sponges on D 3 and 7 (ii). By D 14 (iii) the sponges had tissue and observable small vessels around the edge but the centre of sponge had relatively little cell content. As the experiment progressed, the depth of tissue infiltration and the number of observable vessels increased over D 21 (iv) and D 28 (v). Large tubular structures containing red blood cells were clearly identified by D 35 (vi). Images acquired from the edge of a section at × 20 magnification.

RT-qPCR detected gene transcripts of angiogenic markers and growth factors

Over D 7 – D 21, CD31 (a marker of endothelial cells) appeared to increase from D 7 − 21 but this did not achieve significance (Figure 4.4a). In contrast, PDGFR(β) (a marker of smooth muscle cells, fibroblasts and pericytes) expression did increase significantly (Figure 4.4b). In this model VEGF, a stimulant of angiogenesis, decreased significantly from D 7 – 21 (Figure 4.4c).

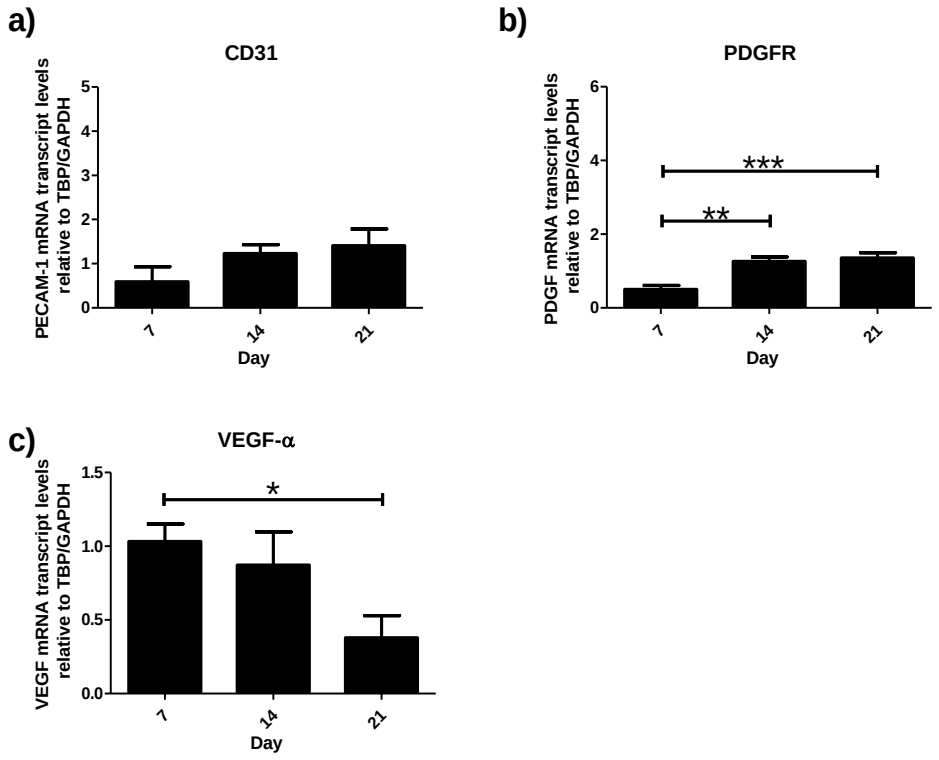

Figure 4.4. Transcript expression of markers of angiogenesis changed over D 7 − D 21. Analysis of gene transcripts of (a) CD31, which does not significantly increase suggesting the quantity of CD31 in the sponges does not change over this time. (b) PDGFR, transcript numbers significantly increased from D 7 to 14 and 21 this receptor is associated with vessel maturation and, therefore, an indication that angiogenesis is ongoing. (c) VEGF (an angiogenic promoter) transcript numbers decreased from D 7 to D 21. Bars represent mean ± SEM (n = 4 – 6) and comparisons where made using a one-way ANOVA followed by Bonferroni post-hoc comparing all data sets (* $P < 0.05$, ** $P < 0.01$, *** $P < 0.001$).

Microscopic analysis of vessels in sponges stained with CD31 and αSMA

Immunostaining for CD31 and α-SMA confirmed the presence of vessels within the sponge (Figure 4.5). Images were analysed in 3 ways: Firstly, the mean fluorescence intensity for the 3 fluorescent channels was calculated (Figure 4.6). CD31 and α-SMA signal intensity both increased from D 3 reaching significance on D 14 and remaining steady thereafter; the DAPI signal for the number of nucleated cells increased steadily over the experiment. These results suggest that vessel growth increased to D 14 and then stabilised, despite increasing cell infiltration. The second method measured the area covered by CD31 and α-SMA signal (Figure 4.7). This suggested the area of vessel incorporation peaked on D 21 then decreased again. The final method required counting all the vessels across the whole section (Figure 4.8). Results suggested that vessel growth actually increased to D 28 then decreases on D 35. This is true even when the total mean is corrected for the area of the sections analysed.

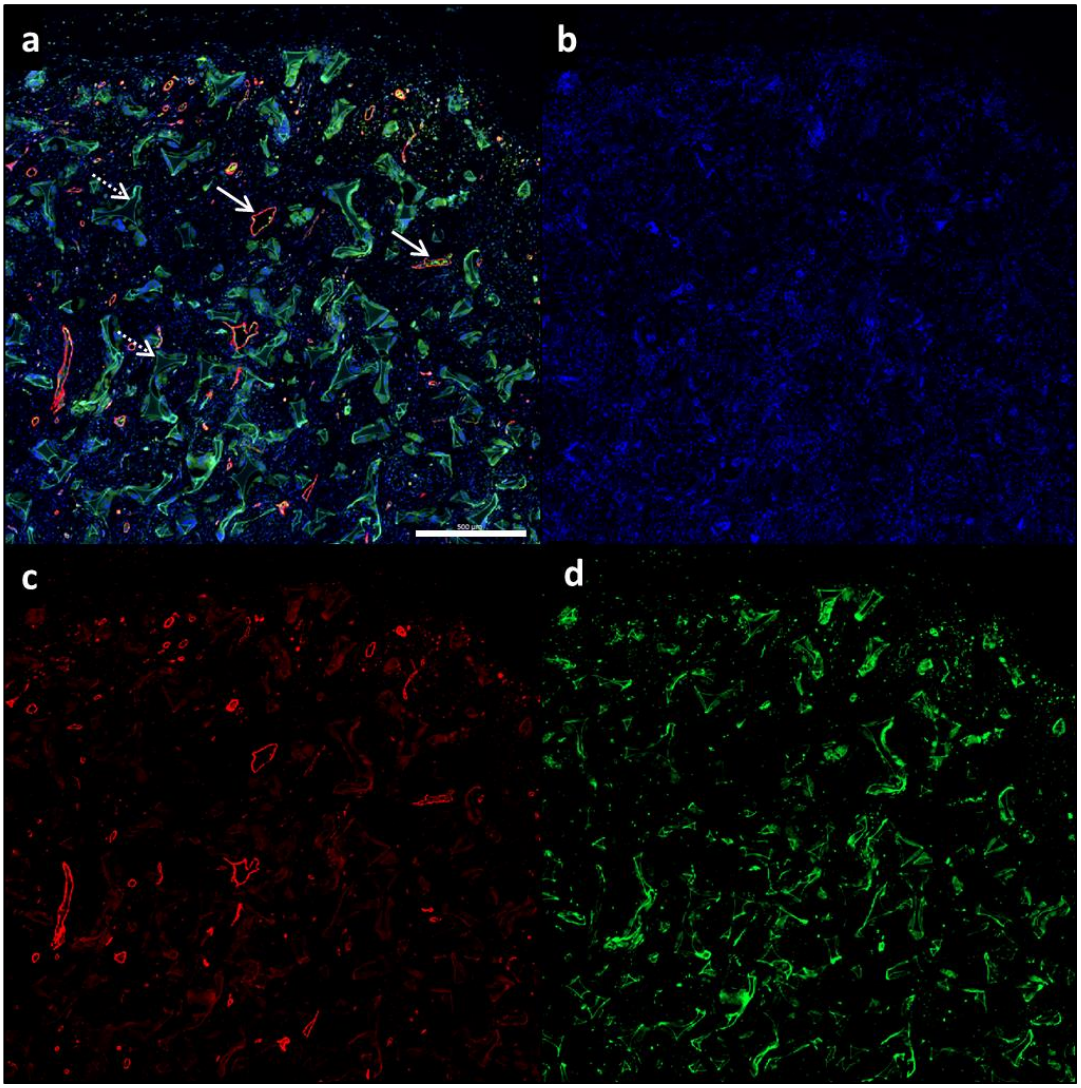

Figure 4.5 Sponges contain an abundance of cells and vessels expressing CD31 and α-SMA. Representative image of sponge tissue collected on D 35: a) composite of images; b) nuclei; c) α-SMA and d) CD31. Dashed arrows: pieces of sponge which have a high auto-fluorescence in the 488 channel; whole arrows: α-SMA and CD31 positive vessels (Scale bar = 500 µm).

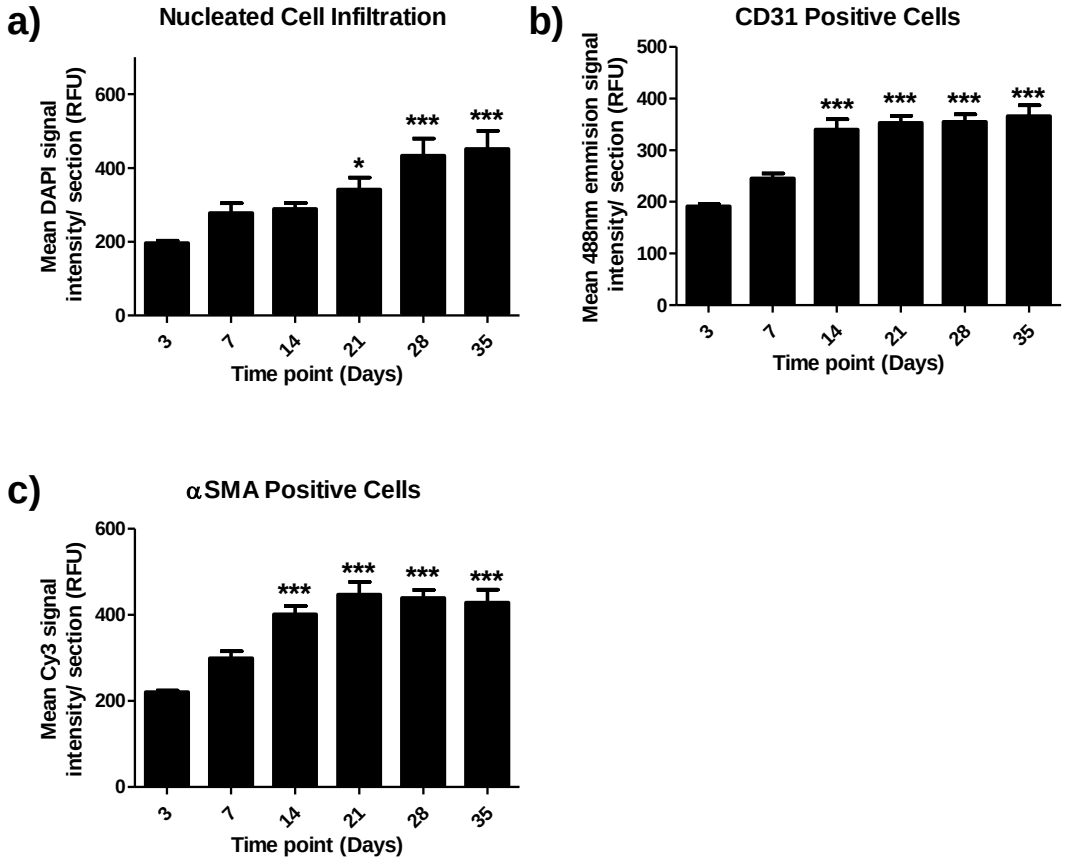

Figure 4.6. The mean fluorescent signal intensity from DAPI, CD31 and α-SMA on sections of sponges collected on D 3 – 35. The fluorescence intensity was measured across the slide under identical conditions in the slide scanner and quantified using the Zen software). a) The measured fluorescence intensity of DAPI stain suggests that the number of nucleated cells steadily increased, reaching significance on D 21 and a maximum on D 28. b) The intensity of stain for CD31 (b) and α-SMA (c) reached a maximum on D 14 and remained steady. Bar represents mean ± SEM (n = 6); (a) comparisons were made using Kruskal-Wallis test followed by a followed by Dunn's multiple comparison; (b) and (c) comparisons were made using a one-way ANOVA followed by a Dunnett's Multiple Comparison Test (* $P < 0.05$, ** $P < 0.01$, *** $P < 0.001$).

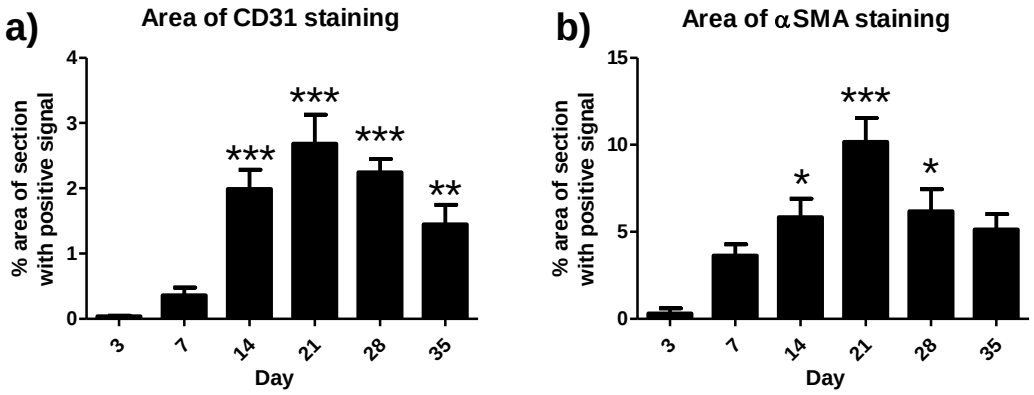

Figure 4.7. The mean area covered by CD31 (a) and α-SMA (b) signal over sections of sponges collected on D 3 – 35. For both signals the area covered increased from D 3 to 21 and then gradually dropped to D 35. Bars represent mean ± SEM (n = 3 – 6) and comparisons were made using a one-way ANOVA followed by Dunnett's multiple comparison tests comparing all data sets to D 3 (* $P < 0.05$, ** $P < 0.01$, *** $P < 0.001$).

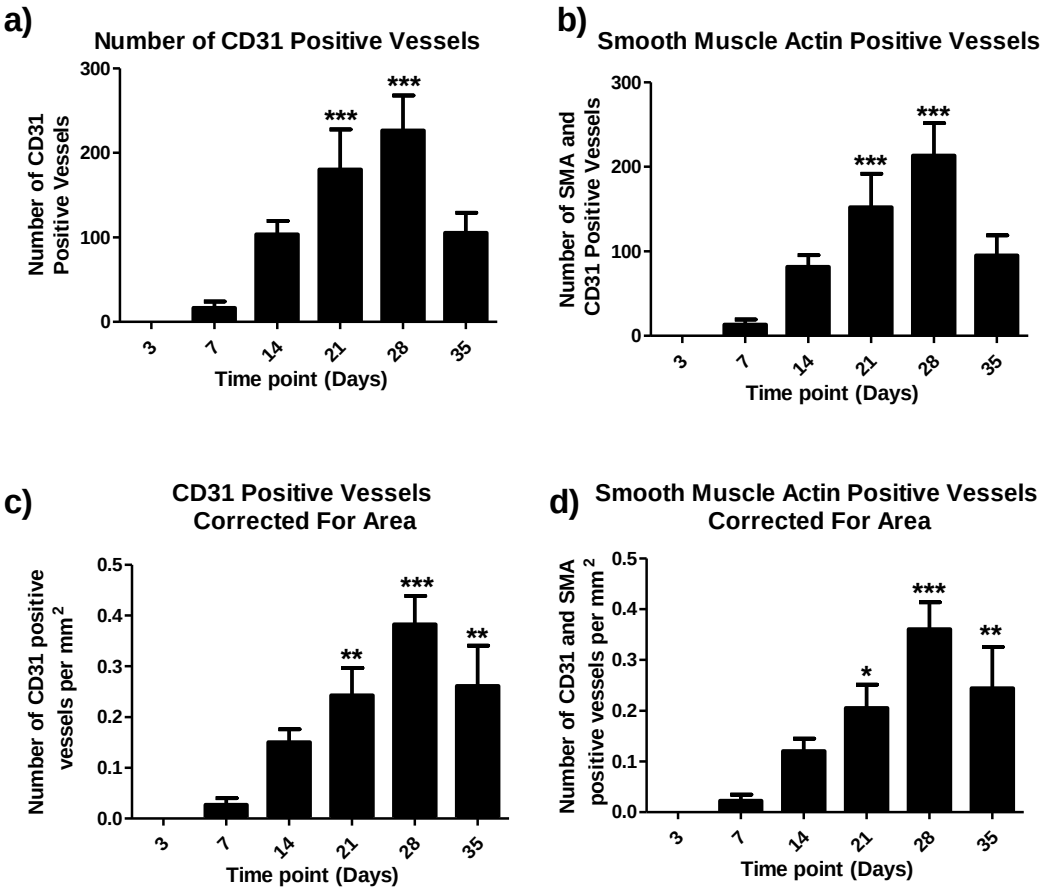

Figure 4.8. The mean number of CD31, or CD31 and α-SMA positive vessels. Profiles for the number of CD31(a) or CD31 with α-SMA (b) positive vessels had similar trends. No vessels were observed on D 3 but they could be observed by D 7, the number increased to reach significance on D 21 and reached a maximum on D 28 followed by a reduction on D 35 (approx. 50%). The total number of vessels was then corrected for the area of tissue section to give (c) and (d) respectively; the pattern was very similar except a relative increase in the number of vessels on D 35, but still resulted in a drop in number compared to D 28. Bars represent mean ± SEM (n = 6) and comparisons where made using a one-way ANOVA followed by Dunnett's multiple comparison tests comparing all data sets to D 3 (* $P < 0.05$, ** $P < 0.01$, *** $P < 0.001$).

4.3.2 Sponge implantation results in an immune response

Inflammatory cytokine present

Gene transcripts for TNFα were present and remained stable over D 7- 21 (Figure 4.9a). In sections stained with H&E, cells with different morphology could be identified at different stages of the angiogenic response. Neutrophil granulocytes (small polymorphonuclear cells, see Figure 4.9b, empty arrow)Figure 4.9. An inflammatory response was observed in the implanted sponges. a) Gene transcripts for TNFα were present and remained stable over D 7- 21. b) Inflammatory cells were present during angiogenesis in this model. Representative H&E stained section from a sponge collected on D 7. Macrophages (solid arrow) and neutrophils (empty arrow) could be identified, image acquired at × 40 magnification, scale bar = 10 μm. Bars represent mean ± SEM (n = 4 – 6) and comparisons were made using a one-way ANOVA followed by Bonferroni Post-hoc tests comparing all data sets ($P > 0.05$).

and macrophages (larger mononuclear cells more cytoplasm, see Figure 4.9b, solid arrow) could be clearly identified at different time points.

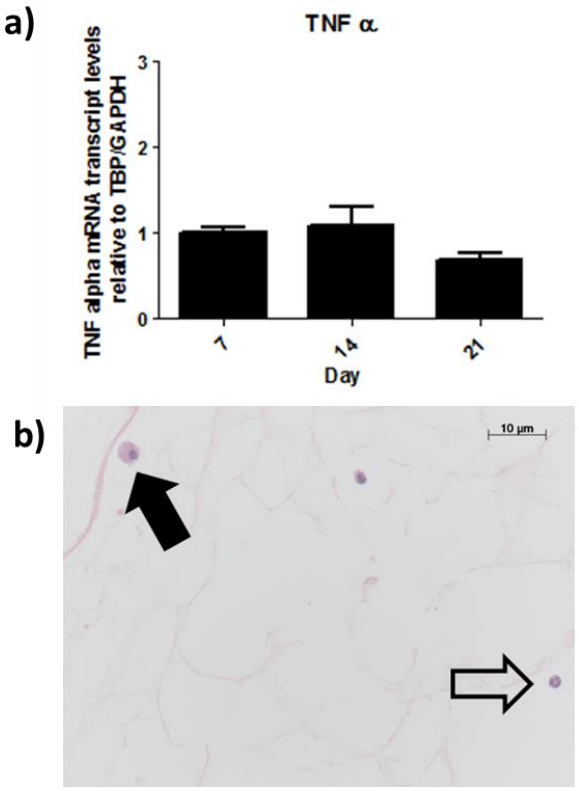

Figure 4.9. An inflammatory response was observed in the implanted sponges. a) Gene transcripts for TNFα were present and remained stable over D 7- 21. b) Inflammatory cells were present during angiogenesis in this model. Representative H&E stained section from a sponge collected on D 7. Macrophages (solid arrow) and neutrophils (empty arrow) could be identified, image acquired at × 40 magnification, scale bar = 10 µm. Bars represent mean ± SEM (n = 4 – 6) and comparisons were made using a one-way ANOVA followed by Bonferroni Post-hoc tests comparing all data sets ($P > 0.05$).

Neutrophil Infiltration peaked on D 3

Neutrophils were easily stained using H&E and identified as polymorphonucleated cells; the number, was highest on D 3 and diminished over time with few cells evident after D 14 (Figure 4.10).

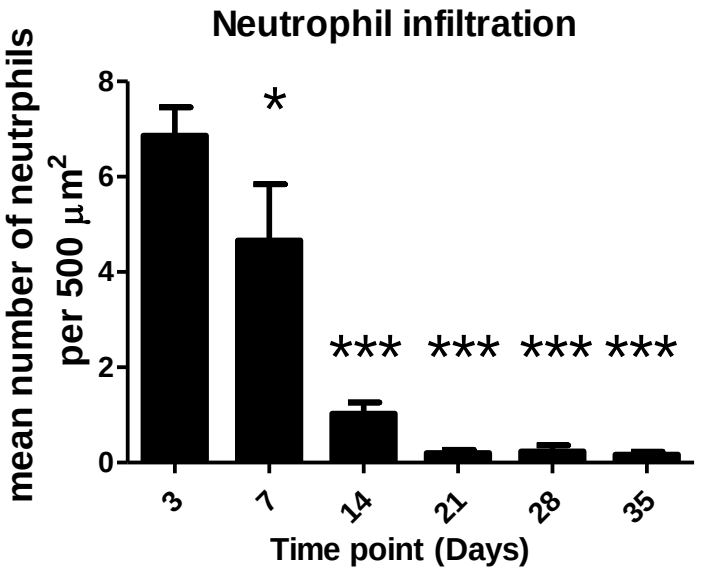

Figure 4.10. Neutrophil number in sponges diminished over time. The number of neutrophils was highest on D 3 and had diminished by D 21. Bars represent mean ± SEM (n = 6) and comparisons were made using a one-way ANOVA followed by Dunnett's multiple comparison test post-hoc comparing all data sets to D 3 (* $P < 0.05$, *** $P < 0.001$).

Macrophage Infiltration peaked on D 28

Sponges were stained for F4/80, a marker for murine macrophages, revealing a large infiltration of these cells (Figure 4.11). The number of macrophages around the edge of the sponge increased to D 14 and then remained steady (Figure 4.12a). However, the depth of macrophage infiltration into the sponges increased to a maximum on D 28 (Figure 4.12b).

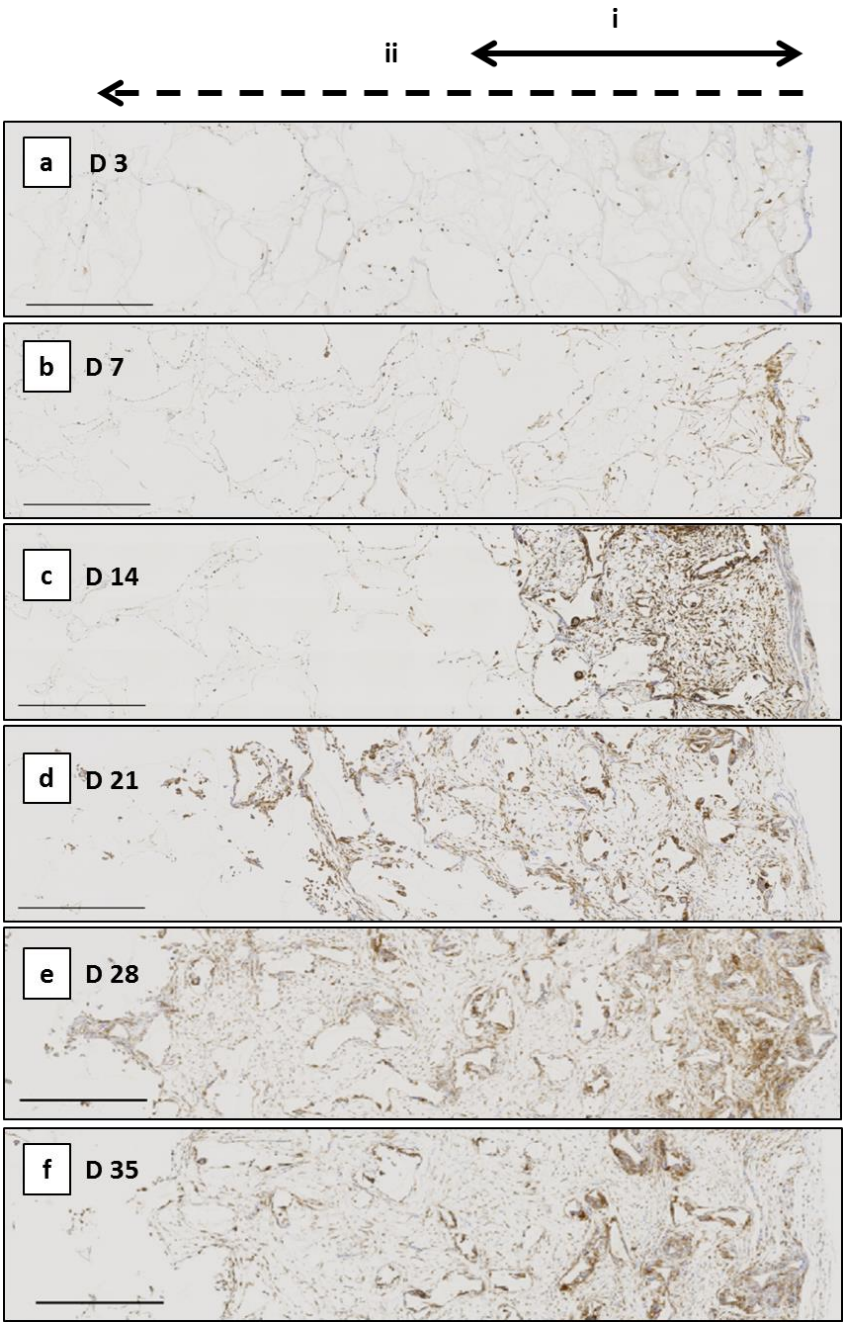

Figure 4.11. Representative images of F4/80 stained sections showing macrophage infiltration into the sponge between D 3 (a) and D 35 (f). There is an increase in F4/80 marker (macrophage infiltration) from the edge (right) towards the centre (left) of the sponge. The mean percentage area of stained was measured from ROI collected near the perimeter of the sponge (solid arrow, i). The depth of macrophage infiltration was measured from the sponge edge, towards the centre, to where the F4/80 stain diminished (dashed arrow, ii). Images were acquired at × 20 magnification and representative images collected (3300 x 880 µm), scale bar = 500 µm.

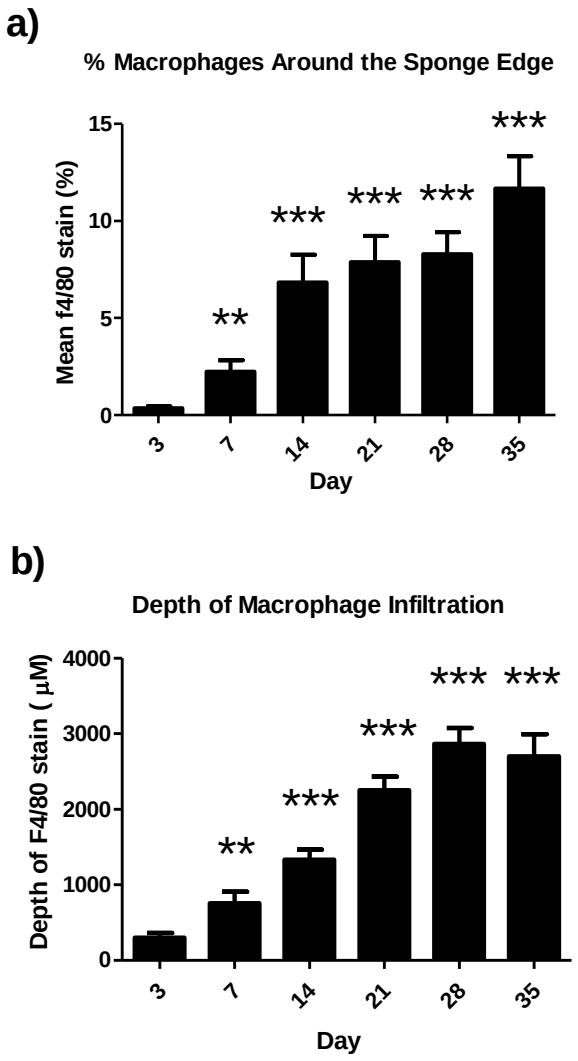

Figure 4.12 Macrophage infiltration increased from D 3 − 28. a) The mean percentage area of F4/80 stain around the sponge edge increased to D 14 whereas infiltration (b) increased steadily to a maximum depth on D 28. Bars represent mean ± SEM (n = 6) and comparisons were made using a one-way ANOVA followed by Dunnett's multiple comparison test post-hoc comparing all data sets to D 3 (** $P < 0.01$, *** $P < 0.001$).

Angiogenesis was detected *in vivo* by FMT imaging.

AngioSense signal was detected *in vivo* by FMT in the sponge model over D 7, 14 and 21 (Figure 4.13a). The mean concentration detected in the sponges was highest on D 7 compared to D 14 and 21 (Figure 4.13b). Sponges were removed and the AngioSense signal was analysed *ex vivo* (Figure 4.14a). However, quantification of the signal showed no changes between measurements from different time points (Figure 4.14b).

a)

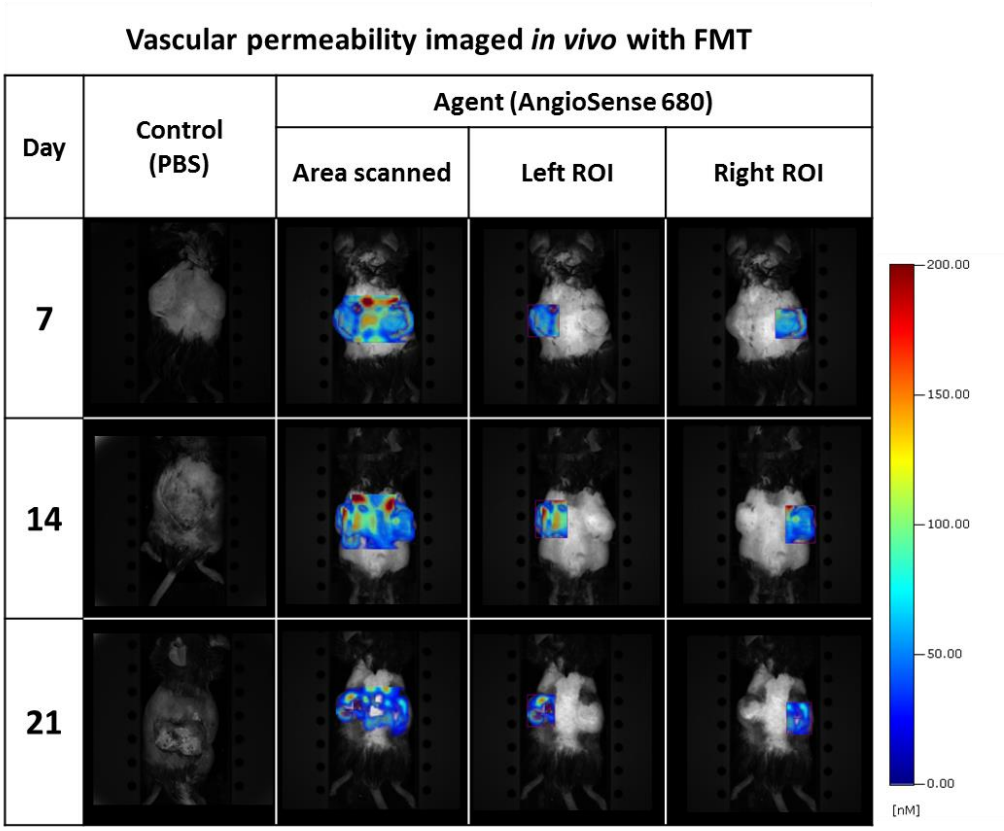

b)

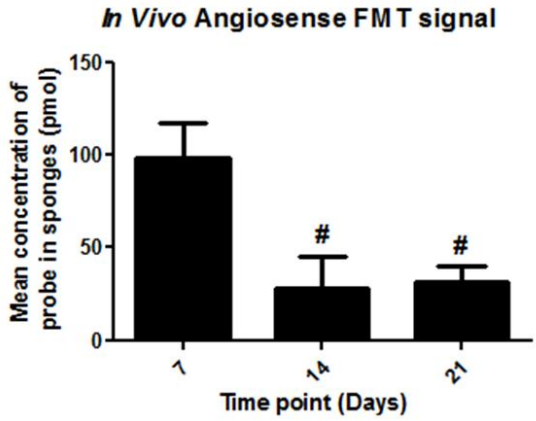

Figure 4.13. AngioSense was detected *in vivo* by FMT imaging on D 7, 14 and 21. a) Representative images from *in vivo* imaging, the "Area Scanned" shows the total signal detected in the scanned area; the "Left ROI" and "Right ROI" show the volume of signal used for quantification. b) The signal was highest on D 7 and then reduced at D 14. Bars represent mean ± SEM (n = 6 − 9) and comparisons were made using a one-way ANOVA followed by Dunn's multiple comparison test comparing data sets to D 7 (# $P < 0.05$).

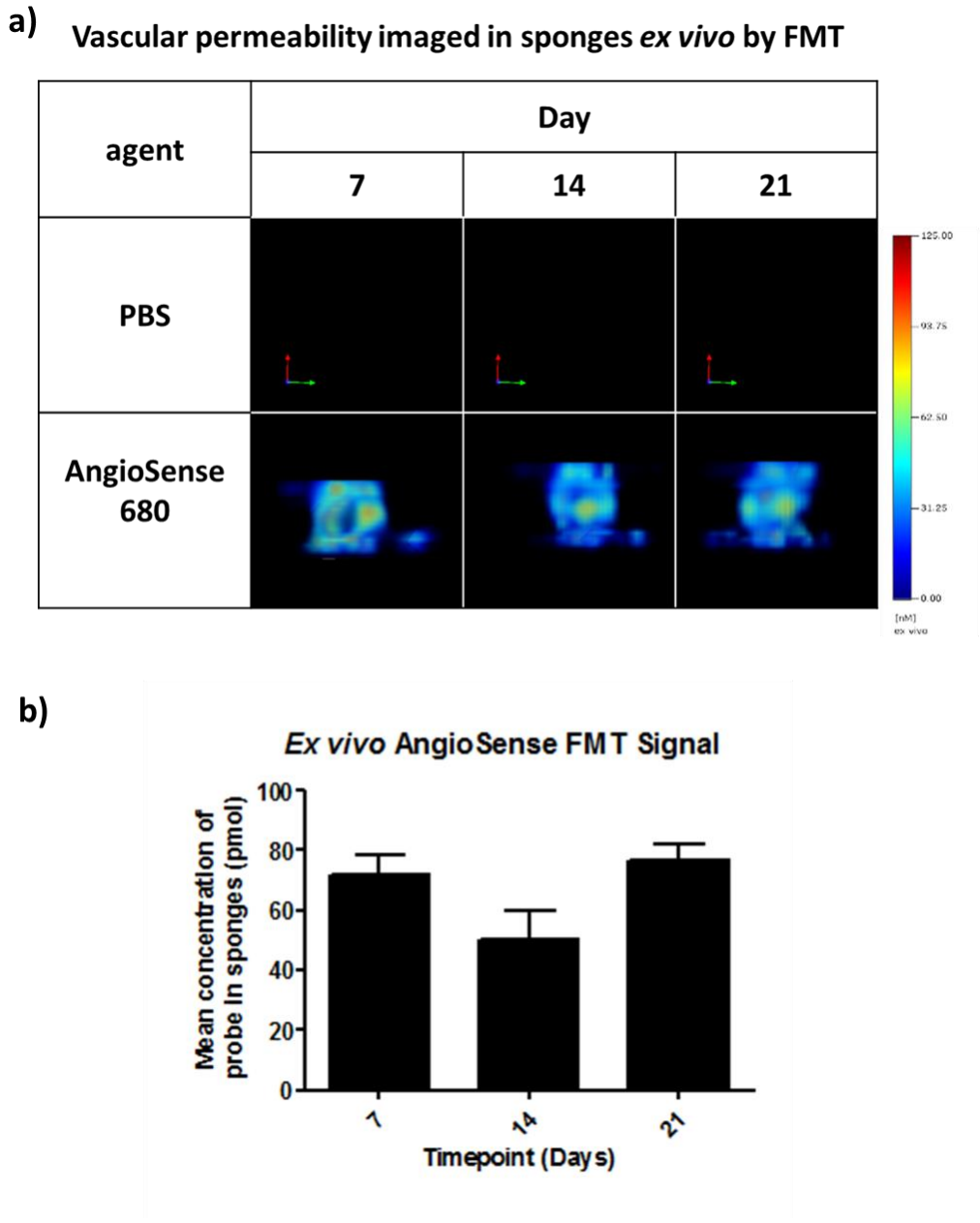

Figure 4.14. AngioSense was detected by FMT in sponges *ex vivo* collected on D 7, 14 and 21. a) Representative images of the total signal detected from a single sponge. This was used to quantify the signal within the sponges. b) The mean concentration of AngioSense 680 detected by FMT imaging in the dissected sponges *ex vivo* did not change significantly over the experiment. Bars represent mean ± SEM (n = 5) and comparisons were made using a one-way ANOVA ($P > 0.05$).

4.3.3 Sponge implantation results in the presence of MMPs

MMP gene expression was detected in the sponges

RT-qPCR analysis of gene transcripts showed that MMP- 2, -9, -10, -12 and -13 were present over the experiment (Figure 4.15). MMP-2 and -13 remained fairly constant whereas MMP-10 was highest on D 14. MMP-9 expression decreased over time whereas, strikingly, MMP-12 increased overtime.

MMP-12 and TIMP-1 protein were present

Interestingly the MMP-12 total protein (zymogen and active) expression was highest in samples collected on D 3 post implantation and steadily decreased to D 21, then appeared to increase again to D 35 (Figure 4.16). The endogenous inhibitor, TIMP-1, was highest on D 3 and diminished by D 7 (Figure 4.17).

MMP-12 activity was highest in sponges collected on D 7

Casein zymography of cell lysates resulted in digested regions (clear/ white) of protease activity at 29 kDa (Figure 4.18a) (Raza *et al*.,2000). Analysis of the gels by densitometry gave quantitative results of the casein digestion by the 29 kDa protein (Figure 4.18b). When the casein gel was treated with marimastat (an MMP inhibitor) the protease action was inhibited by approximately 45% (Figure 4.18c). This technique proved to be challenging and due to limited resources the results here are presented as n = 1.

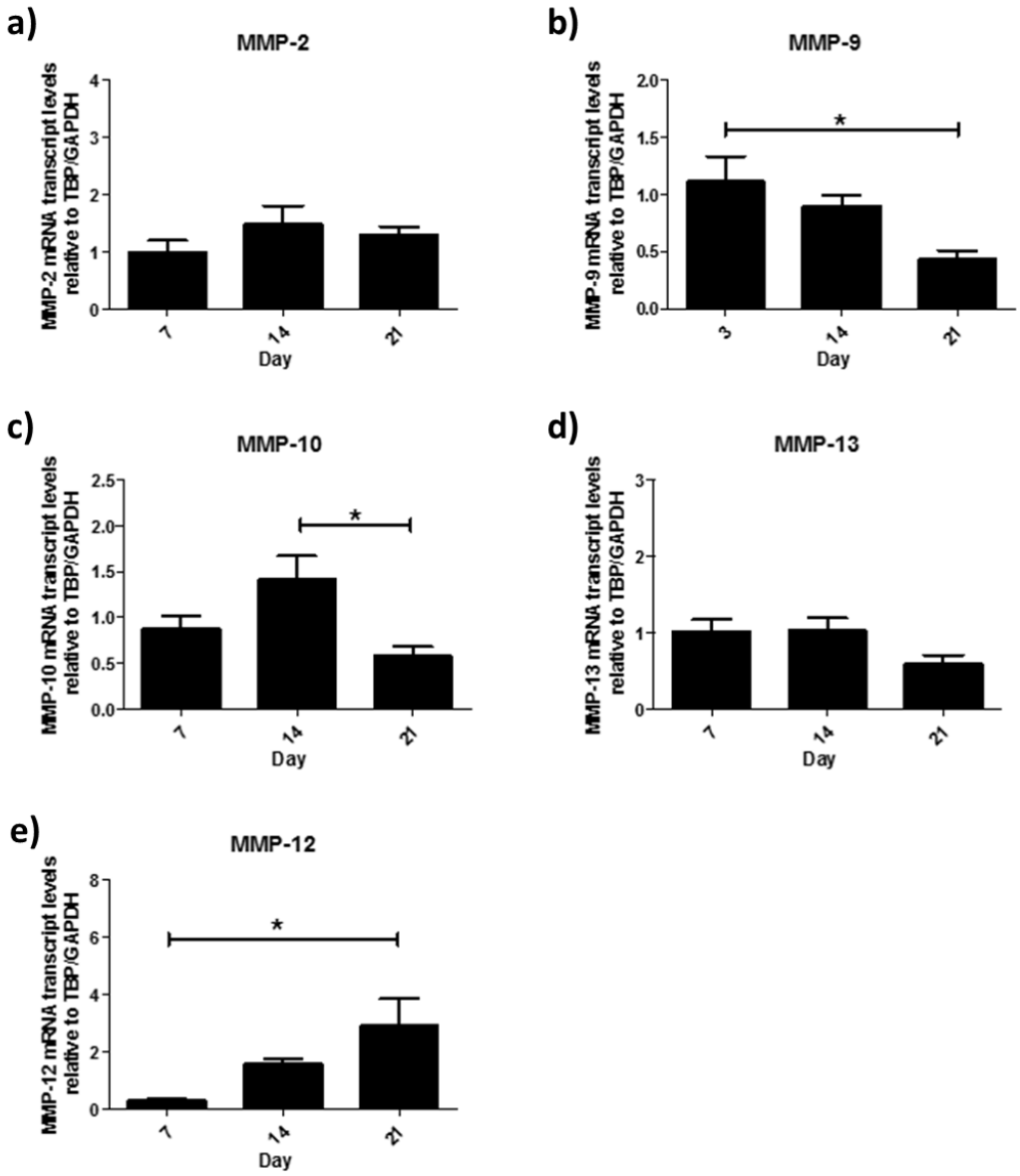

Figure 4.15. MMP-2, -9, -10, -12 and -13 gene transcripts were all present in sponges but had differing profiles over D 7 − 21. RT-qPCR analysis showed that gene transcripts for MMP-2 (a) and 13 (d) remained steady, MMP- 9 (b) and 10 (c) decreased to D 21 whereas MMP-12 (e) expression increased from D 7 − 21. Bars represent mean ± SEM (n = 5 − 6) and comparisons were made using a one-way ANOVA followed by Bonferroni Post-hoc tests comparing all data sets (* $P < 0.05$).

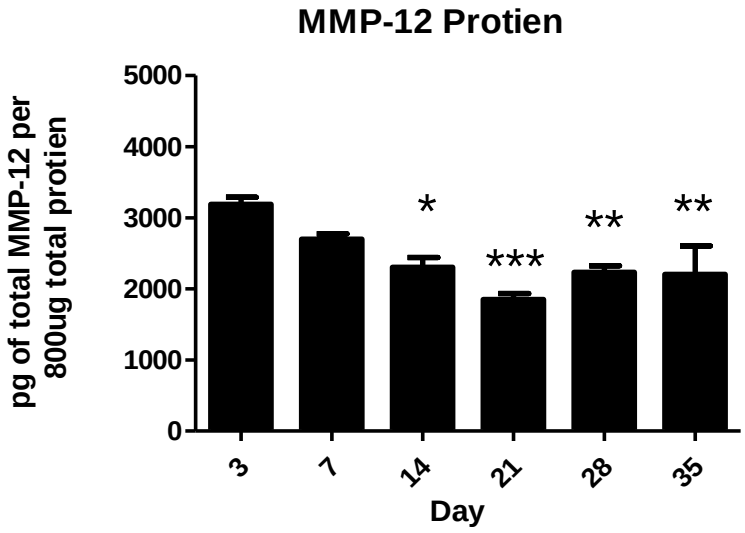

Figure 4.16. MMP-12 protein was present in sponges. MMP-12 protein concentration was highest in sponge tissue lysates from n D 3 which decreased to D 21. Bars represent mean ± SEM (n = 3 − 6) and comparisons were made using a one-way ANOVA followed by Dunnett's multiple comparison tests comparing all data sets to D 3 (* $P < 0.05$, ** $P < 0.01$, *** $P < 0.001$).

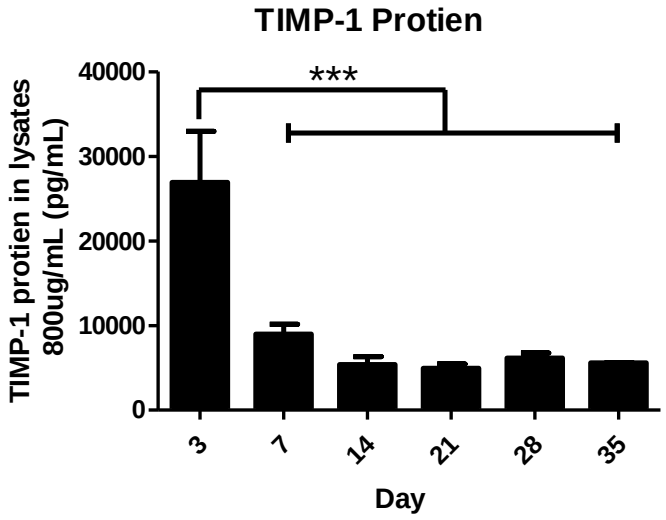

Figure 4.17. TIMP-1 protein was present in sponges. TIMP-1 protein had had the highest concentration in sponges at D 3, this significantly reduced by D 7. Bars represent mean ± SEM (n = 3 − 6) and comparisons were made using a one-way ANOVA followed by Dunnett's multiple comparison tests comparing all data sets to D 3 (*** $P < 0.001$).

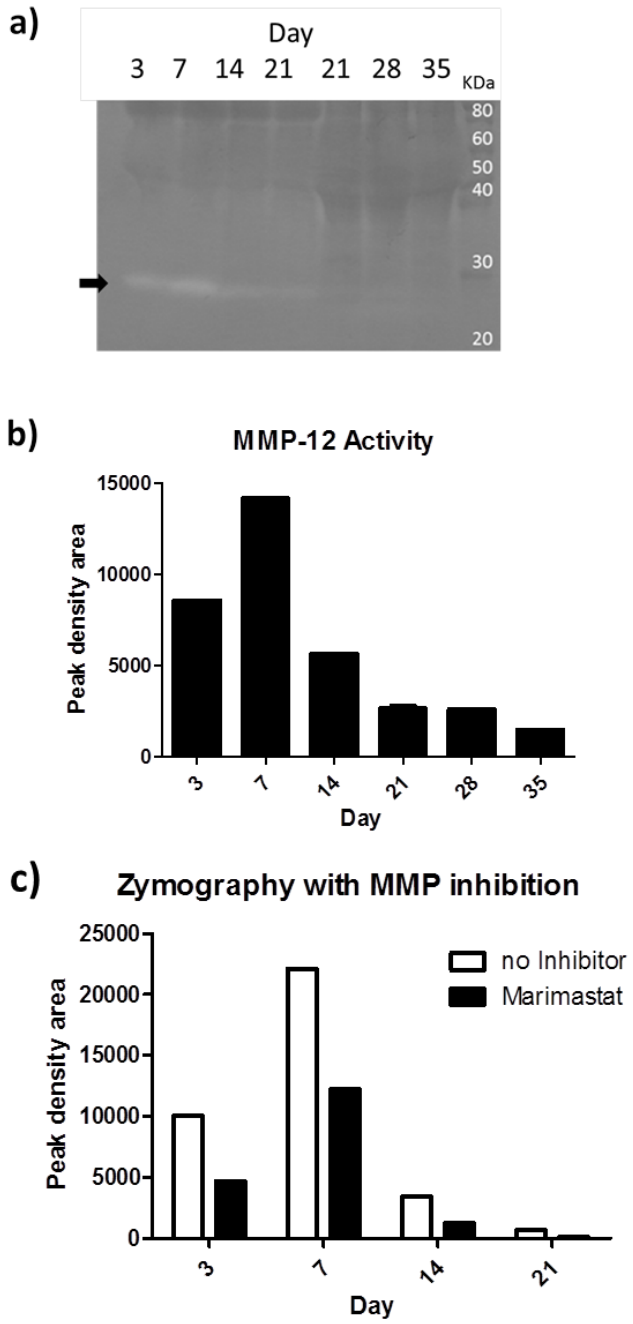

Figure 4.18. MMP-12 activity peaks on D 7. a) A representative image of tissue homogenates from sponges run on a casein gel (lanes 1 − 6 = D 3, 7, 14, 21, 21, 28, 35). White bands of regions of protease digestion of the casein substrate were observed (black arrow). b) Quantification of gel digestion was achieved by densitometry analysis of the 29 kDa band n = 1 − 2. c) Addition of marimastat (50 µM) to the development buffer (24h, 37 °C) appeared to inhibit MMP-12 activity. The Figure shows densitometry analysis of the casein digestion with marimastat (white bars) or without (black bars) n = 1.

MMP activity was detected in sponges *in vivo.*

MMPSense signal was detected *in vivo* by FMT in sponges on D 7, 14 and 21 (Figure 4.19a) but there were no significant changes in the quantified signal (Figure 4.19b). Sponges were then removed and the MMPSense imaged *ex vivo* (Figure 4.20a); quantification of the signal in the sponges also showed no changes between D 7, 14 and 21 (Figure 4.20b).

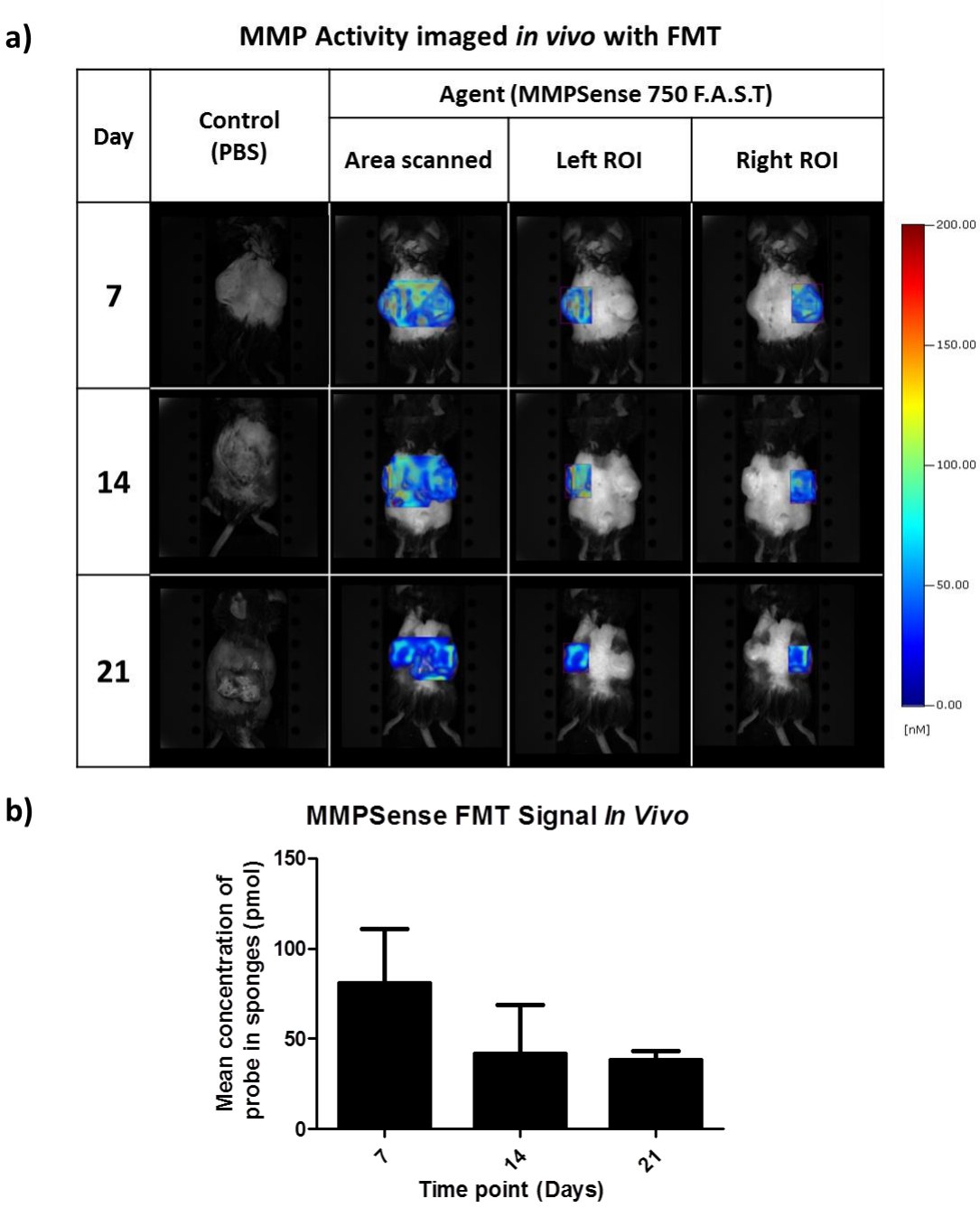

Figure 4.19. MMPSense can be imaged *in vivo* on D 7, 14 and 21. a) Representative images of *in vivo* FMT imaging; "area scanned" shows the total signal detected in the scanned area, the "Right ROI" and "Left ROI" identifies the sponge locations and therefore the signal used for quantification of MMP activity. b) There were no significant changes in the mean concentration of MMPSense detected *in vivo* by FMT imaging of the subcutaneous implanted sponges. Bars represent mean ± SEM (n = 6 − 9) and comparisons where made using a one-way ANOVA ($P > 0.05$).

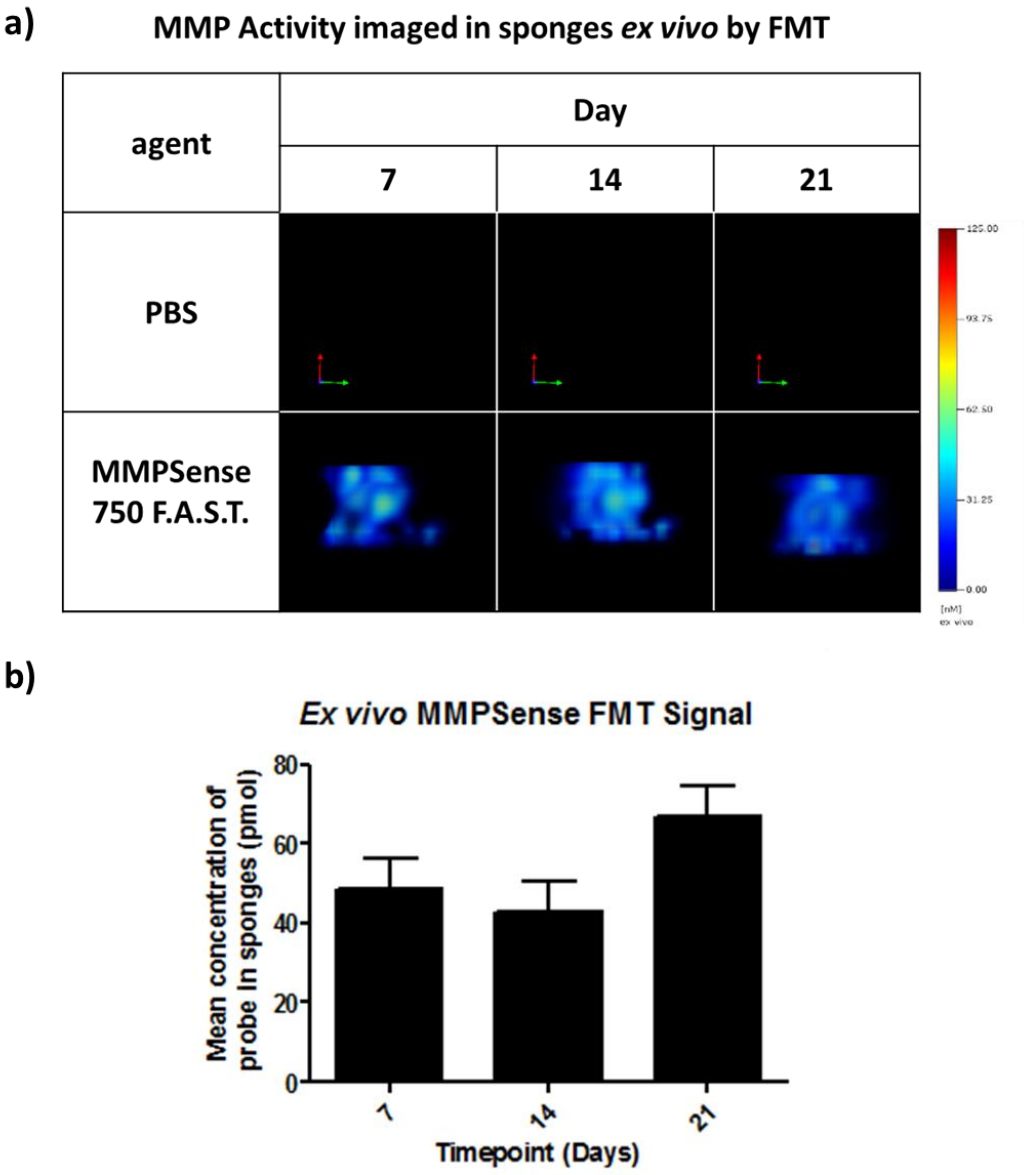

Figure 4.20 . MMPSense can be imaged by FMT in *ex vivo* sponges collected on D 7, 14 and 21. a) Representative *ex vivo* FMT images of MMPSense in sponges on D 7, 14 and 21. b) The total signal detected was used to quantify the MMP activity within the sponges, there were no significant changes detected. Bars represent mean ± SEM (n = 5 − 6) and comparisons were made using a one-way ANOVA ($P > 0.05$).

4.4 Discussion

In this chapter, a preclinical *in vivo* murine model of angiogenesis was established to determine whether MMP activity (particularly MMP-12) is present and can be imaged during angiogenesis. Histological techniques confirmed that this murine model exhibited both a time-dependant inflammatory repose and generation of new vessels. Angiogenesis could be imaged by FMT within the sponges *in vivo* and *ex vivo* using a commercial probe (AngioSense); but this method did not provide precise quantification of angiogenesis consistent with that gained by histology. Secondly, the angiogenic and inflammatory responses in these sponges are accompanied by expression of MMPS, including MMP-12. MMP-12 was present and active during angiogenesis but mRNA expression, protein expression and the protease activity had different temporal profiles over D 7, 14 and 21: peaking on: D 21 for mRNA transcript number, D 3 for protein expression, and D 7 for protease activity. Other MMPs were investigated (MMP- 2, 9, 10, and 13) by analysing mRNA expression; all exhibited transcript expression for D 7 − 35 but had varying profiles. Additionally, in this model MMP activity could be imaged using FMT in the sponges *in vivo* and *ex vivo* with a commercial probe. The data in this chapter support the suitability of this mouse model as a tool for: i) testing MMP-12 targeting inhibitors and imaging compounds and, ii) an investigation into the role of MMP-12 during angiogenesis.

The first model of spontaneous angiogenesis by subcutaneous implantation of a (polyester) sponge was reported in rats in 1987 (Andrade *et al*.,1987), but has since been modified for mice (Hague *et al*., 2002; Illanes *et al*., 2002). This model is attractive as it is very reproducible and the number of vessels can be easily quantified using histological techniques. There have been several successful adaptations of this model to utilise different scaffold materials such as metal meshes, (Schilling *et al*., 1959) other synthetic polymers (polyvinal alcohol, poly urethane) and hydrogels (Kleinman *et al*., 1986; Phelps *et al*., 2010). Furthermore, agents can be administered systemically (via food, water or intravenous injection) or directly via drug

releasing sponge coatings, osmotic minipumps, silastic elastomers or injection into the sponge. For the experiments in this chapter, inexpensive polyurethane sponges were utilised and implanted using a method already established in my supervisor's laboratory (Small *et al*., 2005).

Spontaneous angiogenesis in the subcutaneous sponge implants is facilitated by the porous framework and the host inflammatory response. Post implantation, the infiltration of leukocytes results in the secretion of a cocktail of cytokines and chemokines, producing a proangiogenic response (Leibovich *et al*., 1987; Barcelos *et al*., 2005). The appearance of sponges examined *ex vivo* over D 3 − 35 showed a gradual increase in vessel infiltration, tissue deposition and encapsulation accompanied by compression of the sponge. Consistent with the literature, histological analysis of the sponges showed a steady increase in deposition of fibrovascular tissue containing cells and vessels at different stages of maturation (Xavier *et al*., 2010).

Angiogenesis is a complicated process; during the sprouting phase the surrounding connective tissue and vascular network are broken down and endothelial cells lead the formation of new vessels (Van Hinsbergh & Koolwijk 2008; Rundhaug 2005). These vessels then mature through the recruitment of other cells such as smooth muscle and pericytes (Ribatti *et al*., 2011). These different cell types can be differentiated by fluorescent immunostaining: CD31 (cluster of differentiation 31 but also known as platelet endothelial adhesion molecule-1, PECAM-1) for endothelial cells (Newman 1997); α-SMA (alpha smooth muscle actin) for smooth muscle and pericytes (Skalli *et al*., 1989). CD31 is a 130 kDa type I transmembrane glycoprotein that is expressed at high levels on early and mature endothelial cells at the cell-cell junctions. (Wong *et al*., 2000) It is also expressed to a lesser extent by leukocyte subpopulations (where it facilitates endothelial cell transmigration (Muller, 1995; O'Brien *et al*., 2003), and by platelets in which it facilitates platelet adhesion, aggregation and thrombus

formation (Falati *et al*., 2006; Rosenblum *et al*., 1996). The protein α-SMA is a component of the cell machinery which enables cell contraction in smooth muscle and pericytes; it is also expressed by fibroblasts which are the main producer of fibrous tissue in this model (Goodpaster *et al*., 2008; Hughes & Chan-Ling 2004). DAPI (4',6-diamidino-2-phenylindole) was used as a counter-stain for cell nuclei in these experiments.

The stained sections were analysed in 3 ways. Firstly, the mean intensity of the fluorescence was measured for each channel across each section. Secondly, the percentage area covered by the signal was measured. Finally, the number of vessels was assessed by counting the total number of CD31 and CD31 & α-SMA positive vessels (positively stained structures with a lumen). All three methods gave slightly different profiles for vessel infiltration into the sponge. The variation in the "vessel number" implied by measurements of CD31 and α-SMA staining using these 3 methods could be because: 1) other non-vascular cell types can also be positive for CD31 and α-SMA antigens. 2) The sponges were autofluorescent, resulting in a higher signal intensity and area measured (especially on the green channel/ CD31). 3) Areas of intense staining could be subject to self-quenching (dye-dye energy transfers) resulting in a false lower mean fluorescence intensity signal measured. 4) The counting method was limited to larger vessels as the smaller capillaries or fragments of vessels were much harder to differentiate from artefacts. For the purposes of this study it was decided that the final method provided the most reliable measurement of vessel numbers. This method analysed the whole tissue section and allowed for assessment of actual vessel numbers as opposed to the number of cells expressing the markers. CD31 and α-SMA antibodies have cross reactivity with cell types other than vascular cells. This has also been the preferred method within my supervisor's group. Thus these results were interpreted as showing that vessel numbers increased from D 3 to 28 and then reduced on D 35. This reduction may be due to vascular pruning.

Angiogenesis can also be detected by changes to the expression profiles of cell markers, growth factors and mitogens. The number of mRNA transcripts of VEGF peaked on D 7 and diminished by D 21 as the initiation phase of angiogenesis ended (vessel numbers began to stabilise from D 21). VEGF-induced activation of endothelial cells results in disassembly of VE-cadherin, one of the principal signalling and structural proteins associated with the VE cell-cell adheren junctions (Petzelbauer *et al*., 2000). Disassembly of these junctions increases vascular leakiness and enables the migration of the endothelial cells. These then divide to form the new vessels (Bates 2010). CD31 is highly expressed by endothelial cells and its expression in sponges increased from D 7 – 14 then plateaued despite the actual number of vessels increasing up until D 28. CD31 is not exclusively expressed by this cell type and, therefore, perhaps this is not a true representation of the number of endothelial cells present. Furthermore, a limitation of RT-qPCR is that changes in transcript number may not necessarily mean a change in the number cells expressing it, rather a change in expression from cells already present.

PDGF gene transcription increased from D 7 – 21. Although pro-angiogenic, PDGF is of little importance in the initiation of new blood vessel formation (unlike VEGF) but is more important in the maturation process (Levanon *et al*., 2006). These results support evidence for vascular growth and maturation within the implanted sponges, but RT-qPCR cannot be used as an accurate measurement of angiogenesis in this model.

During the early stages of angiogenesis, VEGF causes an increase in vascular permeability which then returns to basal levels as the new vessel grows and matures (Bates 2010). Basal vascular permeability is essential for the health of normal tissues as it allows the exchange of small molecules, nutrients or waste products. Increased vascular permeability is a key feature of physiological and pathological angiogenesis and is dramatically increased in acute and chronic inflammation. In this study the number of VEGF mRNA transcripts peaked on D 7

and diminished by D 21, this would suggest that vascular permeability during tissue remodelling in this model should be highest on D 7. Vascular leakiness can result in a large efflux of water, macromolecules and inflammatory cells from the vasculature to the interstitium, often leading to in oedema. Sponges collected in this experiment, even as early as D 3, were filled with liquid.

Angiogenesis has previously been measured *in vivo* by monitoring the clearance of a radioactive (Mahadevan *et al*., 1989) or fluorogenic (Lage & Andrade 2000) substance post injection into the sponges (which then diffused into vessels and cleared). This methodology provided useful representation of vascular density in live animals; but needed either radiation or repeated blood sampling and relatively lengthy processing of samples to attain the results. Vascular permeability was quantified in this study using FMT imaging by ascertaining the gain in concentration of the AngioSense probe in the sponges 24 h after iv administration. Vascular permeability was expected to be highest on D 7 during angiogenic spouting and the initial inflammatory response, followed by a reduction as vessels matured and inflammation reduced as the wound healed. The results in this chapter were consistent with this hypothesis as the concentration of this probe measured *in vivo* within the sponges was calculated to be highest on D 7 compared to D 14 and 21. Interestingly, there were no significant changes in the AngioSense signal quantified from *ex vivo* imaging (D 7, 14 and 21). This suggests that this technique was not sufficiently sensitive to detect any changes occurring in (number or functionality of) the vascular network over the experimental period. Furthermore, the increased probe accumulation detected *in vivo* on D 7 is likely to be predominantly in the tissue closely surrounding the sponge (subcutaneous skin and the abdominal muscle). These tissues are undergoing the early stages of angiogenesis and inflammatory remodelling as a result of the surgical insult and presence of the foreign body.

Inflammation plays a key role in the initiation and/or progression of cardiovascular diseases (Stamenkovic 2003). A chronic inflammatory state post sponge implantation helps to stimulate angiogenesis via the production of proangiogenic growth factors (Costa *et al*., 2007). TNFα is a cytokine released systemically during acute inflammation. In the work described in this chapter, TNFα transcript expression remained stable over D 7 − 21 signifying an ongoing inflammatory response. TNFα is also a potent inducer of new blood vessel growth and is also a regulator of wound repair (Leibovich *et al*., 1987). Although its mechanism of action is still unclear, TNFα is also suggested to prime endothelial cells for sprouting once the initial inflammatory response has passed (Sainson *et al*., 2008). This suggests that chronic expression of TNFα in this model primes endothelial cell to undergo angiogenesis.

In early inflammation, resident macrophages recognise foreign or damaged material and secrete pro-inflammatory mediators that recruit polymorphonuclear neutrophils. In this chapter, neutrophils were stained using H&E and identified as small polymorphonuclear cells. As expected, the population of polymorphonuclear cells was highest in sponges collected on D 3 and had diminished by D 14. During inflammation the neutrophil population is replaced by monocytes which differentiate into macrophages. These secrete proteases and phagocytose cell debris. The influx of neutrophils is partially halted through chemokine inactivation by macrophage derived MMP-12 (Dean *et al*., 2008). The marker F4/80 was chosen to stain macrophages because it has limited cross reactivity with other cells present, including fibroblasts (Inoue *et al*., 2005). The density of macrophages close to the edge of the sponge increased from D 3 − 14 and remained steady but, strikingly, the total depth of macrophage infiltration into the sponge increased from D 3 – 28. MMP-12, along with MMP-9, is also suggested to facilitate the infiltration of macrophages (Gong *et al*., 2008; Li *et al*., 2012); in this study MMP-9 transcript levels were high on D 7 as infiltration began, MMP-12 expression gradually increased from D 7 to 21 (this associated well with macrophage infiltration). The

recruited leukocytes release mediators that attract other cells types such as fibroblasts and smooth muscle cells to begin the proliferative phase of wound healing.

Leukocytes are the predominant producers of MMPs which are capable of destroying one or many components of the extracellular matrix. MMPs can also indirectly influence endothelial cell behaviour by release of proangiogenic factors, destruction of angiogenesis inhibitors, or generation of matrix fragments that inhibit angiogenesis, i.e., angiostatin (Cornelius *et al*., 1998; Rundhaug 2005). In this study, MMP activity was detected by FMT in sponges (*in vivo* and *ex vivo*) at similar levels over the time-points investigated (with similar levels detected at D 7, 14 and 21). Persistent signal reflects the ongoing MMP activity during the remodelling process of the surrounding skin and growth of vessels and deposition of tissue into the sponges. The MMPSense probe is activated by a group of MMPs (MMP- 7, -9, -10, -12, -13) and so any changes in the signal detected is unlikely to be in response to a single MMP, particularly MMP-12. Nevertheless, these data confirm MMP activity is present throughout the inflammatory and angiogenic process.

Interestingly, MMP-9 can manipulate vessel development by processing VEGF. ECM bound VEGF can be released by MMP-9 cleavage, when free it promotes angiogenic sprouting. Free VEGF can be truncated by MMP-9 proteolysis which can result in increased vessel diameter (Bergers *et al*., 2000; Lee *et al*., 2005). In this model, MMP-9 and VEGF mRNA transcript levels were high soon after implantation (then decreased from D 7 towards D 21). Soon after sponge implantation, MMP-9 may promote angiogenic sprouting by degrading the ECM and releasing any bound VEGF, but may also provide negative feedback by processing excess free VEGF. The expression of these genes decreased as angiogenesis progressed, consistent with free VEGF being involved in the initiation of vessel formation; not maturation which occurs at the later experimental time points (Bates 2010). MMP-13 mRNA transcripts remained stable over D 7 − 21, MMP-13 null mice have considerably reduced angiogenesis in wound healing

and so its presence may contribute to angiogenesis in this model but the exact mechanism is unclear (Hattori *et al*., 2009). MMP-10 gene expression dropped significantly between D 14 and 21, MMP-10 has been shown to have a dual role *in vitro*; it can promote endothelial cell migration and tube formation (Heo *et al*., 2010) but has also been identified as part of a different pathway which resulted in capillary cell regression and tubular network collapse (Saunders *et al*., 2005). Interestingly, its proangiogenic role was validated *in vivo* as MMP-10 siRNA inhibits angiogenesis in the Matrigel plug assay (Heo *et al*., 2010). Gene transcripts of MMP- 2 are present and remain fairly stable in this model. MMP-2 has been shown to be proangiogenic (Ohno-Matsui *et al*., 2003).

Generally, MMPs are considered to be destructive to the ECM and pro-inflammatory, and their presence is usually considered to be pro-angiogenic. The role of MMP-12 in these processes is less clear cut and it has been suggested to also have anti-angiogenic and anti-inflammatory properties. Consistent with its potential role in regulation of angiogenenesis, the results in this chapter show that both MMP-12 mRNA and protein were present during angiogenesis in the sponges, but interestingly their profiles were almost opposite. The MMP-12 mRNA transcript levels increased from D 7 to 21 whereas protein levels decreased from D 3 to 21. Interestingly Raza and colleagues (2000) also identified that the release of MMP-12 protein from macrophages was not necessarily associated with an increase in mRNA expression (Raza *et al*., 2000). Therefore, there is clearly complex regulation of MMP-12 processing at the transcriptional and translational levels. Currently there is limited literature on the activation pathway for MMP-12 transcription in macrophages but in SMC it may be regulated through phosphatidylinositol-4, 5-bisphosphate 3-kinase (Wu *et al*., 2003). Information on MMP-12 post-transcriptional mRNA regulation is also limited in murine models but in human alveolar macrophages miR-452 suppressed MMP-12 protein expression (Graff *et al*., 2012). Raza and colleges (2000) also demonstrated that plasmin(ogen) and thrombin induced a significant increase in MMP-12 secretion in macrophages via the thrombin G protein-coupled receptor

(protease-activated receptor 1 (PAR-1)) *in vitro*. Once MMP-12 protein is released from the cells it can be activated by proteases (mainly plasmin) in the extracellular space, the active protein can then take part in the biological processes and diseases (Longo *et al*., 2005; Houghton *et al*., 2006). MMPs are released as inactive zymogens into the extracellular space, where they can be activated by other proteases and inhibited by TIMPs. To gain an insight into the relative MMP activity in the sponge tissues over the experiment, zymography was performed (Vandooren *et al*., 2013). Using this technique, we determined MMP-12 activity was present in sponges collected throughout the experiment but it peaked on D 7; unfortunately only an n = 1 was achieved due to challenges in the zymography technique and limited sample and materials available. Therefore, this data provides only a rough guide as to when MMP-12 is most active in this model. Active MMP-12 can degrade several components of the ECM such as collagen, prothrombin and fibrinogen but it predominantly cleaves elastin to facilitate (endothelial, smooth muscle, fibroblasts and monocyte and macrophage) cell migration. Elastin is a highly elastic protein present in the connective tissues of vessel walls and skin that enables them to resume their shape after stretching. Active MMP-12 can also contribute towards the production of angiostatin a potent inhibitor of angiogenesis, from plasminogen (Dong *et al*., 1997); this can inhibit endothelial cell proliferation without affecting that of fibroblasts and SMC (O'Reilly *et al*., 1994). In this study, histological analysis demonstrated that the number of endothelial cells continued to increase in the presence of MMP-12 activity. Angiogenesis is a complex process and, therefore, the production of angiostatin by MMP-12 may be overcome by other proangiogenic factors. Furthermore, MMP-12 activity diminished within the sponges as angiogenesis stabilised, this is despite the continued presence of macrophages in high numbers. However, this study did not distinguish between M1 and M2 macrophage phenotypes, these could be present in different numbers during the study. Additionally, MMP-12 has also been suggested to have some anti-inflammatory regulatory

effects and in this study MMP-12 activity peaked as neutrophil numbers were decreasing and macrophage infiltration began (Bellac *et al*., 2014).

Active MMP-12, like most MMPs, is inhibited endogenously by TIMP-1 coordinating to the active site. TIMP-1 has been shown to inhibit endothelial cell migration *in vitro* (Akahane *et al*., 2004). In this study TIMP-1 concentration was highest in sponges collected on D 3 (100 × TIMP-1 protein compared with MMP-12) at which time the sponges contained no vessels. TIMP-1 may be inhibiting the early stages of angiogenesis by minimising cell proliferation and mobility (Reed *et al*., 2003).

4.4.1 Conclusion

The data presented in this chapter characterised the sponge implantation model which involves angiogenesis, chronic inflammation and the presence of MMPs. Histological and molecular biology techniques contributed valuable information about a remodelling process, but techniques to monitor the process *in vivo* non-invasively would be advantageous. The FMT imaging with commercial probes in this study did provide information on MMP activity and vascular function but had low resolution. Furthermore, the commercial probe provided a generalised picture of MMP activity as it detected a broad spectrum of MMPs. MMP-12 was present during angiogenesis in this model but it's exact role still remains unclear; this could be better investigated using this model with MMP-12 inhibitors, MMP-12 selective FRET probes and MMP-12$^{-/-}$ mice.

Chapter 5

MMP-12 Does Not Inhibit Angiogenesis

5 Chapter 5: MMP-12 Does Not Inhibit Angiogenesis

5.1 Introduction

5.1.1 MMPs

The extracellular matrix (ECM) is the structural connective tissue between cells, comprising collagens, elastin, glycoproteins and fibronectin. Structural changes to the ECM are required for growth and repair (Frantz *et al*., 2010; Hynes, 2009). MMPs are a large family (24+) of zinc dependent proteases, each capable of degrading one or many components of the ECM (Nagase *et al*., 2006). MMPs are under tight regulation (at translation, transcription, secretion, and activation levels), with even the active proteases regulated by endogenous tissue inhibitors of metalloproteinases (TIMPs) (Löffek *et al*., 2011). MMPs are essential for everyday physiological processes but dysregulation of MMP activity is associated with the progression of pathology of many diseases including cancer, inflammatory bowel disease and atherosclerosis (Vu, 2000; O'Sullivan *et al*., 2015; Liang *et al*., 2006; Overall & Kleifeld, 2006).

5.1.2 The role of MMPs in regulating angiogenesis

Matrix metalloproteinases play a dual role during angiogenesis: they are essential for endothelial cell migration and tube formation, but some can also create proteolytic products which are inhibitors of angiogenesis (e.g. angiostatin or endostatin) (Nguyen *et al*., 2001; Cornelius *et al*., 1998; Ferreras *et al*., 2000).

MMPs degrade the basement membrane, ECM components and VE-cadherin endothelial cell-cell adhesions, allowing endothelial cells and pericytes to migrate (Herren *et al*., 1998). Consequently, MMPs overall play a positive role promoting angiogenesis (Bergers *et al*., 2000; Lee *et al*., 2005). Most single MMP knock out (KO) mice do not show severe defects in

angiogenesis, this may be because other MMPs can compensate for the loss due to the cross substrate recognition. Exceptions to this are MMP-1 and -9: MMP-1 KO mice have significant skeletal defects and exhibit a minimal response in *in vivo* angiogenesis assays (Zhou *et al.*, 2000); MMP-9 KO mice exhibit abnormal angiogenesis in the skeletal growth plate during development but this resolves within 3 weeks post-partum (Zhou *et al*., 2000; Vu *et al.*, 1998).

5.1.3 MMP-12 inhibits angiogenesis

MMP-12, also known as macrophage elastase (MME), is predominantly produced by pro-inflammatory macrophages and is considered one of the most important enzymes in the degradation of elastin (but also breaks down fibronectin and collagen IV; Shipley *et al.*, 1996). MMP-12 activity has been shown to be protective against certain diseases. Its activity has been shown to be: cancer protective (Houghton *et al.*, 2006), anti-inflammatory (Dean *et al.*, 2008), anti-bacterial and anti-viral (Houghton *et al.*, 2009; Marchant *et al.*, 2014). But MMP-12 activity is also associated with several cardiovascular diseases including atherosclerosis (Johnson *et al.*, 2011; Yamada *et al.*, 2008), aneurysms (Curci *et al.*,1998; Longo *et al.*, 2005), and acute and chronic arterial stiffening (Liu *et al.*, 2015). Li and colleagues (2012) showed that KO mice exhibited increased angiogenesis of the retina after oxygen-induced retinopathy. Furthermore, tumour samples with increased MMP-12 expression also exhibited reduced vascular content (Margheri *et al.*, 2009; Yang *et al.*, 2001; Gorrin-Rivas *et al.*, 2001; Shi *et al.*, 2006).

MMP-12 can inhibit angiogenesis in two ways: firstly, by the inhibition of plasmin (which is pro-angiogenic) production, and secondly by producing inhibitors of angiogenesis, such as angiostatin and endostatin (Figure 1.12). Cornelius and colleagues found that MMP-12 is the most efficient member of the MMP family for cleaving plasminogen to produce angiostatin, which inhibits endothelial cell proliferation *in vitro.* Macrophages from MMP-12$^{-/-}$ mice

cannot produce angiostatin from plasminogen (Cornelius *et al*., 1998; Serrat *et al*., 2006). MMPs, including MMP-12, can also produce endostatin, a 20 kDa C-terminal fragment of collagen XVIII which also acts as a potent inhibitor of angiogenesis (Ferreras *et al.,* 2000).

The second mechanism linking MMP-12 activity with inhibition of angiogenesis is through its interaction with the uPA/uPAR axis. The uPA/uPAR system has complex functions in inflammation, cancer and cell signalling processes (Crippa, 2007). The endothelial cell uPAR is bound to the cell surface and binds to extracellular pro-uPA, activating it to uPA. The uPA catalyses the production of plasmin from plasminogen in the extracellular space; plasmin cleaves various components of the ECM and is able to activate pro-MMPs leading to further degradation of the matrix. This leaky matrix facilitates the migration of endothelial cells during angiogenesis (Blasi & Carmeliet, 2002). MMP-12 cleaves the full-size endothelial uPAR *in vitro,* generating a truncated form; this may render it unable to sustain its role in promoting angiogenesis via the uPA/uPAR complex *in vivo* (Koolwijk *et al*., 2001; D'Alessio *et al*., 2004; Serrat *et al*., 2006).

Tools to enable interrogation and visualisation of MMP-12 activity *in vitro, ex vivo* and *in vivo* in real-time would allow for assessment of its molecular activity during tissue remodelling in disease and angiogenesis. This project aimed to develop MMP-12 targeting compounds which could be used to clarify its role in angiogenesis. In Chapter 3, an MMP-12 selective inhibitor (HS1-22) and activity FRET probe (HS1-65) were synthesised. In Chapter 4, the *in vivo* sponge implantation model of angiogenesis was characterised and MMP-12 activity was measured to be highest on D 7 in tissue lysates using zymography.

In this chapter HS1-65 was tested as tool to image MMP-12 activity in tissues, initially using well plate assays and tissue lysates, with the aim to use a similar probe to selectively image MMP-12 activity *in vivo*. In addition, HS1-22 was used to inhibit MMP-12 in *ex vivo* and *in vivo* models of angiogenesis.

5.2 Hypothesis and aims

5.2.1 Hypothesis

MMP-12 activity inhibits angiogenesis.

5.2.2 Aims

1. To determine whether the substrate activity probe HS1-65 can detect MMP-12 activity in tissue lysates during angiogenesis in a mouse *in vivo* model of angiogenesis.

2. To determine whether HS1-22 (MMP-12 selective inhibitor) increases angiogenesis in the sponge implantation model and in aortic ring explants.

3. To determine whether MMP-12 deletion increases angiogenesis in the sponge model and in aortic ring explants.

5.3 Methods

5.3.1 Animals

C57BL6/J mice were purchased from Harlan or Charles River, MMP-12 KO mice (B6.129X-Mmp12tm1Sds/J (Shipley *et al.*,1996)) were purchased from The Jackson Laboratories (USA) via Charles River (UK). Animals were housed in groups, where appropriate, and maintained under controlled conditions of light (lights on 08:00 − 20:00) and temperature (21 − 22 ˚C). All mice were housed for at least 1 week, with constant access to food and water before use in experiments.

5.3.2 FRET probe detection of MMP-12 activity in tissue lysates

Study design

The ability to image MMP-12 activity quickly in biological mixtures, tissues and *in vivo* would aid our investigation. Here, the ability to detect MMP-12 activity with HS1-65 (an MMP-12 activity substrate probe) was assessed in lysates of angiogenic tissue (Figure 5.1). *In vitro* zymography analysis of sponge tissue lysates collected over a time course study suggested MMP-12 was most active on D 7 (Figure 4.18) so sponges in C57BL6/J and MMP-12 KO mice were imaged *in vivo* on D 7 by FMT.

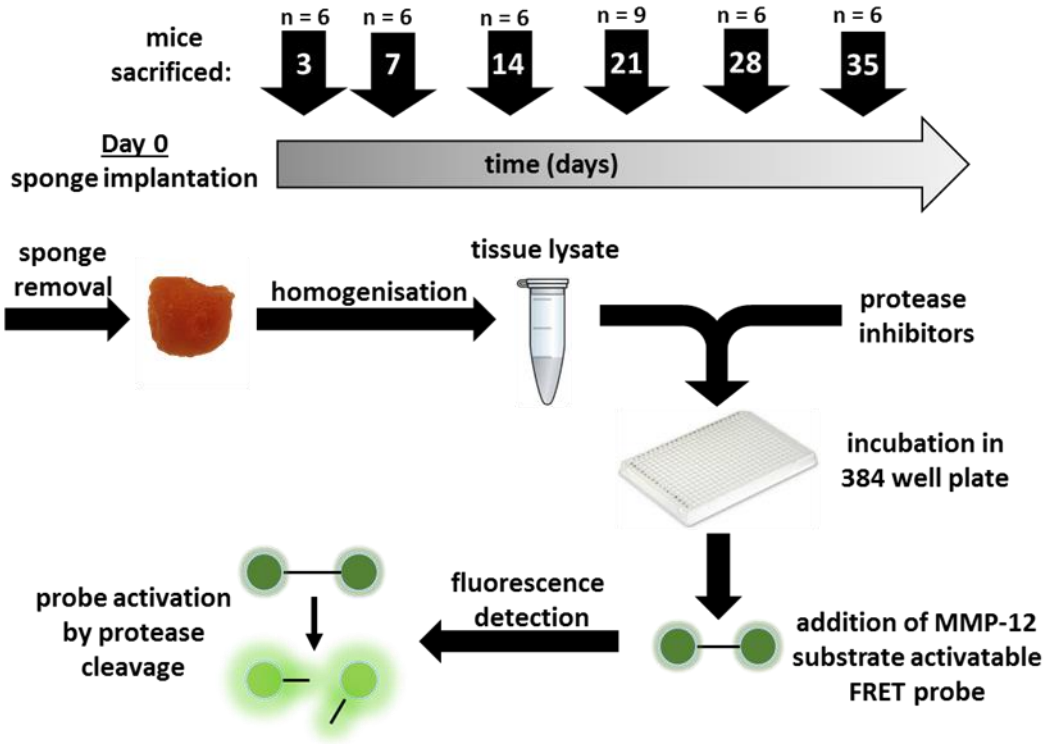

Figure 5.1 Study design: Protease detection in tissue lysates from sponges (D 3 − 35) with an MMP-12 selective probe (HS1-65). C57Bl/6J mice were anesthetised and two 1 cm^3 sponges implanted subcutaneously on the left and right flanks. Mice were sacrificed and sponges removed on D 3, 7, 14, 21, 28, and 35 (n = 6) after implantation. Sponges were homogenised in PBS, the lysate isolated by centrifugation and the protein content calculated using a Bradford's assay. In a 384 well plate, 15 µL reactions were set up in triplicate. Tissue lysates (1.67 µg/mL) were incubated (37 °C, 2 h) with protease inhibitors (marimastat, sivelestat, anti-thrombin III, a protease cocktail block, or MMP buffer, at appropriate concentrations). HS1-65 (10µM) was then added to each well and the proteolysis of HS1-65 monitored in a plate reader over 2 h. Lysates could then be purified and the protease cleavage of HS1-65 confirmed by matrix-assisted laser desorption/ionization - time of flight- mass spectrometry (MALDI-TOF MS).

Surgery, tissue collection and lysate preparation

Sponges were implanted subcutaneously as described in Section 2.9. The sponges were collected on D 3, 7, 14 and 21, cut in half, then either snap frozen on dry ice before storage at −80 °C. One half of the sponge was thoroughly homogenised in 1 mL of PBS. Samples were then centrifuged to isolate the plastic sponge and the supernatant transferred to a new Eppendorf tube. This was repeated and the resulting supernatant was stored at - 80 ˚C. The total protein in the lysate samples was quantified colorimetrically using a Bradford's assay for bovine serum albumin (protocol in Section 2.11).

Plate assay with HS1-65, tissue lysates and MMP inhibitors

Assays with tissue lysates and HS1-65 are described in Section 2.11. Briefly, in a 384 well plate, 15 µL reactions were prepared in triplicate: tissue lysates (D 3 − 35, 5 µL, final concentration 1.67 µg/ µL) were incubated (37 ℃, 1 h) with marimastat (5 µL, final concentration 500 nM) or MMP buffer. Other controls used were: *negative control*, the proteins in the tissue lysate were denatured (95 °C, 5 min); *positive control*, MMPcat-12 (5 µL, 30 nM). The plate was then cooled to 0 °C before HS1-65 was added (5 µL, final concentration 10 µM). Reactions were monitored in a plate reader (37 ℃, ex = 495 nm, em = 525 nm, 2 h). Results were analysed as a fold change in the fluorescent signal (compared to HS1-65 with no treatment).

Plate assay with protease inhibitors

As above but tissue lysates and controls (MMP-12_{cat} or Buffer) were mixed with protease inhibitors (sivelestat (100 µM) or antithrombin III (400 nM) or a protease cocktail block (used neat)) or with MMP buffer, and then incubated (37 °C, 2 h) prior to the addition of HS1-65.

MS analysis of probe cleavage in tissue lysate

Reaction mixtures from tissue lysate plate assays were purified and concentrated using pipette tips containing C18 resin cartridges (Millipore Zip Tip®) (protocol described in Section 2.11). The filtrate was analysed by MALDI-TOF MS as described in Section 1.4.

5.3.3 Pharmacological inhibition or deletion of MMP-12 during *ex vivo* angiogenesis

Study design

The aortic ring assay is a popular quantitative *ex vivo* model of angiogenesis in which developing microvessels undergo many key features of angiogenesis, it has recently been reviewed by Baker and colleagues (Baker *et al.*, 2012). Here we used this assay to test the effects of MMP inhibitors or MMP-12 deletion on angiogenesis (Figure 5.2), the experimental set up is described in Figure 5.3.

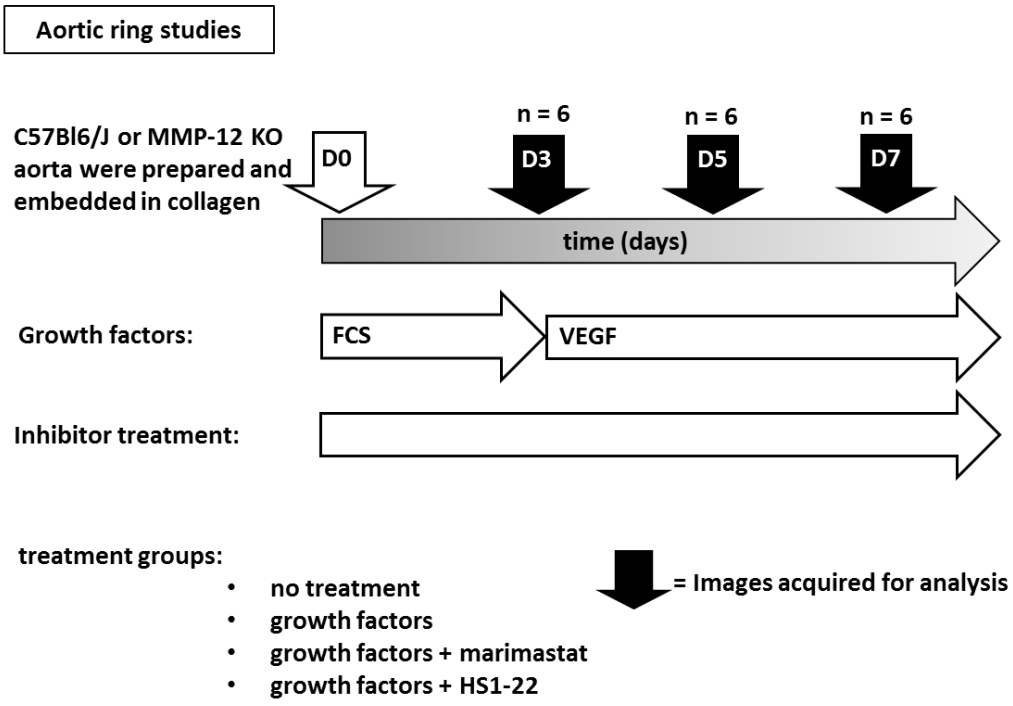

Figure 5.2 Study design: embedded aortae were treated with growth factors and MMP inhibitors. Treatments were made in Opti-MEM supplemented with 2% Foetal calf serum FCS for the first 3 days then VEGF (5 ng/mL) for the rest of the experiment. MMP inhibitors were added to the medium (HS1-22 or marimastat, 25 µM). Microvessel sprouts were counted on days (D) 3, 5 and 7.

Aortic ring assay

The aortic ring assay (Figure 5.3) is described in Section 2.8. Briefly, aorta were carefully dissected out, cleaned and cut into 1 mm rings; these where each embedded in 50 µL of collagen I (rat tail, 1mg/mL in DMEM) in a 96 well plate. Treatments were prepared in Opti-MEM supplemented with 2% Foetal calf serum (FCS) for the first 3 days then VEGF (5 ng/mL) for the rest of the experiment; MMP inhibitors (HS1-22 or marimastat, 25 µM) were also administered in the culture medium which was added on top of the gel (150 µL per well), and was refreshed every 2 − 3 days.

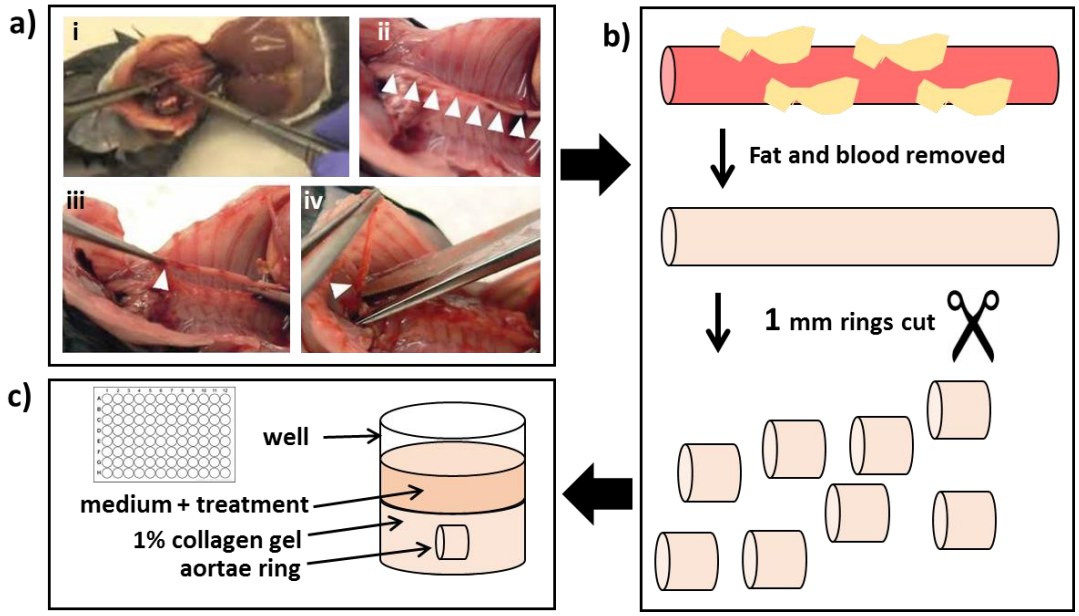

Figure 5.3 Aortic ring assay method. Under a dissecting microscope a) *i*, the thorax of an asphyxiated mouse is dissected to reveal the aorta; *ii-iv*, the aorta (white triangles) is exposed and carefully removed. b) The aorta is placed in DMEM and carefully cleaned by the removal of any excess fat and blood before being cut into 1 mm rings (10- 12 per aorta). c) In a 96 well plate a single ring is embedded in a 1% collagen gel, the treatment is then added to the medium above the gel. Treatments were applied on top of the gel and refreshed every 2-3 days (150 µL per well). Figure adapted from (Baker *et al*., 2012).

Analysis

Images of aortic vessels were captured at × 20 magnification on D 3, 5 and 7 post embedding. The images were randomised and angiogenesis was quantified in two ways (Figure 5.4). Firstly, by counting the number of sprouts and branches from the ring; the mean value of the replicates was taken for each mouse. Secondly, by quantifying the maximum vessel length. The length of the three longest vessels for each aortic ring was quantified using ImageJ; the mean value of the replicates was taken for each mouse.

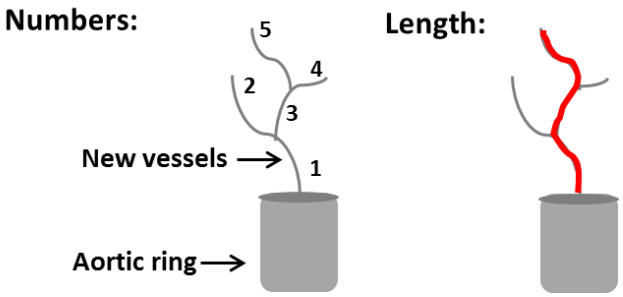

Figure 5.4 Analysis of vessel numbers and lengths in the aortic ring assay. Counting the number of sprouts: each sprout was counted as one, additionally to this, each branch was also counted as one; this illustrative ring sprout would be counted as 5. Vessel length: the length of a branch was measured in ImageJ from the ring to the tip of the microvessel (red line) using the freehand line drawing tool (pixels); the mean length of the three longest was calculated for each ring.

5.3.4 Pharmacological inhibition or deletion of MMP-12 during *in vivo* angiogenesis

Study designs

The *in vivo* subcutaneous sponge implantation model of angiogenesis (Small *et al.*,2005; Andrade *et al.*,1987) was used: firstly, to test pharmacological inhibition of MMP-12 (drug study, Figure 5.5), and secondly to test the effects of MMP-12 deletion using an MMP-12 knockout mouse (MMP-12 KO study, Figure 5.6) (Shipley *et al.*,1996).

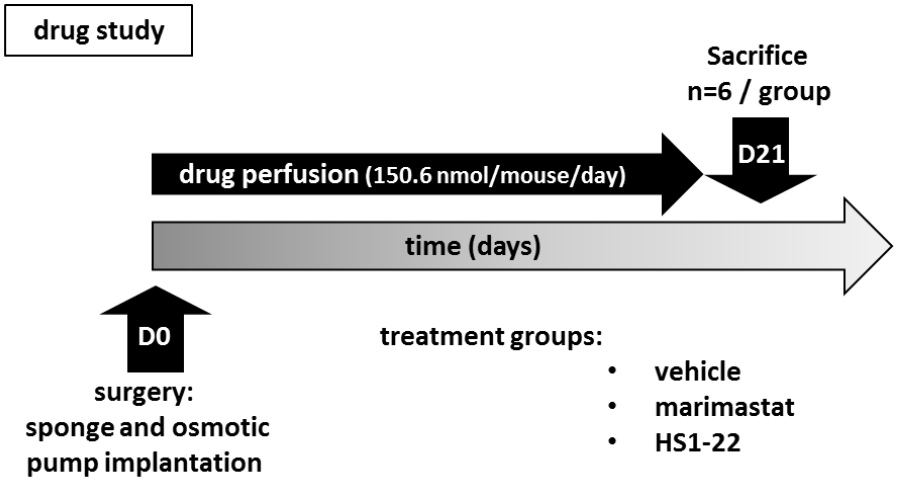

Figure 5.5 Study design: pharmaceutical intervention to inhibit MMPs in a model of angiogenesis. C57Bl6 mice were subcutaneously implanted with a 1 cm^3 sponge connected to an osmotic pump via a catheter. The osmotic pump was filled with either vehicle, marimastat (broad spectrum inhibitor) or HS1-22 (MMP-12 selective inhibitor) (n = 6). Drugs were slowly perfused (0.25 µL/h) into the sponge at 150.6 nmol/mouse/day (marimastat: 2 mg/kg/day or HS1-22: 2.6 mg/kg/day in vehicle (DMSO: propylene glycol : H_2O (1:1:1)). Sponges were removed on D 21, cut in half and samples either fixed or frozen. Angiogenesis was quantified by staining vessels for CD31 and α-SMA, stained vessels were counted under magnification**.**

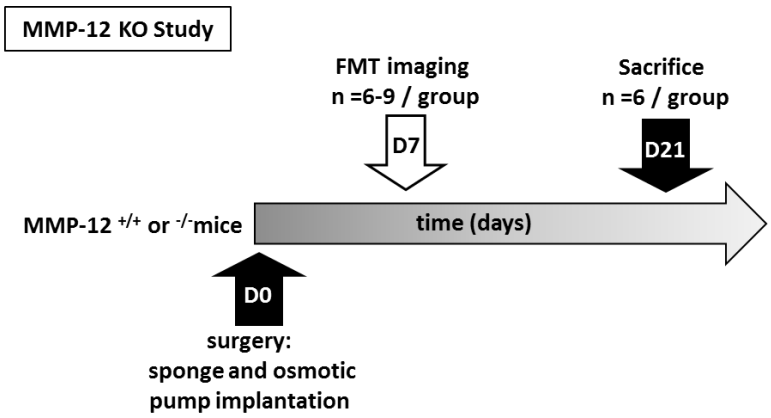

Figure 5.6 Study design, investigation into the effects of MMP-12 deletion in a murine model of angiogenesis. C57Bl6 MMP-$12^{+/+}$ (n = 6) or MMP-$12^{-/-}$ mice (n = 6) were subcutaneously implanted with two 1 cm^3 sponges. On D 7 FMT imaging of angiogenesis and MMP activity was achieved using commercial probes, AngiosSense 680 (AngioSense) and MMPSense 750 F.A.S.T. (MMPSense), respectively. Sponges were removed on D 21, cut in half and samples either fixed or frozen. Aortae were harvested for use in the aortic ring assay. Angiogenesis in sponges was quantified by staining vessels for CD31 and α-SMA, stained vessels were counted under magnification. Gene expression for MMPs and markers of angiogenesis was measured using RT-qPCR.

Pharmacological inhibition of MMP-12 during *in vivo* angiogenesis.

To limit the side effects of systemic administration of the drugs, osmotic mini-pumps were used. Pumps were prepared under sterile conditions, see Appendix 5 for detailed method explanation. Briefly, the catheter and the pump cavity were filled with the desired sterilized drug solution. The pumps were closed and primed prior to surgical implantation (n = 6 / treatment). Pumps and solutions were designed to administer the drug to the mice at 150.6 nmol/mouse/day (marimastat: 2 mg/kg/day, HS1-22: 2.6 mg/kg/day) for 21 days (25g mouse) in DMSO : propylene : glycol : H_2O (1:1:1). This concentration was chosen as it is within the limits of solubility of the drugs in the vehicle, and within the range used in other studies (Chow *et al.*,2008; Skipper *et al.*,2009; Somlyo *et al.*,2003).

Surgery

Each mouse was placed under general anaesthesia. In the MMP-12 KO study, two sponges were subcutaneously implanted in each mouse. In the drug study, the sponge and pump system were implanted subcutaneously in the mouse. The mouse was then allowed to recover. The procedures are described in Section 2.9 and Appendix 1.

Tissue collection

Mice were sacrificed on D 21 and the sponges were collected, cut in half and either snap frozen on dry ice before storage at -80 °C or fixed in 4% PFA (18 h) before storage in 70% ethanol. Organs (heart, liver, lungs, pancreas, and kidneys) were collected and weighed. In the MMP-12 KO study, aortae were collected in DMEM for immediate use in the aortic ring assay.

Histology

Fixed tissues were prepared for histology by embedding in paraffin wax and 5 µm sections were cut for staining and immunohistochemistry. Sections were cut from the centre of each sponge.

In the drug study, one section for each mouse was used for:

1. Staining with haematoxylin and eosin (H&E) to image different cell types and tissue structures.

2. Immunostaining for CD31 and α-SMA to visualise vessel structures.

In the MMP-12 KO study, one section for each mouse was used for:

1. Staining with haematoxylin and eosin (H&E) to image different cell types and tissue structures.

2. Immunostaining for F4.80 to image macrophages.

3. Staining with picrosirius red to image collagen deposition

4. Immunostaining for CD31 and α-SMA to visualise vessel structures.

Whole sections were imaged using a slide scanner. The images were randomised before being analysed by a blinded observer, as discussed in Section 1.12.

MMP-12 KO study FMT imaging and analysis

Mice were placed on an alfalfa free diet to reduce autofluorescence 10 days prior to imaging and injected with MMPSense and AngioSense (Perkin Elmer, 2 nnol) 24 h prior to FMT imaging. Images were acquired and the data were then analysed using the Truequant® software (PerkinElmer) which converted the measured fluorescent signal to the concentration of probe within the sponges. The mean value of probe concentration over the 2 sponges was taken for each mouse, this was then tested for statistical significance. See Section 2.10 and Appendix 1 for the imaging procedures and data analysis; Section 1.4 and Appendix 1 contain more information on FMT and the commercial agents used.

MMP-12 KO study: molecular analysis of gene expression

RNA was isolated from frozen sponges from sponges from the KO study, from this cDNA was synthesised and RT-qPCR was performed. The following genes were investigated: MMP-2, -7, -9, -10, -13, -12, CD31, PDGFR, VEGFα, TNFα, HIF1α, VECAD, VWF, TSP-1 (gene transcripts were normalised against the mean of TBP and GAPDH). The protocols are described in Section 2.13

5.3.5 Statistics

Data were checked for outliers and presented as mean ± SEM. Comparisons were made using Students T-test or ANOVA as appropriate. Some studies are n = 1 or 2 as unpromising leads were not followed up. More detail on statistics used in Section 2.3.

5.4 Results

5.4.1 Protease detection in sponge lysates with an MMP-12 substrate activity probe

HS1-65 is activated in tissue lysates

Reactions with HS1-65 and MMP-12 (catalytic domain) resulted in an 8 fold increase in fluorescence (Figure 5.7). Reactions with tissue lysate (TL, samples were from sponges collected on D 3 − 35) and HS1-65 also resulted in an increase in fluorescence, significantly so for TL samples collected from D 28 and 35 sponges.

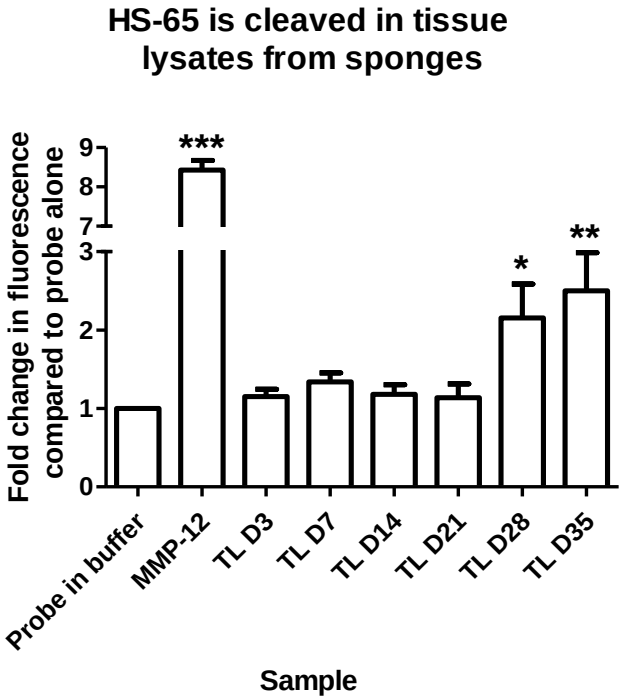

Figure 5.7 HS1-65 is cleaved in tissue lysates from sponges. HS1-65 (10µM) was cleaved in reactions (2 h, 37°C) with MMP-12 (30 nM) and the tissue lysate (TL, 1.67 µg/mL of protein). The fold increase in fluorescence compared to control (probe alone) was calculated. Reactions with MMP-12 and TL from sponges collected on D 28 and D 35 resulted in a significant increase in fluorescence. Bars represent mean ± SEM (n = 3) and comparisons were made using a one-way ANOVA followed by Dunnett's multiple comparison tests comparing all data sets to probe alone (* $P < 0.05$, ** $P < 0.01$, *** $P < 0.001$).

HS1-65 is cleaved by a protease but not an MMP in tissue lysates

MMP-12 pre-treated with marimastat or denatured prior to a reaction with HS1-65 resulted in complete suppression of fluorescence which was comparable to control levels (probe in buffer) (Figure 5.8). Heat denaturation of tissue lysates (TL) prior to the reaction with HS1-65 also resulted in complete suppression of fluorescence. However, TL pre-treated with marimastat prior to a reaction with HS1-65 only resulted in a small suppression of fluorescence on D 7, 28 and 35 TL samples.

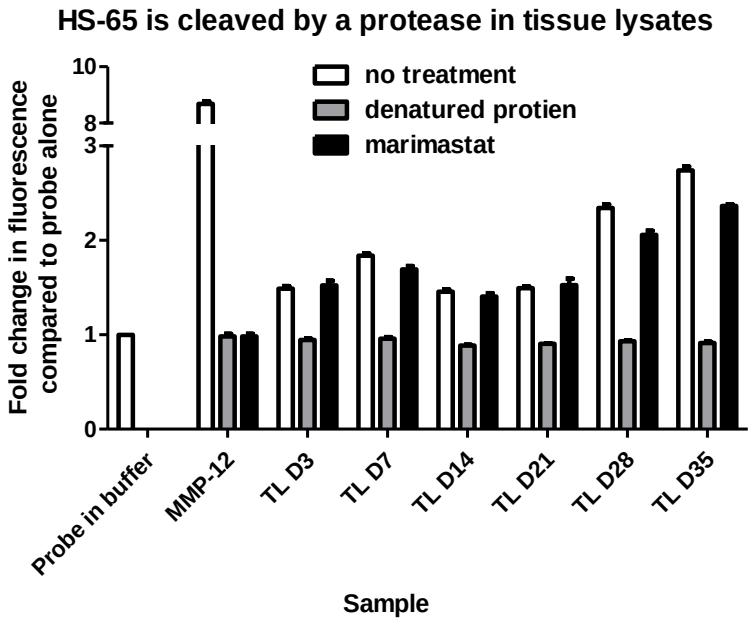

Figure 5.8 Measured fluorescence from HS1-65 substrate activity probe after incubation with tissue lysates (TL), denatured tissue lysates and MMP-12. In a 384 well plate 15 µL reactions were set up in triplicate. The addition of HS1-65 (10µM) to the tissue lysates or MMPcat-12 resulted in an increase in fluorescence (white bars). Denaturing the proteins (TL or MMP-12, grey bars) resulted in complete suppression of fluorescence from HS1-65 levels comparable to HS1-65 incubated with just buffer. The addition of marimastat to the reactions with active TL (black bars) resulted in no large change in fluorescence form HS1-65 on TL D 3, 14 and 21. The MMP-12 incubated with marimastat resulted in complete suppression in fluorescence confirming the marimastat was active. Results are plotted as fold change in fluorescence after 2 h, bar represents mean ± SEM (n = 1 in triplicate), this is one of 2 assays with marimastat (see Appendix 6 for additional results).

MALDI-TOF MS analysis of probe fragments

Tissue lysates (D 3 − 35) (or MMP_{cat}-12) and HS1-65 were incubated for 2 h, the reaction mixtures were then purified and analysed by MALDI-TOF MS. Cleavage of HS1-65 (M^++Na m/z = 1834.9) resulted in a clearly identifiable fragment (M^+ m/z = 787.7) after reaction in MMP_{cat}-12 (Figure 5.9). Spectra with tissue lysates and HS1-65 did not exhibit this distinctive fragment (Figure 5.10).

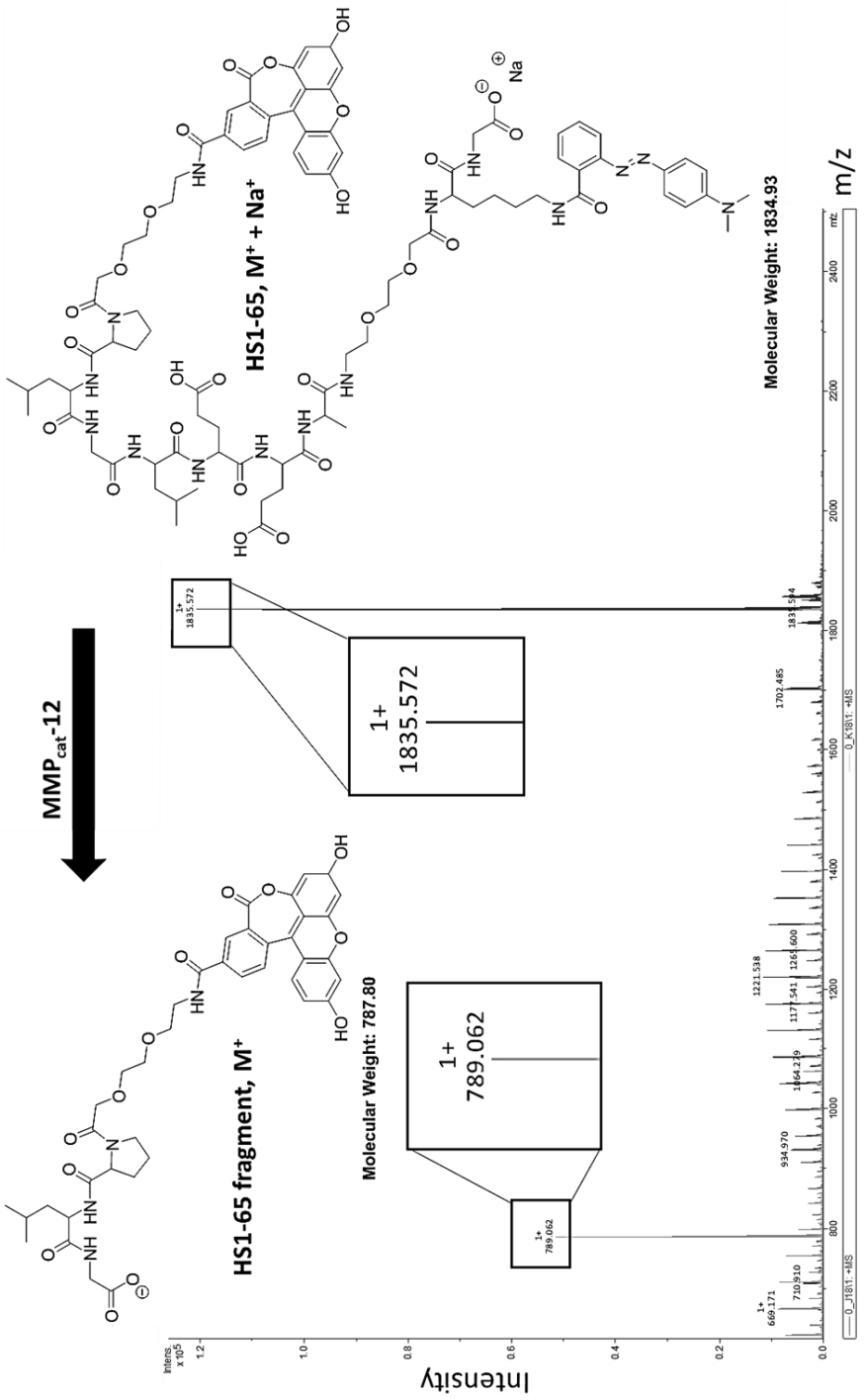

Figure 5.9

Figure 5.9 Analysis of HS1-65 and corresponding cleavage fragment after MMP_{cat}-12 proteolysis using MALDI−TOF MS. HS1-65 was incubated with MMP_{cat}-12 (37 °C, 2h). Samples were purified using pipette tips containing C18 resin cartridges, the filtrate was analysed by MALDI TOF MS. HS1-65 (M^++Na m/z = 1835.57) was cleaved with a clearly identifiable fragment (M^+ m/z 789.06). Other peaks in region 900 to1700 m/z are surfactants in the MMP buffer.

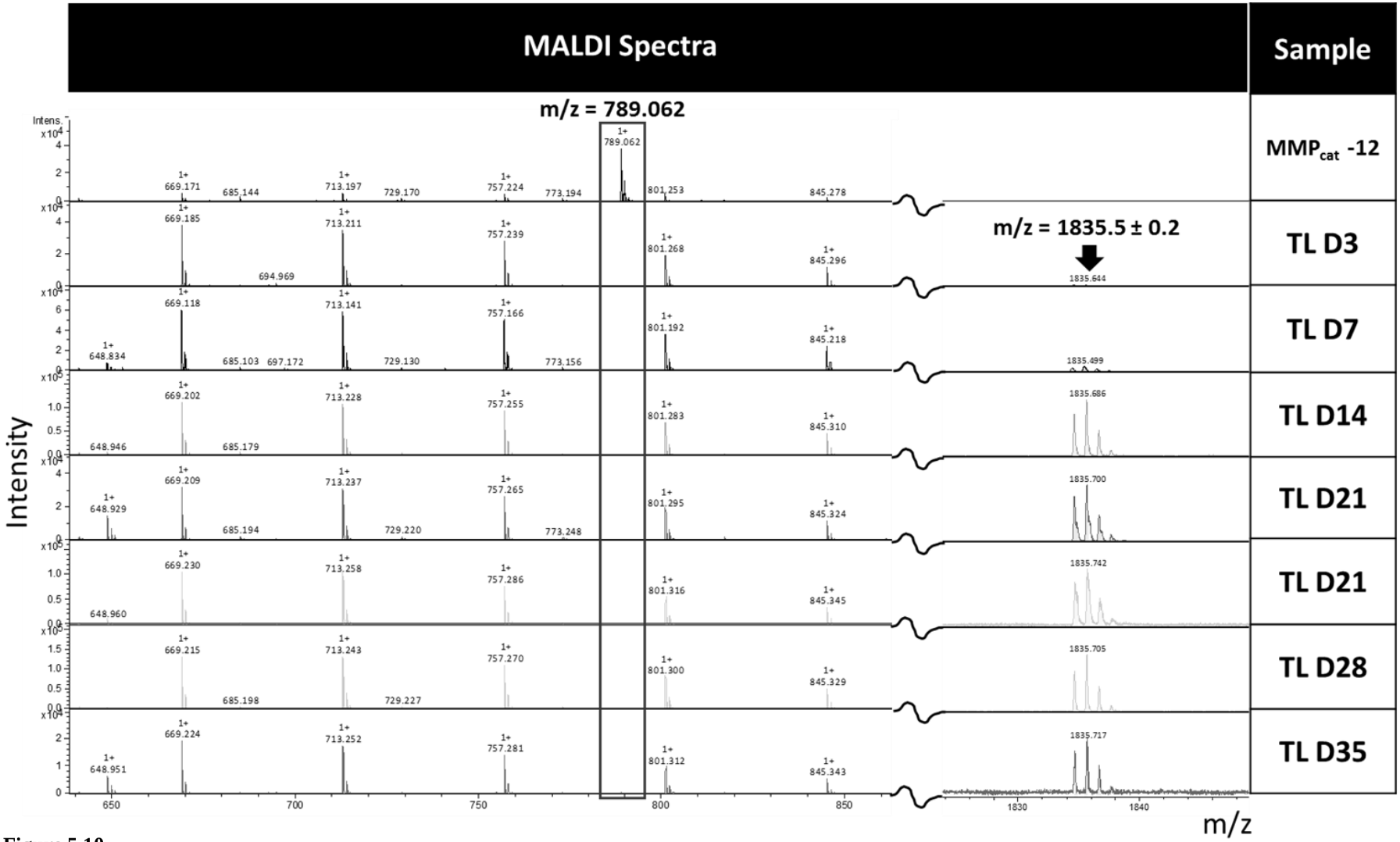
MALDI Spectra
Sample
m/z = 789.062
m/z = 1835.5 ± 0.2
Intens.
Intensity
m/z
MMP$_{cat}$ -12
TL D3
TL D7
TL D14
TL D21
TL D21
TL D28
TL D35

Figure 5.10

Figure 5.10 Analysis of HS1-65 and corresponding cleavage fragment within tissue lysates using MALDI-TOF MS. HS1-65 was incubated with tissue lysates from D 3 − 35 sponges or with MMP_{cat}-12 (37 °C, 2h). Samples were then purified using pipette tips containing C18 resin cartridges, the filtrate was analysed by MALDI TOF MS. HS1-65 was cleaved in all lysates but not by MMP-12, MS spectra confirm that the fragment associated with cleavage by MMP-12 was not present (m/z = 789, region in box) confirming proteolysis by another protease. Other peaks in region 650 to 850 m/z are surfactant in the MMP buffer.

HS1-65 is not cleaved by a serine protease or neutrophil elastase

In an attempt to discover the source of HS1-65 probe activation in the tissue lysates, reactions were challenged with protease inhibitors: i) a commercial broad spectrum protease block, ii) sivelestat (a neutrophil elastase inhibitor), iii) antithrombin III (a serine protease inhibitor). When compared to the experiments with no treatment: the commercial protease blocker virtually abolished the signal from HS1-65 cleavage for all samples (Figure 5.11). The addition of sivelestat or antithrombin III resulted in no change in fluorescence for experiments with tissue lysates collected on D 3 − 21, however, there was a small reduction on D 28 and 35.

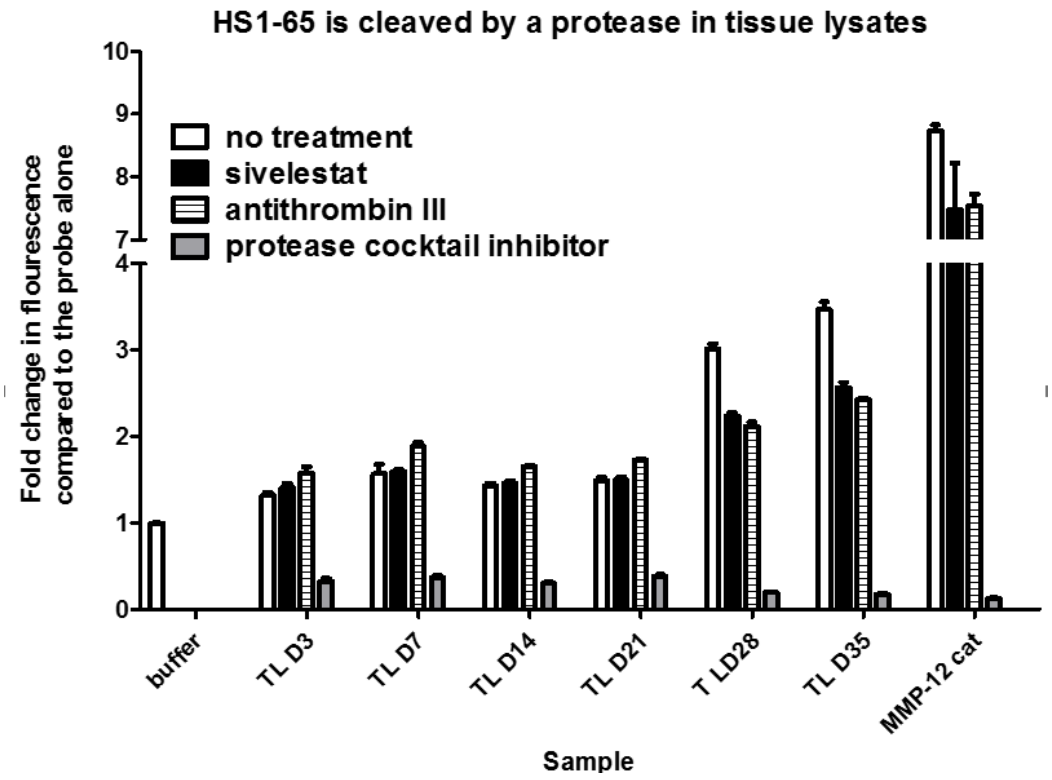

Figure 5.11 HS1-65 is cleaved by a protease in the tissue lysate which is not an MMP, neutrophil or macrophage elastase or a serine protease. In a 384 well plate 15 µL reactions were set up in triplicate as follows: tissue lysates (TL) were challenged with sivelestat (neutrophil elastase inhibitor, black bar, 100 µM), or anti-thrombin II (serine protease inhibitor, striped bar, 100 nM) or a protease inhibitor cocktail (broad spectrum protease inhibitor, grey bars, 0.33 stock) or MMP buffer (white bar), all incubated at 37 °C, 2 h. Subsequently, HS1-65 (10 µM) was added and reactions monitored in a plate reader (ex = 495 nm, em = 525 nm, 37 °C, 2h). HS1-65 was cleaved in all the TL and by MMP-12_{cat}. The addition of sivelestat (black bars) or antithrombin III (stripped bars) to these reactions resulted in no change in the cleavage of HS1-65 for reactions with tissue lysates collected on D 3 − 21; however, there appeared to be a drop in signal on D 28 and D 35. The addition of the protease cocktail block inhibited the cleavage of HS1-65 in all samples, but the fluorescence was quenched over 2 h resulting in a lower than expected fluorescence at the 2 h time point. Results are presented as mean fold change in fluorescence ± SEM, (n = 1 in triplicate).

5.4.2 MMP-12 does not inhibit angiogenesis in the *ex vivo* aortic ring assay

MMP-12 inhibition did not increase microvessel growth in the *ex vivo* aortic ring assay.

Vascular sprouts were observed to grow from the embedded aortic rings (Figure 5.12) and were present in all groups on D 3, 5 and 7 after embedding (Figure 5.13). On D 3, the addition of growth factors to the Opti-MEM control did not alter the number or length of endothelial microvessel sprouts; but by D 5 the numbers increased to almost double ($P < 0.05$ Figure 5.13) but the length was still similar. On D 7 microvessels were present in greater numbers ($P < 0.05$) which were on average 40% longer ($P < 0.05$, Figure 5.14). Interestingly, the addition of marimastat (with growth factors) did not alter vessel length on D 3 but there was a pattern for there to be an increase in vessel numbers compared to microvessels without growth factor or with growth factors and HS1-22, both $P < 0.05$). However by D 7, those aortic rings with the marimastat treatment had fewer microvessels ($P < 0.01$ *vs* growth factors, Figure 5.13) and reduced vessel length ($P < 0.001$ *vs* all groups, Figure 5.14). When HS1-22 (an MMP-12 selective inhibitor) was added to the growth factor treatment there were no statistically significant changes in sprout numbers or length on D 3 or 5; but by D 7 microvessels were shorter then microvessels treated without HS1-22 ($P < 0.001$, Figure 5.14).

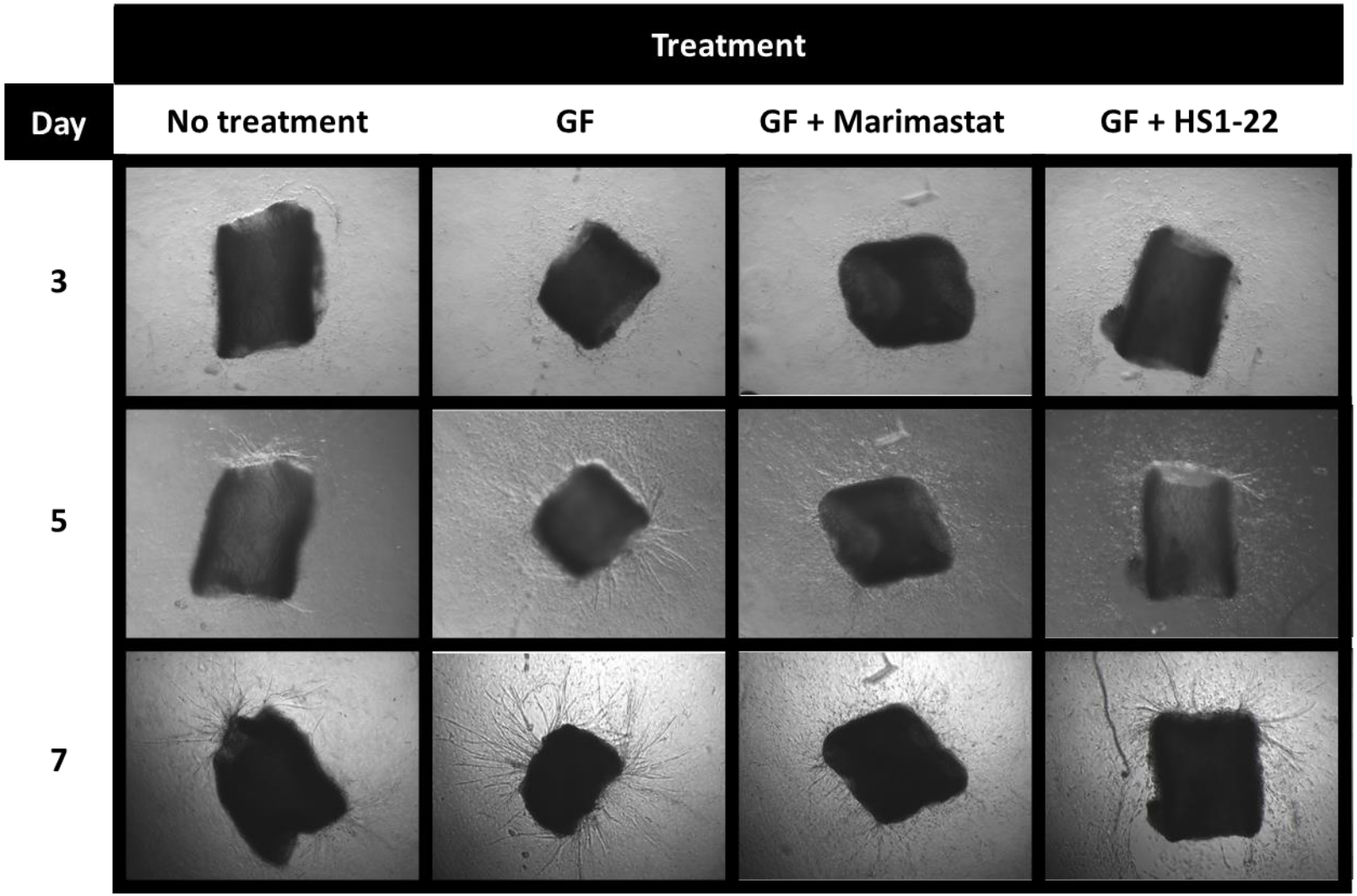

Figure 5.12

Figure 5.12 Representative images from the aortic ring assay. Aortic rings from C57BL6/J mice were embedded in 1% collagen and treated with growth factors (GF) which stimulated the growth of long sprouts. MMP inhibitors (marimastat, a broad spectrum inhibitor or HS1-22 an MMP-12 selective inhibitor; both 25 μM) where added to aortae for the duration of the experiment. Representative images are of rings collected from a single mouse and acquired at × 20 magnification.

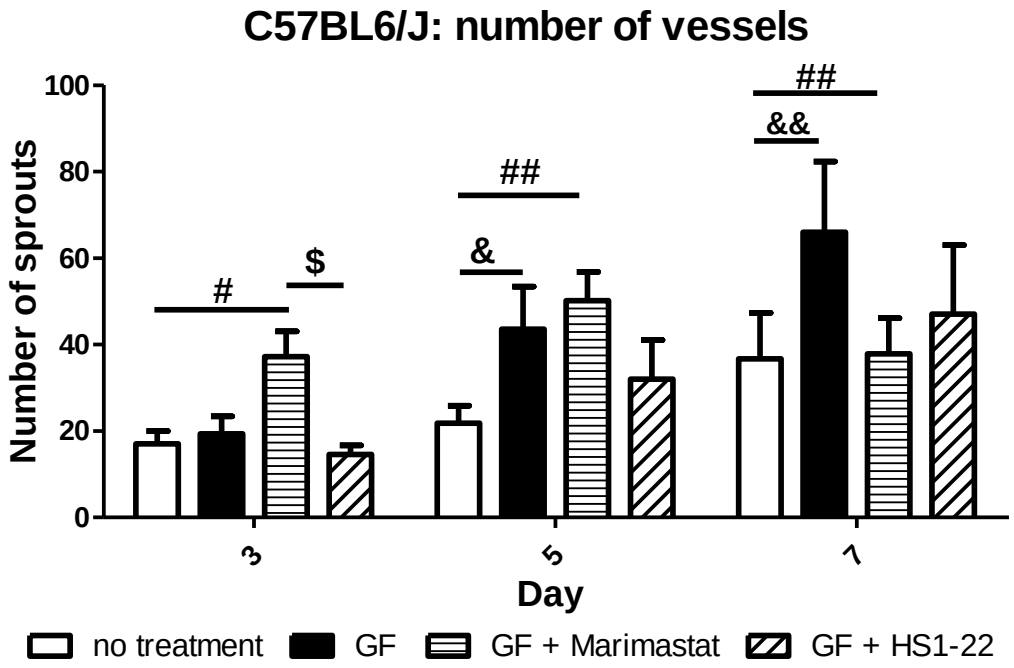

Figure 5.13 Aortic ring assay with growth factors GF and MMP inhibitors: number of sprouts. Vessels were treated with growth factors (solid black) and MMP inhibitors (marimastat or HS1-22, 25 µM). On D 3, marimastat (horizontal lined) almost doubled the number of microvessels from aortic rings compared to those treated with (solid black) or without (white solid) GF treatment. On D 5 the number of marimastat treated microvessels was only statistically higher than those treated without any GF or inhibitors; the addition of GF led to an increase in microvessel number compared to those experiments without GF treatment. By D 7, those aortic vessels treated with just GF had more microvessels that those without GF or those treated with marimastat. The addition of HS1-22 (diagonal lined) to the aortic rings did not significantly alter the number of microvessels compared to those with or without GF. Results are plotted as mean ± SEM, n = 6 in triplicate; statistics: two-way ANOVA followed by a Bonferroni post-hoc test comparing all pairs of columns; marimastat *vs* no treatment (# $P < 0.05$, ## $P < 0.01$); marimastat *vs* HS1-22 ($ $P < 0.05$); GF *vs* no treatment (& $P < 0.05$, $$ $P < 0.01$).

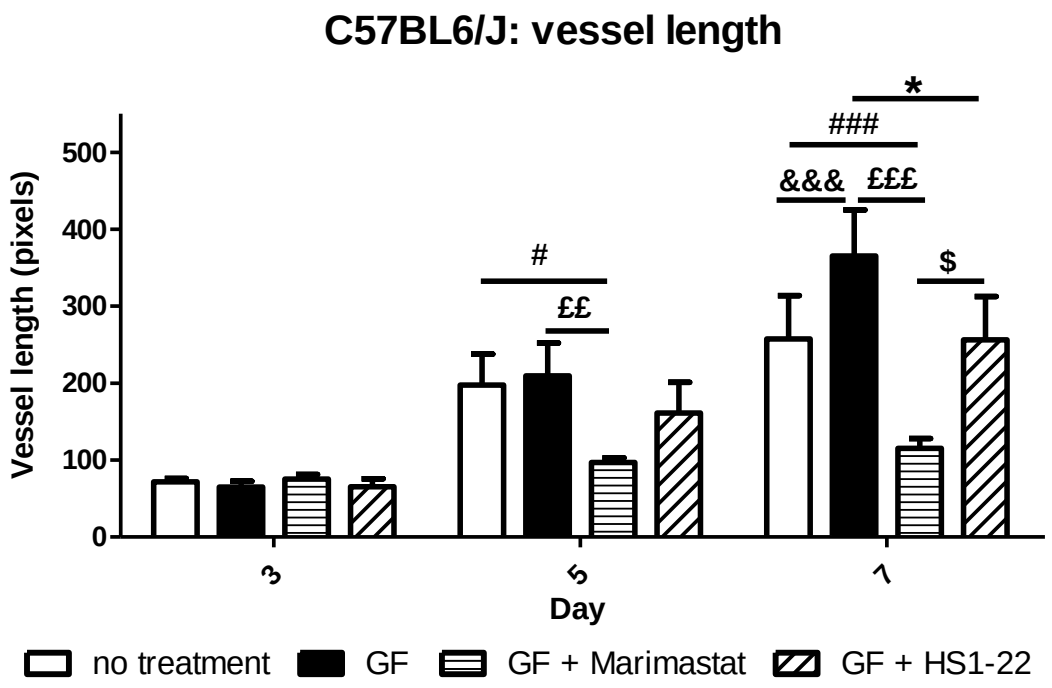

Figure 5.14 Aortic ring assay with growth factors and MMP inhibitors: length of microvessels. On D 3 the length of the microvessels was similar for all treatment groups. On D 5 the length of microvessels was similar for those with (solid black) and without GF (solid white); however, microvessels growing in the presence of marimastat (horizontal lined) had reduced length compared to microvessels treated with GF or without GF. By D 7, vessels treated with GF were longer than those without treatment. Vessels treated with marimastat were shorter than those in all other groups. By D 7, the addition of HS1-22 (diagonal lined) reduced the length of microvessels compared to those treated with GF alone. Results are plotted as mean ± SEM, (n = 6) in triplicate, comparisons where made using two-way ANOVA followed by a Bonferroni post-hoc test comparing all pairs of columns; marimastat *vs* no treatment (### $P < 0.001$); marimastat *vs* GF (££ $P < 0.01$, £££ $P < 0.001$); marimastat *vs* HS1-22 ($ $P < 0.05$); GF *vs* no treatment (&&& $P < 0.001$); GF *vs* HS1-22 (* $P < 0.005$).

MMP-12 gene deletion did not change microvessel growth in the aortic ring assay

Aortic rings were cultured in triplicate from MMP-12 KO and C57BL6/J mice (n = 6 each) in the presence of GF and MMP inhibitors over D 3 − 7. For all time-points assessed, microvessel out-growth was present for both genotypes and for all treatment groups. The deletion of MMP-12 did not result in increase in vessel numbers (Figure 5.15) or length (Figure 5.16) in the presence of GF or MMP inhibitors. Interestingly treatment with HS1-22, an inhibitor designed to be MMP-12 selective, resulted in the same profiles in both MMP-12 KO and C57BL6/J mice.

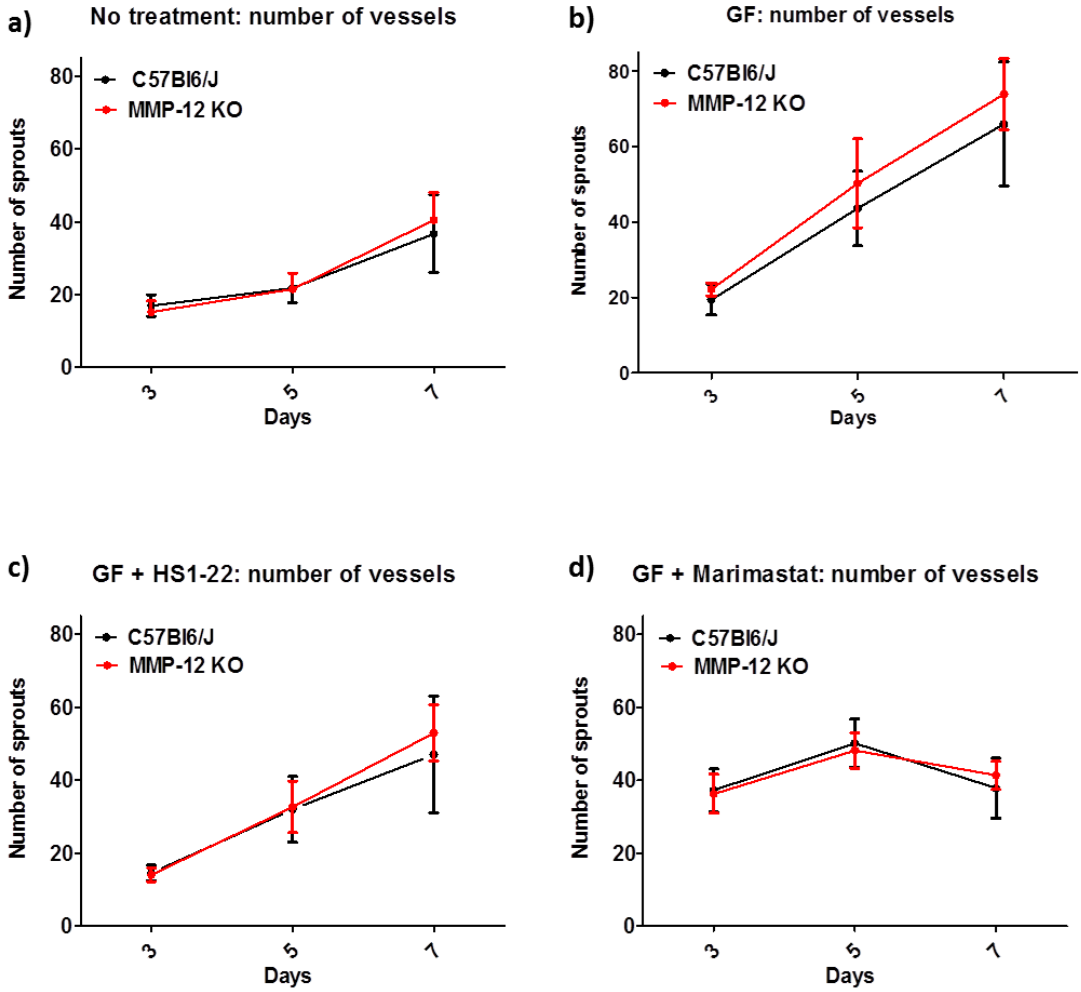

Figure 5.15 Aortic rings deficient in MMP-12 exhibited no differences in vessel numbers and didn't respond differently to growth factors or MMP inhibitors compared to C57BL6/J control. Aortic rings from MMP-12 KO (red line) and C57BL6/J (black line) were treated with (a) and without (b) growth factors (GF, 2% FCS for 3 days followed by VEGF (5 ng/mL). The loss of MMP-12 did not alter microvessels numbers over D 3 − 7. The addition of HS1-22 (MMP-12 selective inhibitor, c) marimastat (broad spectrum MMP inhibitor, d) (both 25 µM) also elicited similar responses for both genotypes. For each treatment, the loss of MMP-12 did not result in any large changes to the overall patterns observed for microvessel numbers over D 3 − 7. Results are plotted as mean ± SEM, (n = 6). Statistics: data were tested with a two-way ANOVA followed by a Bonferroni post-hoc test comparing all treatments, $P > 0.05$.

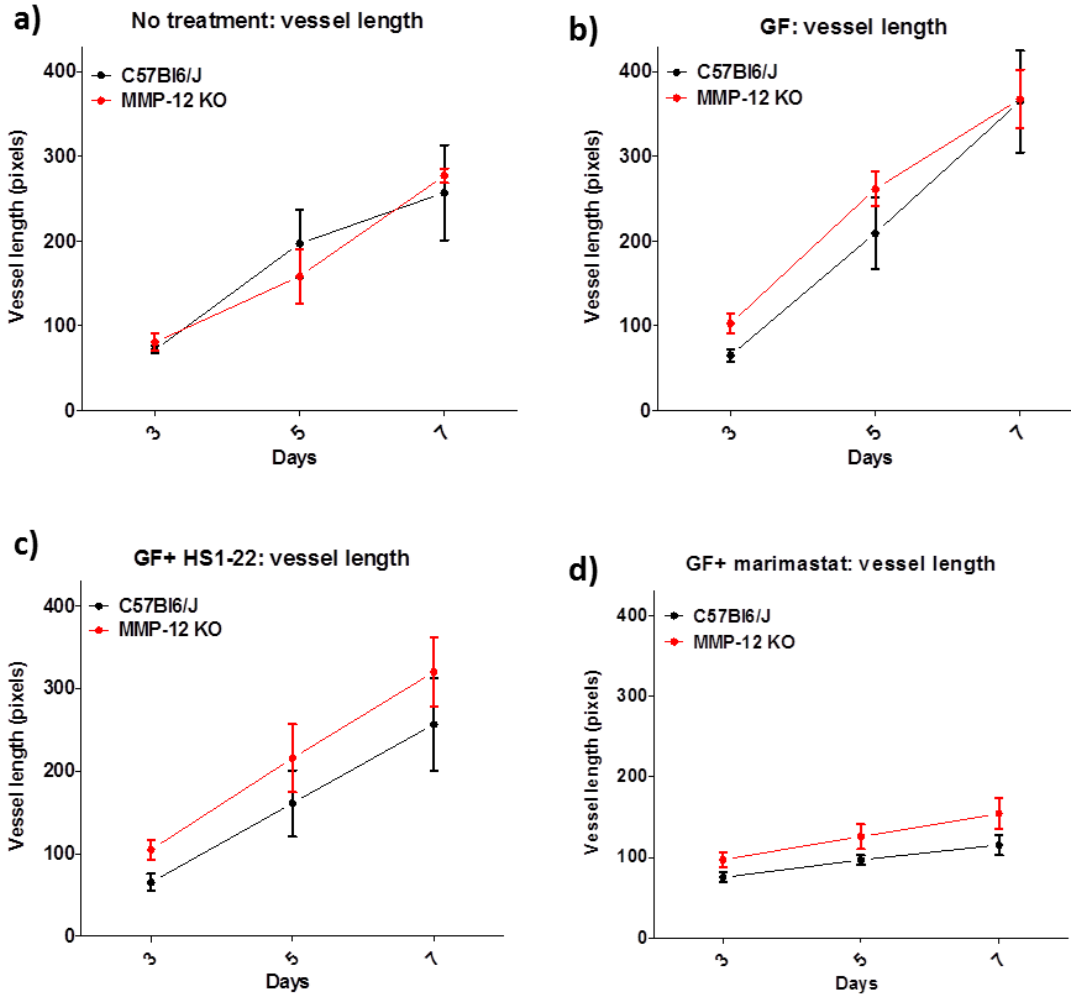

Figure 5.16 Aortic rings deficient in MMP-12 exhibited no differences in vessel length and didn't respond differently to growth factors or MMP inhibitors compared to C57BL6/J controls. Aortic rings from MMP-12 KO (red line) and C57BL6/J (black line) were treated with (a) and without (b) growth factors (GF, 2% FCS for 3 days followed by VEGF (5 ng/mL). The loss of MMP-12 did not alter microvessels numbers over D 3 − 7. The addition of HS1-22 (MMP-12 selective inhibitor, c) marimastat (broad spectrum MMP inhibitor, d) (both 25 µM) also elicited similar responses for both genotypes. For each treatment, the loss of MMP-12 did not result in any large changes to the overall patterns observed for microvessel numbers over D 3 − 7. Results are plotted as mean ± SEM, n = 6 in triplicate. Statistics: data were tested with a two-way ANOVA followed by a Bonferroni post-hoc test comparing all treatments.

5.4.3 MMP-12 Inhibition decreases angiogenesis *in vivo*

MMP-12 inhibition did not alter body weight but did reduce lung size and increase kidney size

MMP inhibitors were administered locally to the sponge using an osmotic mini pump. After 21 days, the administration of marimastat led to an increase in body weight compared to both vehicle and HS1-22 drug treatment (Figure 5.17 (a), both $P < 0.05$). Mice treated with HS1-22 had slightly heavier kidneys compared to controls (Figure 5.17 (f), $P < 0.01$). Interestingly the lung size was significantly smaller in mice treated with marimastat and HS1-22 (Figure 5.17, (d), $P < 0.01$ and $P < 0.001$, respectively). The size of the heart, spleen and liver were unchanged after treatments (Figure 5.17, (b), (c) and (d), respectively).

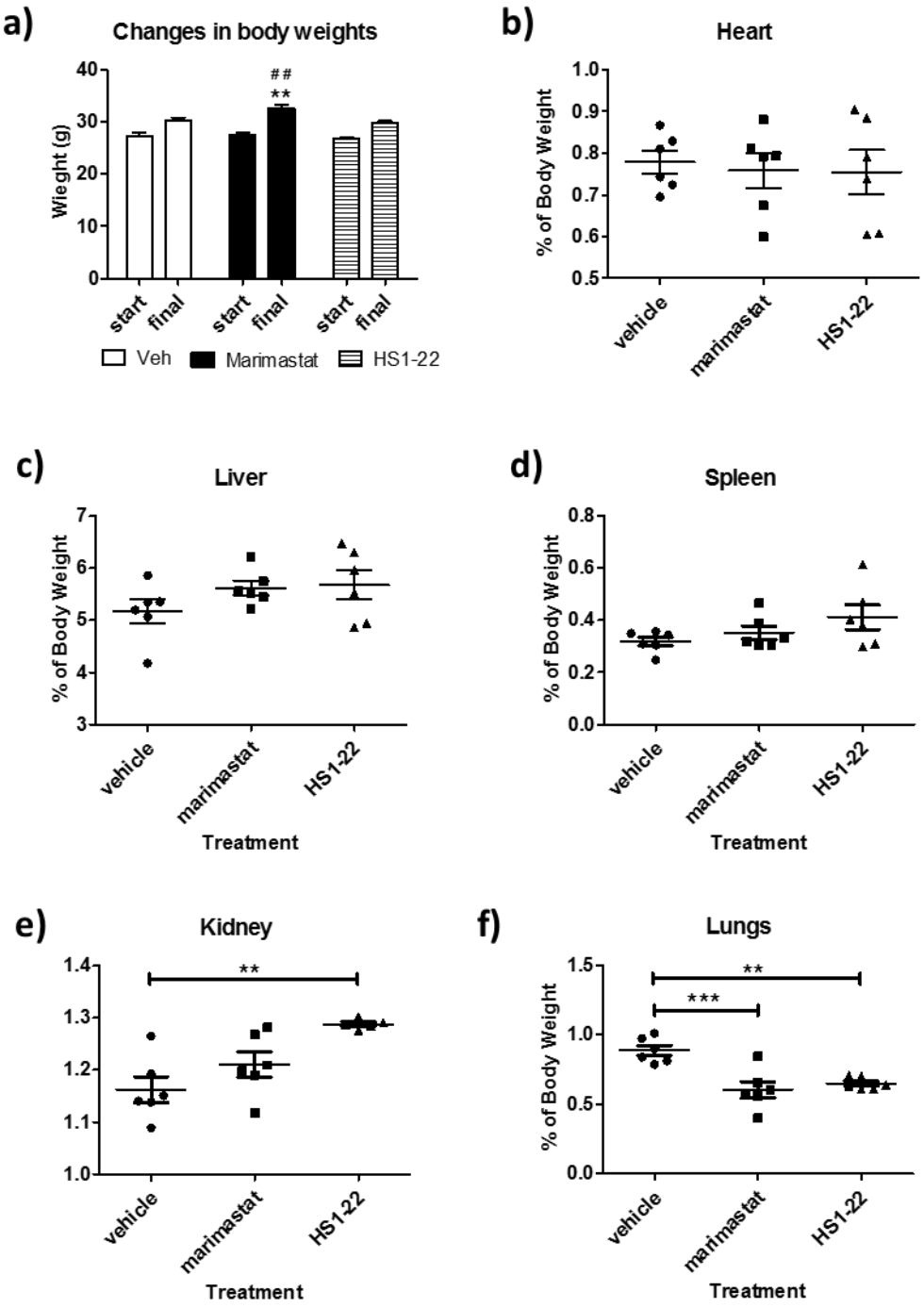

Figure 5.17 Effects of MMP inhibitors on mouse body and organ weights. Administration of marimastat (broad spectrum inhibitor) resulted in increased body weight (a) compared to vehicle (**) and HS1-22 (##, MMP-12 inhibitor). Treatment with marimastat or HS1-22 had no effect on heart (b), liver (c) or spleen (d) weights. Treatment with HS1-22 resulted in mice with heavier kidneys (e, $p < 0.01$). Treatment with marimastat and HS1-22 resulted in reduced lung weights (f, $p < 0.01$ and $p <$

0.001 respectively). Bars or column and error bar represent mean ± SEM (n = 6) and comparisons were made using a one-way ANOVA followed by Bonferroni post-hoc test comparing all data sets (** or ## $P < 0.01$, *** $P < 0.001$).

MMP-12 inhibition decreases angiogenesis

Treatment with marimastat reduced the total number of vessels (Figure 5.18 (a), $P < 0.05$) and the number of vessels positive for CD31 and α-SMA (Figure 5.18 (c), $P < 0.01$) in the sponges compared to the vehicle treated group. There is a pattern for treatment with HS1-22 to also reduce the total number of vessels and the number of vessels positive for CD31 and α-SMA but this didn't achieve significance Figure 5.18 (b),

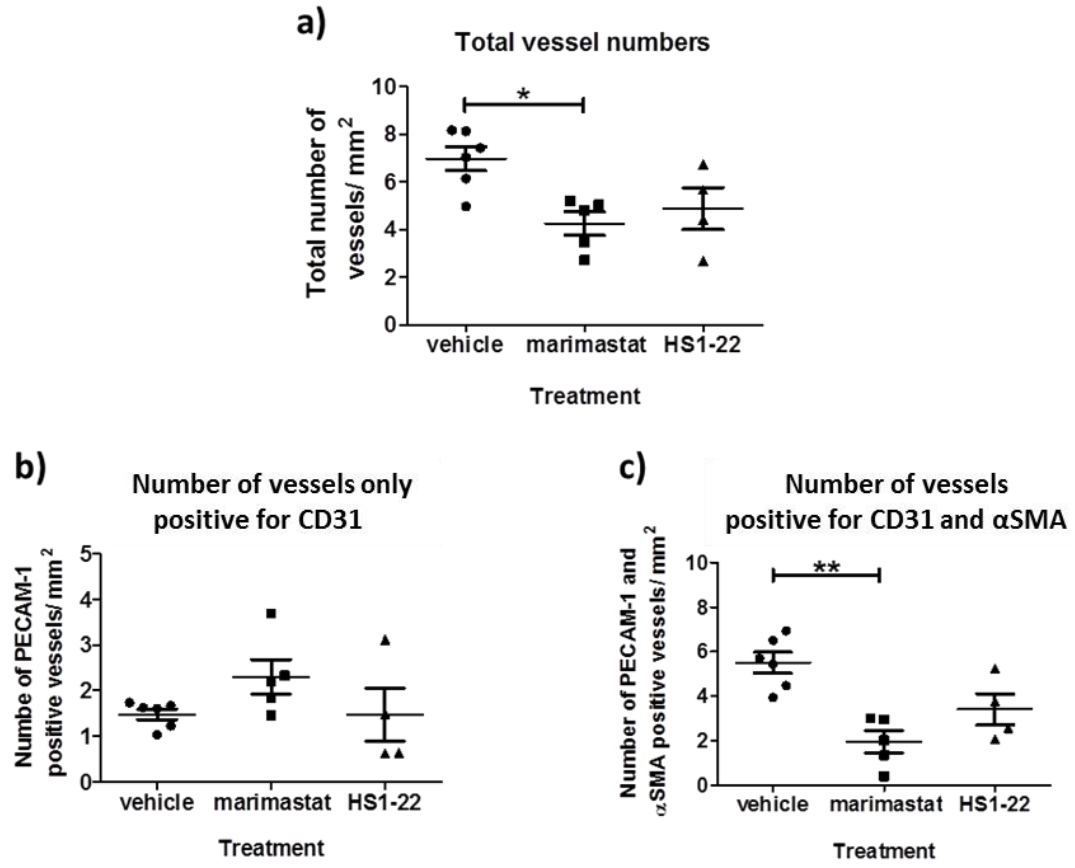

Figure 5.18 Pharmacological inhibition of MMP-12 did not increase angiogenesis. a) Compared to the vehicle, treatment with marimastat resulted in a reduced number of total vessels and treatment with HS1-22 resulted in a pattern for reduced vessel numbers. b) The number of only CD31 positive vessels was unchanged by treatments. c) Compared to the vehicle alone, treatment with marimastat resulted in a reduction in vessels positive for both CD31 and α-SMA, while treatment with HS1-22 resulted in a pattern for reduced CD31 and α-SMA positive vessels. Bars represent mean ± SEM (n = 4 − 6) and comparisons were made using either a one-way ANOVA followed by Bonferroni post-hoc test comparing all data sets (graph a and c) or a Kruskal-Wallis test followed by a Dunn's multiple comparison test (graph b) (* $P < 0.05$, ** $P < 0.01$).

5.4.4 MMP-12 deletion did not alter angiogenesis *in vivo*

MMP-12 KO mice had reduced MMP-12 expression in sponges.

Two sponges were subcutaneously implanted in mice for 21 days. Expression of MMP-12 was significantly reduced in sponges from MMP-12 KO mice compared to the C57BL6/J counterpart (Figure 5.19, $P < 0.01$).

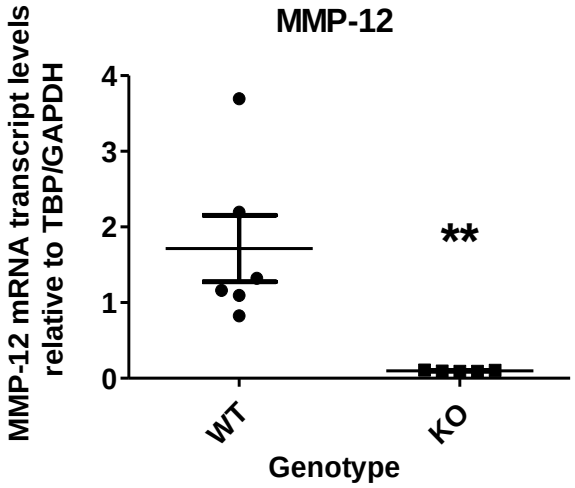

Figure 5.19 MMP-12 expression is significantly reduced in sponges collected from MMP-12 KO mice. Sponges were removed on D 21 after implantation and MMP-12 gene expression measured using RT-qPCR. Bars represent mean ± SEM (n = 5 − 6), comparisons were made using Students t-test (P = 0.0088, ** P < 0.01)

Loss of MMP-12 was not detected *in vivo* using a commercial MMP activity probe and FMT

In vivo FMT imaging of MMPSense in sponges on D 7 resulted in no statistically significant changes in signal detected within the sponges of MMP-12 KO mice (Figure 5.20).

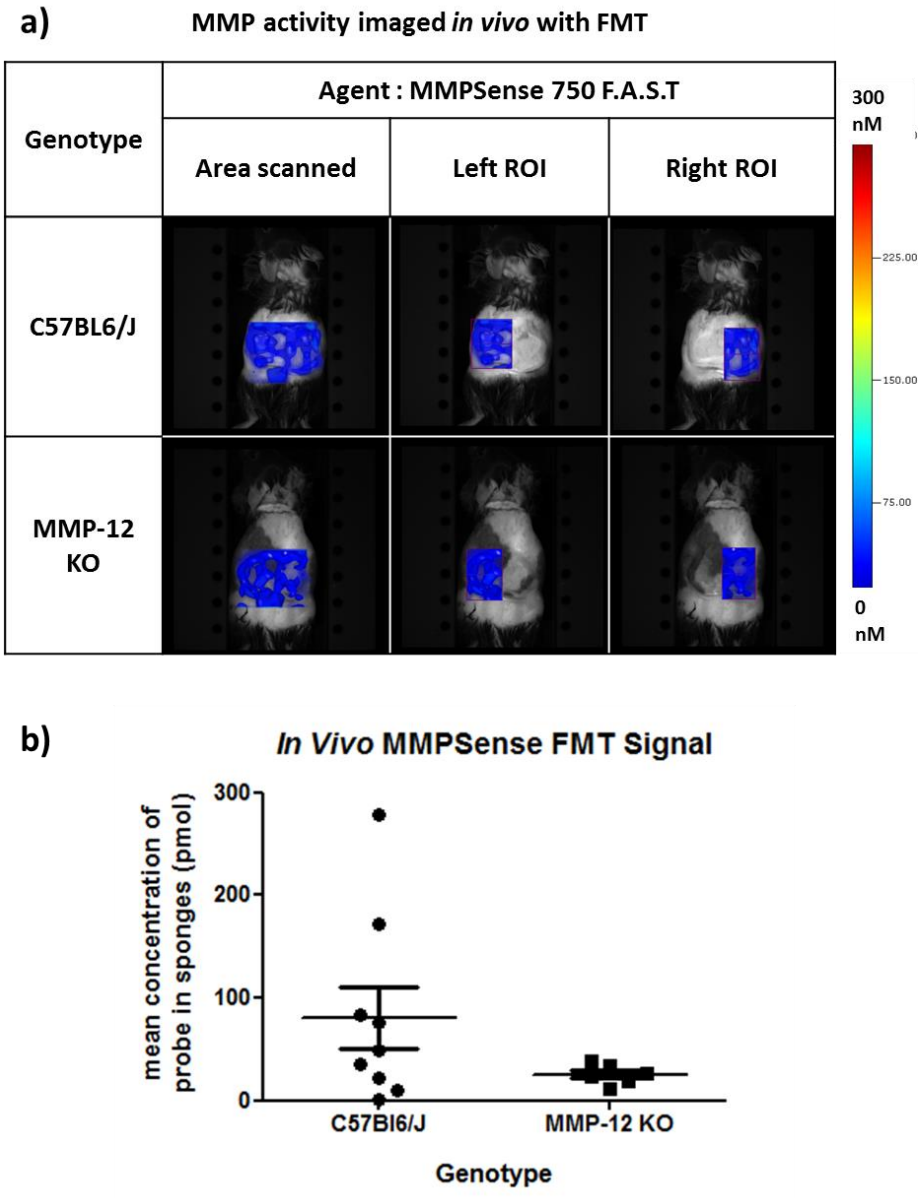

Figure 5.20 FMT imaging of MMP activity on D 7 did not detect the loss of MMP-12 activity *in vivo*. Sponges subcutaneously implanted in MMP-12 KO and C57BL6/J mice a) representative images of the *in vivo* florescent signal acquired by FMT imaging of MMPSense. The "Area scanned" is representative of the signal measured, the left and right regions of interest (ROI) is the signal around

the two subcutaneous sponges. b) The quantified signal around the sponges, MMP activity detected by this method was not significantly different between the two genotypes. Bars represent mean SEM (n = 6 − 9) and comparisons were made using a Students t-test (P = 0.1060).

Loss of MMP-12 expression did not alter body weight but did reduce lung size

Mice were sacrificed on D 21, there was no significant difference in body weight between the C57BL6/J and MMP-12 KO mice (Figure 5.21a). The weights of the heart (b), liver (c), kidney (d), spleen (e) were not different between the genotypes (Figure 5.21). MMP-12 KO mice did have lighter lungs ($P < 0.01$, Figure 5.21f) than C57BL6/J mice.

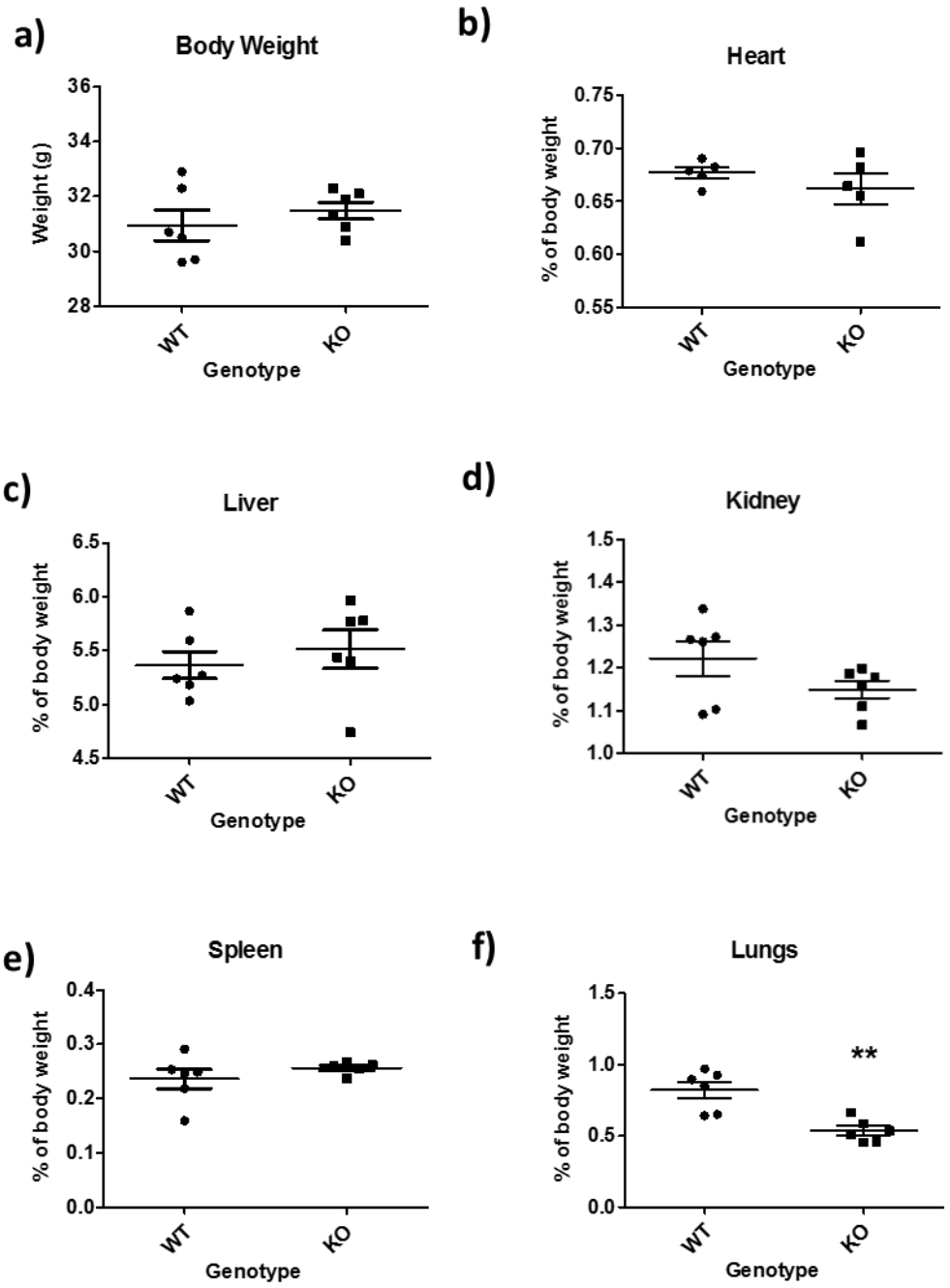

Figure 5.21 No change in body or organ weights, except for the lungs, between the MMP-12 KO and C57BL6/J mice. Mice were sacrificed 21 days after the surgery. There was no significant difference in body weight (a, P = 0.4196), heart (b, P = 0.3503), liver (c, P = 0.5113), kidney (d, P = 0.1465), or spleen (e, P =0.3377) weights between the C57BL6/J and MMP-12 KO mice (P > 0.05). There was a reduction in the weight of lungs (f, P = 0.0016) MMP-12 KO compared to C57BL6/J mice.

Bars represent mean ± SEM (n = 5 − 6) and comparisons were made using a Students t-test (** P < 0.01).

MMP-12 deletion does not alter deposition of collagen in sponges

During dissection it was noted that sponges in MMP-12 KO mice had adhered to each other and were more strongly bound to the surrounding tissue compared to sponges from their C57Bl6/J counterparts (Figure 5.22). Quantification of picrosirius red staining demonstrated that MMP-12 KO did not alter collagen staining in the sponges (Figure 5.23).

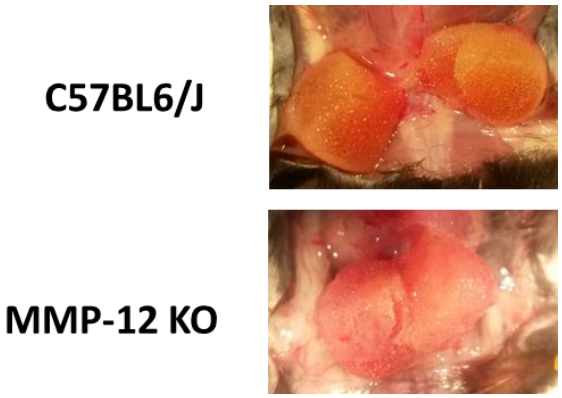

Figure 5.22 Representative images of sponges *ex vivo* after subcutaneous implantation for 21 days in C57BL6/J and MMP-12 KO mice. Sponges in MMP-12 KO mice were generally observed to have adhered to each other and were more tightly bound to the surrounding tissues compared to sponges in C57BL6/J mice.

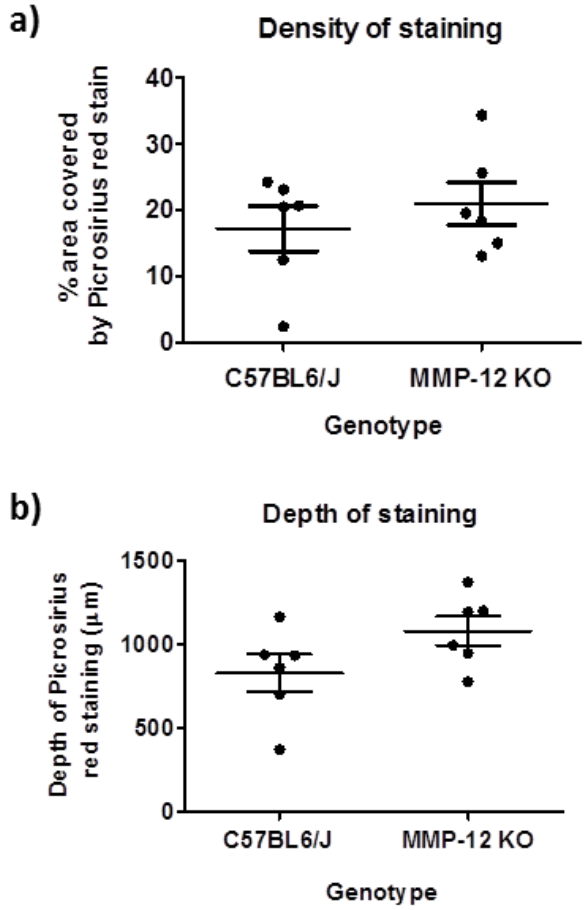

Figure 5.23 Quantification of picroscirius red staining in sponges implanted in C57BL6/J and MMP-12 KO mice. Sponges were removed on D 21 post implantation. The mean density of staining around the edge of the tissue section (a, P = 0.4419) and the mean depth of staining into the sponge (b, P = 0.1021) were both unchanged. Bars represent mean ± SEM (n = 6) and comparisons were made using a Students t-test (P > 0.05).

MMP-12 deletion did not alter the TNFα expression or inflammatory cell infiltration

mRNA was extracted from the sponges and, using RT-qPCR, the relative gene expression of TNFα was measured. There were no differences in the expression of TNFα in sponges from MMP-12 KO mice compared to C57BL6/J controls (Figure 5.24).

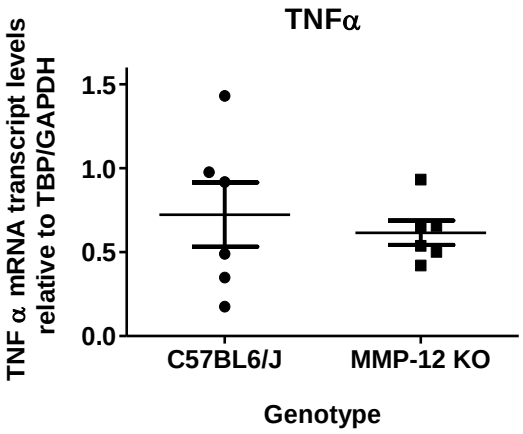

Figure 5.24 Gene transcripts of TNFα remained unchanged in C57BL6/J and MMP-12 KO mice.

Bars represent mean ± SEM (n = 6) and comparisons were made using a Students t-test (P = 0.6105).

MMP-12 deletion did not alter macrophage infiltration

In the sponges the percentage of F4/80 staining around the edge of the sponge (as previously described in Figure 4.11) (Figure 5.25a) and the depth of infiltration into the tissue (Figure 5.25b) were unchanged.

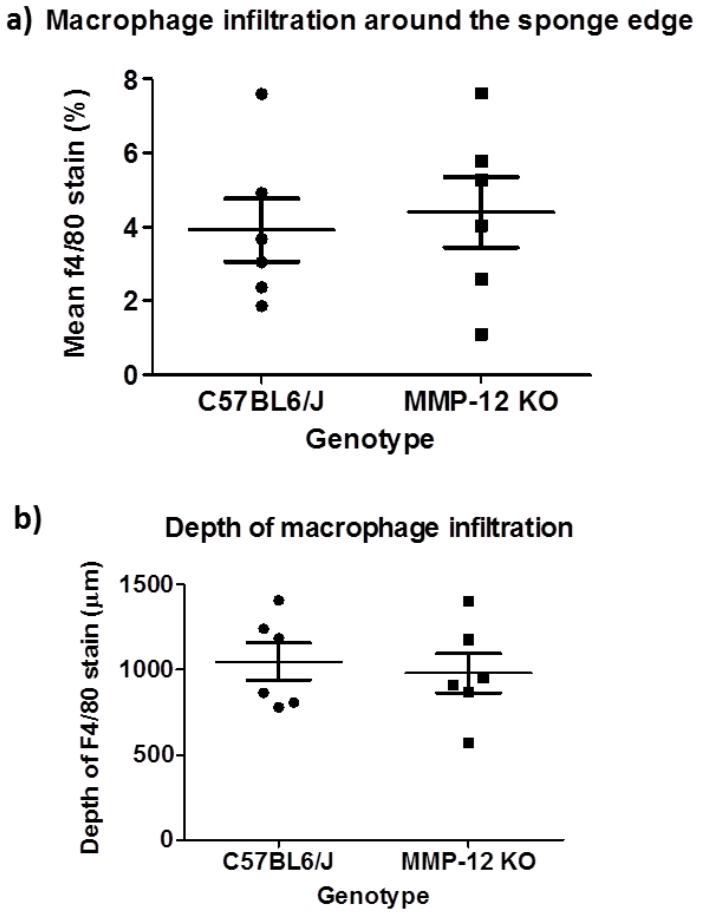

Figure 5.25 Macrophage infiltration was unchanged between C57BL6/J and MMP-12 KO mice. a) The mean percentage area of F4/80 stain around the sponge edge (a, P = 0.7146) and depth of infiltration (b, P = 0.6762) were unchanged. Bars represent mean ± SEM (n = 6) and comparisons were made using a Students t-test (P > 0.05).

MMP-12 deletion did not change AngioSense probe accumulation

Imaging of sponges on D 7 post implantation showed that accumulation of the AngioSense 680 probe was similar in C57BL6/J and MMP-12 KO mice (Figure 5.26)

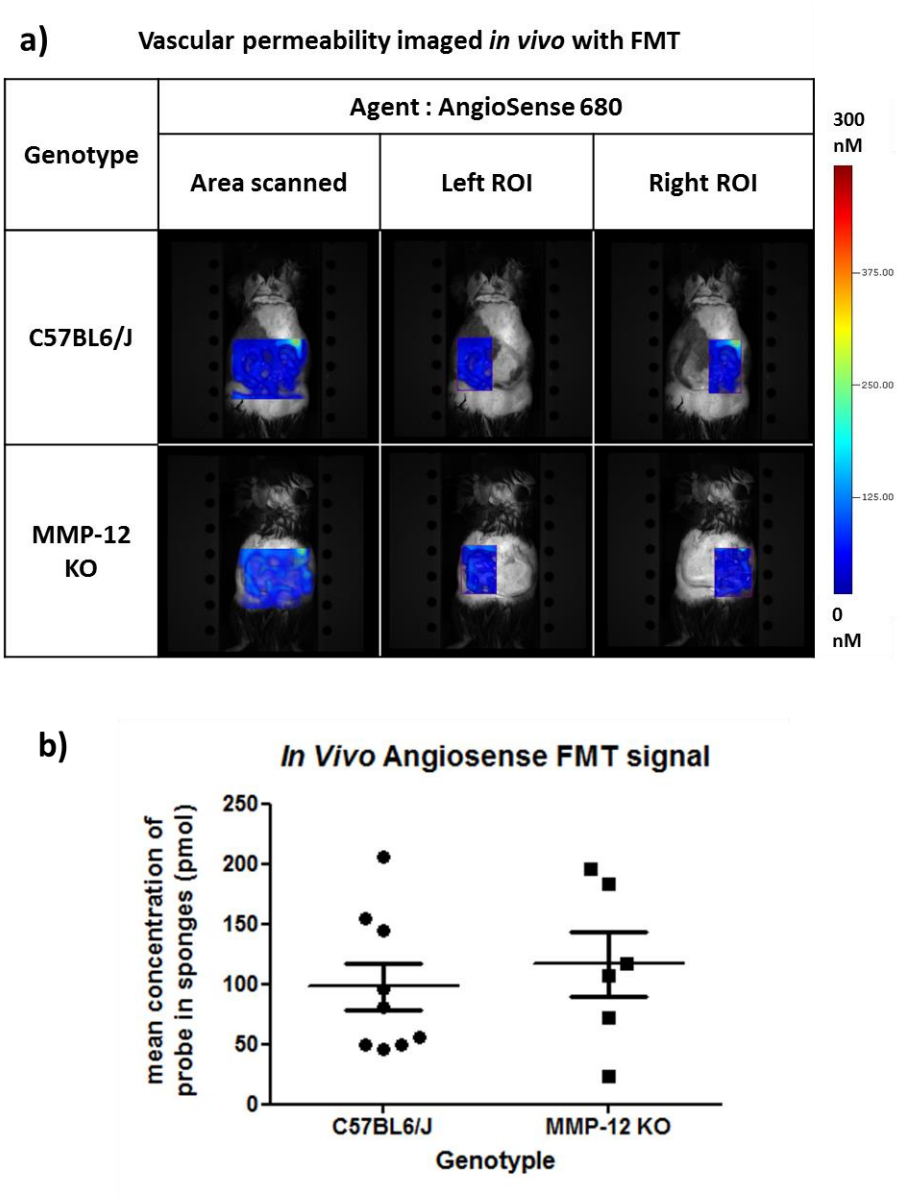

Figure 5.26 MMP-12 deletion did not change vascular permeability *in vivo*. Sponges subcutaneously implanted in MMP-12 KO and C57BL6/J mice. a) Representative images of the *in vivo* fluorescent signal acquired by FMT imaging of AngioSense. The "Area scanned" is representative of the signal measured, the left and right regions of interest (ROI) encompass the signal around the two subcutaneous sponges. b) The mean quantified AngioSense signal around the sponges was similar in C57BL6/J and MMP-12 KO mice ($P = 0.5714$). Bars represent mean ± SEM ($n = 6 - 9$) and comparisons were made using a Students t-test ($P = 0.5714$).

MMP-12 deletion did not increase angiogenesis

Deletion of MMP-12 did not increase the total number of vessels (CD31 or CD31 and α-SMA positive) (Figure 5.27, a). The analysis of the signals detected over the whole section area also identified that there were no changes in the percentage of tissue area covered by CD31, α-SMA or DAPI signals (Figure 5.27, b).

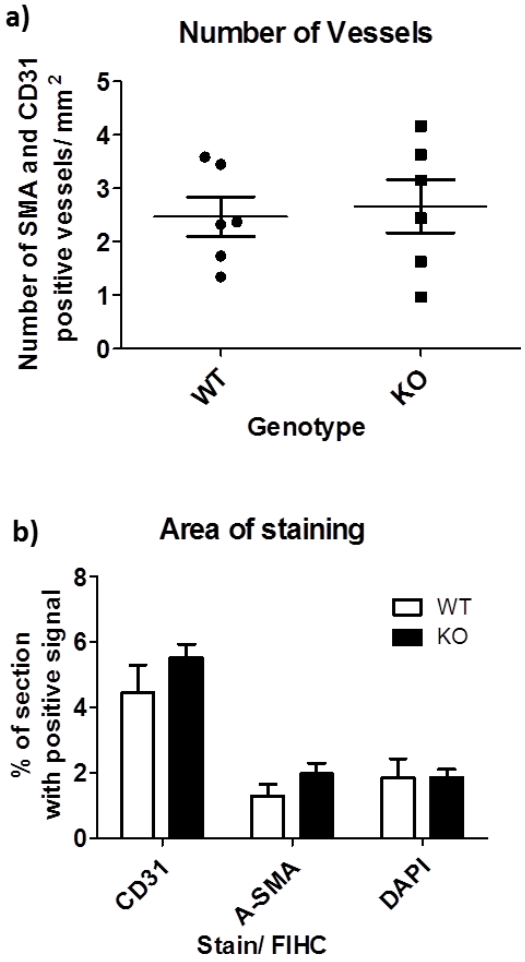

Figure 5.27 Deletion of MMP-12 did not increase angiogenesis *in vivo* in the sponge implantation model. a) Deletion of MMP-12 did not alter the total number of vessels within sponges after 21 days of implantation (P = 0.7600). b) It also did not alter the area stained positive for CD31 (PECAM-1) or α-SMA, suggesting the number of the cells positive for these markers is unchanged. Columns represent mean ± SEM (n = 6), comparisons between genotypes were made using Students t-test P > 0.05.

MMP-12 deletion did not change gene expression of vascular and angiogenic markers.

The expression of hypoxia-inducible factor 1-alpha (HIF-1-α), vascular endothelial growth factor (VEGF) and thrombospondin 1(TSP-1) measured by RT-qPCR was similar in MMP-12 KO and C57BL6/J mice (Figure 5.27Figure 5.28). Expression of CD31 (also known as platelet endothelial cell factor, PECAM-1), vascular cell adhesion molecule (VCAM-1), intercellular cell adhesion molecule (I-CAM), vascular endothelial cadherin molecule (VE-cadherin) and Von Willebrand factor (vWF) were also all unchanged by the deletion of MMP-12 (Figure 5.29). Furthermore, the expression of PDGFRβ (platelet derived growth factor receptor β), a marker of vascular maturation, was also unchanged in the sponge by the loss of MMP-12 activity (Figure 5.29).

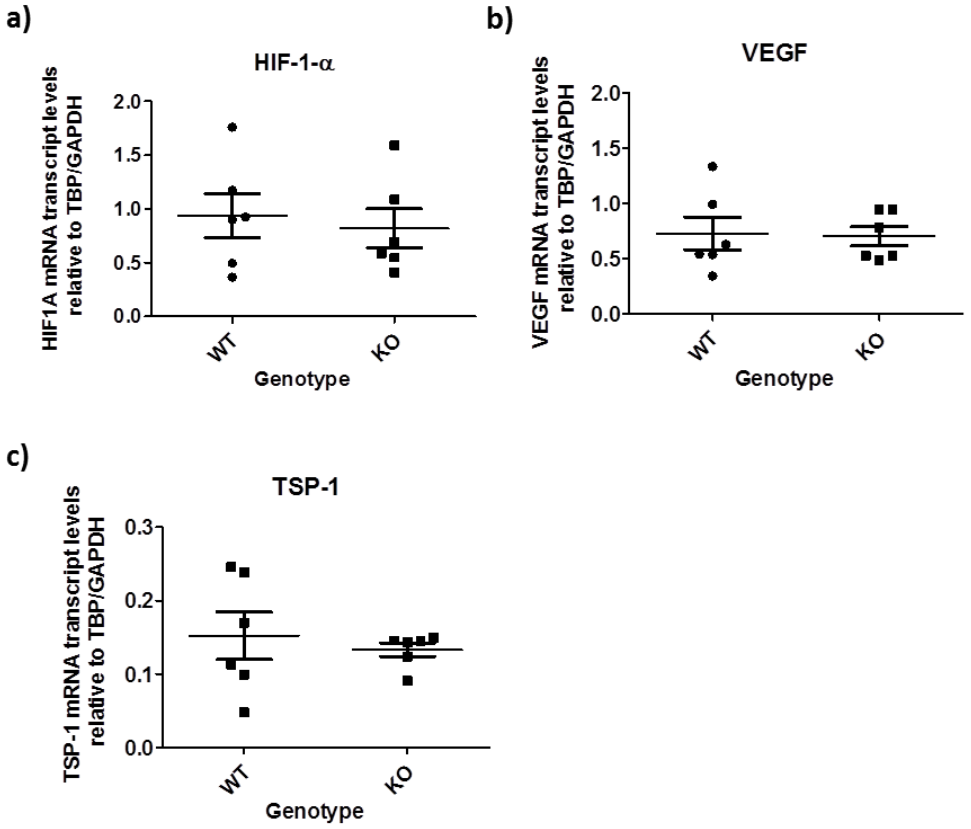

Figure 5.28 Deletion of MMP-12 did not result in a change in mRNA expression of key angiogenic factors. Expression of the pro-angiogenic factors a) HIF-1-α (P = 0.6775) or b) VEGF (P = 0.8818) and the anti-angiogenic TSP-1 (c, P = 0.8182) was similar in C57Bl/6 and MMP KO mice. Bars represent mean ± SEM (n = 6), comparisons were made using Students t-test P > 0.05.

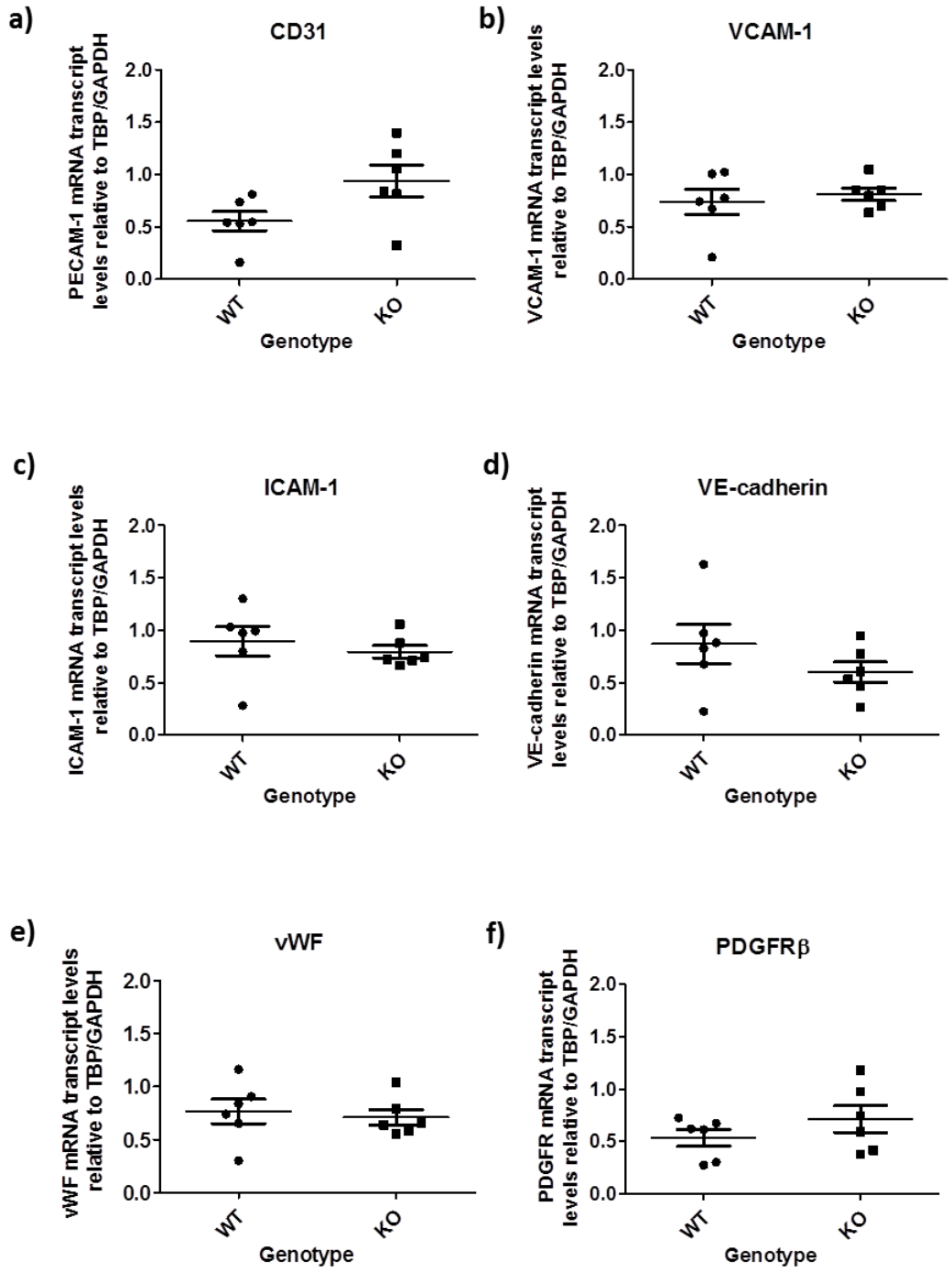

Figure 5.29. Deletion of MMP-12 did not result in a change in mRNA expression of vascular markers. There was no difference in expression of endothelial cell markers: CD31 (a, P = 0.0566), VCAM-1 (b, P =0.5928), ICAM-1 (c, P = 0.5225), VE-cadherin (d, P = 0.2304) and vWF (e, P =0.6850). There was also stable expression of PDGFRβ (f, P = 0.3939) which is associated with vascular maturation. Bars represent mean ± SEM (n = 6), comparisons were made using Students t-test.

5.5 Discussion

In this chapter the role of MMP-12 in angiogenesis was investigated using two MMP-12 targeting compounds (synthesised in Chapter 3, an MMP-12 inhibitor (HS1-22) and an activatable FRET probe (HS1-65)) and MMP-12 KO mice. Out hypothesis was tested in *in vivo* (sponge models, descried in Chapter 4) and *ex vivo* models (lysates from angiogenic tissues or the aortic ring assay) of angiogenesis. This preliminary study found that HS1-65 was non-specifically activated by MMP-12 in the lysates from tissues undergoing angiogenesis (mouse) in an *in vivo* model of angiogenesis. Selective inhibition of MMP-12 with HS1-22 did not increase angiogenesis in the *ex vivo* aortic ring assay (no effect on the numbers of microvessels and decreased their length in the aortic ring assay) or *in vivo* in the sponge assay. Secondly, deletion of MMP-12 also did not increase angiogenesis in the *ex vivo* aortic ring assay (unchanged microvessels numbers and length and the response to MMP inhibitors was unchanged) or *in vivo* in the sponge assay (no change in vessel numbers or gene expression of angiogenic markers). Furthermore, deletion of MMP-12 did not change vascular permeability when measured *in vivo* by FMT (AngioSense 680) and suggestion of a reduction in MMP activity (detected with MMPSense 750) did not reach significance. Overall, these data suggest that MMP-12 activity does not inhibit angiogenesis. This is in contrast to other literature which has shown MMP-12 activity to be anti-angiogenic in an oxygen-induced retinopathy model of angiogenesis (Li *et al*., 2012), and in cancer (Kerkelä *et al*., 2000; Houghton *et al*., 2006)

5.5.1 The FRET probe HS1-65 is activated in tissue lysates but not by MMP-12

A MMP-12 selective FRET probe, HS1-65, with the peptide sequence PLGLEEA (Lim *et al*., 2014; Cobos-Correa *et al*., 2009) was synthesised in-house (Chapter 3). Using *in vitro* assays, this FRET probe was shown to be activated predominantly by MMP-12 and MMP-13 (previously discussed in Chapter 2). Cobos-correa and colleagues (2009) showed that this

peptide sequence was selectively activated by lipopolysaccharide (LPS)-stimulated macrophages expressing MMP-12 from MMP-12 $^{+/+}$ but not MMP-12 $^{-/-}$ mice); whereas Lim and colleagues (2014) used an MMP-12 selective inhibitor to block HS1-65 activation in a preclinical *in vivo* model of collagen-induced arthritis.

It was hypothesised that HS1-65 could be used to detect MMP-12 during angiogenesis in the sponges *in vivo.* In this chapter, HS1-65 was tested to see if it was sensitive enough to detect MMP-12 activity in tissue lysates generated from sponges implanted beneath the skin of control mice for D 3 − 35. HS1-65 was activated in crude tissue lysates but it was shown that this was not mediated selectively by MMP-12, or any other MMP (since activation was not inhibited by marimastat). MALDI-TOF MS analysis of the fragments within the tissue lysate reactions confirmed that the signature fragment detected after MMP-12 cleavage of the probe was not present. The cleavage of HS1-65 by a protease was confirmed using a protease cocktail and by denaturing the proteins present. To gain insight into the protease responsible, reactions were challenged with other protease inhibitors. The probe was not activated by: neutrophil elastase (inhibited by sevilestat) or a serine protease (inhibited by antithrombin III) e.g. trypsin, plasmin, thrombin and the contact activation pathway (Factor X-XII) and kallikrein. Tissue lysates are a complex mixture of cell contents so it will be a challenging process to pursue the protease further.

5.5.2 MMP-12 inhibitor did not promote angiogenesis in the *ex vivo* aortic ring or *in vivo* in the sponge model.

The aortic ring assay was reported by in 1990, but has since been developed to the protocol used in this chapter (Nicosia & Ottinetti 1990; Baker *et al*., 2012). This assay has many attributes that make it a good *in vitro* model of angiogenesis; firstly, it is quick, relatively inexpensive and requires relatively low animal numbers as 10 − 12 rings can be obtained per mouse. Microvessel outgrowths from an intact, multicellular arterial ring develop over a

physiologically-relevant timeline. These tube like structures are clearly visible by microscopy (× 20 magnification) and can have a lumen and be supported by perivascular cells (Nicosia & Ottinetti 1990; Baker *et al*., 2012; McSweeney *et al*., 2010). Finally, this assay allows for simultaneous analysis of microvessel formation when subject to varying treatments in physiologically-relevant, chemically-defined conditions (Nicosia & Ottinetti 1990; Baker *et al*., 2012; McSweeney *et al*., 2010).

Endothelial microvessel out growths (number and length) were enhanced in the presence of growth factors (Baker *et al.,* 2012). FCS contains a rich variety of proteins and growth factors which help maintain cultured cells in an environment in which they can survive, grow, and divide. Plasminogen, present in in FCS, can be activated to plasmin. Plasmin can degrade a variety of proteins (including fibronectin and collagen which are components of the ECM) and can activate MMP-1, -2, -3, -9, -12 and -13 (Davis *et al.,* 2001; Raza *et al.,* 2000; Monea *et al.,* 2002; Carmeliet *et al.,* 1997). Therefore, the presence of plasmin would generally be considered to be proangiogenic (Lacroix *et al.,* 2007). The second growth factor used was VEGF which is a well characterised potent angiogenic promotor; VEGF promotes endothelial cell migration and proliferation (Ferrara *et al.,* 2003).

As predicted, the inhibition of MMP activity (treatment with marimastat) in this study resulted in significantly reduced sprout numbers and stunted vessel growth on D 7. Marimastat has previously been shown to inhibit sprouting in ring assays in a dose-dependent manner (Zhu *et al*., 2000; Burbridge *et al*., 2002). This is consistent with other laboratories which have also highlighted the need for MMP expression during angiogenesis (reviewed by Rundhaug, 2005). Inhibition of MMP activity slows the breakdown of the ECM, restricting endothelial cell migration and the formation of capillaries (Haas *et al*., 1998; Nguyen *et al*., 2001). Marimastat has, however, been shown to minimise vascular regression when added after the angiogenic

growth phase in rat aorta ring assays (Zhu *et al*., 2000). This suggests that MMPs play a dual role in promoting vascular growth and the subsequent pruning and remodelling.

Interestingly, the addition of marimastat unexpectedly increased the number of microvessels on D 3. This is not consistent with other similar experiments which showed marimastat to inhibit the sprouting phase of angiogenesis (Zhu *et al.,* 2000; Burbridge *et al.,* 2002). Marimastat may promote early angiogenesis in this model by inhibiting MMP-dependent production of angiogenic inhibitors, such as angiostatin or endostatin. Interestingly, MMP-7, 9 and 12 can convert plasminogen/plasmin to angiostatin fragments. (Patterson & Sang 1997). Angiostatin inhibits angiogenesis *in vitro* by limiting endothelial cell migration (Cornelius *et al*., 1998; Dong *et al*., 1997; Redlitz *et al*., 1999). Marimastat and HS1-22 both inhibit MMP-12 and so both would be expected to inhibit angiostatin production; however, on D 3 of this study, the selective inhibition of MMP-12 (with HS1-22) did not result in the same increase of microvessel formation as marimastat. These results indicate that the increased angiogenesis with marimastat on D 3 is unlikely to be caused by inhibition of MMP-12. Endostatin can also dramatically inhibit microvessel formation in the aortic ring assay (Kruger *et al*., 2000; Li & Olsen 2004). Endostatin is a 20 kDa C-terminal fragment of collagen XIII (found in the vascular basement membrane), this fragment is the proteolytic product of elastase, cathepsin L and (importantly for this study) by MMP-9, 3, 12 and 13 (Ferreras *et al*., 2000; Halfter *et al.,* 1998). In this assay, the greater angiogenic response observed with MMP inhibition may have been due to reduced synthesis of endostatin. The selective inhibition of MMP-12 did not elicit the same increase in angiogenesis as total MMP inhibition, suggesting that MMPs-3, 9 and 13 could be the important active proteases in this pathway.

Importantly in this study we identified that the selective inhibition of MMP-12 did not affect the number of microvessels on D 3 − 7 but this treatment did result in a slight but significant reduction in vessel length on D 7. This suggests that the inhibition of MMP-12 does not

increase angiogenesis in this assay; if anything, the reverse was true. These results are in contrast to data published by Li and colleagues (2012) that showed loss of MMP-12 gene expression was proangiogenic *in vivo* in a model of oxygen induced retinal ischemia injury. Furthermore, they found that administration of an MMP-12 inhibitor (MMP408 by oral gavage) also increased angiogenesis in the same model. This group also found that pre-treatment with an MMP-12 inhibitor (MMP408; 20 nM, 16 h) did not affect the ability of primary human retinal endothelial cells to form branches in the Matrigel tube formation assay (Li *et al*., 2012). This suggested that either MMP-12 does not play a role in angiogenesis or that MMP-12 activity is not present in this assay. In the work reported in this chapter using the *ex vivo* aortic ring assay, the addition of an MMP-12 selective inhibitor (HS1-22) was not proangiogenic.

In summary, GF simulated microvessel formation in the aortic ring assay but the addition of an MMP-12 inhibitor (HS1-22) did not increase angiogenesis as hypothesised. Marimastat inhibited vessel numbers and length late in the study as expected but there was an increase in sprout numbers in early experiments (D 3) the reason for which is unclear.

A major limitation of the aortic ring assay, and other *in vitro* angiogenesis assays, is the lack of the inflammatory process associated with angiogenesis *in vivo* (Baker *et al*., 2012). As MMP-12 is predominantly secreted by macrophages the lack an inflammatory response limits the number of macrophages present in the environment and, therefore, potentially limits MMP-12 activity. However, adventitial macrophages are present in this assay and are important in regulating tube-like structure formation so there is potential for MMP-12 to be present (Gelati *et al.*, 2008). To test our hypothesis that MMP-12 is an inhibitor of angiogenesis, we next moved into the *in vivo* sponge model (which has MMP-12 activity peaking on D 7 and a time-dependent inflammatory response, as discussed in Chapter 4). We hypothesised that an *in vivo*

model would be a better for testing HS1-22 as it is more representative of the natural angiogenic response compared to the aortic ring assay.

Spontaneous angiogenesis in the subcutaneous sponge implants is facilitated by the porous framework and the host inflammatory response. Post implantation, the infiltration of leukocytes results in the secretion of cytokines and chemokines, producing a pro-angiogenic response (Leibovich *et al.*,1987; Barcelos *et al.*,2005). This model is attractive due to its reproducibility, it's MMP-12 activity, and the ease of vessel number quantification using histological techniques; other advantages are listed in the discussion of Chapter 4

There have been several successful adaptations of the sponge model to utilise different scaffold materials such as metal meshes (Schilling *et al.,* 1959), other synthetic polymers (polyvinal alcohol, poly urethane) and hydrogels (Kleinman *et al.,* 1986; Phelps *et al.,* 2010). Novel polymer coatings have been used to promote attachment, differentiation, and expansion of endothelial cells (Pernagallo *et al.,* 2012). Furthermore, agents can be administered systemically (via food, water, gavage or intravenous injection) or directly via osmotic minipumps (Efron *et al*., 2001), silastic elastomers (Small *et al*., 2005) or injection into the sponge (Hu *et al,*. 1995). In this chapter, MMP inhibitors drugs were administered to polyurethane sponges using osmotic pump attached by a catheter to the sponge. This administration method was chosen as it allowed uninterrupted flow of drug over 3 weeks directly into the sponges and potentially limited any systemic effects of the MMP inhibitors. Sponge implants have previously limited systemic effects of drugs (Small *et al*., 2005); local administration by osmotic pump was intended to have a similar effect in this study and to limit any off target systemic effects of drugs (eg. marimastat causes muscoskeletal toxicity) (Wojtowicz-Praga *et al.,* 1998; Bramhall *et al.,* 2002; Jacobsen *et al.,* 2010).

Overall, marimastat and HS1-22 were well tolerated and there was no loss of body weight. Interestingly there was a small reduction in lung size for both marimastat and HS1-22

treatment. This was mirrored by a similar reduction in lung size in MMP-12 KO mice. MMPs are essential for lung homeostasis and are upregulated in pathological conditions but there is little literature to explain this reduction in lung size observed in this study (Greenlee *et al.*,2007). Mice treated with HS1-22 also exhibited larger kidneys; MMP-12 is present in low levels in the murine kidney but this effect was not mirrored in the mice treated with marimastat or in MMP-12 KO mice so was likely an off-target effect of HS1-22 (Rao *et al.,* 2006). These small but significant changes in organ weights suggests that, despite local administration, there was systemic drug action. Furthermore, it demonstrated that active drug was administered to the sponge.

MMP activity is essential for angiogenesis; it facilitates the breakdown of the ECM and cell migration (Hinsbergh & Koolwijk 2008). In this study, marimastat (2 mg/kg/day) was well tolerated. Histological techniques showed that marimastat inhibited angiogenesis in sponges, specifically, causing a reduction in the number of mature vessels. This is consistent with other studies which also show marimastat as an inhibitor of angiogenesis (Skipper *et al.*,2009; Kimata *et al.*,2002). Therefore, results in this study confirm that MMPs are required for *in vivo* angiogenesis.

Unlike most MMPs, the role of MMP-12 has previously been suggested to be anti-angiogenic *in vitro* and *in vivo* (Li *et al.*,2012; Serrat *et al.*,2006). Results in this chapter revealed that selective pharmacological inhibition of MMP-12 (with HS1-22) did not increase angiogenesis *in vivo* after 21 days of administration. In fact, there was a pattern for fewer vessels, which were less mature, but these differences did not achieve significance. To confirm that MMP-12 did not affect angiogenesis in this *in vivo* sponge model and in the *ex vivo* aortic ring assay, MMP-12 KO mice were utilised.

5.5.3 MMP-12 deletion did not promote angiogenesis in the *ex vivo* aortic ring or *in vivo* in the sponge model.

MMP-12 null mice are commercially available and the MMP-12 deletion is relatively well tolerated. These mice are more prone to viral and bacterial infection and their litter sizes are smaller, ~60% of wildtype (Marchant *et al.*,2014; Houghton *et al.*,2009). Studies have shown that deletion of MMP-12 is protective against atherosclerosis and aortic aneurysms, and is proangiogenic in an oxygen-induced retinopathy/ ischemia model of angiogenesis (Li *et al.*,2012; Johnson *et al.*,2005; Longo *et al.*,2005). Macrophages lacking MMP-12 have limited ability to invade tissues as they cannot cleave components of the ECM to facilitate migration (Li *et al*., 2012). Results in this chapter showed that deletion of MMP-12 had no effect on *ex vivo* angiogenesis (microvessel numbers, length and response to MMP inhibitor treatments remained unchanged in the aortic ring assay) and *in vivo* angiogenesis (vascular permeability (AngioSense and angiogenesis FMT) and total vessel numbers both remained unchanged in sponges).

As discussed above, the inhibition of MMP-12 (treatment with HS1-22) did not statistically increase microvessel formation (number and lengths on D 7) in the aortic ring assay. To examine this further, we next cultured aortae rings from C57BL6/J and MMP-12 KO mice. Compared to their C57BL6/J counterparts, rings lacking MMP-12 did not exhibit any significant changes to the formation of microvessels outgrowths (numbers or length) nor did they respond very differently to the growth factor and MMP inhibitor treatments. Briefly, administration of GF increased angiogenesis and treatment with marimastat, reduced vessel number and length by D 7 in both C57BL6/J and MMP-12 KO mice. Selective inhibition of MMP-12 (with HS1-22) inhibited vessel numbers and lengths by D 7 in both C57BL6/J and MMP-12 KO mice; this suggested that any small changes induced by HS1-22 were off target effects and not due to MMP-12 inhibition.

It was hypothesised that the lack of any pro-angiogenic effect by MMP-12 deletion and inhibition in the *ex vivo* assays could be explained by the lack of a host inflammatory response (although, as previously discussed, macrophages are present in this assay (Gelati et al. 2008)). However, selective inhibition of MMP-12 in the *in vivo* sponge implantation assay also did not increase angiogenesis. To help clarify the role of MMP-12 during *in vivo* angiogenesis, MMP-12 KO mice were utilised in the sponge implantation assay.

E*x vivo* observations showed that sponges implanted in MMP-12 null mice for 21 days were more adhered to each other and the surrounding tissue which suggested that there was greater ECM deposition. Nevertheless, no significant changes in collagen(s) deposition were found by histology. Lack of MMP-12 may lead to greater elastin deposition but this will need to be addressed in future studies.

Sponges in MMP-12 KO mice had significantly diminished MMP-12 expression within the fibrovascular tissue. MMP-12 is predominantly expressed by macrophages (Nénan *et al.,* 2005); C57BL6/J and MMP-12 KO mice exhibited similar levels of macrophage infiltration into their sponges. Macrophages are the major producer of TNFα (Parameswaran & Patial, 2010) and, in this study, TNFα mRNA expression in sponges was unchanged in MMP-12 KO mice. TNFα primes endothelial cells for angiogenic sprouting by inducing tip cell phenotype once the initial inflammatory wave has passed (Sainson *et al.,* 2008). In sponges treated with corticosterone (which is a potent inhibitor of angiogenesis), the angiogenic response was independent of inflammatory cell infiltration and the treatment had a very limited effect on a number of transcripts of inflammatory factors) (Gastaldello, 2015).

The FMT 2500 machine and MMPSense has previously been shown to be sensitive enough to detect increased MMP activity in murine models of gastric and skin cancer (Ding *et al.,* 2012; Al Rawashdeh *et al.,* 2014). In this study, imaging MMP activity within the sponges on D 7 (with MMPSense and FMT) showed that MMP-12 null mice had a pattern for reduced MMP

activity (lower concentration of probe with smaller variability) but this did not reach significance. Firstly, this could be because this study was not powered to detect this difference, by using power calculations and this data, it has been estimated that groups of n = 48 for would be required to prove this hypothesis ($P < 0.05$). Secondly, the MMPSense probe, which is designed to detect a spectrum of MMP activities (MMP- 2, 7, 9, 12 and 13), was not sensitive enough to detect the selective loss of MMP-12 activity within the sponges (Groves *et al.,* 2010). Additionally, other MMPs have substrates in common with MMP-12 (Table 1.1) and so may have partially compensated for the loss of MMP-12 activity, in which case there is possible genetic redundancy *in vivo*. Compensation by other MMPs has previously been observed: global deletion of MMP-9 resulted in increased expression of MMP-3 and 13 in myocardial tissue post myocardial infarction (Ducharme *et al.,* 2000); in postpartum uterine involution, deletion of MMP-7 resulted in increased expression of MMP-3 and 10, whereas the deletion of MMP-3 resulted in an increase in MMP-7 and 10.

Interestingly in this study, MMP-12 KO mice exhibited no changes to angiogenesis in the *in vivo* sponge implantation assay. No changes in vascular permeability (a characteristic which increases in vessels undergoing active angiogenesis) were detected *in vivo* in sponges in MMP-12 KO mice (AngioSense with FMT) or in total vessel numbers on D 21 post implantation. Consistent with these results, deletion of MMP-12 had no effect on VEGF (an angiogenic promotor) or TSP-1 (an angiogenic inhibitor) gene expression in the sponges. VEGF-induced activation of endothelial cells results in disassembly of VE-cadherin, one of the principal signalling and structural proteins associated with the VE cell-cell adherens junction (Petzelbauer *et al.,* 2000). Disassembly of these junctions increases vascular leakiness and enables the migration of the endothelial cells, these then divide to form the new vessels (Bates 2010). Further to this, the expression of TSP-1, an inhibitor of angiogenesis, was also unaltered (Lawler *et al.,* 2002). TSP-1 inhibits angiogenesis by inhibiting endothelial cell migration,

proliferation, survival, and apoptosis and by antagonizing the activity of VEGF (Lawler & Lawler, 2012).

Consistent with the histological analysis of vessels, gene expression for markers of endothelial cells (VE-cadherin, CD31, VCAM-1 and ICAM-1) also remained unchanged between sponges from MMP-12 KO and C57BL6/J mice. CD31 was the closest to a significant change between the two genotypes ($P = 0.0566$), power calculations estimate that a groups of $n = 9$ would have been sufficient to prove if this was a real change. CD31 is an adhesion molecule expressed by endothelial cells is suggested to facilitate the trans-endothelial migration phase of leukocytes (Muller, 1995; Wakelin *et al*., 1996). CD31 is expressed by endothelial cells but also by macrophages (McKenney *et al.*, 2001), therefore any change in gene expression of this marker cannot be assumed to be solely from a change in endothelial cell numbers. VCAM-1 also mediates the adhesion of leukocytes to inflamed endothelium; when in its soluble form VCAM-1 is reported to exhibit angiogenic activity *in vivo* through mediating endothelial cell chemotaxis (Koch *et al.*,1995). VCAM-1 is also suggested to be required for blood vessel maturation via the integrin α4β1–VCAM-1–mediated adhesion between endothelial and mural cells (Fukushi *et al.*,2000). Endothelial cells and macrophages both express ICAM-1 which is important for stabilising cell−cell interactions and facilitating leukocyte endothelial transmigration (Lawson & Wolf 2009). Platelet derived growth factor receptor (PDGFR) is also important in the maturation process as it stimulates pericyte and smooth muscle recruitment (Levanon *et al.*, 2006), its gene expression also remained unchanged in sponges from MMP-12 KO mice. This supports the histological analysis of angiogenesis within the sponges implanted in MMP-12 null mice: the loss of MMP-12 during *in vivo* angiogenesis did not alter angiogenesis. Deletion of MMP-12 also did not affect adipose tissue associated angiogenesis in mice on a high fat diet (Bauters *et al*., 2013).

5.5.4 Conclusion

The inhibition or deletion of MMP-12 did not promote angiogenesis in *in vivo* or *ex vivo* murine assays. HS1-22 had off target effects making the associated studies into the effect of MMP-12 during angiogenesis less reliable. FMT imaging was successfully used to image MMP activity (MMPSense) and angiogenesis (AngioSense) but levels detected were unchanged between MMP-12 KO and C57BL6/J mice. HS1-65 was found to be cleaved in sponge tissue lysates by a protease other than MMP-12.

To conclude, firstly, commercial molecular imaging probes are useful tools for non-invasively gaining information on a tissue micro-environment, but selective imaging of MMP-12 activity in sponges is still to be achieved. Secondly, MMP-12 is not an inhibitor of angiogenesis in the assays used in this chapter.

Chapter 6

General Conclusions, Limitations and Future Directions

6 Chapter 6: General Conclusions, Limitations and Future Directions

6.1 Introduction

The vascular network provides nutrients and removes waste from tissues. A healthy network of blood vessels supports tissue maintenance, growth and repair but structural and functional abnormalities in the network can contribute towards disease. Poor blood supply can cause ischemia in tissues, leading to myocardial infarction (Thygesen *et al.,* 2012), or stroke (Prabhakaran *et al.,* 2015). Conversely, increased blood supply to tumours is associated with increased tumour growth and metastasis, leading to poor prognosis (Folkman, 2007). The ability to image the structure of the vessel network and blood flow could contribute towards the assessment of a particular disease state. Furthermore, advancements in molecular analysis could contribute towards a greater understanding of the molecular environment of diseases. For example, changes in enzyme activities and signalling molecules that contribute to altered angiogenesis. Pharmacological manipulation to stimulate or inhibit angiogenesis represents an attractive therapeutic opportunity in cancer biology, tissue regeneration and even obesity (Folkman, 2007; Cao & Langer, 2010; Yoo & Kwon, 2013).

The activity of matrix metalloproteinases (MMPs) is associated with increased vessel growth and the progression of several cardiovascular diseases (CVD) (Van Hinsbergh & Koolwijk 2008). Interestingly, MMP-12 is suggested to inhibit vessel growth but its precise role is still unclear (Li *et al.,* 2012). It has been suggested that MMP-12 inhibits angiogenesis by the generation of inhibitory molecules and by the inhibition of plasminogen activation (Figure 1.12) (Ferreras *et al.,* 2000; Cornelius *et al.,* 1998; D'Alessio *et al.,* 2004; Koolwijk *et al.,* 2001). The ability to selectively image and/or manipulate MMP-12 activity *in vivo* could contribute towards a better understanding of its role during blood vessel formation and in

diseases in which it is suggested to have an active role such as atherosclerosis (Liang *et al*., 2006), arthritis (Liu *et al*., 2004) and aneurysms (Longo *et al*., 2005).

The aim of work presented in the thesis was conducted to gain a greater understanding of the precise role of active MMP-12 during angiogenesis. Thus, commercial and in-house synthesised MMP inhibitors and FRET probes were used to address the hypothesis that MMP-12 activity is anti-angiogenic.

6.2 Research summary, limitations and future work

6.2.1 Overview

The work described in this thesis was conducted to test the hypothesis: MMP-12 activity inhibits angiogenesis. Firstly, an MMP-12 inhibitor was applied to *ex vivo* and *in vivo* angiogenesis assays. These showed that inhibition of MMP-12 activity did not result in an increased angiogenesis. Secondly, MMP-12 knock out (KO) mice were used in *ex vivo* and *in vivo* angiogenesis assays; once again impaired MMP-12 activity did not increase angiogenesis. Tools to image angiogenesis and MMP, in particular MMP-12, activity non-invasively during angiogenesis were tested as part of these studies.

6.2.2 MMP-12 inhibition did not promote angiogenesis

To answer the hypothesis, initially an MMP-12 inhibitor was synthesised and tested for potency and selectivity using recombinant *in vitro* assays and then used in the *ex vivo* aortic ring and *in vivo* sponge assays of angiogenesis.

A potent, low-toxic, MMP-12 selective inhibitor was synthesised

The MMP-12 selective inhibitor, HS1-22, was structurally similar to MMP408 (discussed in Section 1.6.4) (Li *et al.*, 2009). It was hoped that a small rearrangement of moieties (from MMP408 to HS1-22) would allow for future labelling with a fluorophore (for optical molecular imaging of MMP-12) without significant loss of potency or selectivity towards MMP-12. HS1-22 was synthesised in 6 steps from commercially available reagents. The compound was purified by HPLC and analysed using 1D and 2D NMR and MS techniques. *In vitro* recombinant enzyme assays confirmed that HS1-22 was very selective for MMP-12 (but also slightly inhibited MMP-2) in a panel of selected MMPs. IC_{50} assays showed that HS1-22 was a potent inhibitor for MMP-12 (but marimastat (broad spectrum (Wojtowicz-

Praga *et al.,* 1998)) and AZD1236 (MMP-9 and 12 (Dahl *et al.,* 2012)) were more potent); these results also suggested that there was a compromise between potency and selectivity for MMP inhibitors. An MTT assay also showed HS1-22 to be non-toxic at concentrations below 100 μM. Consequently, this compound was taken forward to *ex vivo* and *in vivo* angiogenesis assays. To summarise, HS1-22 is a potent MMP-12 inhibitor with low toxicity.

Inhibition of MMP-12 did not promote angiogenesis

The hypothesis that MMP-12 activity contributes to inhibition of angiogenesis was tested using HS1-22 in *ex vivo* and *in vivo* angiogenesis assays. It was hypothesized that inhibition of MMP-12 by HS1-22 would promote vessel growth in these assays. Firstly, HS1-22 was tested as an angiogenesis promoter in the *ex vivo* aortic ring assay (assay reviewed by Baker *et al.,* 2012). MMP inhibitors were administered to aortic rings and the number and lengths of microvessel outgrowths measured. A broad spectrum inhibitor of MMPs (marimastat) reduced micro-vessel numbers and length. This was consistent with the work of Zhu and colleagues (2000). The selective inhibition of MMP-12 (with HS1-22) did not alter the number of vessel outgrowths but did decrease the vessel length by D 7. This result was contrary to the hypothesis that selective inhibition of MMP-12 would increase angiogenesis. A possible reason for this was that the contribution of macrophages, the main source of MMP-12, is limited in this assay (number due to the lack of a systemic inflammatory component). It should be noted, however, that inflammatory cells present in the adventitia of the aortic rings have been shown to contribute to tube formation in this assay (Gelati *et al.,* 2008). A subsequent investigation described in this thesis showed that the microvessel outgrowths from MMP-12 KO mice did not respond differently to the MMP inhibitor treatments (by D 7, marimastat reduced microvessel numbers, and both HS1-22 and marimastat inhibited vessel lengths) compared to those from C57BL6/J mice. This confirmed that any effects of HS1-22 in this assay were unlikely to be the result of MMP-12 inhibition. Results obtained using the *ex vivo* assay

suggest that MMP-12 does not have a role in inhibiting angiogenesis. However, the aortic ring assay has its limitations, primarily that angiogenesis occurs in the absence of a systemic inflammatory response (and, therefore, potentially lacks MMP-12 secreting macrophages) and the tissue is not exposed to blood-borne or tissue-derived factors (Baker *et al.,* 2012). Therefore, the next stage was to test the hypothesis in *in vivo* model of angiogenesis with an inflammatory response.

An *in vivo* model of angiogenesis with defined expression and activity profiles of MMP-12 was developed. The subcutaneous sponge implantation model of angiogenesis is well established and regularly used in the Hadoke group (Small *et al.,* 2005; Andrade *et al.,* 1987). At the beginning of this project, the precise role and activity profile of MMP-12 in this model was unknown. The expression and activity of MMPs in the subcutaneous sponge implantation model was characterised over a 35 day period. MMP-12 was present in this model: gene expression (increased D 7-21), protein expression (decreased D 7 - 21) and activity (peaked on D 7) were all measured. Firstly, these data served as a guide to the presence of MMP-12 activity during angiogenesis in this model, and secondly, it highlighted the complexity of the patterns of MMP activation and regulation.

To test our hypothesis, that MMP-12 is an inhibitor of angiogenesis, HS1-22 and marimastat were administered for 21 days directly into the sponge via an osmotic pump. It was intended that direct administration to the sponge would minimise systemic effects. Administration of marimastat led to a small but significant increase in body weight and a reduction of lung weight; mice treated with HS1-22 exhibited larger kidneys and smaller lungs. Therefore, this indicated that local administration was not sufficient to prevent systemic effects of these drugs. Sponges from mice treated with marimastat showed a significant reduction in both the total number of vessels and the number of CD31 and α-SMA positive vessels. This is consistent with other studies showing that inhibition of MMP activity inhibits angiogenesis (Wada *et al.,*

2003). Mice treated with HS1-22 also had a pattern suggesting a reduction in total and mature vessels but this did not reach significance. These data do not support the hypothesis that MMP-12 inhibits angiogenesis.

To summarise, an MMP-12 selective inhibitor was synthesised in-house but this compound did not promote angiogenesis in *ex vivo* or *in vivo* assays.

Limitations and future experiments

Broad spectrum MMP inhibitors (including marimasat) were first developed as anti-cancer treatments but failed to provide the breakthrough hoped for; this was in-part due to their musculoskeletal toxicity (Cathcart *et al*., 2015). It was suggested that inhibitors targeting specific MMPs would limit these side effects (Cathcart *et al*., 2015), but this hypothesis is still to be definitively proven. In this study, MMP-12 inhibition with HS1-22 was hypothesised to inhibit angiogenesis but this was not proven. There are several avenues for future work regarding HS1-22 and the assays used:

Does HS1-22 alter endothelial cell behaviour in vitro?

An MMP-12 inhibitor (MMP408) was shown to not affect the ability of endothelial cells to form branches in the Matrigel tube formation assay (Li *et al.*, 2012). The effects of HS1-22 on endothelial cell behaviour could also be tested in a similar manner using the Matrigel tube formation assay (Arnaoutova *et al.*, 2009) or the endothelial scratch assay (Liang *et al.*, 2007).

Does the aortic ring assay have MMP-12 expression and activity?

In this study HS1-22 was tested as a proangiogenic drug using the aortic ring assay. Although macrophages are known to be present in this assay (Gelati *et al*., 2008), the presence of MMP-12 in this assay is still unknown. To better understand of the effects of HS1-22 on aortic ring microvessel outgrowths, the presence of MMP-12 in this assay could be investigated. MMP-

12 gene expression in the aortic rings during angiogenesis could be measured using RT-qPCR (Baker *et al*., 2012). Alternatively, MMP-12 activity in the vessel tissues could perhaps be measured using zymography (Vandooren *et al*., 2013).

Does HS1-22 inhibit angiogenesis in another model of angiogenesis?

An MMP-12 inhibitor (MMP408) was shown to promote angiogenesis in an oxygen-induced retinopathy model of angiogenesis (Li *et al.*, 2012). HS1-22 could be tested in this angiogenesis assay. Angiogenesis in tumours, retinopathy and cardiac ischaemia may be regulated in different ways, so it is conceivable that MMPs may contribute differently in models of these conditions. Other angiogenesis assays in which HS1-22 could be tested *in vivo* include the chick chorioallantoic membrane (CAM) assay or zebra fish. However, they each have their own limitations- including not being mammal based (both reviewed by Norrby, 2006).

Does MMP408 inhibit angiogenesis in the sponge implantation assay?

Compound MMP408 was the compound HS1-22 was based on and is also a potent MMP-12 inhibitor. It was previously used to support that MMP-12 is an inhibitor in the OIR model of angiogenesis. MMP408 could be used in this sponge model to verify the results from HS1-22. Should it elicit a similar response in sponges, it would confirm that selective MMP-12 inhibition is not proangiogenic.

Can HS1-22 be labelled and used to image MMP-12?

Selective imaging of MMP-12 activity could allow for better understanding of its role during angiogenesis and disease. Compound HS1-22 was chosen for this study due to the potential to conjugate it to a fluorogenic reporter group without impacting the compounds potency greatly (discussed in Section 1.6.4). Although labelling of HS1-22 was not undertaken for this study due to limited resources, future studies could do this (Figure 6.1).

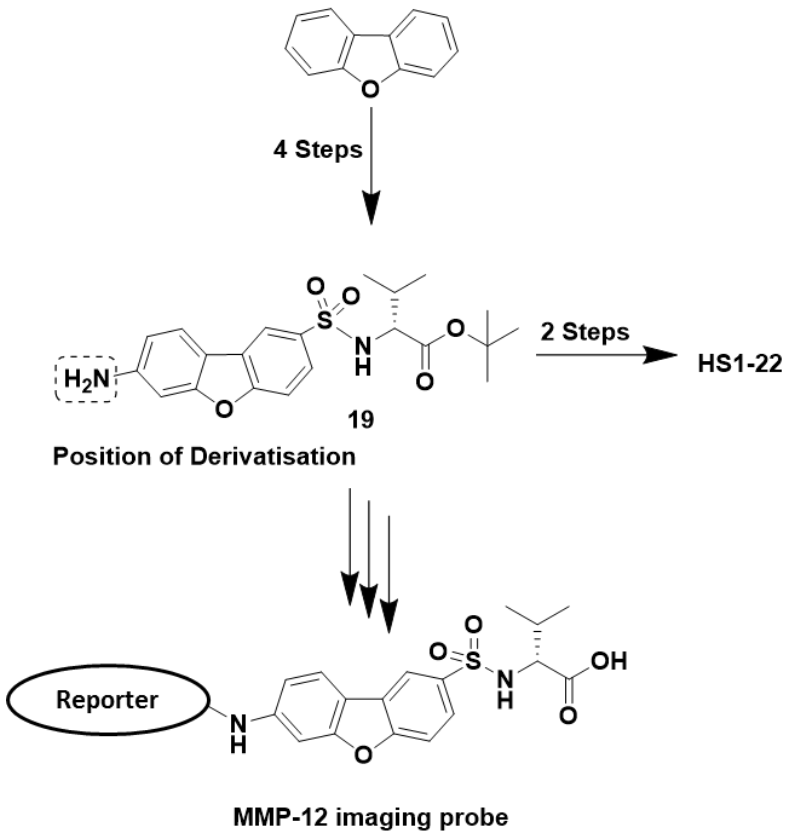

Figure 6.1 Synthetic strategy for the synthesis of a reporter labelled MMP-12 inhibitor. Synthetic divergence to make an imaging probe (rather than HS1-22) would occur from compound **19**, with the amine acting as a handle. HS1-22 could be modified to incorporate a range of reporters for imaging; for example, Gd-DOTA for MRI, Cy5.5 or Cy7 for optical imaging, ^{18}F for PET or a microbubble for ultrasound.

6.2.3 MMP-12 deletion did not inhibit angiogenesis.

Inhibition of MMP-12 did not promote angiogenesis in either the *ex vivo* aortic ring assay or *in vivo* sponge implantation models of angiogenesis. This was not consistent with our hypothesis that MMP-12 contributes to inhibition of angiogensis. To clarify these results MMP-12 KO mice or their tissues were utilised in both of these angiogenesis assays.

In the *ex vivo* aortic ring assay, characteristics of microvessel outgrowths (number or length) from the aortic rings from MMP-12 KO mice were similar to those from C57BL6/J mice. Also the response to MMP inhibitor treatments (marimastat and HS1-22) was not affected by genetic deletion of MMP-12. Again, as discussed above, this may be due to a lack of MMP-12 activity in this assay. Next, the effect of MMP-12 deletion on angiogenesis was assessed in the *in vivo* sponge assay. Results showed that the number of vessels in subcutaneous sponges was unchanged between those from C57BL6/J and MMP-12 KO mice. Additionally, the gene expression of vascular marker (CD31, VCAM-1, VE-cadherin, PDGFRβ), angiogenesis promotors (VEGF, HIF-1-α) and inhibitors (TSP-1) was unchanged by MMP-12 KO. The data collected using MMP-12 KO mice suggest that MMP-12 activity does not inhibit angiogenesis in this model.

To summarise, deletion of MMP-12 did not promote angiogenesis in *ex vivo* or *in vivo* assays.

Limitations and future experiments

Does MMP-12 inhibit angiogenesis in another model of angiogenesis?

Animal models of disease and tissue remodelling, although useful tools, do not always develop and behave exactly like the corresponding process in humans. As such, results and conclusions drawn from their use should be interpreted with some caution. Deletion of MMP-12 in the sponge implantation assay did not affect vessel number or gene expression. However, MMP-12 deletion has been shown to inhibit angiogenesis after oxygen induced retinopathy (Li *et al.*, 2012). Angiogenesis in different tissues occurs under different biological conditions (for example, tissues have different ECM compositions and specialised cell behaviours). Furthermore, there are differences between developmental, physiological and pathological angiogenesis (reviewed by Chung & Ferrara, 2011). Angiogenesis in tumours, retinopathy and

cardiac ischaemia may be regulated in different ways. It is also conceivable that MMPs may contribute differently in each of these conditions.

In cancer, angiogenesis is required to support tumour growth when the tumour size exceeds 1− 2 mm diameter, and later facilitates metastasis. Tumour cells release a host of factors including HIFs, FGF and VEGF to stimulate angiogenesis (Chung & Ferrara, 2011). However, the resulting tumour vessels are structurally and functionally abnormal, typically the network has irregular branching, different vessel diameters and poor perfusion (Jain 2005; Nagy *et al.*, 2010). The vessel walls are also leaky, which facilitates cancer cell access to the vessel lumen (Hashizume *et al*., 2000). Tumour cells and endothelial cells can line the lumen of the vessels (Chang *et al.*, 2000), but unlike the endothelial cells, these tumour endothelial cells can transform to a mesenchymal state and migrate to new tissues which can result in metastasis (Voulgari & Pintzas, 2009).

Inflammation has long been associated with cancer development. Macrophages have been implicated in cancer pathogenesis and tumours with a high macrophage content have increased vascularity and poor prognosis (Pollard, 2009; Chung *et al.*, 2010). MMMP-12 is predominantly secreted by macrophages, can degrade components of the ECM and is required for macrophage migration across the basement membrane (Shipley *et al.*, 1996; Gronski *et al.*, 1997). MMP-12 deletion has already been shown to increase tumour growth and metastasis in model of lung cancer (Lewis lung metastases) (Houghton *et al.*, 2006). Selective inhibition of MMP-12 (with HS1-22) could be tested as an anti-cancer therapy in a similar model of lung cancer. Alternatively, a model of proliferating capillary haemangiomas could be used. These tumours are clinically treated with glucocorticoids to supress inflammation and angiogenesis (Folkman *et al.*, 1983; Logie *et al.*, 2010; Hasan *et al.*, 2000). A model of capillary haemangiomas may be a useful assay to test whether MMP-12 inhibition results in greater angiogenesis in tumours.

In the sponge model, does the expression and activity of other MMPs in the MMP-12 KO mice change compared to C57BL6/J mice?

Many MMPs have the same substrates and, therefore, there is scope for redundancy (Table 1.1). There is evidence from other single MMP KO models that other MMPs up-regulate to compensate for the loss (Ducharme *et al.*, 2000; Rudolph-Owen *et al.*, 1997). It would be interesting to determine whether there is an increase in expression and activity of other MMPs in the sponges as a result of deletion of MMP-12.

Why does MMP-12 inhibition and MMP-12 deletion result in mice with lighter lungs?

In both *in vivo* studies (the pharmacological inhibition and genetic deletion of MMP-12), it was noted that loss of MMP-12 activity resulted in mice with smaller lungs; the reason for this is unknown. The lungs comprise of highly vascularised tissues rich in elastin, the major substrate for MMP-12. It is already known that increased MMP-12 activity can exacerbate COPD (Molet *et al.*, 2005). Histological analysis of lungs from MMP-12 KO and HS1-22 treated mice could reveal key changes in tissue structure on a cellular level, including the vasculature.

To date there is little understanding of the precise role of MMP-12 during embryonic development, and although not fatal, MMP-12 deletion does result in reduced litter sizes (60% of wild type (The Jackson Laboratory, 2016)). MMP-12 KO mice do not have MMP-12 activity during embryonic development but still have a functional cardiovascular system, therefore the role of MMP-12 is not essential to angiogenesis regulation in the embryo. Further investigation into MMP-12 during development, especially its role in angiogenesis, is required.

6.2.4 Molecular imaging of angiogenesis, total MMP and MMP-12 activity

Optical molecular imaging is developing traction in the field of medical imaging (Bu *et al.*, 2013; Osborn & Jaffer, 2013; Garland *et al.*, 2016). Optical imaging has many advantages including using non-ionizing radiation and non-bulky, easily maintained equipment which could be used for bedside diagnostics. Currently there is a broad range of commercially-available reagents for preclinical imaging, as well as novel probes developed by other research groups designed to provide insight into the molecular environment of cells and tissues (Peterson, 2011; Groves, 2010; Waschkau *et al.*, 2013). In this study, commercially available AngioSense and MMPSense agents were used to image angiogenesis and MMP activity, using fluorescent molecular tomography (FMT), in subcutaneously implanted sponges *in vivo*.

Angiogenesis was imaged in sponges with AngioSense and FMT

Non-invasive imaging of angiogenesis using AngioSense and FMT was used to help address our hypothesis: MMP-12 is an inhibitor of angiogenesis. In the time-course study, *in vivo* imaging of sponges detected an increase in vascular permeability, a characteristic of early angiogenesis, in sponges on D 7 compared to D 14 and 21. As D 7 would represent an early stage of angiogenesis in this model we hypothesised that the increased signal was due to increased angiogenesis within the sponges. Interestingly, imaging of the D 7 sponges *ex vivo* did not identify this difference. This discrepancy between the *in vivo* and *ex vivo* measurements of vascular permeability in sponges on D 7 may be due vascular changes in tissues immediately surrounding the sponges *in vivo*. Interestingly, the peak in angiogenesis (measured *in vivo*) and the peak in MMP-12 activity (measured by zymography) where both on D 7. Therefore, it was possible that MMP-12 may be having the greatest effect on angiogenesis at this time point. However, in the MMP-12 KO study, angiogenesis in sponges was imaged on D 7 but no changes were detected between C57BL6/J and MMP-12 KO mice (imaged *in vivo* by FMT

with AngioSense). These data were supported by histological and gene expression analysis from the same sponges collected on D 21 which showed that vessel numbers and angiogenic markers were unchanged by MMP-12 KO (discussed above).

AngioSense and FMT can be used to image vascular permeability, a marker of early angiogenesis, in sponges. This tool successfully identified those sponges undergoing early angiogenesis (*in vivo* signal was highest in sponges from D 7 compared to D 14 and 21) and provided an indirect measurement of early angiogenesis in sponges. This was consistent with the observed increase vessel numbers (measured with histology) and changes in gene expression of vascular and angiogenesis markers (measured with RT-qPCR); both provided evidence for ongoing angiogenesis over D 7 − 21.

MMP activity was imaged in sponges with MMPSense and FMT

MMPs are understood to be important in regulating cell movement and behaviour. MMP activity is generally assumed to be pro-angiogenic. In the sponge implantation model MMP-12 activity was measured using zymography, which suggested it was highest in sponges on D 7. In this study, MMP activity was imaged *in vivo* using FMT and MMPSense; MMPSense can be used to image the activity of MMP- 7, -9, -10, -12 and -13.

In the time-course study, *in vivo* and *ex vivo* imaging of sponges detected no significant changes to MMP activity in sponges on D 7, 14 and 21. However, MMPs have different substrates and roles in regulating cell movement and behaviour during angiogenesis (Table 1.1, Page-McCaw *et al*., 2007), so the active MMPs on D 3 may be different from those on D 21. Supporting this, MMP gene expression profiles were shown to vary between D 7 and 21; for example, MMP-12 expression increased whereas MMP-9 expression decreased. Furthermore, the variability in the probe concentration measured *in vivo* in the sponges was highest on D 7 compared to D 14 and 21. This is perhaps due to variations in MMP activity

over the time course, but were most apparent on D 7 during the early inflammatory and antigenic response. By D 21, as angiogenesis stabilised, the MMP activity signal had the lowest variability. Therefore, FMT and MMPSense can be used to image MMP activity in sponges *in vivo* but cannot be used to infer changes in the activities of individual MMPs.

In the MMP-12 KO study, it was hoped that the loss of MMP-12 activity could be detected in subcutaneous sponges *in vivo* with FMT imaging and MMPSense. MMP activity measured *in vivo* appeared to be lower in sponges from MMP-12 KO mice but this did not reach significance. Therefore, MMPSense and FMT is a potential method to detect MMP-12 activity in sponges *in vivo*, but this requires further investigation to confirm.

MMPSense and FMT imaging were successfully used to make a measurement of MMP activity in sponges *in vivo* but it was unable detect changes in the activity of specific MMPs in the sponge model over time.

MMP-12 activity could not be selectively imaged with HS1-65 in tissue lysates

MMPs comprise a large family of enzymes with different functions (Page-McCaw *et al.*, 2007). The ability to image the activity of a single, specific MMP could allow for better understating of its role during tissue remodelling and disease. Currently, optical molecular imaging probes to image selective MMPs are not commercially available. In this thesis, it was hypothesised that MMP-12 activity was anti-angiogenic, so the ability to selectively detect MMP-12 activity non-invasively *in vivo* during angiogenesis was of interest.

In this study a small family of MMP-12 selective FRET probes was synthesised using solid phase peptide synthesis (SPPS) based on those published by Cobos-Correa and colleagues (2009). Probe HS1-65 was shown to be selective for MMP-12 using recombinant enzymes

(but was also cleaved by MMP-13 and slightly by MMP-10); total selectivity in these probes is difficult due to the high homology between MMPs. Next, tissue lysates (TL) were generated from subcutaneous sponges implanted form 3 – 35 days. HS1-65 was cleaved in the TL samples but this was subsequently shown not to be a result of MMP-12 activity (using MALDI-TOF MS analysis). Protease inhibitors were used to show that HS1-65 was cleaved by a protease but not by another MMP, neutrophil elastase or a serine protease. The protease in the TL which cleaved HS-65 is still unknown. Therefore, due to limited success and limited resources this part of the study was not extended.

To summarise; firstly, commercial imaging agents and FMT can be used to image MMP activity and angiogenesis in the sponge model of angiogenesis. Secondly HS1-65 was shown to be selective for MMP-12 in recombinant assays but was not selectively activated in TL samples.

Limitations and future experiments

In vivo 3D optical molecular imaging techniques are still relatively new compared to other 3D MRI, PET and CT imaging technologies. The imaging resolution of *in vivo* of optical molecular imaging techniques, such as FMT, is poor compared to the latter techniques. Possibilities for human translation of optical molecular imaging techniques are also still limited for several reasons: firstly, the tissue penetration depth of imaging is still limited to a few cm due to light scattering within tissues. Secondly, equipment for molecular imaging is still in development and not readily available in hospitals. Finally, there are few commercial agents currently available for use in humans, and pathways for clinical agent approval are still challenging. For optical molecular imaging to become a routine tool for diagnostics, these limitations need to be resolved.

In this study, there are several avenues for future work regarding optical molecular imaging:

Can FMT and AngioSense be used to measure vascular density in sponges?

AngioSense when imaged within an hour of administration has been used as a blood pool agent and so can be used to image the vasculature. Imaging at this time-point in sponges could provide a non-invasive measurement of the blood pool and, therefore, of vascular density. However, this measurement has been identified to be challenging due to the low signal to noise ratio in the tissues (Ardeshirpour *et al.*, 2011) .

Can FMT and MMPSense be used to measure the loss of MMP-12 activity in vivo?

MMPSense and FMT did detect a pattern for a reduction MMP activity signal in sponges implanted in KO mice but this did not reach significance. In this study, the MMP-12 KO mice were shipped from the United States of America at great expense, so due to limited resources the numbers in this assay could not be increased during this study.

Can HS1-65 be used to image MMP-12 activity on cells or sponge tissues?

HS1-65 was tested in TL but was shown to be unselectively cleaved. Assays using TL are somewhat crude; TL are complex mixtures which contain both intracellular and extracellular components. Assays which are more representative of the *in vivo* environment use whole live cells or tissues. MMP-12 selective probes could be tested on cultured macrophages (Cobos-Correa *et al.,* 2009) or *ex vivo* diseased tissues (Jager *et al.,* 2016).

Can an MMP-12 selective FRET probe be used to image MMP-12 activity selectively in vivo?

An MMP-12 selective FRET probe, similar to HS1-65, has been used in image MMP-12 activity *in vivo* in a preclinical model of arthritis (Lim *et al.,* 2014). This FRET probe utilised the PLGLEEA substrate sequence and near infra-red dyes which make it suitable for *in vivo* imaging. This FRET probe could be synthesised in-house tested as tool to measure MMP-12 activity in the sponges *in vivo*.

6.3 Summary of conclusions

Molecular imaging is an exciting field of research with potential to improve diagnostic medicine and facilitate personalised medicine. Research in this thesis used commercial and in-house synthesised MMP inhibitors and FRET probes to address the hypothesis that MMP-12 activity is anti-angiogenic. The major findings were:

- HS1-22 can be synthesised in 6 steps and was shown to be a potent and selective inhibitor for MMP-12 using recombinant enzyme assays. Inhibition of MMP-12 with HS1-22 did not increase angiogenesis in *in vivo* or *ex vivo* angiogenesis assays.

- Deletion of MMP-12 did not increase angiogenesis in *in vivo* or *ex vivo* angiogenesis assays.

- Commercial imaging probes can be used to image angiogenesis and MMP activity in sponges *in vivo* and *ex vivo*.

- HS1-65, an activity FRET robe, was synthesised in house using SPPS and shown to be selective for MMP-12 using recombinant enzyme assays. But HS1-65 was non-specifically cleaved in tissue lysates by an unknown protease.

To conclude, the work described in this thesis revealed that MMP-12 is not an inhibitor of angiogenesis in the models used in this thesis.

7 References

Adams, R.H. & Alitalo, K., 2007. Molecular regulation of angiogenesis and lymphangiogenesis. *Nature Reviews. Molecular Cell Biology*, 8(6), pp.464–478.

Aggarwal, S., Qamar, A., Sharma, V. & Sharma, A., 2011. Abdominal aortic aneurysm: A comprehensive review. *Experimental and Clinical Cardiology*, 16(1), pp.11–15.

Akahane, T., Akahane, M., Shah, A., Connor, C.M. & Thorgeirsson, U.P., 2004. TIMP-1 inhibits microvascular endothelial cell migration by MMP-dependent and MMP-independent mechanisms. *Experimental Cell Research*, 301(2), pp.158–167

Akram, A.R., Avlonitis, N., Lilienkampf, A., Perez-Lopez, A.M., McDonald, N., Chankeshwara, S.V., Scholefield, E., Haslett, C., Bradley, M. & Dhaliwal, K., 2015. A labelled-ubiquicidin antimicrobial peptide for immediate in situ optical detection of live bacteria in human alveolar lung tissue. *Chemical. Science*, 6(12), pp. 6971–6979.

Amblard, M.., Fehrentz, J. & Martinez, J., Subra, G., 2006. Methods and protocols of modern solid phase Peptide synthesis. *Molecular Biotechnology*, 33(3), pp.239–254.

Andersen, C.L., Jensen, J.L. & Ørntoft, T.F., 2004. Normalization of real-time quantitative reverse transcription-PCR data: a model-based variance estimation approach to identify genes suited for normalization, applied to bladder and colon cancer data sets. *Cancer research*, 64(15), pp.5245–5250.

Andrade, S.P., Fan, T.P. & Lewis, G.P., 1987. Quantitative *in-vivo* studies on angiogenesis in a rat sponge model. *British Journal of Experimental Pathology*, 68, pp.755–766.

Annabi, B., Shedid, D., Ghosn, P., Kenigsberg, R.L., Desrosiers, R.R., Bojanowski, M.W., Beaulieu, E., Nassif, E., Moumdjian, R. & Beliveau, R., 2002. Differential regulation of matrix metalloproteinase activities in abdominal aortic aneurysms. *Journal of Vascular Surgery*, 35(3), pp.539–546.

Ardeshirpour, Y., Chernomordik, V., Capala, J., Hassan, M., Zielinsky, R., Griffiths, G., Achilefu, S., Smith, P. & Gandjbakhche, A., 2011. Using in-vivo fluorescence imaging in personalized cancer diagnostics and therapy, an image and treat paradigm. *Technology in Cancer Research & Rreatment*, 10(6), pp.549–560.

Arnaoutova, I., George, J., Kleinman, H.K. & Benton, G., 2009. The endothelial cell tube formation assay on basement membrane turns 20: State of the science and the art. *Angiogenesis*, 12(3), pp.267–274.

Aslam, T., Miele, A., Chankeshwara, S.V., Megia-Fernandez, A., Michels C., Akram, A.R., McDonald, N., Hirani, N., Haslett, C., Bradley, M. & Dhaliwal, K., 2015. Optical molecular imaging of lysyl oxidase activity – detection of active fibrogenesis in human lung tissue. *Chemical Science*, 6(8), pp.4946–4953.

Avlonitis, N., Debunne, M., Aslam, T., McDonald, N., Haslett, C., Dhaliwal, K. & Bradley, M., 2013. Highly specific, multi-branched fluorescent reporters for analysis of human neutrophil elastase. *Organic & Biomolecular Chemistry*, 11(26), pp.4414–4418.

Baker, A.H., Edwards, D.R. & Murphy, G., 2002. Metalloproteinase inhibitors: biological actions and therapeutic opportunities. *Journal of Cell Science*, 115(Pt 19), pp.3719–3727.

Baker, M. Robinson, S.D, Lechertier, T., Barber, P.R., Tavora, B., D'Amico, G., Jones, D.T., Vojnovic, B. & Hodivala-Dilke, K., 2012. Use of the mouse aortic ring assay to study angiogenesis. *Nature Protocols*, 7, pp.89–104.

Barcelos, L.S., Talvani, A., Teixeira, A.S., Vieira, L.Q., Cassali, G.D., Andrade, S.P. & Teixeira, M.M., 2005. Impaired inflammatory angiogenesis, but not leukocyte influx, in mice lacking TNFR1. *Journal of Leukocyte Biology*, 78(2), pp.352–358

Barnwell, N., Briggner, L., Cole, A., Eriksson, A., Jacob, P., Vaz, L. & Andew, W., 2007. A new crystalline form g of (5s) -5- [4- (5-chloro-pyridin-2- yloxy) -piperidine-1-sulfonylmethyl] - 5 - methyl -imidazolidine - 2,4-dione (i) and intermediates thereof. WO 2007106022 A2

Bates, D.O., 2010. Vascular endothelial growth factors and vascular permeability. *Cardiovascular Research*, 87(2), pp.262–271.

Bauters, D., Van Hul, M. & Lijnen, H.R., 2013. Macrophage elastase (MMP-12) in expanding murine adipose tissue. *Biochimica et Biophysica Acta - General Subjects*, 1830(4), pp.2954–2959.

Belaaouaj, A.S., Shipley, J., Kobayashi, D.K., Zimonjic, D.B., Popescu, N., Silverman, G.A. & Shapiro, S.D., 1995. Human Macrophage Metalloelastase. *Journal of Biological Chemistry*, 270(24), pp.14568–14575.

Bellac, C.L., Dufour, A., Krisinger, M.J., Loonchanta, A., Starr, A.E., Auf dem Keller, U., Lange, P.F., Goebeler, V., Kappelhoff, R., Butler, G.S., Burtnick, L.D., Conway, E.M., Roberts, C.R. & Overall, C.M., 2014. Macrophage matrix metalloproteinase-12 dampens inflammation and neutrophil influx in arthritis. *Cell Reports*, 9(2), pp.618–632.

Bergers, G., Brekken, R., McMahon, G., Vu, T.H., Itoh, T., Tamaki, K., Tanzawa, K., Thorpe, P., Itohara, S., Werb, Z, & Hanahan, D., 2000. Matrix metalloproteinase-9 triggers the angiogenic switch during carcinogenesis. *Nature Cell Biology*, 2(10), pp.737–744.

Blasi, F. & Carmeliet, P., 2002. uPAR: a versatile signalling orchestrator. *Nature Reviews. Molecular CellBiology*, 3(12), pp.932–943.

Bramhall, S.R. Schulz, J., Nemunaitis, J., Brown, P.D., Baillet, M. & Buckels, J.A.C., 2002. A double-blind placebo-controlled, randomised study comparing gemcitabine and marimastat with gemcitabine and placebo as first line therapy in patients with advanced pancreatic cancer. *British Journal of Cancer*, 87(2), pp.161–167.

Bu, L., Ma, X., Tu, Y., Shen, B. & Cheng, Z., 2013. Optical image-guided cancer therapy. *Current Pharmaceutical Biotechnology*, 14(8), pp.723–732.

Burbridge, M.F., Cogé, F., Galizzi, J.P., Boutin, J.A., West, D.C. & Tucker, G.C., 2002. The role of the matrix metalloproteinases during *in vitro* vessel formation. *Angiogenesis*, 5(3), pp.215–226.

Burrage, P.S., Mix, K.S. & Brinckerhoff, C.E., 2006. Matrix metalloproteinases: role in arthritis. *Frontiers in Bioscience : a Journal and Virtual Library*, 11, pp.529–543.

Cao, Y. & Langer, R., 2010. Optimizing the delivery of cancer drugs that block angiogenesis. *Science Translational Medicine*, 2(15), p.15ps3.

Carmeliet, P., Moons, L., Lijnen, R., Baes, M., Lemaître, V., Tipping, P., Drew, A., Eeckhout, Y., Shapiro, S., Lupu, F. & Collen, D., 1997. Urokinase-generated plasmin activates MMPs during aneurysm formation. *Nature Genetics*, 17(4), pp.439–444.

Cathcart, J., Pulkoski-Gross, A. & Cao, J., 2015. Targeting matrix metalloproteinases in cancer: Bringing new life to old ideas. *Genes & Diseases*, 2(1), pp.26–34.

Chang, Y.S, di Tomaso, E., McDonald, D.M., Jones, R., Jain, R.K. & Munn, L.L., 2000. Mosaic blood vessels in tumors: frequency of cancer cells in contact with flowing blood. *Proceedings of the National Academy of Sciences*, 97(26), pp.14608–14613.

Channe G., Mahesh, B. & Gowda, S., 2001. Zinc-catalyzed ammonium formate reductions: Rapid and selective reduction of aliphatic and aromatic nitro compounds. *Indian Journal of Chemistry - Section B Organic and Medicinal Chemistry*, 40(1), pp.75–77.

Chen, H., Feng, Y., Xu, Z. & Ye, T., 2005. The total synthesis and reassignment of stereochemistry of dragonamide. Tetrahedron, 61(47), pp.11132–11140.

Chhabra, S.R., Hothi, B., Evans, D.J., White, P.D., Bycroft, B.W. & Chan, W.C., 1998. An appraisal of new variants of Dde amine protecting group for solid phase peptide synthesis. *Tetrahedron Letters*, 39(12), pp.1603–1606.

Chiou, A.C., Chiu, B. & Pearce, W.H., 2001. Murine aortic aneurysm produced by periarterial application of calcium chloride. *The Journal of Surgical Research*, 99, pp.371–376.

Chow, J.C., Chiu, B. & Pearce, W.H., 2008. Metalloproteinase- and gamma-secretase-mediated cleavage of protein-tyrosine phosphatase receptor type Z. *The Journal of Biological Chemistry*, 283(45), pp.30879–89.

Choyke, P.L., Alford, R., Simpson, H.M., Duberman, J., Craig Hill, G., Ogawa, M., Regino, C. & Kobayashi, H., 2009. Toxicity of organic fluorophores used in molecular imaging: Literature review. *Molecular Imaging*, 8(6), pp.341–354.

Chung, A.S. & Ferrara, N., 2011. Developmental and Pathological Angiogenesis. *Annual Review of Cell and Developmental Biology*, 27(1), pp.563–584.

Chung, A.S., Lee, J. & Ferrara, N., 2010. Targeting the tumour vasculature: insights from physiological angiogenesis. *Nature Reviews. Cancer*, 10(7), pp.505–514.

Cobos-Correa, A., Trojanek, J.B., Diemer, S., Mall, M.A. & Schultz, C., 2009. Membrane-bound FRET probe visualizes MMP12 activity in pulmonary inflammation. *Nature Chemical Biology*, 5, pp.628–630.

Cornelius, L.A., Nehring, L.C., Harding, E., Bolanowski, M., Welgus, H.G., Kobayashi, D.K., Pierce, R.A. & Shapiro, S.D., 1998. Matrix metalloproteinases generate angiostatin: effects on neovascularization. *Journal of Immunology*, 161(12), pp.6845–6852.

Costa, C., Incio, J. & Soares, R., 2007. Angiogenesis and chronic inflammation: cause or consequence? *Angiogenesis*, 10(3), pp.149–66.

Crippa, M.P., 2007. Urokinase-type plasminogen activator. *The International Journal of Biochemistry & Cell Biology*, 39(4), pp.690–694.

Curci, J.A., Liao, S., Huffman, M.D, Shapiro, S.D. & Thompson, R.W., 1998. Expression and localization of macrophage elastase (matrix metalloproteinase-12) in abdominal aortic aneurysms. *The Journal of Clinical Investigation*, 102(11), pp.1900–1910.

Czarny, B., Stura, E.A., Devel, L., Vera, L., Cassar-Lajeunesse, E., Beau, F., Calderone, V., Fragai, M., Luchinat, C. & Dive, V., 2013. Molecular determinants of a selective matrix metalloprotease-12 inhibitor: Insights from crystallography and thermodynamic studies. *Journal of Medicinal Chemistry*, 56(3), pp.1149–1159.

D'Alessio, S., Fibbi, G., Cinelli, M., Guiducci, S., Del Rosso, A., Margheri, F., Serrati, S., Pucci, M., Kahaleh, B., Fan, P., Annunziato, F., Cosmi, L., Liotta, F., Matucci-Cerinic, M. & Del Rosso, M., 2004. Matrix metalloproteinase 12-dependent cleavage of urokinase receptor in systemic sclerosis microvascular endothelial cells results in impaired angiogenesis. *Arthritis and Rheumatism*, 50(10), pp.3275–3285.

Dahl, R., Titlestad, I., Lindqvist, A., Wielders, P., Wray, H., Wang, M., Samuelsson, V., Mo, J. & Holt, A., 2012. Effects of an oral MMP-9 and -12 inhibitor, AZD1236, on biomarkers in moderate/severe COPD: A randomised controlled trial. *Pulmonary Pharmacology and Therapeutics*, 25(2), pp.169–177.

Davis, G.E., Pintar, K.A., Salazar, R. & Maxwell, S.A., 2001. Matrix metalloproteinase-1 and -9 activation by plasmin regulates a novel endothelial cell-mediated mechanism of collagen gel contraction and capillary tube regression in three-dimensional collagen matrices. *Journal of Cell Science*, 114(5), pp.917–30.

Dean, R.A., Cox, J.H., Bellac, C.L., Doucet, A., Starr, A.E. & Overall, C.M., 2008. Macrophage-specific metalloelastase (MMP-12) truncates and inactivates ELR^+ CXC chemokines and generates CCL2, -7, -8, and -13 antagonists: Potential role of the macrophage in terminating polymorphonuclear leukocyte influx. *Blood*, 112(8), pp.3455–3464.

Deguchi, J.O., Aikawa, E., Libby, P., Vachon, J.R., Inada, M., Krane, S.M., Whittaker, P. & Aikawa, M., 2005. Matrix metalloproteinase-13/collagenase-3 deletion promotes collagen accumulation and organization in mouse atherosclerotic plaques. *Circulation*, 112(17), pp.2708–2715.

Demedts, I.K., Morel-Montero, A., Lebecque, S., Pacheco, Y., Cataldo, D., Joos, G.F., Pauwels, R. & Brusselle, G.G., 2006. Elevated MMP-12 protein levels in induced sputum from patients with COPD. *Thorax*, 61(3), pp.196–201.

Devel, L., Rogakos, V., David, A., Makaritis, A., Beau, F., Cuniasse, P., Yiotakis, A. & Dive, V., 2006. Development of selective inhibitors and substrate of matrix metalloproteinase-12. *The Journal of Biological Chemistry*, 281(16), pp.11152–11160.

Dhaliwal, K., Alexander, L., Escher, G., Unciti-Broceta, A., Jansen, M., Mcdonald, N., Cardenas-Maestre, J.M., Sanchez-Martin, R., Simpson. J., Haslett, C. & Bradley M., 2011. Multi-modal molecular imaging approaches to detect primary cells in preclinical models. *Faraday Discuss.*, 149, pp.107–114.

Dhanabal, M., Ramchandran, R., Waterman, M.J., Lu, H., Knebelmann, B., Segal, M. & Sukhatme, V.P., 1999. Endostatin induces endothelial cell apoptosis. *The Journal of Biological Chemistry*, 274(17), pp.11721–11726.

Díaz-Mochón, J.J., Bialy, L. & Bradley, M., 2004. Full orthogonality between Dde and Fmoc: The direct synthesis of PNA-peptide conjugates. *Organic Letters*, 6(7), pp.1127–1129.

Ding, S., Eric Blue, R., Chen, Y., Scull, B., Kay Lund, P. & Morgan, D., 2012. Molecular imaging of gastric neoplasia with near-infrared fluorescent activatable probes. *Molecular Imaging*, 11(6), pp.507–15.

Dong, Z., Kumar, R., Yang, X. & Fidler, I.J., 1997. Macrophage-derived metalloelastase is responsible for the generation of angiostatin in Lewis lung carcinoma. *Cell*, 88(6), pp.801–810.

Dubois, B., D'Hooghe, M.B., De-Lepeleire, K., Ketelaer, P., Opdenakker, G. & Carton, H., 1998. Toxicity in a double-blind, placebo-controlled pilot trial with D-penicillamine and metacycline in secondary progressive multiple sclerosis. *Multiple.Sclerosis.*, 4(2), pp.74–78.

Ducharme, A., Frantz, S., Aikawa, M., Rabkin, E., Lindsey, M., Rohde, L.E., Schoen, F., Kelly, R.A., Werb, Z., Libby, P. & Lee, R.T., 2000. Targeted deletion of matrix metalloproteinase-9 attenuates left ventricular enlargement and collagen accumulation after experimental myocardial infarction. *Journal of Clinical Investigation*, 106(1), pp.55–62.

Efron, D.T., Most, D., Shi, H., Tantry, U.S. & Barbul, A., 2001. A novel method of studying wound healing. *The Journal of Surgical Research*, 98(1), pp.16–20.

Egginton, S., 2009. Invited review: activity-induced angiogenesis. *Pflugers Archiv European Journal of Physiology*, 457(5), pp.963–977.

Falati, S., Patil, S., Gross, P.L., Stapleton, M., Merrill-Skoloff, G., Barrett, N.E., Pixton, K.L., Weiler, H., Cooley, B., Newman, D.K., Newman, P.J., Furie, B.C., Furie, B. & Gibbins, J.M., 2006. Platelet PECAM-1 inhibits thrombus formation *in vivo*. *Blood*, 107(2), pp.535–541.

Ferrara, N., Gerber, H. & LeCouter, J., 2003. The biology of VEGF and its receptors. *Nature Medicine*, 9(6), pp.669–676.

Ferreras, M., Felbor, U., Lenhard, T., Olsen, B.R. & Delaissé, J., 2000. Generation and degradation of human endostatin proteins by various proteinases. *Federation of European Biochemical Societies Letters*, 486(3), pp.247–251.

Folkman, J., Langer, R., Linhardt, R.J., Haudenschild, C. & Taylor, S., 1983. Angiogenesis inhibition and tumor regression caused by heparin or a heparin fragment in the presence of cortisone. *Science (New York, N.Y.)*, 221(4612), pp.719–725.

Folkman, J., 2007. Angiogenesis: an organizing principle for drug discovery? *Nature reviews. Drug Discovery*, 6(4), pp.273–286.

Formato, M., Farina, M., Spirito, R., Maggioni, M., Guarino, A., Cherchi, G.M., Biglioli, P., Edelstein, C. & Scanu, A.M., 2004. Evidence for a Proinflammatory and Proteolytic Environment in Plaques from Endarterectomy Segments of Human Carotid Arteries. *Arteriosclerosis, Thrombosis, and Vascular Biology*, 24(1), pp.129–135.

Forsythe, J.A., Jiang, B.H., Iyer, N.V., Agani., F., Leung, S.W., Koos, R.D. & Semenza, G.L., 1996. Activation of vascular endothelial growth factor gene transcription by hypoxia-inducible factor 1. *Molecular and Cellular Biology*, 16(9), pp.4604–13.

Frangioni, J.V., 2003. *In vivo* near-infrared fluorescence imaging. *Current Opinion in Chemical Biology*, 7(5), pp.626–634.

Frantz, C., Stewart, K.M. & Weaver, V.M., 2010. The extracellular matrix at a glance. *Journal of Cell Science*, 123(24), pp.4195–4200.

Fukushi, J., Ono, M., Morikawa, W., Iwamoto, Y. & Kuwano, M., 2000. The activity of soluble VCAM-1 in angiogenesis stimulated by IL-4 and IL-13. *Journal of Immunology*, 165(5), pp.2818–23.

Galis, Z.S., Sukhova, G.K., Lark, M.W. & Libby, P., 1994. Increased expression of matrix metalloproteinases and matrix degrading activity in vulnerable regions of human atherosclerotic plaques. *The Journal of Clinical Investigation*, 94(6), pp.2493–2503.

Garland, M., Yim, J.J. & Bogyo, M., 2016. A Bright Future for Precision Medicine: Advances in Fluorescent Chemical Probe Design and Their Clinical Application. *Cell Chemical Biology*, 23(1), pp.122–136.

Gastaldello, A., 2015. Ph.D. Thesis: Mechanisms of action of 5 apha -tetrahydrocorticosterone, a novel anti-inflammatory glucocorticoid. *The University of Edinburgh.*

Gelati, M., Aplin, A.C, Fogel, E., Smith, K.D. & Nicosia, R.F., 2008. The angiogenic response of the aorta to injury and inflammatory cytokines requires macrophages. *Journal of Immunology*, 181(8), pp.5711–5719.

Gill, S.E. & Parks, W.C., 2008. Metalloproteinases and their inhibitors: Regulators of wound healing. *International Journal of Biochemistry and Cell Biology*, 40(6-7), pp.1334–1347.

Goldman, S. & Shalev, E., 2004. MMPS and TIMPS in ovarian physiology and pathophysiology. *Frontiers in Bioscience*, 9, pp.2474–2483.

Gomis-Rüth, F.X., Maskos, K., Betz, M., Bergner, A., Huber, R., Suzuki, K., Yoshida, N., Nagase, H., Brew, K., Bourenkov, G.P., Bartunik, H. & Bode, W., 1997. Mechanism of inhibition of the human matrix metalloproteinase stromelysin-1 by TIMP-1. *Nature*, 389(6646), pp.77–81.

Gong, Y., Hart, E., Shchurin, A. & Hoover-Plow, J., 2008. Inflammatory macrophage migration requires MMP-9 activation by plasminogen in mice. *The Journal of Clinical Investigation*, 118(9), pp.3012–3024.

Goodpaster, T., Legesse-Miller, A., Hameed, M.R., Aisner, S.C., Randolph-Habecker, J. & Coller, H., 2008. An immunohistochemical method for identifying fibroblasts in formalin-fixed, paraffin-embedded tissue. *The Journal of Histochemistry and Cytochemistry : Official Journal of the Histochemistry Society*, 56(4), pp.347–358.

Gorrin-Rivas, M.J., Arii, S., Mori, A., Kanda, Y. & Imamura, M., 2001. Mouse macrophage metalloelastase gene delivery by HVJ-cationic liposomes in experimental antiangiogenic gene therapy for murine CT-26 colon cancer. *International Journal of Cancer*, 93(5), pp.731–735.

Gossas, T. & Danielson, H.U., 2006. Characterization of Ca_2^+ interactions with matrix metallopeptidase-12: implications for matrix metallopeptidase regulation. *The Biochemical journal*, 398(3), pp.393–398.

Graff, J.W., Powers, L.S., Dickson, A.M., Kim, J., Reisetter, A.C., Hassan, I.H., Kremens, K.W., Gross, T.J., Wilson, M.E. & Monick, M.M., 2012. Cigarette smoking decreases global microRNA expression in human alveolar macrophages. *PloS one*, 7(8), p.e44066.

Greenlee, K.J., Werb, Z. & Kheradmand, F., 2007. Matrix metalloproteinases in lung: multiple, multifarious, and multifaceted. *Physiological Reviews*, 87(1), pp.69–98.

Gronski, T.J., Martin, R.L., Kobayashi, D.K., Walsh, B.C., Holman, M.C., Huber, M., Van Wart, H.E. & Shapiro, S.D., 1997. Hydrolysis of a broad spectrum of extracellular matrix proteins by human macrophage elastase. *The Journal of Biological Chemistry*, 272(18), pp.12189–12194.

Groves, K., Kossodo, S., Handy, E., Jensen, J., Blusztajn, A., Cuneo, G., Peterson, J.D. & Rajopadhye, M., 2010. *In Vivo* imaging of treatment effects using a novel infrared labeled agent MMPSense750 FAST, Poster.

Haas, T.L., Davis, S.J. & Madri, J.A., 1998. Three-dimensional type I collagen lattices induce coordinate expression of matrix metalloproteinases MT1-MMP and MMP-2 in microvascular endothelial cells. *The Journal of Biological Chemistry*, 273(6), pp.3604–10.

Hague, S., MacKenzie, I.Z., Bicknell, R. & Rees, M.C.P., 2002. *In-vivo* angiogenesis and progestogens. *Human Reproduction*, 17, pp.786–793.

Halfter, W., Dong, S., Schurer, B. & Cole, G.J., 1998. Collagen XVIII is a basement membrane heparan sulfate proteoglycan. *Journal of Biological Chemistry*, 273(39), pp.25404–25412.

Harris, L.M., Faggioli, G.L., Fiedler, R.R., Curl, G.R. & Ricotta, J.J., 1991. Ruptured abdominal aortic aneurysms: Factors affecting mortality rates. *Journal of Vascular Surgery*, 14(6), pp.812–820.

Hasan, Q., Tan, S.T., Gush, J., Peters, S.G. & Davis, P.F., 2000. Steroid therapy of a proliferating hemangioma: Histochemical and molecular changes. *Pediatrics*, 105(1), pp.117–121.

Hashizume, H., Baluk, P., Morikawa, S., McLean, J.W., Thurston, G., Roberge, S., Jain, R.K. & McDonald, D.M., 2000. Openings between defective endothelial cells explain tumor vessel leakiness. *The American Journal of Pathology*, 156(4), pp.1363–1380.

Hattori, N., Mochizuki, S., Kishi, K., Nakajima, T., Takaishi, H., D'Armiento, J. & Okada, Y., 2009. MMP-13 plays a role in keratinocyte migration, angiogenesis, and contraction in mouse skin wound healing. *The American Journal of Pathology*, 175(2), pp.533–546.

Hautamaki, R.D., Kobayashi, D.K., Senior, R.M. & Shapiro, S.D., 1997. Requirement for macrophage elastase for cigarette smoke-induced emphysema in mice. *Science*, 277(5334), pp.2002–2004.

Heissig, B., Hattori, K., Friedrich, M., Rafii, S. & Werb, Z., 2003. Angiogenesis: vascular remodeling of the extracellular matrix involves metalloproteinases. *Current Opinion in Hematology*, 10(2), pp.136–41.

Hellström, M., Kalén, M., Lindahl, P., Abramsson, A. & Betsholtz, C., 1999. Role of PDGF-B and PDGFR-beta in recruitment of vascular smooth muscle cells and pericytes during embryonic blood vessel formation in the mouse. *Development*, 126(14), pp.3047–3055.

Hensley, H.H., Roder, N.A., Brien, S.W.O., Bickel, L.E., Xiao, F., Litwin, S. & Connolly, D.C., 2012. Combined *In Vivo* Molecular and Anatomic Imaging for Detection of Ovarian Carcinoma – Associated Protease Activity and Integrin Expression in Mice. *Neoplasia*, 14(6), pp.451–462.

Heo, S.H., Choi, Y.J., Ryoo, H.M. & Cho, J.Y., 2010. Expression profiling of ETS and MMP factors in VEGF-activated endothelial cells: Role of MMP-10 in VEGF-induced angiogenesis. *Journal of Cellular Physiology*, 224(3), pp.734–742.

Hermus, L., van Dam, G.M. & Zeebregts, C.J., 2010. Advanced Carotid Plaque Imaging. *European Journal of Vascular and Endovascular Surgery*, 39(2), pp.125–133.

Herren, B., Levkau, B., Raines, E.W. & Ross, R., 1998. Cleavage of beta-catenin and plakoglobin and shedding of VE-cadherin during endothelial apoptosis: evidence for a role for caspases and metalloproteinases. *Molecular Biology of the Cell*, 9(6), pp.1589–1601.

Heymans, S., Luttun, A., Nuyens, D., Theilmeier, G., Creemers, E., Moons, L., Dyspersin, G.D., Cleutjens, J.P., Shipley, M., Angellilo, A., Levi, M., Nübe, O., Baker, A., Keshet, E., Lupu, F., Herbert, J.M., Smits, J F., Shapiro, S.D., Baes, M., Borgers, M., Collen, D., Daemen, M.J. & Carmeliet, P., 1999. Inhibition of plasminogen activators or matrix metalloproteinases prevents cardiac rupture but impairs therapeutic angiogenesis and causes cardiac failure. *Nature Medicine*, 5(10), pp.1135–1142.

Hidalgo, M. & Eckhardt, S.G., 2001. Development of Matrix Metalloproteinase Inhibitors in Cancer Therapy. *JNCI Journal of the National Cancer Institute*, 93(3), pp.178–193.

Houghton, A.M., Grisolano, J.L., Baumann, M.L., Kobayashi, D.K., Hautamaki, R.D., Nehring, L.C., Cornelius, L.A. & Shapiro, S.D., 2006. Macrophage elastase (matrix metalloproteinase-12) suppresses growth of lung metastases. *Cancer Research*, 66(12), pp.6149–55.

Houghton, A.M., Hartzell, W.O., Robbins, C.S., Gomis-Rüth, F.X. & Shapiro, S.D., 2009. Macrophage elastase kills bacteria within murine macrophages. *Nature*, 460(7255), pp.637–641.

de la Hoz, A., Diaz-Ortiz, A. & Moreno, A., 2005. Microwaves in organic synthesis. Thermal and non-thermal microwave effects. *Chemical Society Reviews*, 34(2), pp.164–178.

Hu, D., Hiley, C., Smither, R., Gresham, G. & Fan, T., 1995. Correlation of Xe-133 clearance, blood-flow and histology in the rat sponge model for angiogenesis - Further-studies with angiogenic modifiers. *Laboratory Investigation*, 72(5), pp. 601–610.

Hu, J., Van den Steen, P., Sang Q. & Opdenakker G., 2007. Matrix metalloproteinase inhibitors as therapy for inflammatory and vascular diseases. *Nature Reviews. Drug Discovery*, 6(6), pp.480–498.

Hu, X. & Beeton, C., 2010. Detection of functional matrix metalloproteinases by zymography. *Journal of Visualized Experiments*, (45), pii 2445.

Hughes, S. & Chan-Ling, T., 2004. Characterization of smooth muscle cell and pericyte differentiation in the rat retina *in vivo*. *Investigative Opthalmology & Visual Science*, 45(8), p.2795.

Hynes, R.O., 2009. The extracellular matrix: not just pretty fibrils. *Science*, 326(5957), pp.1216–1219.

Ibarra, J.M., Jimenez, F., Martinez, H.G., Clark, K. & Ahuja, Seema S.S., 2011. MMP-activated fluorescence imaging detects early joint inflammation in collagen-antibody-induced arthritis in CC-chemokine receptor-2-null mice, *in-vivo*. *International Journal of Inflammation*, 2011(8), pp.691587.

Illanes, J., Dabancens, A., Acuña, O., Fuenzalida, M., Guerrero, A., Lopez, C. & Lemus, D., 2002. Effects of betamethasone, sulindac and quinacrine drugs on the inflammatory neoangiogenesis response induced by polyurethane sponge implanted in mouse. *Biological Research*, 35 (3−4), pp.339–345.

Inoue, T., Plieth, D., Venkov, C.D., Xu, C. & Neilson, E.G., 2005. Antibodies against macrophages that overlap in specificity with fibroblasts. *Kidney International*, 67(6), pp.2488–2493.

Ishibashi, S., Brown, M.S., Goldstein, J.L., Gerard, R.D., Hammer, R.E., Herz, J. & Ishibashi, S., 1993. Hypercholesterolemia in low density lipoprotein receptor knockout mice and its reversal by adenovirus-mediated gene delivery. *The Journal of Clinical Investigation*, 92(2), pp.883–893.

Isidro-Llobet, A., Álvarez, M. & Albericio, F., 2009. Amino acid-protecting groups. *Chemical Reviews*, 109(6), pp.2455–2504.

Iyer, S., Visse, R., Nagase, H. & Acharya, K.R., 2006. Crystal Structure of an Active Form of Human MMP-1. *Journal of Molecular Biology*, 362(1), pp.78–88.

Jacobsen, J., Major Jourden, J., Miller, M. & Cohen, S., 2010. To bind zinc or not to bind zinc: An examination of innovative approaches to improved metalloproteinase inhibition. *Biochimica et Biophysica acta - Molecular Cell Research*, 1803(1), pp.72–94.

Jager, N., Wallis de Vries, B., Hillebrands, J., Harlaar, N., Tio, R., Slart, R., van Dam, G., Boersma, H., Zeebregts, C. & Westra, J., 2016. Distribution of matrix metalloproteinases in human atherosclerotic carotid plaques and their production by smooth muscle cells and macrophage subsets. *Molecular Imaging and Biology*, 18(2), pp.283–291.

Jain, R.K., 2003. Molecular regulation of vessel maturation. *Nature Medicine*, 9(6), pp.685–693.

Jain, R.K., 2005. Normalization of tumor vasculature: an emerging concept in antiangiogenic therapy. *Science*, 307(5706), pp.58–62.

James, M.L. & Gambhir, S.S., 2012. A molecular imaging primer: modalities, imaging agents, and applications. *Physiological. Reviews.*, 92(2), pp.897–965.

Jares-Erijman, E.A. & Jovin, T.M., 2003. FRET imaging. *Nature Biotechnology*, 21(11), pp.1387–1395.

Jguirim-Souissi, I., Jelassi, A., Addad, F., Hassine, M., Najah, M., Hamda, K.B., Maatouk, F., Farhat, M.B., Bouslema, A., Rouis, M. & Slimane, M.N., 2007. Plasma metalloproteinase-12 and tissue inhibitor of metalloproteinase-1 levels and presence, severity, and outcome of coronary artery disease. *American Journal of Cardiology*, 100(1), pp.23–27.

Johnson, D.E., Hinohara, T., Selmon, M.R., Braden, L.J. & Simpson, J.B., 1990. Primary peripheral arterial stenoses and restenoses excised by transluminal atherectomy: a histopathologic study. *Journal of the American College of Cardiology*, 15(2), pp.419–425.

Johnson, J., Devel, L., Czarny, B., George, S., Jackson, C., Rogakos, V., Beau, F., Yiotakis, A., Newby, A. & Dive, V., 2011. A selective matrix metalloproteinase-12 inhibitor retards atherosclerotic plaque development in apolipoprotein E-knockout mice. *Arteriosclerosis, Thrombosis, and Vascular Biology*, 31(3), pp.528–535.

Johnson, J.L, George, S.A., Newby, A.C. & Jackson, C.L., 2005. Divergent effects of matrix metalloproteinases 3, 7, 9, and 12 on atherosclerotic plaque stability in mouse brachiocephalic arteries. *Proceedings of the National Academy of Sciences of the United States of America*, 102, pp.15575–15580.

Johnson, J.L., Fritsche-Danielson, R., Behrendt, M., Westin-Eriksson, A., Wennbo, H., Herslof, M., Elebring, M., George, S.J., McPheat, W.C. & Jackson, C.L., 2006. Effect of broad-spectrum matrix metalloproteinase inhibition on atherosclerotic plaque stability. *Cardiovascular Research*, 71(3), pp.586–595.

Kaijzel, E.L., Van Heijningen, P.M, Wielopolski, P.A., Vermeij, M., Koning, G.A., Van Cappellen, W.A., Que, I., Chan, A., Dijkstra, J., Ramnath, N.W.N., Hawinkels, L.J.A.C., Bernsen, M.R., Löwik, C.W.G.M. & Essers, J., 2010. Multimodality imaging reveals a gradual increase in matrix metalloproteinase activity at aneurysmal lesions in live fibulin-4 mice. *Circulation: Cardiovascular Imaging*, 3(5), pp.567–577.

Keeling, B.W., Armstrong, P.A., Stone, P.A., Bandyk, D.F. & Shames, M.L., 2005. An overview of matrix metalloproteinases in the pathogenesis and treatment of abdominal aortic aneurysms. *Vascular and Endovascular Surgery*, 39(6), pp.457–64.

Keereweer, S., Van Driel, P.B., Snoeks, T.J., Kerrebijn, J.D., Baatenburg de Jong, R.J., Vahrmeijer, A.L., Sterenborg, H.J. & Löwik, C.W., 2013. Optical image-guided cancer surgery: Challenges and limitations. *Clinical Cancer Research*, 19(14), pp.3745–3754.

Kent, C.K., Zwolak, R.M., Egorova, N.N., Riles, T.S., Manganaro, A., Moskowitz, A.J., Gelijns, A.C. & Greco, G., 2010. Analysis of risk factors for abdominal aortic aneurysm in a cohort of more than 3 million individuals. *Journal of Vascular Surgery*, 52(3), pp.539–48.

Kerkelä, E., Ala-Aho, R., Jeskanen, L., Rechardt, O., Grénman, R., Shapiro, S.D., Kähäri, V.M. & Saarialho-Kere, U., 2000. Expression of human macrophage metalloelastase (MMP-12) by tumor cells in skin cancer. *The Journal of Investigative Dermatology*, 114(6), pp.1113–9.

Kerkelä, E., Ala-aho, R., Klemi, P., Grénman, S., Shapiro, S.D., Kähäri, V.M. & Saarialho-Kere, U., 2002. Metalloelastase (MMP-12) expression by tumour cells in squamous cell carcinoma of the vulva correlates with invasiveness, while that by macrophages predicts better outcome. *Journal of Pathology*, 198(2), pp.258–269.

Kessenbrock, K., Plaks, V. & Werb, Z., 2010. Matrix Metalloproteinases: Regulators of the Tumor Microenvironment. *Cell*, 141(1), pp.52–67.

Keumi, T., Tomioka, N., Hamanaka, K., Kakihara, H., Morita, T., Kitajima, H. & Fukushima, M., 1991. Positional reactivity of dibenzofuran in electrophilic substitutions. *The Journal of Organic Chemistry*, 56(15), pp.4671–4677.

Kim, Y.M., Hwang, S., Kim, Y.M., Pyun, B.J., Kim, T.Y., Lee, S.T., Gho, Y.S. & Kwon, Y.G., 2002. Endostatin blocks vascular endothelial growth factor-mediated signaling via direct interaction with KDR/Flk-1. *Journal of Biological Chemistry*, 277(31), pp.27872–27879.

Kimata, M., Otani, Y., Kubota, T., Igarashi, N., Yokoyama, T., Wada, N., Yoshimizu, N., Fujii, M., Kameyama, K., Okada, Y., Kumai, K. & Kitajima, M., 2002. Matrix metalloproteinase inhibitor, marimastat, decreases peritoneal spread of gastric carcinoma in nude mice. *Japanese Journal of Cancer Research :Gann*, 93(7), pp.834–841.

Klán, P., Literák, J. & Relich, S., 2001. Molecular photochemical thermometers: investigation of microwave superheating effects by temperature dependent photochemical processes. *Journal of Photochemistry and Photobiology A: Chemistry*, 143(1), pp.49–57.

Kleinman, H.K., McGarvey, M.L., Hassell, J.R., Star, V.L., Cannon, F.B., Laurie, G.W. & Martin, G.R., 1986. Basement membrane complexes with biological activity. *Biochemistry*, 25(2), pp.312–318.

Koch, A.E., Halloran, M.M., Haskell, C.J. Shah, M.R. & Polverini, P.J., 1995. Angiogenesis mediated by soluble forms of E-selectin and vascular cell adhesion molecule-1. *Nature*, 376(6540), pp.517–519.

Koolwijk, P., Sidenius, N., Peters, E., Sier, C.F.M., Hanemaaijer, R., Blasi, F. & Van Hinsbergh, V.W.M., 2001. Proteolysis of the urokinase-type plasminogen activator receptor by metalloproteinase-12: Implication for angiogenesis in fibrin matrices. *Blood*, 97(10), pp.3123–3131.

Koppisetti, R.K., Fulcher, Y.G., Jurkevich, A., Prior, S.H., Xu, J., Lenoir, M., Overduin, M. & Van Doren, S.R., 2014. Ambidextrous binding of cell and membrane bilayers by soluble matrix metalloproteinase-12. *Nature Communications*, 5, p.5552.

Krock, B., Skuli, N. & Simon, M.C., 2011. Hypoxia-induced angiogenesis: good and evil. *Genes & Cancer*, 2(12), pp.1117–33.

Kruger, E.A., Duray, P.H., Tsokos, M.G., Venzon, D.J., Libutti, S.K., Dixon, S.C., Rudek, M.A., Pluda, J., Allegra, C. & Figg, W.D., 2000. Endostatin inhibits microvessel formation in the *ex vivo* rat aortic ring angiogenesis assay. *Biochemical and Biophysical Research Communications*, 268(1), pp.183–91.

Lacroix, R., Sabatier, F., Mialhe, A., Basire, A., Pannell, R., Borghi, H., Robert, S., Lamy, E., Plawinski, L., Camoin-Jau, L., Gurewich, V., Angles-Cano, E. & Dignat-George, F., 2007. Activation of plasminogen into plasmin at the surface of endothelial microparticles: A mechanism that modulates angiogenic properties of endothelial progenitor cells *in vitro*. *Blood*, 110(7), pp.2432–2439.

Lage, A.P. & Andrade, S.P., 2000. Assessment of angiogenesis and tumor growth in conscious mice by a fluorimetric method. *Microvascular Research*, 59(2), pp.278–285.

Lagente, V., Le Quement, C. & Boichot, E., 2009. Macrophage metalloelastase (MMP-12) as a target for inflammatory respiratory diseases. *Expert Opinion on Therapeutic Targets*, 13(3), pp.287–295.

Lang, R., Kocourek, A., Braun, M., Tschesche, H., Huber, R., Bode, W. & Maskos, K., 2001. Substrate specificity determinants of human macrophage elastase (MMP-12) based on the 1.1 A crystal structure. *Journal of Molecular Biology*, 312(4), pp.731–742.

Laschke, M.W., Giebels, C. & Menger, M.D., 2011. Vasculogenesis: A new piece of the endometriosis puzzle. *Human Reproduction Update*, 17(5), pp.628–636.Lawler, J., 2002. Thrombospondin-1 as an endogenous inhibitor of angiogenesis and tumor growth. *Journal of Cellular and Molecular Medicine*, 6(1), pp.1–12.

Lawler, P.R. & Lawler, J., 2012. Molecular basis for the regulation of angiogenesis by thrombospondin-1 and -2. *Cold Spring Harbor Perspectives in Medicine*, 2(5), a006627.

Lawson, C. & Wolf, S., 2009. ICAM-1 signaling in endothelial cells. *Pharmacological reports*, 61(1), pp.22–32.

Lee, H.M., Ciancio, S.G., Tuter, G., Ryan, M.E., Komaroff, E. & Golub, L.M., 2004. Subantimicrobial dose doxycycline efficacy as a matrix metalloproteinase inhibitor in chronic periodontitis patient is enhanced when combined with a non-steriodal anti-inflammatory drug. *Journal of Periodontology*, 75(3), pp.453–463.

Lee, S., Jilani, S.M., Nikolova, G.V., Carpizo, D. & Iruela-Arispe, M.L., 2005. Processing of VEGF-A by matrix metalloproteinases regulates bioavailability and vascular patterning in tumors. *The Journal of Cell Biology*, 169(4), pp.681–691.

Lee, S., Vinegoni, C., Feruglio, P.F., Fexon, L., Gorbatov, R., Pivoravov, M., Sbarbati, A., Nahrendorf, M. & Weissleder, R., 2012. Real-time *in vivo* imaging of the beating mouse heart at microscopic resolution. *Nature Communications*, 3, p.1054.

Leibovich, S.J., Polverini, P.J., Shepard, H.M., Wiseman, D.M., Shively, V. & Nuseir, N., 1987. Macrophage-induced angiogenesis is mediated by tumour necrosis factor-alpha. *Nature*, 329(6140), pp.630–632.

Levanon, K., Varda-Bloom, N., Greenberger, S., Barshack, I., Goldberg, I., Orenstein, A., Breitbart, E., Shaish, A. & Harats, D., 2006. Vascular wall maturation and prolonged angiogenic effect by endothelial-specific platelet-derived growth factor expression. *Pathobiology*, 73(3), pp.149–158.

Li, J., Wang, J.J., Peng, Q., Chen, C., Humphrey, M.B., Heinecke, J. & Zhang, S.X., 2012. Macrophage metalloelastase (MMP-12) deficiency mitigates retinal inflammation and pathological angiogenesis in ischemic retinopathy. *PLoS ONE*, 7(12) e52699.

Li, Q. & Olsen, B.R., 2004. Increased angiogenic response in aortic explants of collagen XVIII/endostatin-null mice. *The American Journal of Pathology*, 165(2), pp.415–24.

Li, W., Li, J., Wu, Y., Wu, J., Hotchandani, R., Cunningham, K., McFadyen, I., Bard, J., Morgan, P., Schlerman, F., Xu, X., Tam, S., Goldman, S.J., Williams, C., Sypek, J. & Mansour, T.S., 2009. A selective matrix metalloprotease 12 inhibitor for potential treatment of chronic obstructive pulmonary disease (COPD): discovery of (S)-2-(8-(methoxycarbonylamino)dibenzo[b,d]furan-3-sulfonamido)-3-methylbutanoic acid (MMP408). *Journal of Medicinal Chemistry*, 52, pp.1799–1802.

Li, W., Li, J., Wu, A., Wu, J., Hotchandani, R., Tam, S., Mansour, T., Sypek, J.P. & Mcfadyen, I., 2008. Tricyclic compounds as matrix metalloproteinase inhibitors.WO2008137816 A2.

Liang, C.C., Park, A.Y. & Guan, J.L., 2007. *In vitro* scratch assay: a convenient and inexpensive method for analysis of cell migration *in vitro*. *Nature Protocols*, 2(2), pp.329–33.

Liang, J., Liu, E., Yu, Y., Kitajima, S., Koike, T., Jin, Y., Morimoto, M., Hatakeyama, K., Asada, Y., Watanabe, T., Sasaguri, Y., Watanabe, S. & Fan, J., 2006. Macrophage metalloelastase accelerates the progression of atherosclerosis in transgenic rabbits. *Circulation*, 113(16), pp.1993–2001.

Lim, N.H., Meinjohanns, E., Bou-Gharios, G., Gompels, L.L., Nuti, E., Rossello, A., Devel, L., Dive, V., Meldal, M. & Nagase, H., 2014. *In vivo* imaging of matrix metalloproteinase 12 and matrix metalloproteinase 13 activities in the mouse model of collagen-induced arthritis. *Arthritis and Rheumatology*, 66(3), pp.589–598.

Lindholt, J.S., Vammen, S., Fasting, H., Henneberg, E.W. & Heickendorff, L., 2000. The plasma level of matrix metalloproteinase 9 may predict the natural history of small abdominal aortic aneurysms. A preliminary study. *European Journal of Vascular and Endovascular Surgery*, 20(3), pp.281–285.

Liu, M., Sun, H., Wang, X., Koike, T., Mishima, H., Ikeda, K., Watanabe, T., Ochiai, N. & Fan, J., 2004. Association of increased expression of macrophage elastase (matrix metalloproteinase 12) with rheumatoid arthritis. *Arthritis and Rheumatism*, 50(10), pp.3112–3117.

Liu, P., Sun, M. & Sader, S., 2006. Matrix metalloproteinases in cardiovascular disease. *The Canadian Journal of Cardiology*, 22(Suppl B), pp.25B–30B.

Liu, S.L., Bae, Y.H., Yu, C., Monslow, J., Hawthorne, E.A., Castagnino, P., Branchetti, E., Ferrari, G., Damrauer, S.M., Puré, E. & Assoian, R.K., 2015. Matrix metalloproteinase-12 is an essential mediator of acute and chronic arterial stiffening. *Scientific Reports*, article number 17189.

Löffek, S., Schilling, O. & Franzke, C.W., 2011. Biological role of matrix metalloproteinases: a critical balance. *The European Respiratory Journal*, 38(1), pp.191–208.

Logie, J.J., Ali, S., Marshall, K.M., Heck, M.M.S.., Walker, B.R. & Hadoke, P.W.F., 2010. Glucocorticoid-mediated inhibition of angiogenic changes in human endothelial cells is not caused by reductions in cell proliferation or migration. *PLoS ONE*, 5(12), e14476.

Longo, G., Xiong, W., Greiner, T.C., Zhao, Y., Fiotti, N. & Baxter, T.B., 2002. Matrix metalloproteinases 2 and 9 work in concert to produce aortic aneurysms. *The Journal of Clinical Investigation*, 110(5), pp.625–32.

Longo, M.G., Buda, S.J., Fiotta, N., Xiong, W., Griener, T., Shapiro, S. & Baxter, T.B., 2005. MMP-12 has a role in abdominal aortic aneurysms in mice. *Surgery*, 137(4), pp.457–562.

Mackay, M., Pérez-López, A.M., Bradley, M., Lilienkampf, A., 2016. Eliminating caspase-7 and cathepsin B cross-reactivity on fluorogenic caspase-3 substrates. *Molecular BioSystems.*, 12(3), pp.693–696.

Magnussen, H., Watz, H., Kirsten, A., Wang, M., Wray, H., Samuelsson, V., Mo, J. & Kay, R., 2011. Safety and tolerability of an oral MMP-9 and -12 inhibitor, AZD1236, in patients with moderate-to-severe COPD: a randomised controlled 6-week trial. *Pulmonary Pharmacology & Therapeutics*, 24(5), pp.563–70.

Mahadevan, V., Hart, I.R. & Lewis, G.P., 1989. Factors influencing blood supply in wound granuloma quantitated by a new *in vivo* technique. *Cancer Research*, 49(2), pp.415–419.

Marchant, D.J., Bellac, C.L., Moraes, T.J., Wadsworth, S.J., Dufour, A., Butler, G.S., Bilawchuk, L.M., Hendry, R.G., Robertson, A.G., Cheung, C.T., Ng, J., Ang, L., Luo, Z., Heilbron, K., Norris, M.J., Duan, W., Bucyk, T., Karpov, A., Devel, L., Georgiadis, D., Hegele, R.G., Luo, H., Granville, D.J., Dive, V., McManus, B.M. & Overall, C.M., 2014. A new transcriptional role for matrix metalloproteinase-12 in antiviral immunity. *Nature Medicine*, 20 (5) pp.493−502.

Margheri, F., Serrati, S., Lapucci, A., Giusti, B., Pucci, M., Torre, E., Bianchini, F., Calorini, L., Albini, A., Ventura, A., Fibbi, G & Del Rosso, M., 2009. Systemic sclerosis-endothelial cell antiangiogenic pentraxin 3 and matrix metalloprotease 12 control human breast cancer tumor vascularization and development in mice. *Neoplasia*, 11(10), pp.1106–1115.

Matsumoto, S., Kobayashi, T., Katoh, M., Saito, S, Ikeda, Y., Kobori, M., Masuho, Y. & Watanabe, T., 1998. Expression and localization of matrix metalloproteinase-12 in the aorta of cholesterol-fed rabbits: relationship to lesion development. *The American Journal of Pathology*, 153(1), pp.109–119.

McKenney, J.K., Weiss, S.W. & Folpe, A.L., 2001. CD31 expression in intratumoral macrophages: a potential diagnostic pitfall. *The American Journal of Surgical Pathology*, 25(9), pp.1167–73.

McSweeney, S.J., Hadoke, P.W., Kozak, A.M., Small, G.R., Khaled, H., Walker, B.R. & Gray, G.A., 2010. Improved heart function follows enhanced inflammatory cell recruitment and angiogenesis in 11βHSD1-deficient mice post-MI. *Cardiovascular Research*, 88(1), pp.159–167.

Merrifield, R.B., Stewart, J.M. & Jernberg, N., 1966. Instrument for automated synthesis of peptides. *Analytical Chemistry*, 38(13), pp.1905–1914.

Mito, J.K., Ferrer, J.M., Brigman, B.E., Lee, C.L., Dodd, R.R., Eward, W.C., Marshall, L.F., Cuneo, K.C., Carter, J.E., Ramasunder, S., Kim, Y., Lee, W.D., Griffith, L.G., Bawendi, M.G. & Kirsch, D.G., 2012. Intraoperative detection and removal of microscopic residual sarcoma using wide-field imaging. *Cancer*, 118(21), pp.5320–5330.

Molet, S., Belleguic, C., Lena, H., Germain, N., Bertrand, C. P., Shapiro, S.D., Planquois, J.M., Delaval, P. & Lagente, V., 2005. Increase in macrophage elastase (MMP-12) in lungs from patients with chronic obstructive pulmonary disease. *Inflammation Research*, 54(1), pp.31–36.

Monea, S., Lehti, K., Keski-Oja, J. & Mignatti, P., 2002. Plasmin activates pro-matrix metalloproteinase-2 with a membrane-type 1 matrix metalloproteinase-dependent mechanism. *Journal of Cellular Physiology*, 192(2), pp.160–170.

Montet, X., Figueiredo, J.L., Alencar, H., Ntziachristos, V., Mahmood, U. & Weissleder, R., 2007. Tomographic fluorescence imaging of tumor vascular volume in mice. *Radiology*, 242(3), pp.751–758.

Montet, X., Ntziachristos, V., Grimm, J. & Weissleder, R., 2005. Tomographic fluorescence mapping of tumor targets. *Cancer Research*, 65(14), pp.6330–6336.

Morales, R., Perrier, S., Florent, J.M., Beltra, J., Dufour, S., De Mendez, I., Manceau, P., Tertre, A.C., Moreau, F., Compere, D., Dublanchet, A. & O'Gara, M., 2004. Crystal structures of novel non-peptidic, non-zinc chelating inhibitors bound to MMP-12. *Journal of Molecular Biology*, 341(4), pp.1063–1076.

Morell, M., Nguyen Duc, T., Willis, A.L., Syed, S., Lee, J., Deu, E., Deng, Y., Xiao, J., Turk, B.E., Jessen, J.R., Weiss, S.J. & Bogyo, M., 2013. Coupling protein engineering with probe design to inhibit and image matrix metalloproteinases with controlled specificity. *Journal of the American Chemical Society*, 135(24), pp.9139–9148.

Morgan, A.R., Rerkasem, K., Gallagher, P.J., Zhang, B., Morris, G.E., Calder, P.C., Grirable, R.F., Eriksson, P., McPheat, W.L., Shearman, C.P. & Ye, S., 2004. Differences in matrix metalloproteinase-1 and matrix metalloproteinase-12 transcript levels among carotid atherosclerotic plaques with different histopathological characteristics. *Stroke*, 35(6), pp.1310–1315.

Moser, T.L., Stack, M.S., Asplin, I., Enghild, J.J., Højrup, P., Everitt, L., Hubchak, S., Schnaper, H.W. & Pizzo, S.V., 1999. Angiostatin binds ATP synthase on the surface of human endothelial cells. *Proceedings of the National Academy of Sciences of the United States of America*, 96(6), pp.2811–2816.

Müller, A., Krämer, S.D., Meletta, R., Beck, K., Selivanova, S.V., Rancic, Z., Kaufmann, P.A., Vos, B., Meding, J., Stellfeld, T., Heinrich, T.K., Bauser, M., Hütter, J., Dinkelborg, L.M., Schibli, R. & Ametamey, S.M., 2014. Gene expression levels of matrix metalloproteinases in human atherosclerotic plaques and evaluation of radiolabeled inhibitors as imaging agents for plaque vulnerability. *Nuclear Medicine and Biology*, 41(7), pp.562–669

Muller, W.A., 1995. The role of PECAM-1 (CD31) in leukocyte emigration: studies *in vitro* and *in vivo*. *Journal of Leukocyte Biology*, 57(4), pp.523–528.

Murphy, G., Houbrechts, A., Cockett, M.I., Williamson, R.A., O'Shea, M. & Docherty, A.J., 1991. The N-terminal domain of tissue inhibitor of metalloproteinases retains metalloproteinase inhibitory activity. *Biochemistry*, 30(33), pp.8097–102.

Murray, J.K., Aral, J. & Miranda, L.P., 2011. Solid-phase peptide synthesis using microwave irradiation. *Methods in Molecular Biology*, 716, pp.73–88.

Nagase, H., Visse, R. & Murphy, G., 2006. Structure and function of matrix metalloproteinases and TIMPs. *Cardiovascular Research*, 69(3), pp.562–573.

Nagase, H. & Woessner, J.F., 1999. Matrix metalloproteinases. *The Journal of Biological Chemistry*, 274(31), pp.21491–21494.

Nagy, J.A., Chang, S.H., Shih, S.C., Dvorak, A.M. & Dvorak, H.F., 2010. Heterogeneity of the tumor vasculature. *Seminars in Thrombosis and Hemostasis*, 36(3), pp.321–331.

Nakashima, Y., Plump, A.S., Raines, E.W., Breslow, J.L. & Ross, R., 1994. ApoE-deficient mice develop lesions of all phases of atherosclerosis throughout the arterial tree. *Arteriosclerosis and Thrombosis and Vascular Biology*, 14(1), pp.133–140.

Nénan, S., Boichot, E., Lagente, V. & Bertrand, C.P., 2005. Macrophage elastase (MMP-12): A pro-inflammatory mediator? *Memorias do Instituto Oswaldo Cruz*. 100(suppl 1), pp. 167–172.

Newby, A.C., 2005. Dual role of matrix metalloproteinases (matrixins) in intimal thickening and atherosclerotic plaque rupture. *Physiological Reviews*, 85(1), pp.1–31.

Newby, A.C., 2006. Matrix metalloproteinases regulate migration, proliferation, and death of vascular smooth muscle cells by degrading matrix and non-matrix substrates. *Cardiovascular Research*, 69(3), pp.614–624.

Newman, P.J., 1997. The biology of PECAM-1. *Journal of Clinical Investigation*, 99(1), pp.3–8.

Ng, K.T., Qi, X., Kong, K.L., Cheung, B.Y., Lo, C.M., Poon, R.T., Fan, S.T. & Man, K., 2011. Overexpression of matrix metalloproteinase-12 (MMP-12) correlates with poor prognosis of hepatocellular carcinoma. *European Journal of Cancer*, 47(15), pp.2299–2305.

Nguyen, M., Arkell, J. & Jackson, C.J., 2001. Human endothelial gelatinases and angiogenesis. *International Journal of Biochemistry and Cell Biology*, 33(10), pp.960–970.

Nicosia, R.F. & Ottinetti, A., 1990. Growth of microvessels in serum-free matrix culture of rat aorta. A quantitative assay of angiogenesis *in vitro*. *Laboratory Investigation; a Journal of Technical Methods and Pathology*, 63(1), pp.115–122.

Nolting, D.D., Gore, J.C. & Pham, W., 2011. Near-infrared dyes: Probe development and applications in optical molecular imaging. *Current Organic Synthesis*, 8(4), pp.521–534.

Norrby, K., 2006. *In vivo* models of angiogenesis. *Journal of Cellular and Molecular Medicine*, 10(3), pp.588–612.

Ntziachristos, V., Bremer, C. & Weissleder, R., 2003. Fluorescence imaging with near-infrared light: new technological advances that enable *in vivo* molecular imaging. *European Radiology*, 13, pp.195–208.

Nury, C., Bregant, S., Czarny, B., Berthon, F., Cassar-Lajeunesse, E. & Dive, V., 2013. Detection of endogenous matrix metalloprotease-12 active form with a novel broad spectrum activity-based probe. *The Journal of Biological Chemistry*, 288(8), pp.5636–44.

O'Brien, C.D., Lim, P., Sun, J. & Albelda, S.M., 2003. PECAM-1-dependent neutrophil transmigration is independent of monolayer PECAM-1 signaling or localization. *Blood*, 101(7), pp.2816–2825.

O'Reilly, M.S., Holmgren, L., Shing, Y., Chen, C., Rosenthal, R.A., Moses, M., Lane, W.S., Cao, Y., Helene S.E. & Folkman, J., 1994. Angiostatin: A novel angiogenesis inhibitor that mediates the suppression of metastases by a Lewis lung carcinoma. *Cell*, 79(2), pp.315–328.

O'Reilly, M.S., Boehm, T., Shing, Y., Fukai, N., Vasios, G., Lane, W.S., Flynn, E., Birkhead, J.R., Olsen, B.R. & Folkman, J., 1997. Endostatin: an endogenous inhibitor of angiogenesis and tumor growth. *Cell*, 88(2), pp.277–285.

O'Sullivan, S., Gilmer, J.F. & Medina, C., 2015. Matrix Metalloproteinases in inflammatory bowel disease: an update. *Mediators of Inflammation*, 2015: 964131.

O-Charoenrat, P., Rhys-Evans, P. & Eccles, S., 2002. A synthetic matrix metalloproteinase inhibitor prevents squamous carcinoma cell proliferation by interfering with epidermal growth factor receptor autocrine loops. *International Journal of Cancer*, 100(5), pp.527–533.

Ohno-Matsui, K., Uetama, T., Yoshida, T., Hayano, M., Itoh, T., Morita, I. & Mochizuki, M., 2003. Reduced retinal angiogenesis in MMP-2-deficient mice. *Investigative Ophthalmology & Visual Science*, 44(12), pp.5370–5375.

Osborn, E.A. & Jaffer, F.A., 2013. The advancing clinical impact of molecular imaging in CVD. *JACC. Cardiovascular imaging*, 6(12), pp.1327–41.

Overall, C.M. & Kleifeld, O., 2006. Tumour microenvironment - opinion: validating matrix metalloproteinases as drug targets and anti-targets for cancer therapy. *Nature Reviews. Cancer*, 6(3), pp.227–239.

Page-McCaw, A., Ewald, A.J. & Werb, Z., 2007. Matrix metalloproteinases and the regulation of tissue remodelling. *Nature Reviews. Molecular Cell Biology*, 8(3), pp.221–33.

Paiva, K.B.S. & Granjeiro, J.M., 2014. Bone tissue remodeling and development: Focus on matrix metalloproteinase functions. *Archives of Biochemistry and Biophysics*, 561, pp.74–87.

Palasek, S.A., Cox, Z.J. & Collins, J.M., 2007. Limiting racemization and aspartimide formation in microwave-enhanced Fmoc solid phase peptide synthesis. *Journal of Peptide Science*, 13(3), pp.143–148.

Parameswaran, N. & Patial, S., 2010. Tumor necrosis factor-α signaling in macrophages. *Critical Reviews in Eukaryotic Gene Expression*, 20(2), pp.87–103.

Patterson, B.C. & Sang, Q.A., 1997. Angiostatin-converting enzyme activities of human matrilysin (MMP-7) and gelatinase B/type IV collagenase (MMP.9). *Journal of Biological Chemistry*, 272(46), pp.28823–28825.

Pepper, M.S., 2001. Role of the matrix metalloproteinase and plasminogen activator-plasmin systems in angiogenesis. *Arteriosclerosis, Thrombosis, and Vascular Biology*, 21(7), pp.1104–1117.

Pernagallo, S., Tura, O., Wu, M., Samuel, K., Diaz-Mochon, J.J., Hansen, A., Zhang, R., Jackson, M., Padfield, G.J., Hadoke, P.W.F., Mills, N., Turner, M.L., Iredale, J.P., Hay, D.C. & Bradley, M., 2012. Novel biopolymers to enhance endothelialisation of intra-vascular devices. *Advanced Healthcare Materials*, 1(5), pp.646–656.

Peterson, J.D., 2011. Comparison of PerkinElmer vascular pre-clinical fluorescent imaging agents in oncology and inflammation research.*Perkinelmer.Inc*. Application note: preclinical imaging, pp.1–10.

Petzelbauer, P., Halama, T. & Gröger, M., 2000. Endothelial adherens junctions. *The Journal of Investigative Dermatology. Symposium Proceedings*, 5(1), pp.10–13.

Phelps, E.A., Landázuri, N., Thulé, P.M., Taylor, R.W. & García, A.J., 2010. Bioartificial matrices for therapeutic vascularization. *Proceedings of the National Academy of Sciences of the United States of America*, 107(8), pp.3323–8.

Pollard, J.W., 2009. Trophic macrophages in development and disease. *Nature Reviews. Immunology*, 9(4), pp.259–70.

Prescott, M.F., Sawyer, W.K., Von Linden-Reed, J., Jeune, M., Chou, M. Caplan, S.l. & Jeng, A.Y., 1999. Effect of matrix metalloproteinase inhibition on progression of atherosclerosis and aneurysm in LDL receptor-deficient mice overexpressing MMP-3, MMP-12, and MMP-13 and on restenosis in rats after balloon injury. *Annals of the New York Academy of Sciences*, 878, pp. 179–190.

Rao, V.H., Meehan, D.T., Delimont, D., Nakajima, M., Wada, T., Gratton, M.A. & Cosgrove, D., 2006. Role for macrophage metalloelastase in glomerular basement membrane damage associated with alport syndrome. *The American Journal of Pathology*, 169(1), pp.32–46.

Rasmussen, H.S. & McCann, P.B., 1997. Matrix metalloproteinase inhibition as a novel anticancer strategy: A review with special focus on Batimastat and Marimastat. *Pharmacology and Therapeutics*, 75(1), pp.69–75.

Al Rawashdeh, W., Arns, S., Gremse, F., Ehling, J., Knüchel-Clarke, R., Kray, S., Spöler, F., Kiessling, F. & Lederle, W., 2014. Optical tomography of MMP activity allows a sensitive noninvasive characterization of the invasiveness and angiogenesis of Scc xenografts. *Neoplasia*, 16(3), pp.235–246.

Raza, S.L., Nehring, L.C., Shapiro, S.D. & Cornelius, L.A., 2000. Proteinase-activated receptor-1 regulation of macrophage elastase (MMP-12) secretion by serine proteinases. *The Journal of Biological Chemistry*, 275(52), pp.41243–41250.

Redlitz, A., Daum, G. & Sage, E.H., 1999. Angiostatin diminishes activation of the mitogen-activated protein kinases ERK-1 and ERK-2 in human dermal microvascular endothelial cells. *Journal of Vascular Research.*, 36(1), pp.28–34.

Reed, M.J., Koike, T., Sadoun, E., Sage, H.E. & Puolakkainen, P., 2003. Inhibition of TIMP1 enhances angiogenesis *in vivo* and cell migration *in vitro*. *Microvascular Research*, 65(1), pp.9–17.

Ribatti, D., Vacca, A., Nico, B., Roncali, L. & Dammacco, F., 2001. Postnatal vasculogenesis. *Mechanisms of Development*, 100(2), pp.157–163.

Ribatti, D., Nico, B. & Crivellato, E., 2011. The role of pericytes in angiogenesis. *International Journal of Developmental Biology*, 55(3), pp.261–268.

Ripplinger, C.M., Kessinger, C.W., Li, C., Kim, J.W., McCarthy, J.R., Weissleder, R., Henke, P.K., Lin, C.P. & Jaffer, F.A., 2012. Inflammation modulates murine venous thrombosis resolution *in vivo*: Assessment by multimodal fluorescence molecular imaging. *Arteriosclerosis, Thrombosis, and Vascular Biology*, 32, pp.2616–2624.

Roque, M., Fallon, J.T., Badimon, J.J., Zhang, W.X., Taubman, M.B. & Reis, E.D., 2000. Mouse model of femoral artery denudation injury associated with the rapid accumulation of adhesion molecules on the luminal surface and recruitment of neutrophils. *Arteriosclerosis, Thrombosis, and Vascular Biology*, 20(2), pp.335–342.

Rosenblum, W.I., Nelson, G.H., Wormley, B., Werner, P., Wang, J. & Shih, C.C., 1996. Role of platelet-endothelial cell adhesion molecule (PECAM) in platelet adhesion/aggregation over injured but not denuded endothelium *in vivo* and *ex vivo*. *Stroke*, 27(4), pp.709–11.

Ross, R., 1999. Atherosclerosis−an inflammatory disease. *The New England Journal of Medicine*, 340(2), pp.115–126.

Rudolph-Owen, L.A., Hulboy, D.L., Wilson, C.L., Mudgett, J & Matrisian, L.M., 1997. Coordinate expression of matrix metalloproteinase family members in the uterus of normal, matrilysin-deficient, and stromelysin-1-deficient mice. *Endocrinology*, 138(11), pp.4902–4911.

Rundhaug, J.E., 2005. Matrix metalloproteinases and angiogenesis. *Journal of Cellular and Molecular Medicine*, 9(2), pp.267–285.

Rush, T.S. & Powers, R., 2004. The application of X-ray, NMR, and molecular modeling in the design of MMP inhibitors. *Current Topics in Medicinal Chemistry*, 4(12), pp.1311–1327.

Saarialho-Kere, U.K., Kerkelä, E., Jeskanen, L., Hasan, T., Pierce, R., Starcher, B., Raudasoja, R., Ranki, A., Oikarinen, A. & Vaalamo, M., 1999. Accumulation of matrilysin (MMP-7) and macrophage metalloelastase (MMP- 12) in actinic damage. *Journal of Investigative Dermatology*, 113(4), pp.664–672.

Saghatelian, A., Jessani, N., Joseph, A., Humphrey, M. & Cravatt, B.F., 2004. Activity-based probes for the proteomic profiling of metalloproteases. *Proceedings of the National Academy of Sciences of the United States of America*, 101(27), pp.10000–10005.

Sainson, R.C.A., Johnston, D.A., Chu, H.C., Holderfield, M.T., Nakatsu, M.N., Crampton, S., Davis, J., Conn, E. & Hughes, C., 2008. TNF primes endothelial cells for angiogenic sprouting by inducing a tip cell phenotype. *Blood*, 111(10), pp.4997–5007.

Sata, M., Maejima, Y., Adachi, F., Fukino, K., Saiura, A., Sugiura, S., Aoyagi, T., Imai, Y., Kurihara, H., Kimura, K., Omata, M., Makuuchi, M., irata, Y & Nagai, R., 2000. A mouse model of vascular injury that induces rapid onset of medial cell apoptosis followed by reproducible neointimal hyperplasia. *Journal of Molecular and Cellular Cardiology*, 32(11), pp.2097–2104.

Saunders, B.W., Bayless, K.J. & Davis, G.E., 2005. MMP-1 activation by serine proteases and MMP-10 induces human capillary tubular network collapse and regression in 3D collagen matrices. *Journal of Cell Science*, 118(Pt 10), pp.2325–2340.

Schäfers, M., Riemann, B., Kopka, K., Breyholz, H.j., Wagner, S., Schäfers, K.P., Law, M.P., Schober, O. & Levkau, B., 2004. Scintigraphic imaging of matrix metalloproteinase activity in the arterial wall *in vivo*. *Circulation*, 109(21), pp.2554–2559.

Schilling, J.A., Joel, W. & Shurley, H.M., 1959. Wound healing: a comparative study of the histochemical changes in granulation tissue contained in stainless steel wire mesh and polyvinyl sponge cylinders. *Surgery*, 46(4), pp.702–710.

Scholtes, V.P., Johnson, J.L., Jenkins, N., Sala-Newby, G.B., de Vries, J.P., de Borst, G.J., de Kleijn, D.P., Moll, F.L., Pasterkamp, G. & Newby, A.C., 2012. Carotid atherosclerotic plaque matrix metalloproteinase-12-positive macrophage subpopulation predicts adverse outcome after endarterectomy. *Journal of the American Heart Association*, 1(6), e001040.

Serratì, S., Cinelli, M., Margheri, F., Guiducci, S., Del Rosso, A., Pucci, M., Fibbi, G., Bazzichi, L., Bombardieri, S., Matucci-Cerinic, M. & Del Rosso, M., 2006. Systemic sclerosis fibroblast inhibit *in vitro* angiogenesis by MMP-12-dependent cleavage of the endothelial cell urokinase receptor. *Journal of Pathology*, 210(2), pp.240–248.

Shamsara, J., Shahir-Sadr, A., Shamsara, J. & Shahir-Sadr, A., 2014. A predictive HQSAR model for a series of tricycle core containing MMP-12 inhibitors with dibenzofuran ring. *International Journal of Medicinal Chemistry*, 2014:Article ID 630807.

Shapiro, S.D., Kobayashi, D.K. & Ley, T.J., 1993. Cloning and characterization of a unique elastolytic metalloproteinase produced by human alveolar macrophages. *The Journal of Biological Chemistry*, 268(32), pp.23824–23829.

Shi, H., Xu, J.M., Hu, N.Z., Wang, X.L., Mei, Q. & Song, Y.L., 2006. Transfection of mouse macrophage metalloelastase gene into murine CT-26 colon cancer cells suppresses orthotopic tumor growth, angiogenesis and vascular endothelial growth factor expression. *Cancer Letters*, 233(1), pp.139–150.

Shi, J., Son, M.Y., Yamada, S., Szabova, L., Kahan, S., Chrysovergis, K., Wolf, L., Surmak, A. & Holmbeck, K., 2008. Membrane-type MMPs enable extracellular matrix permissiveness and mesenchymal cell proliferation during embryogenesis. *Developmental Biology*, 313(1), pp.196–209.

Shifren, A. & Mecham, R.P., 2006. The stumbling block in lung repair of emphysema: elastic fiber assembly. *Proceedings of the American Thoracic Society*, 3(5), pp.428–433.

Shipley, J.M., Wesselschmidt, R.L., Kobayashi, D.K., Ley, T.J. & Shapiro, S.D., 1996. Metalloelastase is required for macrophage-mediated proteolysis and matrix invasion in mice. *Proceedings of the National Academy of Sciences of the United States of America*, 93(9), pp.3942–3946.

Skalli, O., Pelte, M F., Peclet, M C., Gabbiani, G., Gugliotta, P., Bussolati, G., Ravazzola, M. & Orci, L., 1989. Alpha-smooth muscle actin, a differentiation marker of smooth muscle cells, is present in microfilamentous bundles of pericytes. *The Journal of Histochemistry and Cytochemistry*, 37(3), pp.315–321.

Skipper, J.B., McNally, L.R., Rosenthal, E.L., Wang, W. & Buchsbaum, D.J., 2009. *In vivo* efficacy of marimastat and chemoradiation in head and neck cancer xenografts. *ORL; Journal for Oto-rhino-laryngology and its Related Specialties*, 71(1), pp.1–5.

Small, G.R., Hadoke, P.W.F., Sharif, I., Dover, A.R., Armour, D., Kenyon, C., Gray, G.A. & Walker, B.R., 2005. Preventing local regeneration of glucocorticoids by 11beta-hydroxysteroid dehydrogenase type 1 enhances angiogenesis. *Proceedings of the National Academy of Sciences of the United States of America*, 102(34), pp.12165–12170.

Smith, H.W., & Marshall, C.J., 2010. Regulation of cell signalling by uPAR. *Nature Reviews. Molecular Cell Biology*, 11(1), pp.23–36.

Somlyo, A.V., Phelps, C., Dipierro, C., Eto, M., Read, P., Barrett, M., Gibson, J.J., Burnitz, C.M., Myers, C. & Somlyo, A P., 2003. Rho kinase and matrix metalloproteinase inhibitors cooperate to inhibit angiogenesis and growth of human prostate cancer xenotransplants. *The Federation of American Societies for Experimental Biology Journal*, 17(12), pp.223–234.

Sparano, J.A., Bernardo, P., Stephenson, P., Gradishar, W.j, Ingle, J.N., Zucker, S. & Davidson, N.E., 2004. Randomized phase III trial of marimastat versus placebo in patients with metastatic breast cancer who have responding or stable disease after first-line chemotherapy: Eastern Cooperative Oncology Group trial E2196. *Journal of Clinical Oncology*, 22(23), pp.4683–90.

Stamenkovic, I., 2003. Extracellular matrix remodelling: the role of matrix metalloproteinases. *The Journal of Pathology*, 200, pp.448–464.

Stawikowski, M. & Fields, G.B., 2012. Introduction to peptide synthesis. *Current Protocols in Protein Science*, Chapter 18.

Sternlicht, M.D. & Werb, Z., 2001. How matrix metalloproteinases regulate cell behavior. *Annual Review of Cell and Developmental Biology*, 17, pp.463–516.

Subirós-Funosas, R., Prohens, R., Barbas, R., El-Faham, A. & Albericio, F., 2009. Oxyma: An efficient additive for peptide synthesis to replace the benzotriazole-based HOBt and HOAt with a lower risk of explosion. *Chemistry - A European Journal*, 15(37), pp.9394–9403.

Taniguchi, T. & Takaoka, A., 2002. The interferon-α/β system in antiviral responses: A multimodal machinery of gene regulation by the IRF family of transcription factors. *Current Opinion in Immunology*, 14(1), pp.111–116.

The Jackson Laboratory, 2016. B6.129X-Mmp12tm1Sds/J JAX mouse strain datasheet. *The Jackson Laboratory*, datasheet - 004855.

Thygesen, K., Alpert, J.S., Jaffe A.S., Simoons, M.L., Chaitman B.R. & White H.D., 2012. Third universal definition of myocardial infarction. *Nature Reviews. Cardiology*, 9(11), pp.620–633.

TOCRIS, 2015. Angiogenesis, Cancer Research Product Guide. *TOCRIS*, Edition 3., pp.28.

Troyan, S.l, Kianzad, V., Gibbs-Strauss, S.L., Gioux, S, Matsui, A., Oketokoun, R., Ngo, L., Khamene, A., Azar, F. & Frangioni, J.V., 2009. The FLARE intraoperative near-infrared fluorescence imaging system: a first-in-human clinical trial in breast cancer sentinel lymph node mapping. *Annals of Surgical Oncology*, 16(10), pp.2943–52.

Troyanovsky, B., Levchenko, T., Månsson, G., Matvijenko, O. & Holmgren, L., 2001. Angiomotin: an angiostatin binding protein that regulates endothelial cell migration and tube formation. *The Journal of Cell Biology*, 152(6), pp.1247–54.

Urano, Y., Asanuma, D., Hama, Y., Koyama, Y., Barrett, T., Kamiya, M., Nagano, T., Watanabe, T., Hasegawa, A., Choyke, P.L. & Kobayashi, H., 2009. Selective molecular imaging of viable cancer cells with pH-activatable fluorescence probes. *Nature Medicine*, 15(1), pp.104–9.

Vaalamo, M., Kariniemi, A.L., Shapiro, S.D. & Saarialho-Kere, U., 1999. Enhanced expression of human metalloelastase (MMP-12) in cutaneous granulomas and macrophage migration. *Journal of Investigative Dermatology*, 112(4), pp.499–505.

Valença, S.S., da Hora, K., Castro, P., Moraes, V.G., Carvalho, L. & Porto, L.C., 2004. Emphysema and metalloelastase expression in mouse lung induced by cigarette smoke. *Toxicologic Pathology*, 32(3), pp.351–356.

Van Hinsbergh, V.W.M. & Koolwijk, P., 2008. Endothelial sprouting and angiogenesis: Matrix metalloproteinases in the lead. *Cardiovascular Research*, 78(2), pp.203–212.

Vandooren, J., Geurts, N., Martens, E., Van den Steen, P.E. & Opdenakker, G., 2013. Zymography methods for visualizing hydrolytic enzymes. *Nature Methods*, 10(3), pp.211–20.

Vincenti, M.P. & Brinckerhoff, C.E., 2002. Transcriptional regulation of collagenase (MMP-1, MMP-13) genes in arthritis: integration of complex signaling pathways for the recruitment of gene-specific transcription factors. *Arthritis Research*, 4(3), pp.157–164.

Visse, R. & Nagase, H., 2003. Matrix metalloproteinases and tissue inhibitors of metalloproteinases: Structure, function, and biochemistry. *Circulation Research*, 92(8), pp.827–839.

Voulgari, A. & Pintzas, A., 2009. Epithelial-mesenchymal transition in cancer metastasis: Mechanisms, markers and strategies to overcome drug resistance in the clinic. *Biochimica et Biophysica Acta - Reviews on Cancer*, 1796(2), pp.75–90.

Vu, T.H.& Werb Z., 2000. Matrix metalloproteinases: effectors of development and normal physiology. *Genes & Development*, 14(17), pp.2123–2133.

Vu, T.H., Shipley, J.M., Bergers, G., Berger, J.E., Helms, J.A., Hanahan, D., Shapiro, S.D., Senior, R.M. & Werb, Z., 1998. MMP-9/gelatinase B is a key regulator of growth plate angiogenesis and apoptosis of hypetrophic chondrocytes. *Cell*, 93(3), pp.411–422.

Wada, N., Otani, Y., Kubota, T., Kimata, M., Minagawa, A., Yoshimizu, N., Kameyama, K., Saikawa, Y., Yoshida, M., Furukawa, T., Fujii, M., Kumai, K., Okada, Y. & Kitajima, M., 2003. Reduced angiogenesis in peritoneal dissemination of gastric cancer through gelatinase inhibition. *Clinical and Experimental Metastasis*, 20(5), pp.431–435.

Wagner, S., Breyholz, H.J., Höltke, C., Faust, A., Schober, O., Schäfers, M. & Kopka, K., 2009. A new 18F-labelled derivative of the MMP inhibitor CGS 27023A for PET: Radiosynthesis and initial small-animal PET studies. *Applied Radiation and Isotopes*, 67(4), pp.606–610.

Wakelin, M.W., Sanz, M.J., Dewar, A.A., Albelda, S.M., Larkin, S.W., Boughton-Smith, N., Williams, T.J., & Nourshargh, S., 1996. An anti-platelet-endothelial cell adhesion molecule-1 antibody inhibits leukocyte extravasation from mesenteric microvessels *in vivo* by blocking the passage through the basement membrane. *The Journal of Experimental Medicine*, 184(1), pp.229–239.

Wallis de Vries, B.M., Hillebrands, J.L., van Dam, G.M., Tio, R.A., de Jong, J.S., Slart, R.H. & Zeebregts, C.J., 2009. Multispectral near-infrared fluorescence molecular imaging of matrix metalloproteinases in a human carotid plaque using a matrix-degrading metalloproteinase-sensitive activatable fluorescent probe. *Images in Cardiovascular Medicine*, 119(20), e534-e536.

Waschkau, B., Faust, A., Schäfers, M. & Bremer, C., 2013. Performance of a new fluorescence-labeled MMP inhibitor to image tumor MMP activity *in vivo* in comparison to an MMP-activatable probe. *Contrast Media and Molecular Imaging*, 8(1), pp.1–11.

Whelan, C.J., 2004. Metalloprotease inhibitors as anti-inflammatory agents: an evolving target? *Current Opinion in Investigational Drugs*, 5(5), pp.511–6. A

Willmann, J.K., van Bruggen, N., Dinkelborg, L.M. & Gambhir, S.S., 2008. Molecular imaging in drug development. *Nature Reviews. Drug Discovery*, 7(7), pp.591–607.

Withers, K., Carolan-Rees, G. & Dale, M., 2013. Pipeline™ embolization device for the treatment of complex intracranial aneurysms: a NICE medical technology guidance. *Applied Health Economics and Health Policy*, 11(1), pp.5–13.

Wojtowicz-Praga, S., Torri, J., Johnson, M., Steen, V., Marshall, J., Ness, E., Dickson, R., Sale, M., Rasmussen, H.S., Chiodo, T.A. & Hawkins, M.J., 1998. Phase I trial of Marimastat, a novel matrix metalloproteinase inhibitor, administered orally to patients with advanced lung cancer. *Journal of Clinicol Oncology*, 16(6), pp.2150–2156.

Wong, C.W., Wiedle, G., Ballestrem, C., Wehrle-Haller, B., Etteldorf, S., Bruckner, M., Engelhardt, B., Gisler, R.H. & Imhof, B.A., 2000. PECAM-1/CD31 trans-homophilic binding at the intercellular junctions is independent of its cytoplasmic domain; evidence for heterophilic interaction with integrin alphavbeta3 in Cis. *Molecular Biology of the Cell*, 11(9), pp.3109–3121.

Wu, L., Tanimoto, A., Murata, Y., Sasaguri, T., Fan, J., Sasaguri, Y. & Watanabe, T., 2003. Matrix metalloproteinase-12 gene expression in human vascular smooth muscle cells. *Genes to Cells : Devoted to Molecular & Cellular Mechanisms*, 8(3), pp.225–234.

Xavier, D.O., Amaral, L.S., Gomes, M.A., Rocha, M.A., Campos, P.R., Cota, B.D., Tafuri, L.S, Paiva, A.M., Silva, J.H., Andrade, S.P. & Belo, A.V., 2010. Metformin inhibits inflammatory angiogenesis in a murine sponge model. *Biomedicine and Pharmacotherapy*, 64(3), pp.220–225.

Xu, Z., Shi, H., Li, Q., Mei, Q., Bao, J., Shen, Y. & Xu, J., 2008. Mouse macrophage metalloelastase generates angiostatin from plasminogen and suppresses tumor angiogenesis in murine colon cancer. *Oncology Reports*, 20(1), pp.81–88.

Yabluchanskiy, A., Ma, Y., Iyer, R.P., Hall, M.E. & Lindsey, M.L., 2013. Matrix metalloproteinase-9: Many shades of function in cardiovascular disease. *Physiology*, 28(6), pp.391–403.

Yamada, S., Wang, K.Y., Tanimoto, A., Fan, J., Shimajiri, S., Kitajima, S., Morimoto, M., Tsutsui, M., Watanabe, T., Yasumoto, K. & Sasaguri, Y., 2008. Matrix metalloproteinase 12 accelerates the initiation of atherosclerosis and stimulates the progression of fatty streaks to fibrous plaques in transgenic rabbits. *The American Journal of Pathology*, 172(5), pp.1419–1429.

Yamamoto, K., Higashi, S., Kioi, M., Tsunezumi, J., Honke, K. & Miyazaki, K., 2006. Binding of active matrilysin to cell surface cholesterol sulfate is essential for its membrane-associated proteolytic action and induction of homotypic cell adhesion. *Journal of Biological Chemistry*, 281(14), pp.9170–9180.

Yang, W., Arii, S., Gorrin-Rivas, M., Mori, A., Onodera, H. & Imamura, M., 2001. Human macrophage metalloelastase gene expression in colorectal carcinoma and its clinicopathologic significance. *Cancer*, 91(7), pp.1277–1283.

Yang, X., Dong, Y., Zhao, J., Sun, H., Deng, Y., Fan, J. & Yan, Q., 2007. Increased expression of human macrophage metalloelastase (MMP-12) is associated with the invasion of endometrial adenocarcinoma. *Pathology Research and Practice*, 203(7), pp.499–505.

Yoo, S.Y. & Kwon, S.M., 2013. Angiogenesis and its therapeutic opportunities. *Mediators of Inflammation*, 2013, Article ID 127170.

Yusuke I., Kiyoko I., Arinobu T. & Kuni O., 2008. Diet and abdominal autofluorescence detected by *in vivo* fluorescence imaging of living mice. *Molecular Imaging*, 7(1), pp.21–27.

Zhang, C.C., Yan, Z., Giddabasappa, A., Lappin, P.B., Painter, C.L., Zhang, Q., Li, G., Goodman, J., Simmons, B., Pascual, B., Lee, J., Levkoff, T., Nichols, T. & Xie, Z., 2014. Comparison of dynamic contrast-enhanced MR, ultrasound and optical imaging modalities to evaluate the antiangiogenic effect of PF-03084014 and sunitinib. *Cancer Medicine*, 3(3), pp.462–471.

Zhang, H., Li, Y. & Xu, G., 2007. Human macrophage metalloelastase expression in gastric cancer and its relationship with gastric cancer prognosis. *Journal of Experimental & Clinical Cancer Research*, 26(3), pp.361–366.

Zhang, Q., Bindokas, V., Shen, J., Fan, H., Hoffman, R.M. & Xing, H.R., 2011. Time-course imaging of therapeutic functional tumor vascular normalization by antiangiogenic agents. *Molecular Cancer Therapeutics*, 10(7), pp.1173–1184.

Zhou, Z., Apte, S.S., Soininen, R., Cao, R., Baaklini, G.Y., Rauser, R.W., Wang, J., Cao, Y. & Tryggvason, K., 2000. Impaired endochondral ossification and angiogenesis in mice deficient in membrane-type matrix metalloproteinase I. *Proceedings of the National Academy of Sciences of the United States of America*, 97(8), pp.4052–7.

Zhu, W.H., Guo, X., Villaschi, S. & Francesco N.R., 2000. Regulation of vascular growth and regression by matrix metalloproteinases in the rat aorta model of angiogenesis. *Laboratory Investigation; a Journal of Technical Methods and Pathology*, 80(4), pp.545–555.

Zou, Y., Qi, Y., Roztocil, E. & Davies, M.G., 2009. Patterns of gelatinase activation induced by injury in the murine femoral artery. *The Journal of Surgical Research*, 154(1), pp.135–42.

Zucker S., Cao, J., & Molloy C.J., 2001. Anticancer Drug Development: Chapter 6, Role of matrix metalloproteinases and plasminogen activatr in cancer invasion and metastasis: Thaeraputic stratergies, *B. C. Baguley & D. J. Kerr, eds., Academic Press,* pp 91-122.

Zucker, S. & Vacirca, J., 2004. Role of matrix metalloproteinases (MMPs) in colorectal cancer. *Cancer Metastasis Reviews*, 23 (1−2), pp.101–17.

Appendix 1: Methodological Detail

MTT assay

The toxicity of compounds was assessed using the colorimetric MTT (3-(4,5-dimethylthiazol-2-yl)-2,5-diphenyltetrazolium bromide) assay. The MTT assay assesses cell metabolic activity. NAD(P)H-dependent cellular oxidoreductase enzymes may, under defined conditions, reflect the number of viable cells present. Compounds of interest are used to treat cells (normally incubated for 24 h) before the MTT assay is conducted. When MTT is added, and if the cells are viable, there is a colour change from yellow to purple (Figure A1.1). Comparisons are made between healthy cells (without treatment) and those cells which received treatment prior to the MTT assay.

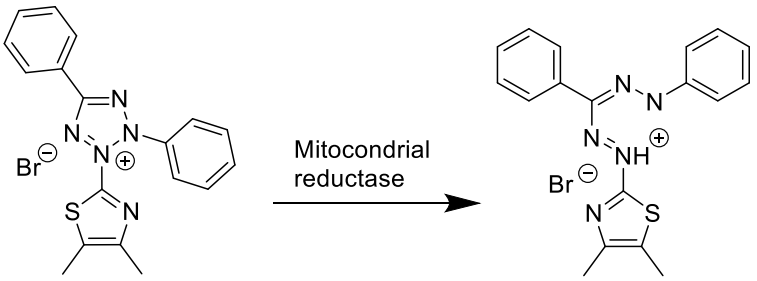

Figure A1.1 The MMT assay assesses the number of viable cells present by making a measurement of cell metabolic activity, specifically of NAD(P)H dependant cellular oxidases. Mitochondrial reductase enzymes are capable of reducing the tetrazolium dye MTT to insoluble formazan. Compounds of interest are incubated with the cells prior to the MTTT assay. Cell metabolism (and therefore viability) is reflected in the conversion of MTT and the resulting colour change from yellow to purple which can be measured using a plate reader. Comparisons are made between healthy cells and treated cells.

Osmotic minipumps and implantation surgery

Osmotic mini pumps were chosen as the means of MMP inhibitor (marimasat and HS1-22) administration as this approach ensured the compound reached the sponge at a steady rate. It was also envisaged at this method would minimise any systemic effects of the drugs. The vehicle chosen was similar to that used in other studies and the dose selected (150.6 nmol/mouse/day) was equivalent to or lower than that used in previous studies administering MMPIs (Chow *et al*., 2008; O-Charoenrat *et al*., 2002; Skipper *et al*., 2009; Somlyo *et al*., 2003).

Mini pump preparation and surgery

Drugs were administered to mice at 150.6 nmol/mouse/day (Marimastat: 2 mg/kg/day, HS1-22: 2.6 mg/kg/day) for 21 days (25g mouse) in DMSO:propylene glycol: H_2O (1:1:1). Pumps were prepared under sterile conditions (Figure). Briefly, a catheter was attached to a flow moderator before it and the pump cavity were filled with the desired drug solution (sterilised by micro filtration 0.22 μM pore size) using a syringe with a blunt needle. The metal tubing of the flow moderator was then inserted into the pump cavity. The pumps were primed prior to surgery. Surgery was conducted as described in Section 2.9.3.

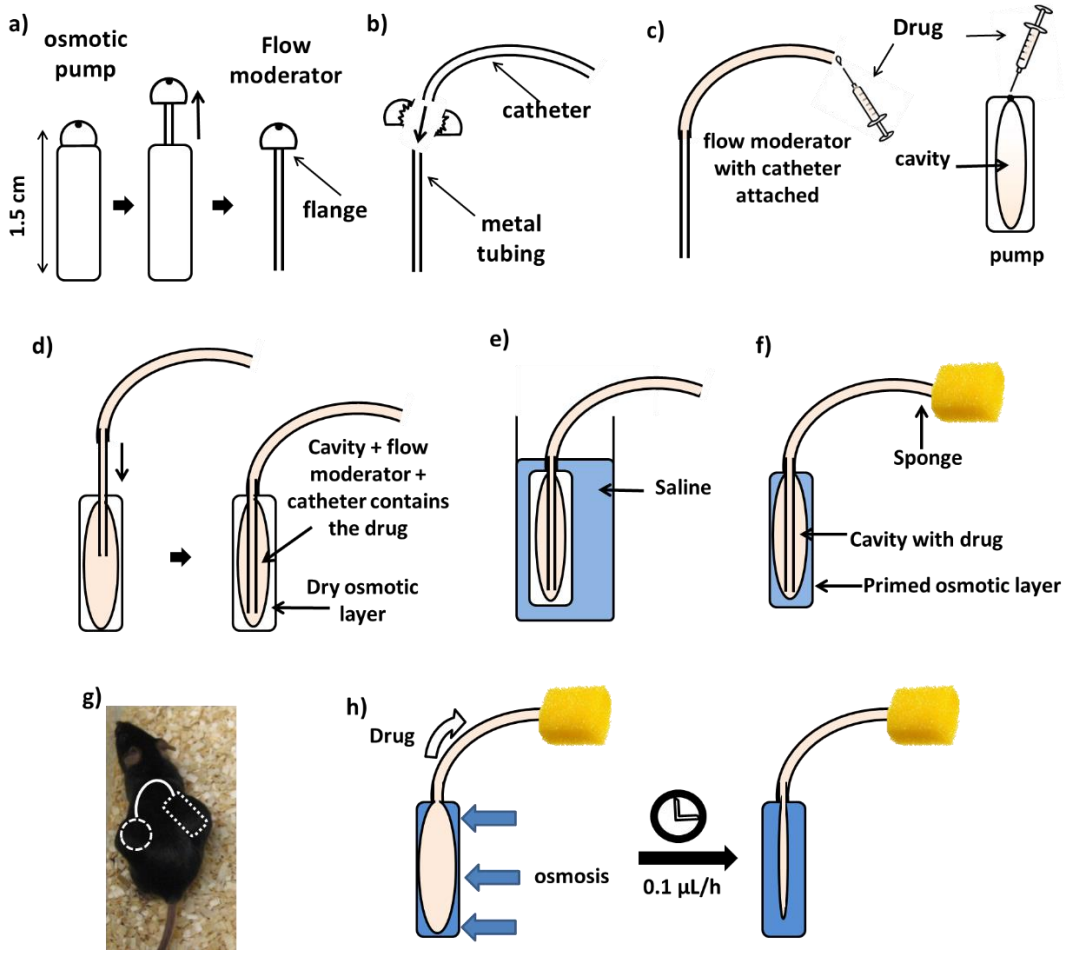

Figure A1.2 Preparation and use of the osmotic minipump. a) The flow moderator was isolated from the pump; b) the flange was broken off the flow moderator using a scalpel to reveal the metal tubing to which the catheter was attached (covered 2 - 3 mm); c) the tubing and pump (held vertically with forceps) were slowly filled with the desired solution using a syringe with a blunt needle. d) The metal tube (flow moderator) was then carefully inserted back into the pump. The pumps were then primed (incubated in saline, 37 °C, 48 h); f) prior to surgery, the catheter was inserted into the sponge and glued in place; g) the mouse was anaesthetised and a subcutaneous pocket was made under their dorsal skin, the sponge (long dash) was then inserted followed by the pump (short dash) and then the remaining catheter (solid) was tucked in before closing the wound; h) *in vivo* the osmotic pump slowly absorbs fluid which slowly presses on the cavity containing the drug, this forces it out of the pump and up the catheter delivering it to the sponge at a steady rate (0.1 µl/h for up to 28 days).

FMT

FMT machine

Fluorescence molecular tomography (FMT) is a tomographic near infra-red (NIR) imaging modality that is suitable for *in vivo* imaging of small animals. The FMT™ 2500 system is designed for preclinical research and utilises complex algorithms to construct a 3D image of detected signal. The process requires trans-illumination of the subject rather than the surface illumination used for epifluorescent assessment (Ntziachristos *et al.,* 2003). This 3D imaging helps to resolve the ambiguity of depth and size of the detected signal affecting 2D imaging.

The instrument operates on two near-infrared channels (excited at 670 nm and 746 nm, emitting at 700 nm and 775 nm respectively), which facilitates the imaging of 2 agents within the same mouse to attain more information on the biological molecular processes present. Furthermore, the FMT machine is able to determine the concentration of the probe detected within a selected region of interest (ROI). There is a wide range of optical imaging agents for different targets, most area available for use in both channels and are supplied by Perkin-Elmer. In this project AngioSense 680 and MMPSense 750 FAST were used to measure vascular leakiness and MMP activity, respectively, *in vivo.*

Preparation

Mice were fed an alfalfa free diet (Teklad 2914 maintenance diet, Harlan) for at least 10 days prior to imaging to eliminate auto-fluorescence in the gut (Inoue *et al*., 2008). Imaging agents were reconstituted, under sterile conditions, with PBS (1.2 mL/ vial); agents were combined (2.4 mL) to create a mixture for administration. With assistance from Gary Borthwick, 24 h prior to imaging the mice were warmed in an incubator (30 °C, 15 min) and briefly anaesthetised (Isoflurane). Imaging agents (200 µL, containing 2 nmol of each agent or PBS as a control) were administered by an intravenous tail vein injection and the mouse allowed to recover.

Imaging *in vivo*

Mice were weighed and anaesthetised using isoflurane (for the duration of the experiment). Hair was removed from the chest and abdomen using clippers followed by application of depilitory cream (Veet, Reckitt Benckiser Group). After 2-3 min (or when the hair became loose) the mouse was thoroughly rinsed using warm water and then dried using paper towels. The mouse was temporarily removed from the anaesthetic rig and promptly positioned in the cassette so that the tissue of interest was in the centre. The cassette was closed to a setting of 17 and then placed in the FMT 2500 machine with the ROI facing up. The inner and outer doors of the machine were closed and anaesthesia resumed (before the mouse revived). The TrueQuant software was used to obtain the data; the acquisition time was 3 − 4 minutes for each agent used. The mouse could then be removed from the chamber and either allowed to recover or culled by a schedule 1 method, as required.

Imaging *ex vivo*

Once mice had been killed, sponges were carefully removed from the carcass and placed in a cylindrical dish (approx. 3 cm diameter, 2 cm deep) and covered gently with tissue mimic solution (PerkinElmer) while taking care not to squeeze the sponge. The dish was placed in the cassette and imaged in the FMT machine as described below. The acquisition time was approx. 2 min for each agent. After scanning, each sponge was gently cleaned in PBS and then cut in half and either fixed in paraformaldehyde solution (24 h and then stored in 70% ethanol) or snap frozen on dry ice and subsequently stored at - 80 ˚C.

Data acquisition

The TrueQuant software was used to acquire data as follows:

Under the experiment tab: a data base was created for the experiment with the required groups, subject (mouse) numbers and the selected agents used in the experiment.

Under the scan tab: the system required basic information (the depth of cassette, agent to be imaged (only one scanned at a time)); then the preliminary reflectance image could be acquired. Using the reflectance image, the scan field was drawn around the ROI to have < 50 laser source positions (Figure 2.2). The “add to reconstruction queue” was checked and the subject scanned by pressing the “scan” button.

ELISA

An enzyme-linked immunosorbent assay (ELISA) allows the quantification of an antigen in a protein mixture by the use of selective antibodies and a colour change to identify a substance. In this project, two "sandwich ELISA assays" were utilised to measure MMP-12 and its endogenous inhibitor TIMP-1 in the sponges (Figure 4).

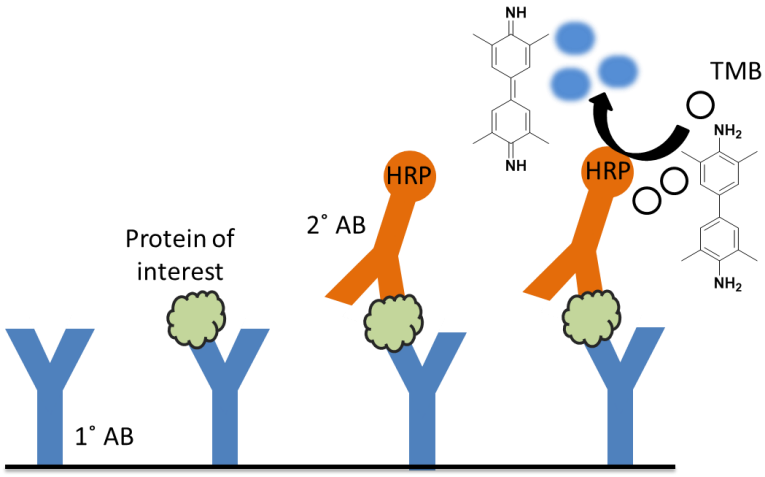

Figure A1.4 Sandwich ELISA technique. The protein of interest within the sample is attached to the plate surface by specific selective antibodies. Then, a second specific antibody is applied over the surface so it can also bind to the protein. The second antibody is either directly conjugated to an enzyme such as horse radish peroxidase (HRP) or a biotin moiety (and an avidin–HRP antibody is then applied). In the final step, an enzyme substrate such as 3,3',5,5'-Tetramethylbenzidin (TMB) is added; the subsequent reaction produces a colour change from clear to blue. The rate of colour change is proportional to the concentration of the protein of interest in the sample. This reaction can be stopped with an acidic solution (colour change from blue to yellow) to allow absorbance measurements in a plate reader. The concentration of the protein of interest within a sample are determined using a standard curve.

Appendix 2: MALDI-TOF-MS of FRET Probes

Matrix-assisted laser desorption/ionization mass spectrometry (MALDI MS) was used to confirm the mass of the synthesised Förster resonance energy transfer (FRET) probes.

HS1-58

MALDI MS: calculated for $C_{97}H_{133}N_{15}O_{27}^{+}$ $[M]^{+}$ 1940.2, found 1940.14.

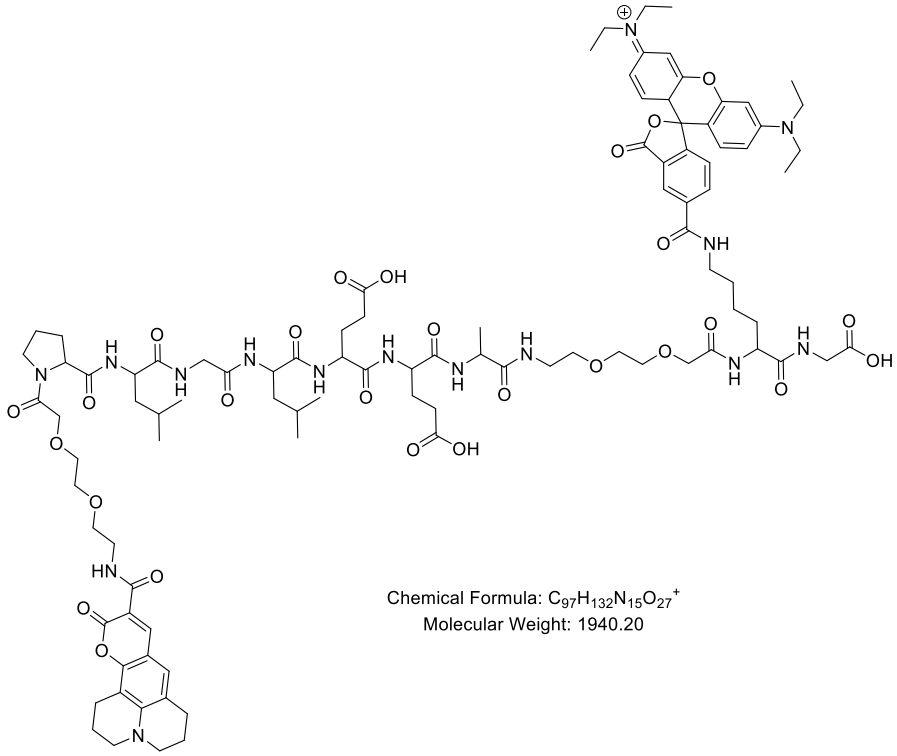

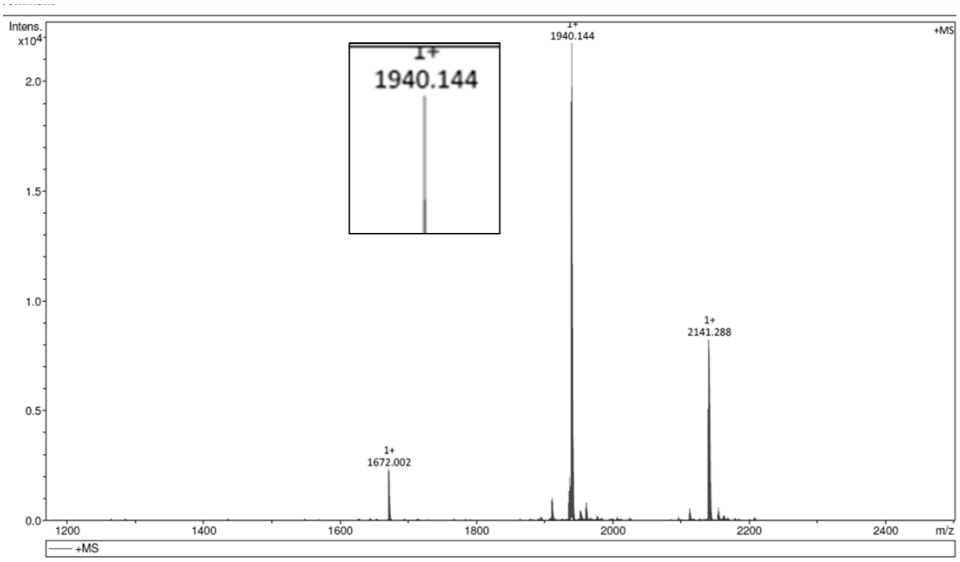

HS1-59

MALDI Mass Spectrometry: calculated for $C1_{102}H_{129}N_{14}O_{30}^{+}$ $[M]^{+}$ 2031.22 found 2031.68.

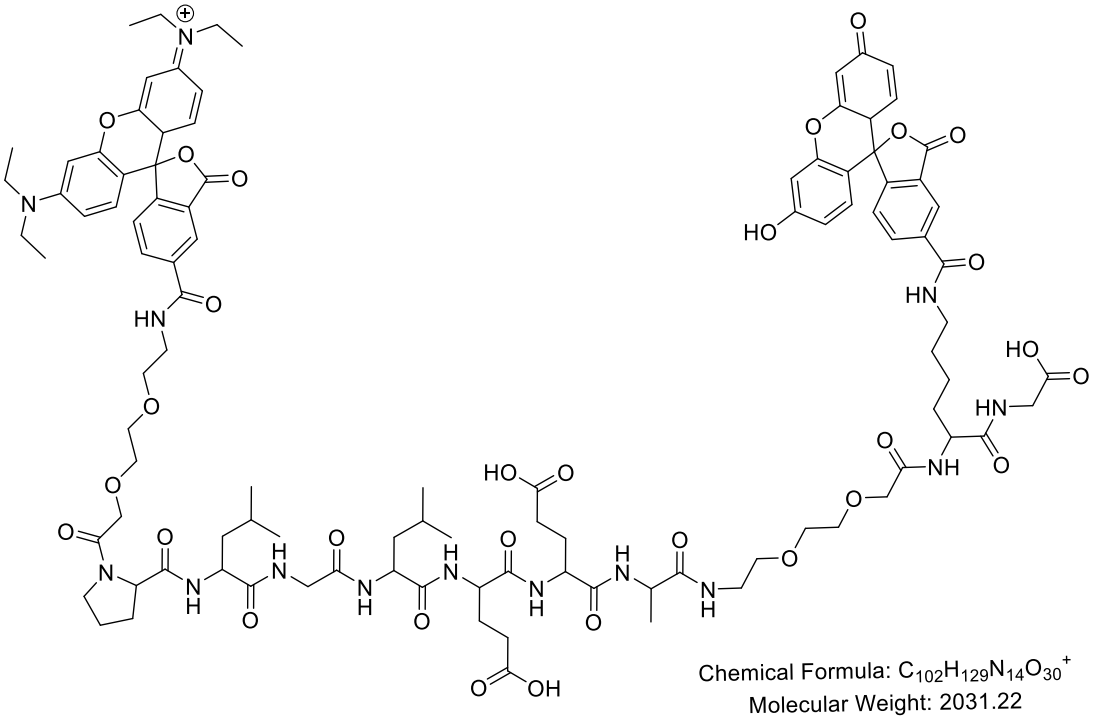

Chemical Formula: $C_{102}H_{129}N_{14}O_{30}^{+}$
Molecular Weight: 2031.22

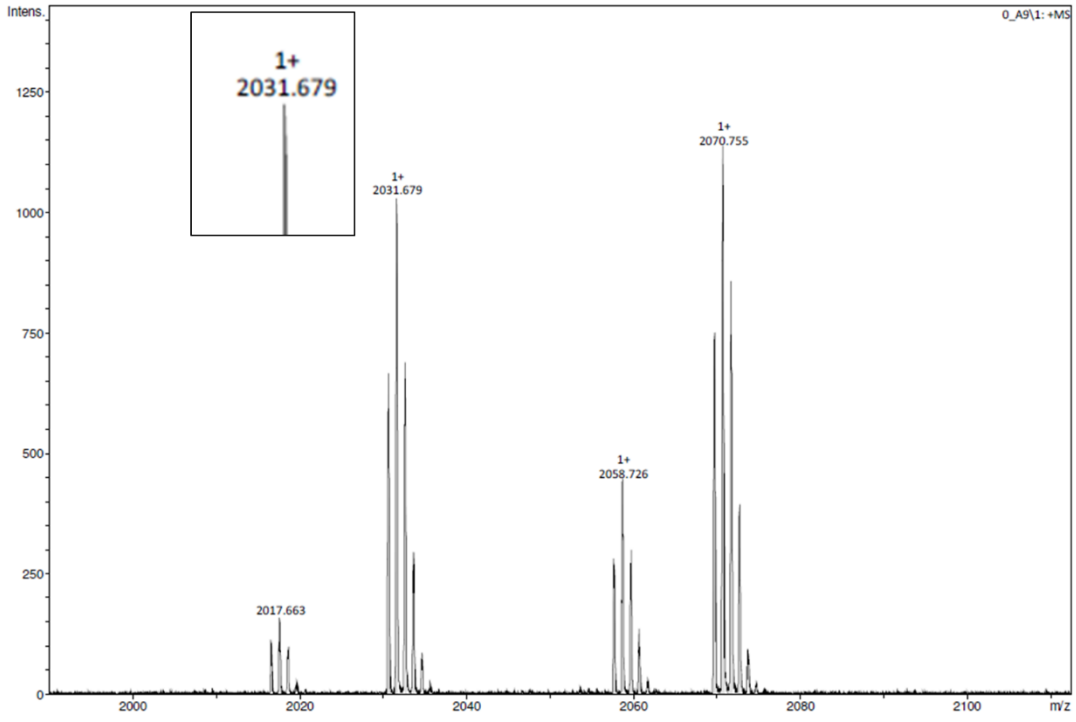

HS1-65

MALDI Mass Spectrometry: calculated for $C_{88}H_{113}N_{15}O_{27}Na$ $[M+Na]^+$ 1835.95 found 1835.6.

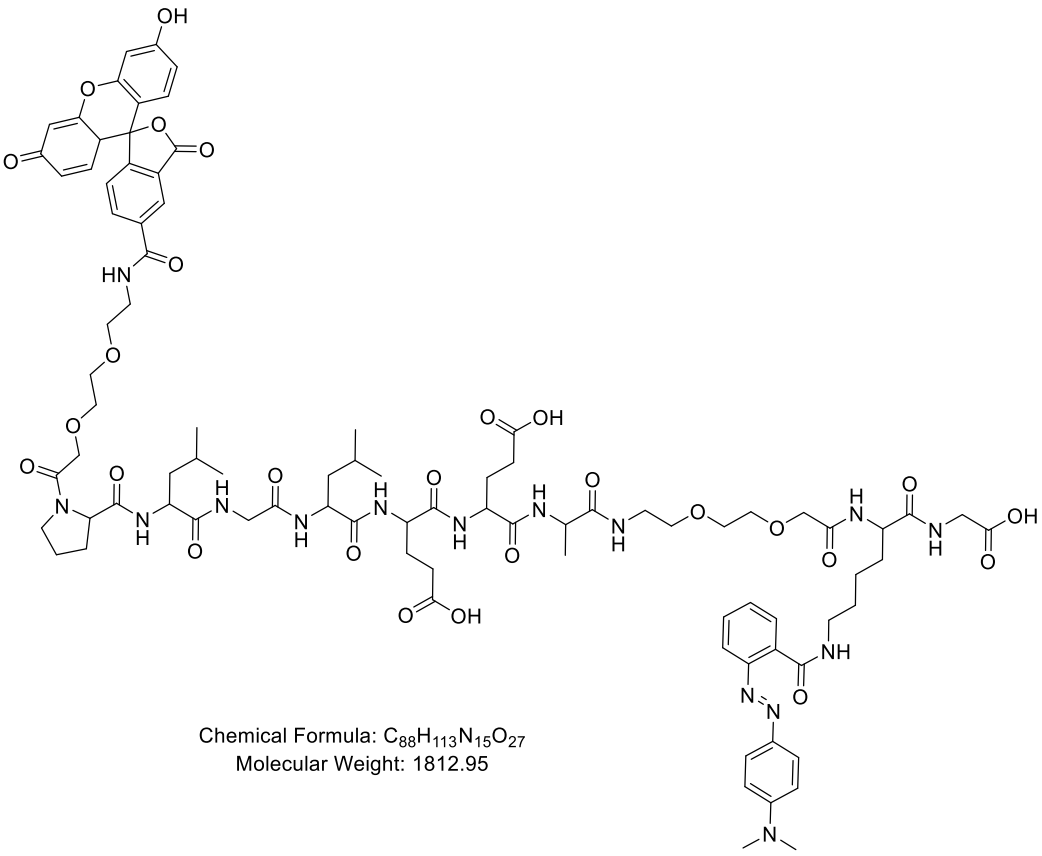

Chemical Formula: $C_{88}H_{113}N_{15}O_{27}$
Molecular Weight: 1812.95

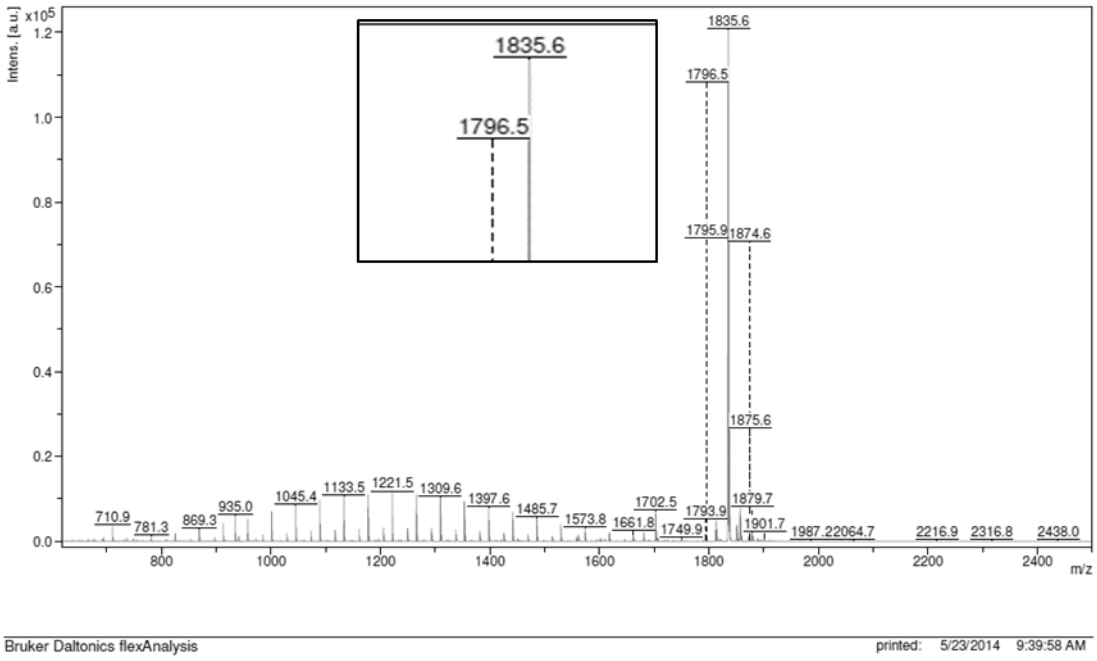

Appendix 3: HPLC ELSD Traces

High performance liquid chromatography (HPLC) was used to separated compounds and impurities within samples to check for purity. Compounds were separated along a concentration gradient (5% to 95%) of acetonitrile (ACN) in water. Compounds where detected using an evaporative light scattering detector (ELSD) and light absorbance at selective wavelengths. The HPLC-ELSD traces are presented here, the signal detected after 14 min is an artefact of the system. HPLC-ELSD traces for the FRET probes are presented in Figure A3.1. HPLC-ELSD traces for HS1-22 and synthesis intermediates are presented in Figure A3.2.

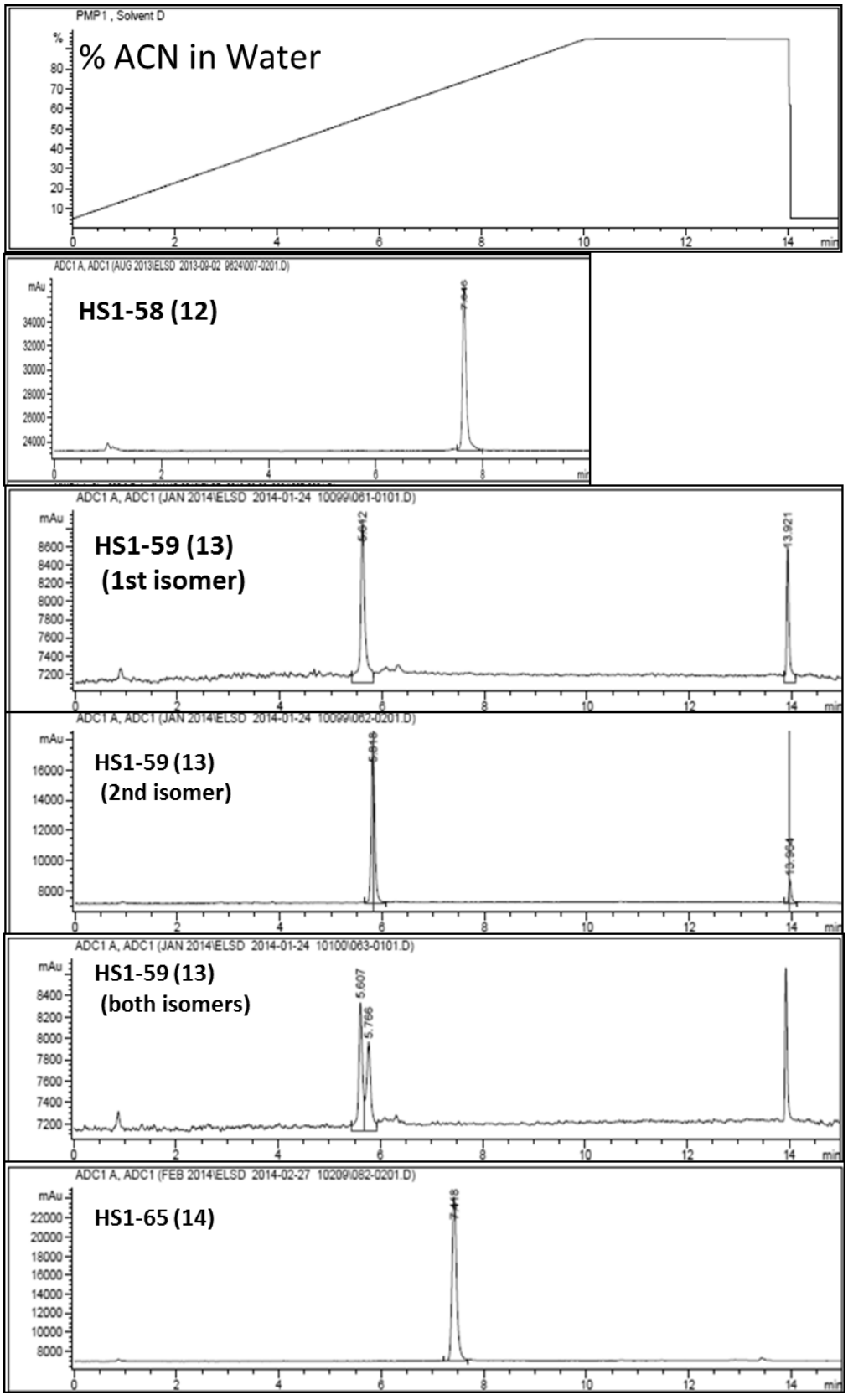

Figure A3.1 HPLC ELSD traces of FRETporbes

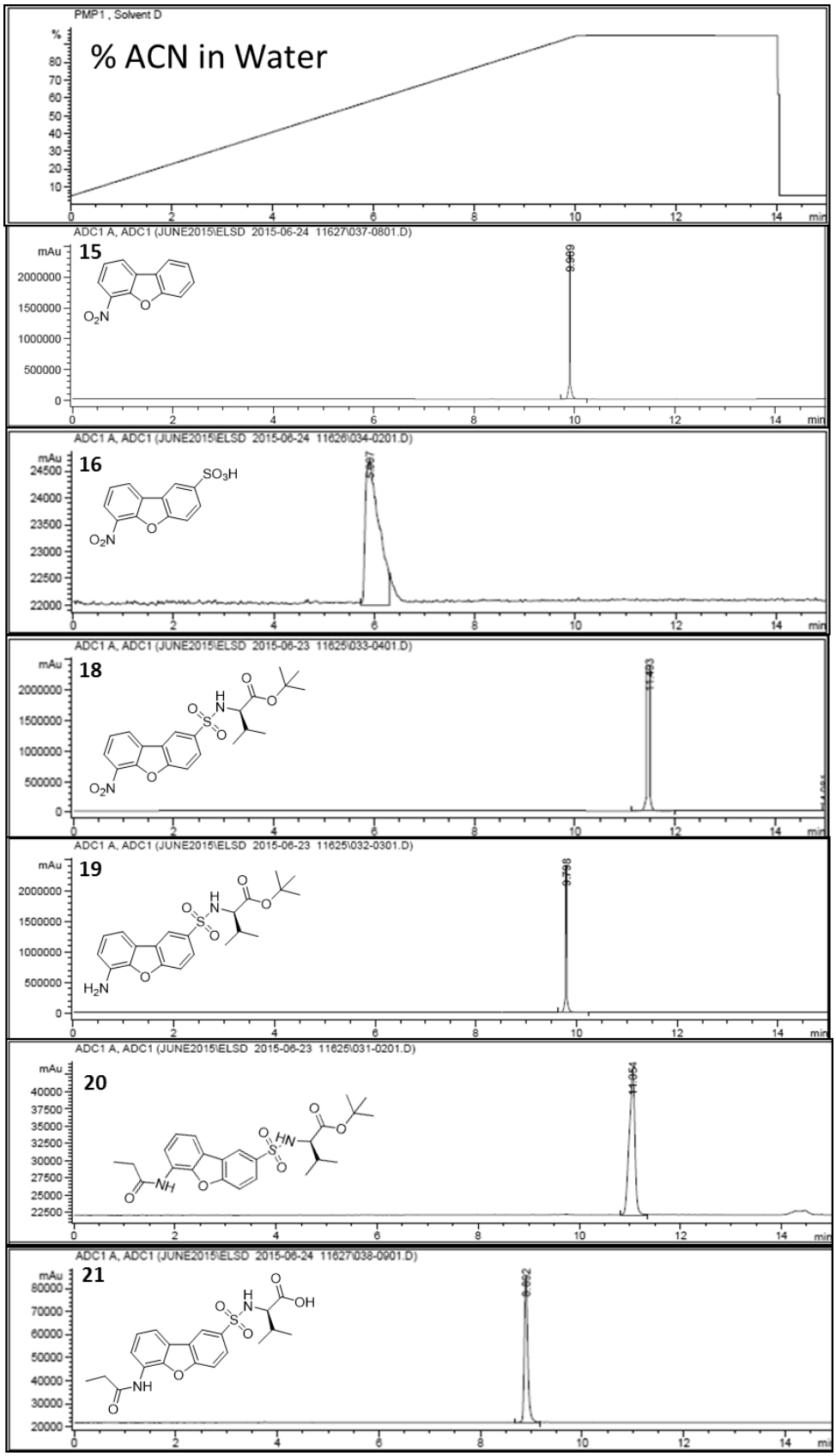

Figure A3.2 HPLC ELSD traces for HS1-22 (21) and synthesis intermediates

Appendix 4: Absorbance of Dyes and FRET Probes for Yield Determination

The absorption of fluorophores and FRET probes was measured (as described in section 2.5.6) (Figure A4.1). It was determined that the absorption of Rhodamine B or FAM could be used to measure the concentration of the probe due to minimal overlap with the second corresponding fluorophore of the FRET probe. To create a standard curve, the absorption of RhodB or FAM at various concentrations (25 – 200 μM) was measured using a nanodrop. This data was potted so that linear best fit lines could be drawn and associated equations determined (Figure A4.2). This equation was used to determine the concentration of the FRET probe. The FRET probe was diluted (1/10, 1/50/ 1/100) and the absorbance of the solutions was measured. Absorbance was measured at the wavelength of the conjugated fluorophore (FAM or Rhodamine B, 495 nm or 546 nm respectively). The absorbance measurement between 0 and 1 was used to calculate the concentration of the probe sample using a standard curve. The concentration of the stock mixture was then calculated depending on the dilution of the sample.

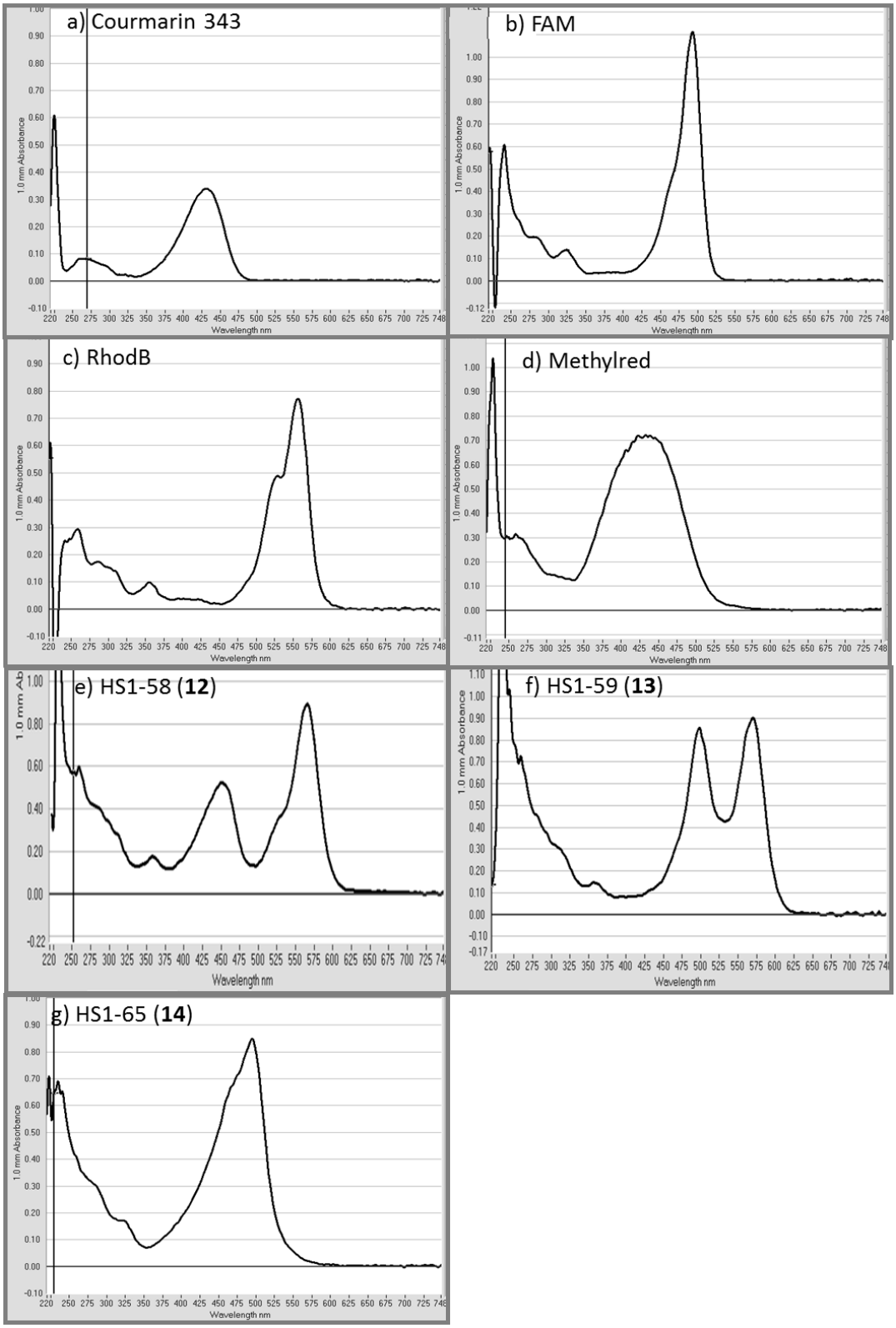

Figure A4.1 Spectra showing the absorption of dyes and FRET probes

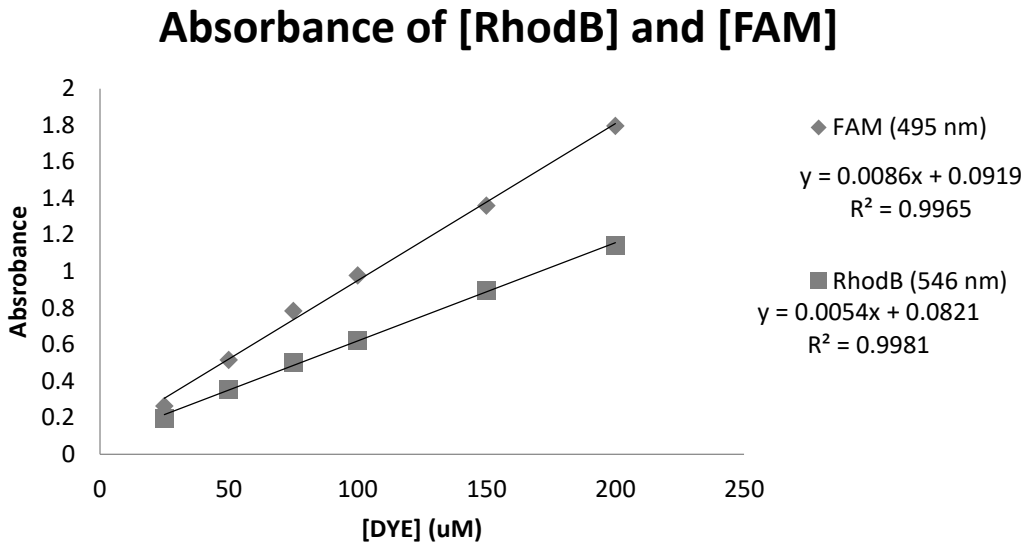

Figure A4.2 The absorption of light by RhodB and FAM at concentrations between 25 and 200 µM. A linear best fit line was drawn for each and the respective equations determined. Data is presented as mean (n = 1 in duplicate).

Appendix 5: RT-qPCR Data For Sponges Collected on D 21 – 35

To investigate the role of MMP-12 during angiogenesis *in vivo* the sponge model was utilised as described in (Section 2.9 and Chapter 4). Gene expression of vascular markers, and angiogenesis markers and MMPs were analysed in sponges collected from D 3 – 35. Two studies were conducted, firstly sponges where collected during early angiogenesis (D 3 – 21), secondly sponges were collected during later angiogenesis (D 21 – 35). The D 3 sponges showed little expression of these genes (likely due to the lack of biological tissue), and therefore any analysis of the gene expression in relation to the other time points in this study was not possible. Four housekeeping genes were assessed for the sponge model of which TBP and GAPDH had the lowest mean variation in gene expression between groups D 7 – 21 and D 21 – 35(Table 2.7). Data from D 7 – 21 is presented in Chapter 4 and here (labelled as "early"), data from D 21- 35 (labelled as "late") is just presented in this appendix (Figures A5.1, A5.2 and A5.3). To check for consistency in gene expression between the two studies, sponges from D 21 from both the "early" and "late" studies were also compared.

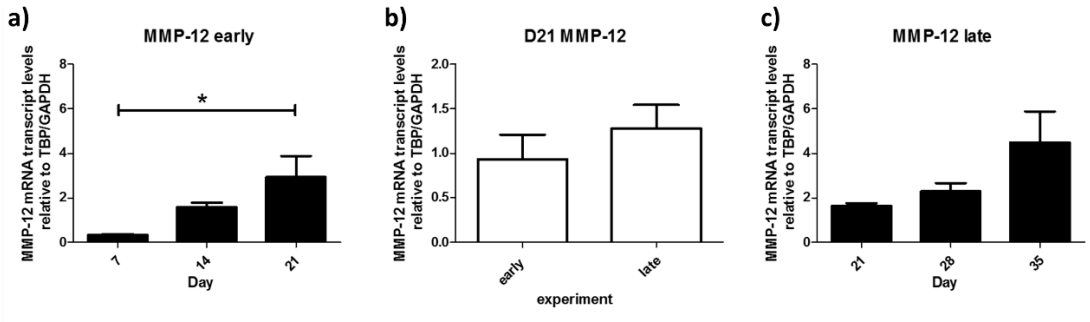

Figure A5.1 Gene transcripts of MMP-12 in sponge. a) early time course experiments = D 7 – 21, b) To check for consistency in gene expression between the two studies, sponges from D 21 from both the early and late studies were also compared. c) late time course experiments = D 21 – 35. Bars represent mean ± SEM (n = 6) and comparisons for (b) were made using a Students t-test ($P > 0.05$); comparisons for (a) and (c) were made using a one-way ANOVA followed by Bonferroni Post-hoc tests comparing all data sets (* $P < 0.05$).

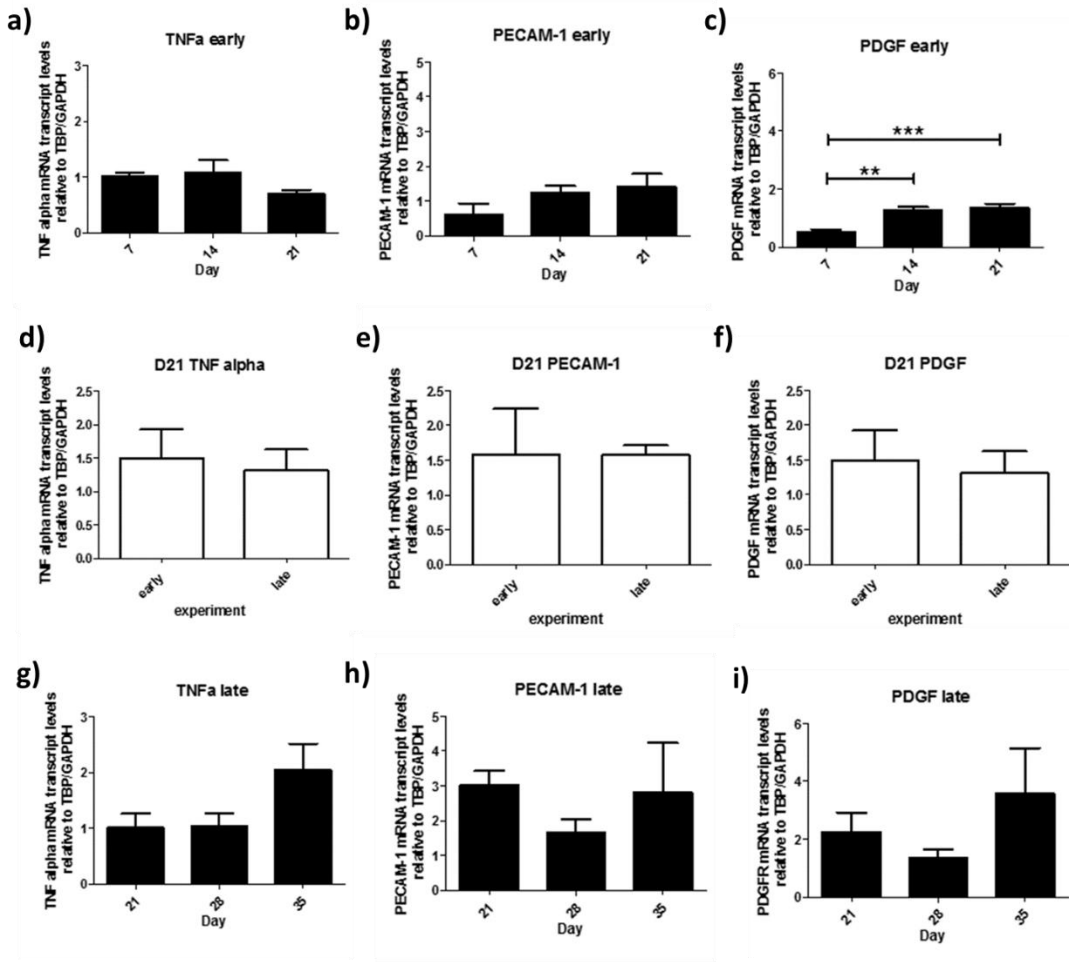

Figure 0.1 Gene transcripts of TNF, PECAM-1 and PDGF in sponges. a-c) gene expression of early time course experiments (D 7 – 21) for TNFα, PECAM-1 (CD31) and PDGF respectively. d-f) To check for consistency in gene expression between the two studies, sponges from D 21 from both the "early" and "late" studies were also compared for TNFα, PECAM-1 (CD31) and PDGF gene expression. g-h) gene expression in late time course experiments (D 21 – 35) for TNFα, PECAM-1 (CD31) and PDGF respectively. Bars represent mean ± SEM (n = 5 − 6) and comparisons for (d-f) were made using a Students t-test ($P > 0.05$); comparisons for (a-c) and (g-i) were made using a one-way ANOVA followed by Bonferroni Post-hoc tests comparing all data sets (** $P < 0.01$, *** $P < 0.001$).

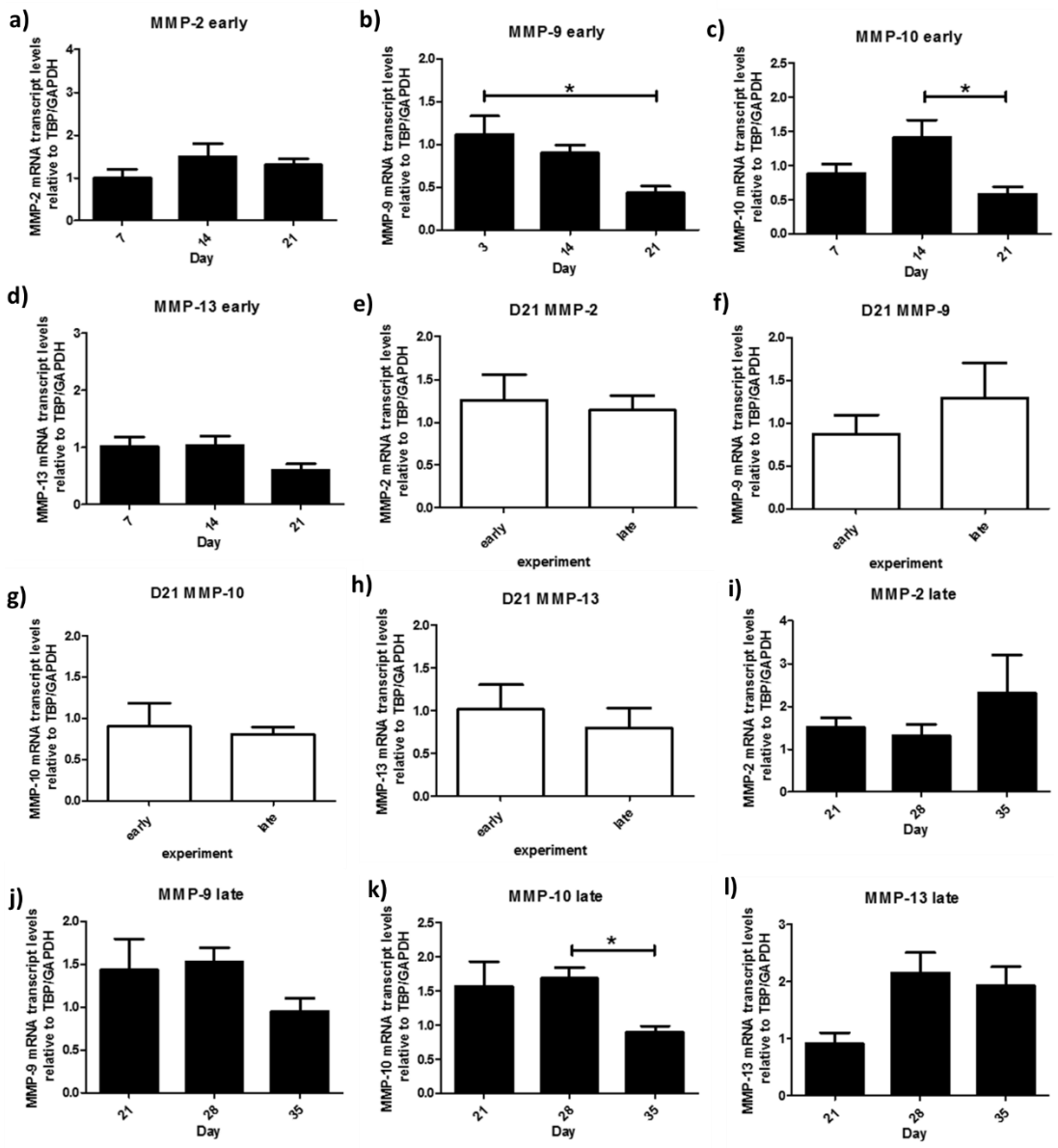

Figure A5.3 Gene transcripts of MMP-2, 9, 10 and 13 in sponges. a-d) Gene expression in the early time course experiments (D 7 – 21) for MMP-2, -9, -10 and -13 respectively. e-h) To check for consistency in gene expression between the two studies, sponges from D 21 from both the "early" and "late" studies were also compared for MMP-2, -9, -10 and -13 respectively. i-l) Gene expression in the late time course experiments (D 21 – 35) for MMP-2, -9, -10 and -13 respectively. Bars represent mean ± SEM (n = 5 − 6) and comparisons for (e-h) were made using a Students t-test ($P > 0.05$); comparisons for (a-d) and (i-l) were made using a one-way ANOVA followed by Bonferroni Post-hoc tests comparing all data sets (* $P < 0.05$).

Appendix 6: Permissions For Use of Figures

Figures from open access did not need permission to use. Permission for other figures used in this thesis are listed here. All figures in this where modified form the original cited figure

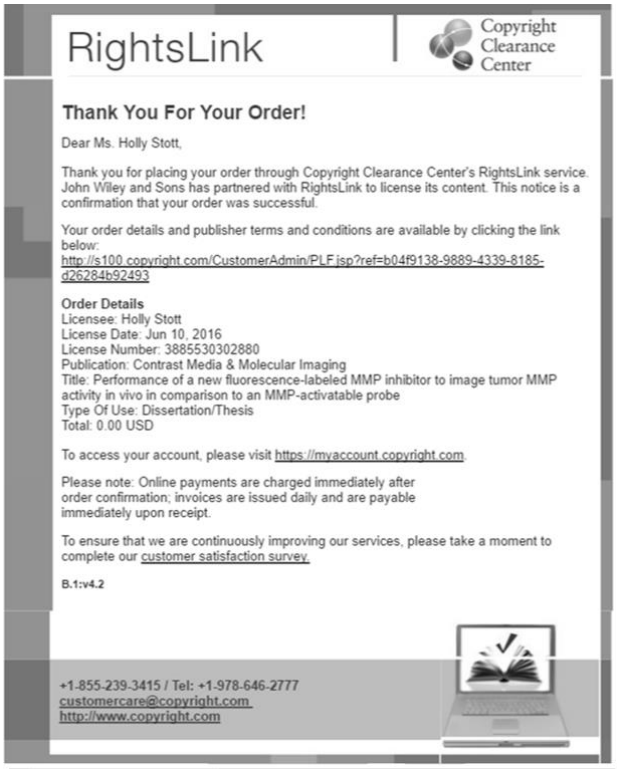

RightsLink | Copyright Clearance Center

Thank You For Your Order!

Dear Ms. Holly Stott,

Thank you for placing your order through Copyright Clearance Center's RightsLink service. John Wiley and Sons has partnered with RightsLink to license its content. This notice is a confirmation that your order was successful.

Your order details and publisher terms and conditions are available by clicking the link below:
http://s100.copyright.com/CustomerAdmin/PLF.jsp?ref=b04f9138-9889-4339-8185-d26284b92493

Order Details
Licensee: Holly Stott
License Date: Jun 10, 2016
License Number: 3885530302880
Publication: Contrast Media & Molecular Imaging
Title: Performance of a new fluorescence-labeled MMP inhibitor to image tumor MMP activity in vivo in comparison to an MMP-activatable probe
Type Of Use: Dissertation/Thesis
Total: 0.00 USD

To access your account, please visit https://myaccount.copyright.com.

Please note: Online payments are charged immediately after order confirmation; invoices are issued daily and are payable immediately upon receipt.

To ensure that we are continuously improving our services, please take a moment to complete our customer satisfaction survey.

B.1:v4.2

+1-855-239-3415 / Tel: +1-978-646-2777
customercare@copyright.com
http://www.copyright.com

RightsLink | Copyright Clearance Center

Thank You For Your Order!

Dear Ms. Holly Stott,

Thank you for placing your order through Copyright Clearance Center's RightsLink service. John Wiley and Sons has partnered with RightsLink to license its content. This notice is a confirmation that your order was successful.

Your order details and publisher terms and conditions are available by clicking the link below:
http://s100.copyright.com/CustomerAdmin/PLF.jsp?ref=3fdc25a3-9c6a-49d3-827a-f630df772b90

Order Details
Licensee: Holly Stott
License Date: Jun 10, 2016
License Number: 3885520293290
Publication: Arthritis & Rheumatology
Title: In Vivo Imaging of Matrix Metalloproteinase 12 and Matrix Metalloproteinase 13 Activities in the Mouse Model of Collagen-Induced Arthritis
Type Of Use: Dissertation/Thesis
Total: 0.00 USD

To access your account, please visit https://myaccount.copyright.com.

Please note: Online payments are charged immediately after order confirmation; invoices are issued daily and are payable immediately upon receipt.

To ensure that we are continuously improving our services, please take a moment to complete our customer satisfaction survey.

B.1:v4.2

+1-855-239-3415 / Tel: +1-978-646-2777
customercare@copyright.com
http://www.copyright.com

RightsLink | Copyright Clearance Center

Thank You For Your Order!

Dear Ms. Holly Stott,

Thank you for placing your order through Copyright Clearance Center's RightsLink service. Nature Publishing Group has partnered with RightsLink to license its content. This notice is a confirmation that your order was successful.

Your order details and publisher terms and conditions are available by clicking the link below:
http://s100.copyright.com/CustomerAdmin/PLF.jsp?ref=bf39c209-f5b5-4df8-b4bb-d03058ebfb3e

Order Details
Licensee: Holly Stott
License Date: Jun 10, 2016
License Number: 3885510734923
Publication: Nature Chemical Biology
Title: Membrane-bound FRET probe visualizes MMP12 activity in pulmonary inflammation
Type Of Use: reuse in a dissertation / thesis
Total: 0.00 USD

To access your account, please visit https://myaccount.copyright.com.

Please note: Online payments are charged immediately after order confirmation; invoices are issued daily and are payable immediately upon receipt.

To ensure that we are continuously improving our services, please take a moment to complete our customer satisfaction survey.

B.1:v4.2

+1-855-239-3415 / Tel: +1-978-646-2777
customercare@copyright.com
http://www.copyright.com

RightsLink | Copyright Clearance Center

Thank You For Your Order!

Dear Ms. Holly Stott,

Thank you for placing your order through Copyright Clearance Center's RightsLink service. Nature Publishing Group has partnered with RightsLink to license its content. This notice is a confirmation that your order was successful.

Your order details and publisher terms and conditions are available by clicking the link below:
http://s100.copyright.com/CustomerAdmin/PLF.jsp?ref=853cc98a-4ad2-444f-b7c8-75d1d2a33315

Order Details
Licensee: Holly Stott
License Date: Jun 10, 2016
License Number: 3885340537658
Publication: Nature Reviews Molecular Cell Biology
Title: Matrix metalloproteinases and the regulation of tissue remodelling
Type Of Use: reuse in a dissertation / thesis
Total: 0.00 USD

To access your account, please visit https://myaccount.copyright.com.

Please note: Online payments are charged immediately after order confirmation; invoices are issued daily and are payable immediately upon receipt.

To ensure that we are continuously improving our services, please take a moment to complete our customer satisfaction survey.

B.1:v4.2

+1-855-239-3415 / Tel: +1-978-646-2777
customercare@copyright.com
http://www.copyright.com

RightsLink | Copyright Clearance Center

Thank You For Your Order!

Dear Ms. Holly Stott,

Thank you for placing your order through Copyright Clearance Center's RightsLink service. Elsevier has partnered with RightsLink to license its content. This notice is a confirmation that your order was successful.

Your order details and publisher terms and conditions are available by clicking the link below:
http://s100.copyright.com/CustomerAdmin/PLF.jsp?ref=2aacdf4b-66e0-45e0-950a-d76a34a07412

Order Details
Licensee: Holly Stott
License Date: Jun 10, 2016
License Number: 3885450565827
Publication: Cell Chemical Biology
Title: A Bright Future for Precision Medicine: Advances in Fluorescent Chemical Probe Design and Their Clinical Application
Type Of Use: reuse in a thesis/dissertation
Total: 0.00 USD

To access your account, please visit https://myaccount.copyright.com.

Please note: Online payments are charged immediately after order confirmation; invoices are issued daily and are payable immediately upon receipt.

To ensure that we are continuously improving our services, please take a moment to complete our customer satisfaction survey.

B.1:v4.2

+1-855-239-3415 / Tel: +1-978-646-2777
customercare@copyright.com
http://www.copyright.com

RightsLink | Copyright Clearance Center

Thank You For Your Order!

Dear Ms. Holly Stott,

Thank you for placing your order through Copyright Clearance Center's RightsLink service. Nature Publishing Group has partnered with RightsLink to license its content. This notice is a confirmation that your order was successful.

Your order details and publisher terms and conditions are available by clicking the link below:
http://s100.copyright.com/CustomerAdmin/PLF.jsp?ref=e686dac9-008f-4994-843f-8d335ed6cf69

Order Details
Licensee: Holly Stott
License Date: Jun 10, 2016
License Number: 3885450087067
Publication: Nature Reviews Drug Discovery
Title: Molecular imaging in drug development
Type Of Use: reuse in a dissertation / thesis
Total: 0.00 USD

To access your account, please visit https://myaccount.copyright.com.

Please note: Online payments are charged immediately after order confirmation; invoices are issued daily and are payable immediately upon receipt.

To ensure that we are continuously improving our services, please take a moment to complete our customer satisfaction survey.

B.1:v4.2

+1-855-239-3415 / Tel: +1-978-646-2777
customercare@copyright.com
http://www.copyright.com